



**SYNTHESIS OF NOVEL PHOSPHININE
COORDINATION COMPOUNDS AND
THEIR REACTIVITY TOWARD SMALL
MOLECULES**

Dissertation zur Erlangung des
Doktorgrades der Naturwissenschaften

DOCTOR RERUM NATURALIUM

am Institut für Anorganische Chemie
der Fakultät für Chemie und Pharmazie
der Universität Regensburg

vorgelegt von

JULIA LEITL

aus Aschau am Inn

Regensburg 2020

To my grandpa.

Der experimentelle Teil der vorliegenden Arbeit wurde von November 2016 bis März 2020 unter Anleitung von Prof. Dr. Robert Wolf am Institut für Anorganische Chemie der Universität Regensburg angefertigt.

Diese Arbeit wurde angeleitet von:	Prof. Dr. Robert Wolf
Promotionsgesuch eingereicht am:	13.07.2020
Tag der mündlichen Prüfung:	25.09.2020
Promotionsausschuss: Vorsitz:	Prof. Dr. Manfred Scheer
Erstgutachter:	Prof. Dr. Robert Wolf
Zweitgutachter:	Prof. Dr. Christian Müller
Dritter Prüfer:	Prof. Dr. Frank-Michael Matysik

PROLOGUE

This doctoral thesis reports on the synthesis and characterization of novel phosphinine coordination compounds and their reactivity toward small molecules. *Chapter 1* gives a general overview of phosphinine chemistry, discussing their rich coordination chemistry and application in catalysis. *Chapter 2* reports on the selective halogenation of an anionic phosphinine iron(0) complex, which led to the formation of rare halogenated phosphacyclohexadienyl complexes. *Chapter 3* shows the reactivity of a phospho-bora-norbornadiene with nitriles and alkynes. The results show phosphinine derivatives incorporating a Lewis acidic site can possess frustrated Lewis pair (FLP) type reactivity. In *Chapter 4*, the synthesis of pyridyl-phosphinine-based phosphinoborates is discussed. *Chapter 5* reports on the facile splitting of carbon dioxide by an anionic pyridyl-phosphinine iron(0) complex. *Chapter 6* addresses the synthesis on a homoleptic pyridyl-phosphinine nickel(0) complex which is capable of splitting carbon-halide bonds. Finally, *Chapter 7* summarizes all results of this thesis followed by a brief outlook on the future of phosphinine chemistry.

PROLOG

Diese Dissertation beschreibt die Synthese und Charakterisierung von neuen Phosphininverbindungen und deren Reaktivität gegenüber kleinen Molekülen. *Kapitel 1* gibt einen generellen Überblick über die Phosphinchemie wieder. Die Vielfältigkeit von Phosphininen spiegelt sich in ihrer reichhaltigen Koordinationschemie und ihren Einsatz in der Katalyse wider. *Kapitel 2* thematisiert die selektive Halogenierung eines anionischen Phosphinin-Eisen(0)-Komplexes unter Bildung von halogenierten Phosphacyclohexadienylkomplexen. In *Kapitel 3* wird der Einsatz von Phosphininen in frustrierten Lewis-Paaren (FLP) beschrieben. Hierbei zeigt ein Phosphaboranorbornadien eine FLP-artige Reaktivität gegenüber Nitrilen und Alkinen. In *Kapitel 4* wird die Synthese von Pyridylphosphinin-basierten Phosphinoboranen diskutiert. *Kapitel 5* berichtet von der einfachen Spaltung von Kohlenstoffdioxid durch einen anionischen Pyridylphosphinin-Eisen(0)-Komplex. *Kapitel 6* beschreibt die Synthese eines homoleptischen Pyridylphosphinin-Ni(0)-Komplexes, welcher in der Lage ist, Kohlenstoff-Halogen-Bindungen zu spalten. *Kapitel 7* fasst alle Ergebnisse dieser Arbeit zusammen und gibt einen kurzen Ausblick in zukünftige Forschungsgebiete der Phosphinin-Chemie.

List of Abbreviations

18c-6	[18crown-6]
BAr ^F ₄	tetrakis(3,5-bis(trifluoromethyl)phenyl)borate
bd	broad doublet
bs	broad singlet
Bu	butyl
cod	1,5-cyclooctadiene
Cp	cyclopentadiene
Cp*	1,2,3,4,5-pentamethylcyclopentadiene
DFT	density functional theory
DME	1,2-dimethoxyethane
EPR	electron spin resonance
m	multiplet
Me	methyl
mes	mesityl
nbd	2,5-norbornadiene
NMR	nuclear magnetic resonance
Ph	phenyl
s	singlet
THF	tetrahydrofuran
TPP	2,4,6-triphenylphosphinine
t	triplet
TMS	tris(trimethylsilyl)
δ	chemical shift

Table of Contents

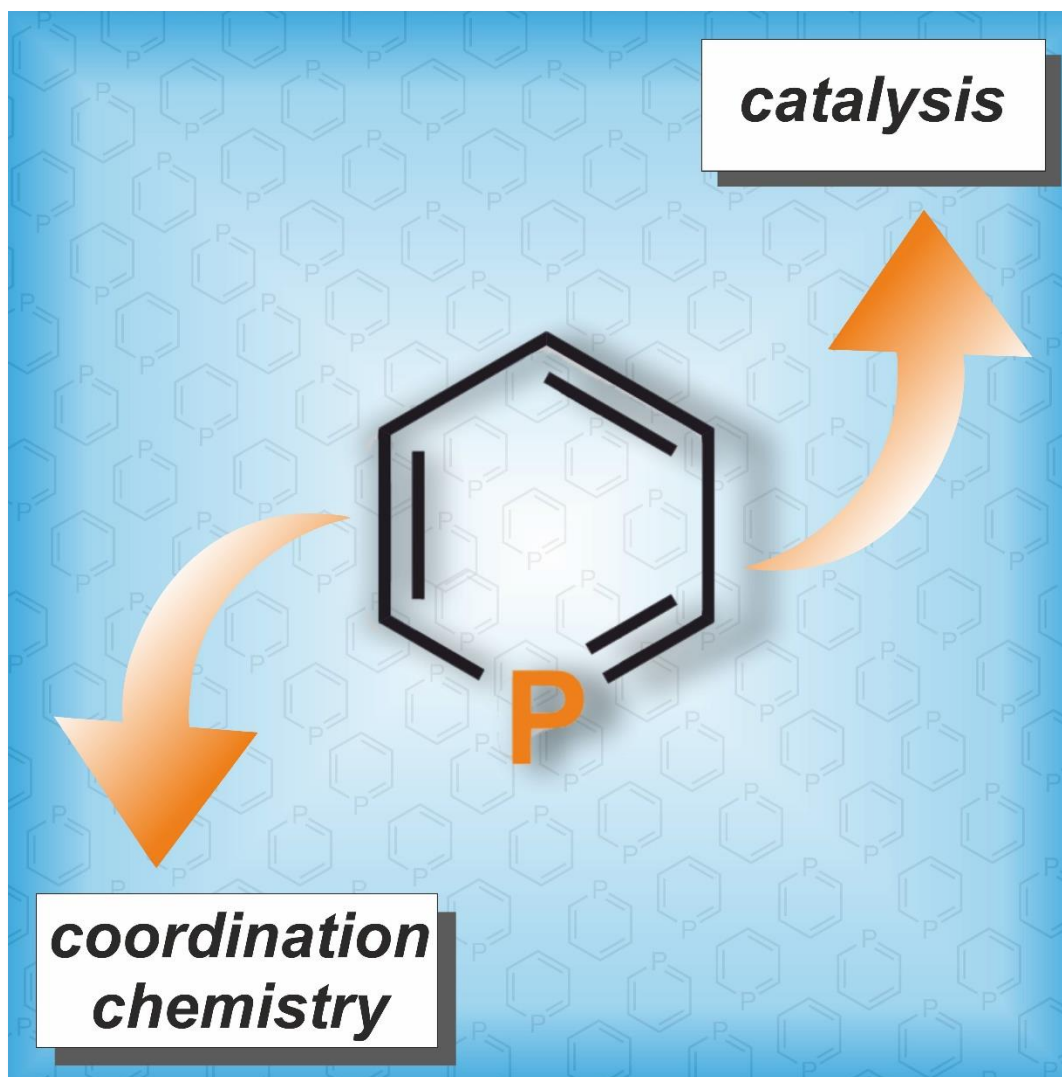
Chapter 1	1
Introduction	1
Chapter 2	21
<i>Halide-Substituted Phosphacyclohexadienyl Iron Complexes: Covalent Structures vs. Ion Pairs</i>	
Introduction	22
Results and Discussions	23
Conclusion	30
Experimental	31
References	35
Supporting Information	37
Chapter 3	38
<i>A Phosphinine-Derived 1-Phospha-7-Bora-Norbornadiene: Frustrated Lewis Pair Type Activation Toward Triple Bonds</i>	
Introduction	39
Results and Discussions	40
Conclusion	53
Experimental	54
References	61
Supporting Information	63
Chapter 4	64
<i>2-(2'-Pyridyl)-4,6-Diphenylphosphinine as Platform for the Synthesis of Phosphorus/Boron-Based Lewis Pairs</i>	
Introduction	65
Results and Discussions	68
Conclusion	77
Experimental	79
References	83
Supporting Information	85

Chapter 5	111
<i>Facile C=O Bond Splitting of Carbon Dioxide Induced by Metal-Ligand Cooperativity in a Phosphinine Iron(0) Complex</i>	
Introduction	112
Results and Discussions	113
Conclusion	119
Experimental	120
References	124
Supporting Information	125
Chapter 6	126
<i>Phosphorus-Analogues of [Ni(bpy)₂]: Synthesis and Application in Carbon-Halogen Bond Activation</i>	
Introduction	127
Results and Discussions	128
Conclusion	139
Experimental	140
References	145
Supporting Information	147
Chapter 7	148
Summary and Conclusion	148
List of Publications	155
Curriculum Vitae	156
Acknowledgement	157
Appendix	159

Chapter 1

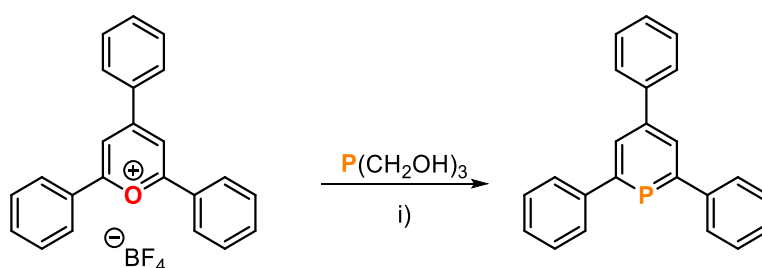
Introduction

Phosphinines – Versatile Ligands in Coordination Chemistry and Homogenous Catalysis



1.1 The discovery of phosphinines

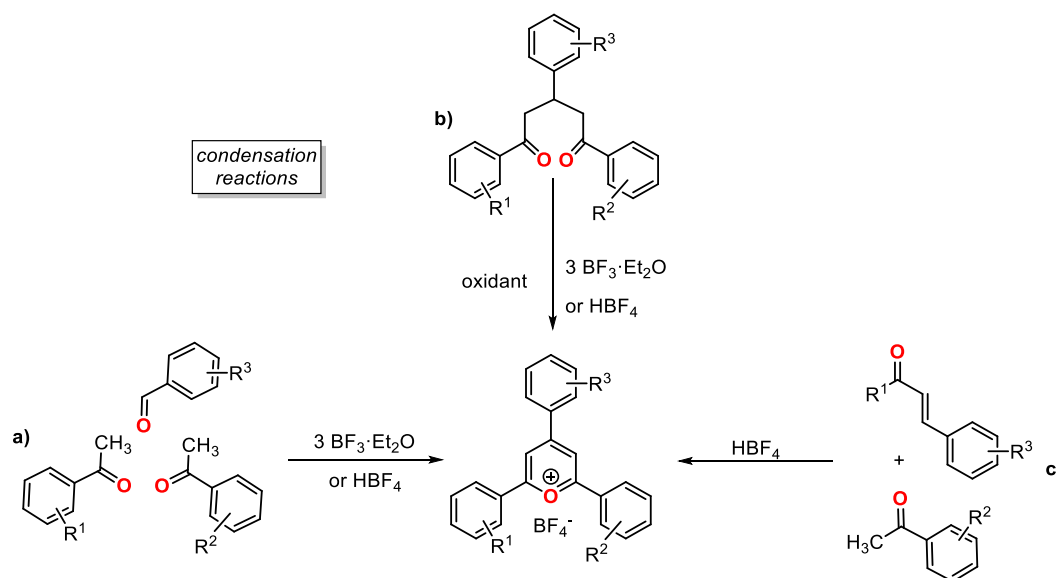
For a large part of chemical research history, it was believed that $p\pi-p\pi$ multiple bonds could not occur for heavier main group elements.^[1] The “double bond rule” purports that elements with a quantum number greater than two, are not able to form multiple bonds with themselves or with other elements.^[2] This was disproved in the last century by the isolation of low coordinate / multiply bonded compounds containing phosphorus, silicon and their heavier congeners.^[3-5] Unsaturated compounds containing phosphorus were of particular interest due to being analogous to carbon.^[6] These two elements have a diagonal relationship in the periodic table of elements, which results in similar reactivity. The Pauling electronegativity values (2.55 for C and 2.19 for P) as well as the van der Waals radii (1.70 Å for C and 1.80 Å for P) are similar, and, as a result, strong covalent C–P bonds (bond dissociation energies for C–C = 605 kJ·mol⁻¹ and P–C = 507.5 kJ·mol⁻¹) can be formed.^[7] The synthesis of 2,4,6-triphenylphosphabenzene, also known as triphenylphosphinine (TPP), in 1966 by Märkl demonstrated that phosphorus-containing heterocycles possessing P–C multiple bonds or P–C sp^2 -hybridization can actually exist.^[8] TPP was synthesized by reaction of a pyrylium salt with a phosphorus(III) source, e.g. P(CH₂OH)₃ (Scheme 1). Märkl’s seminal work on the synthesis of phosphinines was a fundamental breakthrough in main group chemistry. It allowed easy access to low coordinate phosphorus compounds which *hitherto* only existed in the form of unstable phosphalkynes or phosphacyanides.^[9,10] Phosphinines subsequently proved to have promising applications in coordination chemistry and catalysis and were intensively investigated by the groups of Märkl, Dimroth, Ashe III, Elschenbroich, Mathey, Le Floch, Zenneck and Müller.



Scheme 1. First synthesis of TPP by Märkl; i) pyridine, $-3 \text{ CH}_2\text{O}$, $-\text{H}_2\text{O}$, $-\text{HBF}_4$.

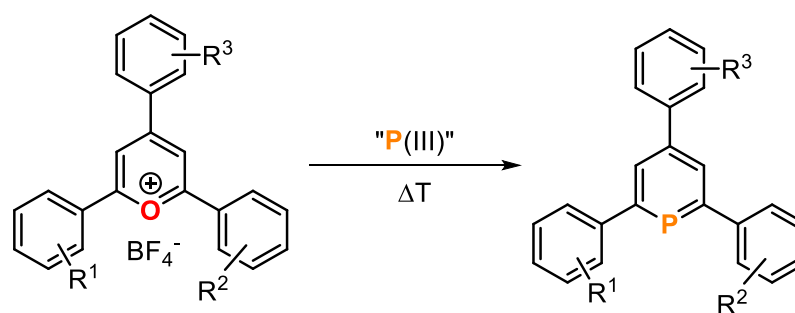
1.2 Synthetic routes toward phosphinines

Numerous synthetic routes to phosphinines have been developed over the past five decades. The following describes the most common synthetic procedures for these six-membered heterocycles. As mentioned above, Märkl used the pyrylium salt 2,4,6-triphenylpyrylium tetrafluoroborate for the original synthesis of TPP (Scheme 1).^[8] Pyrylium salts are a common precursor for the synthesis of phosphinines because of the easy introduction of various functional groups and substituents in specific positions of the heterocycle (Scheme 2).^[11]



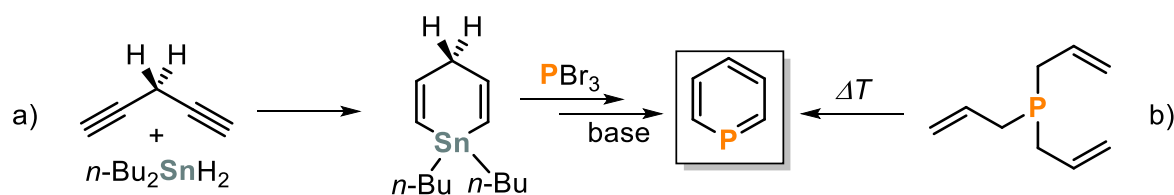
Scheme 2. Different synthetic routes to pyrylium salts.

Synthesizing pyrylium salts *via* the condensation of aldehydes and ketones is ideal as the starting materials are generally commercially available or easily accessible synthetically (a, Scheme 2).^[12] Pyrylium salts can also be synthesized through two other routes: the cyclization of aromatic 1,5-diketones with BF_3/HBF_4 (b, Scheme 2) or reacting a chalcone with acetophenone derivatives in the presence of HBF_4 (c, Scheme 2)^[13]. The final step of the phosphinine synthesis is the O^+/P exchange reaction of the pyrylium salt with a phosphorus (III) compound such as PH_3 or more nucleophilic agents such as $\text{P}(\text{CH}_2\text{OH})_3$ ^[14] or $\text{P}(\text{SiMe}_3)_3$ ^[15]. With this route, high purity phosphinines can be isolated. However, yields of the isolated products typically are low to moderate (i.e. in the range of 10 – 50%).



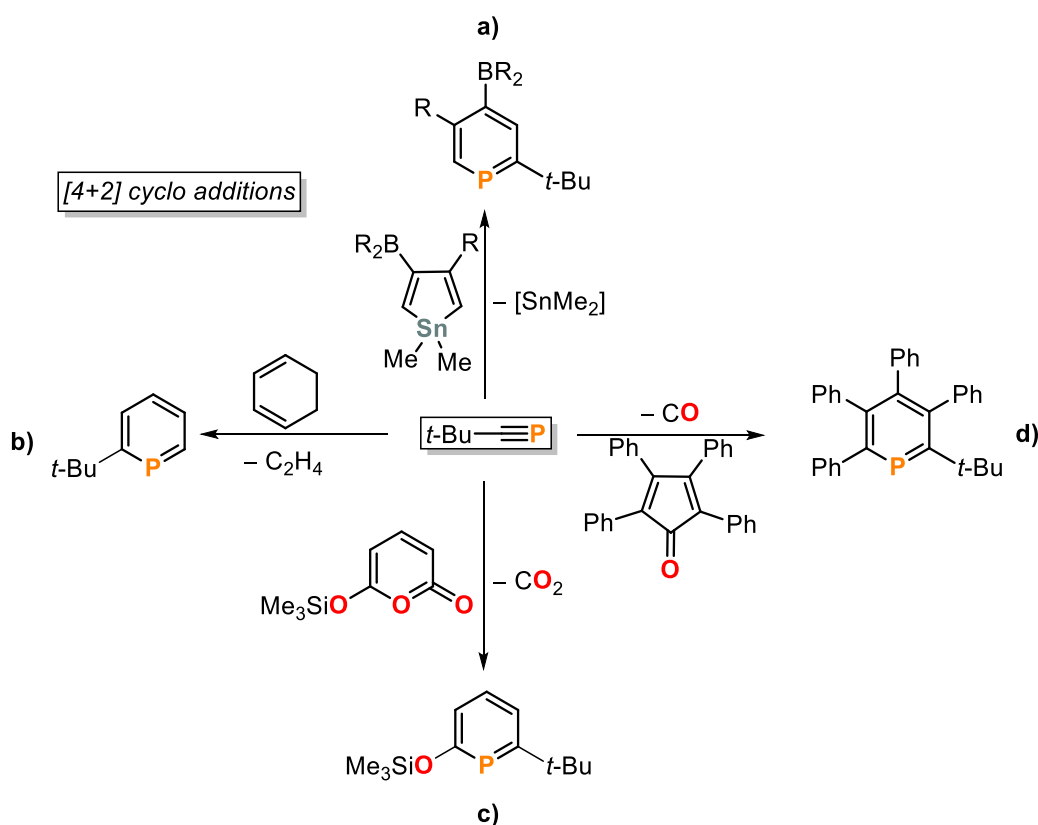
Scheme 3. Synthesis of phosphinines *via* pyrylium salt route.

Another common route for the synthesis of phosphinines was reported by Ashe III, who was able to obtain the unsubstituted parent phosphinine PC_5H_5 *via* tin exchange reaction from a stanna-cyclohexadiene (a, Scheme 4).^[16] An alternative preparation of PC_5H_5 is the thermolysis of tris(allyl)phosphine at 700 °C (b, Scheme 4).^[17]



Scheme 4. Synthesis of parent phosphinine *via* a) stannacyclopentadiene and by b) thermolysis.

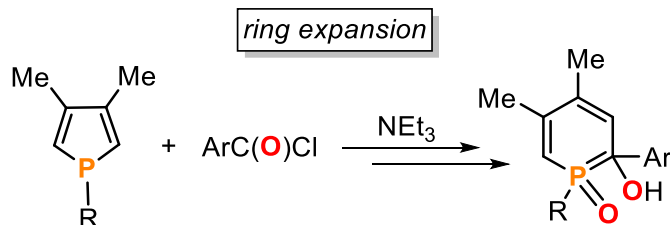
A versatile precursor for the synthesis of substituted phosphinines are phosphoalkynes. These low-coordinate phosphorus compounds can act as dienophiles in [4+2] cycloadditions with different dienophilic systems (Scheme 5). All of these reactions involve a cycloaddition as the first step followed by subsequent elimination of an organic fragment. For example, *tert*-butylphosphoalkyne can be treated with activated stannols (a, Scheme 5)^[18] or heated in the presence of 1,3-cyclohexadienes (b, Scheme 5)^[19] to form phosphinines in good yields *via* the elimination of dimethyl tin and ethene respectively (Scheme 5). Regitz and co-workers described the synthesis of phosphinines *via* [4+2] cycloaddition of *tert*-butylphosphoalkyne and pyrones (c, Scheme 5)^[20] or cyclopentadienes (d, Scheme 5)^[21] with release of CO₂ and CO respectively.



Scheme 5. Synthesis of phosphinines *via tert*-butyl phosphoalkyne.

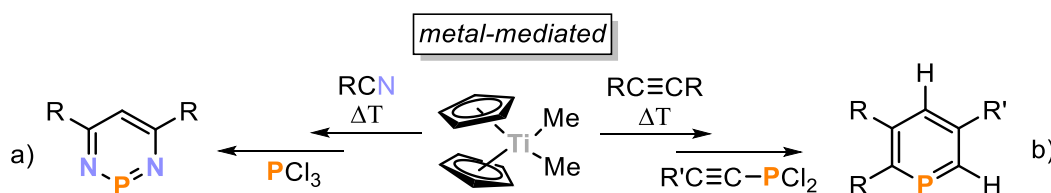
Another prevalent tool for the synthesis of phosphinines is the one-step ring expansion reactions of phospholes.^[22] The original reaction, first conducted by Mathey, involved the hydrolysis of a mixture of phosphole, aromatic acid chloride and triethylamine (Scheme

6).^[23] The ring expansion is highly dependent on the substituents of the phosphole and acid chloride. Too bulky substituents (R and Ar) or alkyl substituents on the acid chloride prevent phosphinine formation.



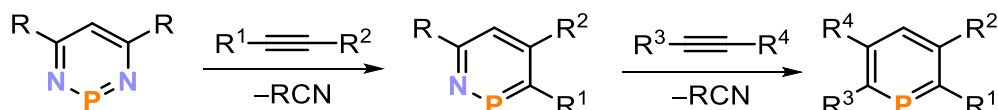
Scheme 6. Synthesis of phosphinines from phospholes.

A less frequently employed method for the formation of phosphinines are metal-mediated syntheses. Titanacycle transfer reactions are very useful for the synthesis of pnictogen containing heterocycles.^[3] Cp_2TiMe_2 can be used for the formation of 1,3,2-diazaphosphinines *via* N–Ti, N–P bond metathesis (a, Scheme 7).^[24] It can also act as a mediator for the formation of 2,3,5-substituted phosphinines, which involves a thermal rearrangement, an intramolecular [4+2] cycloaddition and a [1,5]-hydrogen shift (b, Scheme 7).^[25]



Scheme 7. Titanium-mediated syntheses of phosphinines.

It was later found that nitrogen containing P heterocycles also proved to be effective precursors for the synthesis of 2,3,5,6-tetra-substituted phosphinines. The two-step reaction starts with [4+2] cycloaddition of an alkyne at elevated temperatures (70 °C) which affords a 1,2-azaphosphinine with the release of nitrile. Addition of a second equivalent of alkyne leads to the formation of the desired tetra-functionalized phosphinine.^[24,26]



Scheme 8. Synthesis of 2,3,5,6-tetrafunctional phosphinines *via* reaction of 1,3,2-diazaphosphinines with alkynes.

Chromium-^[27], iron-^[28] and hafnium^[29]-mediated syntheses have also been established for the synthesis of phosphinines, but the pyrylium salt route is still the most employed due to being the easiest, most efficient and cheapest method to obtain substituted phosphinines.

1.3 Electronic and structural properties of phosphinines

Due to their unique electronic and structural properties, phosphinines have been intensively employed as ligands in coordination chemistry and homogeneous catalysis. General features of these heterocycles are their planar structure and aromaticity.^[30] The molecular structure generally features equal C–C bond lengths (1.395 Å), which are close to the values in benzene, and short P–C bonds (mean distance: 1.749 Å). The aromaticity of the parent phosphine was estimated to amount to 97% of benzene.^[31] Moreover, the electronic properties of phosphinines differ significantly from their lighter homologues, pyridines, as demonstrated by photoelectron and electron transmission spectroscopy and theoretical calculations.^[32–35] An analysis of the frontier molecular orbitals of phosphinines reveals that the lone pair of electrons resides in the HOMO–2. The P-lone pair of electrons occupies a more diffuse, partially delocalized and less directional orbital compared to pyridine, which makes phosphinine a comparably weaker σ -donor. Electrophilic attack on the P atom in phosphinines hardly occurs due to the fact that the electron density on the P atom has strong 3s-orbital character (about 63%) which leads to low basicity ($pK_a(\text{C}_5\text{H}_6\text{P}^+) = -16.1 \pm 1$ in aqueous solutions).^[36] Due to their symmetry the HOMO–1 and HOMO are able to form π -donor interactions with metal d-orbitals of suitable symmetry in transition metal complexes. More importantly, the low-lying LUMO orbital provides phosphinines with great π -acceptor abilities (Figure 1).^[11] This property is essential for the formation of transition metal complexes.

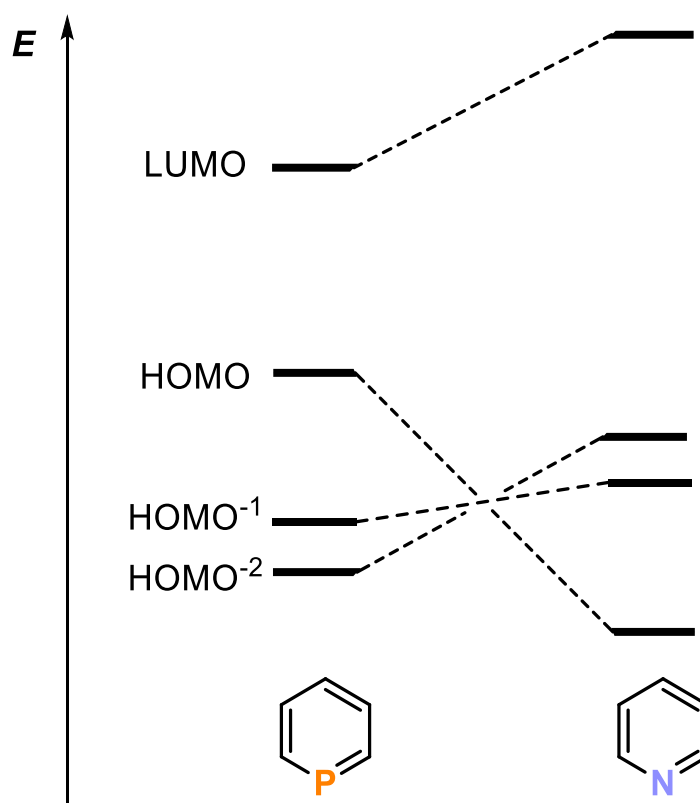


Figure 1. Qualitative MO-diagram; comparison of the frontier orbitals of phosphinine (left) and pyridine (right).

A classical tool for the quantification of the electron donor properties of a ligand is the Tolman electronic parameter χ .^[37] The Tolman parameter allows the comparison of different phosphorus ligands with each other. The parameter χ is the result of IR stretching frequencies of phosphorous donor ligand (L) nickel carbonyl complexes $\text{LNi}(\text{CO})_3$, whereby $(t\text{Bu}_3\text{P})\text{Ni}(\text{CO})_3$ serves as reference. High χ values indicate strong π -acceptor properties, which arise from little π -back donation from the metal center to the CO ligand. The comparison of phosphinines with other P-ligands shows that they have higher values for the CO stretching frequencies in their corresponding Ni complexes and thus are stronger π -acceptors (Figure 2).^[11, 38, 39]

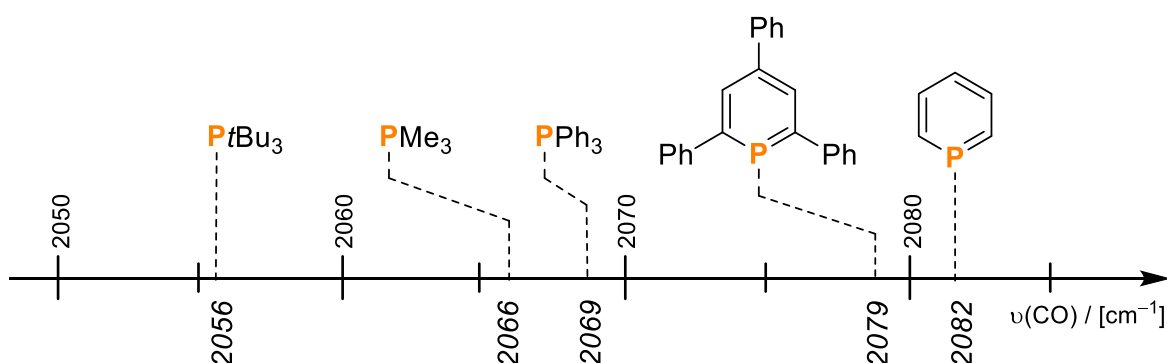


Figure 2. Tolman electronic parameters of P containing ligands determined by IR CO stretching frequencies (in $[\text{cm}^{-1}]$) of $\text{LNi}(\text{CO})_3$ ($\text{L} = \text{PtBu}_3, \text{PMe}_3, \text{PPh}_3, \text{TPP}, \text{PC}_5\text{H}_5$).

Along with electronic properties the choice of substituent is important in terms of the steric demand of the phosphinine. In order to describe the steric situation of a ligand, the Tolman steric parameter θ (= cone angle) can be utilized.^[37] The value θ gives a general idea about the steric hinderance around the P-centre in phosphine ligands. However, in terms of phosphinine ligands, which are plane molecules, the occupancy angles α and β along the orthogonal planes x and y in the heterocycle are more suitable for the description of the steric situation (Figure 3).^[33] The values of the occupancy angles of TPP, measured from the geometry of its calculated structure, are $\alpha = 216^\circ$ and $\beta = 54^\circ$. The steric demand in the y plane is lower than in the x plane, thus phosphinines are better described as a flattened cone rather than a perfectly cylindrical one, which is the case for phosphines.^[33]

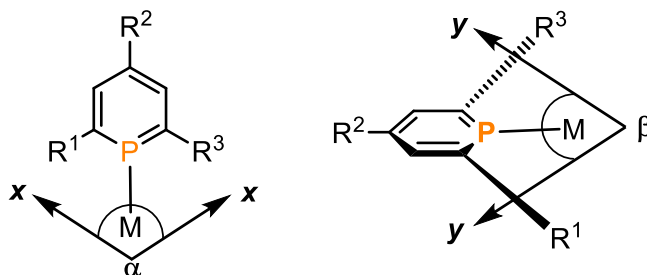


Figure 3. Occupancy angles α and β in phosphinines.

1.4 Phosphanes as ligands for transition metal complexes

As mentioned, the electronic properties of phosphines (see section 1.3) make them highly attractive ligands in coordination chemistry and are able to adopt a range of different coordination modes (Figure 4). Phosphines possess a lone pair of electrons, located at the P atom, allowing them to form η^1 -complexes *via* σ -coordination (a, Figure 4). Due to a low-lying LUMO, the π -acceptor ability of phosphines is very high, which enables the formation of π -complexes such as η^6 -complexes (b, Figure 4). The combination of σ -donor and π -acceptor properties offer several coordination sites on the ligand allowing the formation of dinuclear phosphine complexes (c and d, Figure 4). Adding a substituent to the P atom forms λ^4 -phosphines, also referred as phosphacyclohexadienyl anions, and they coordinate mostly in a η^5 -mode to the metal center (e, Figure 4). There is also the rare η^4 -mode (f, Figure 4), which is presented by just a few examples.

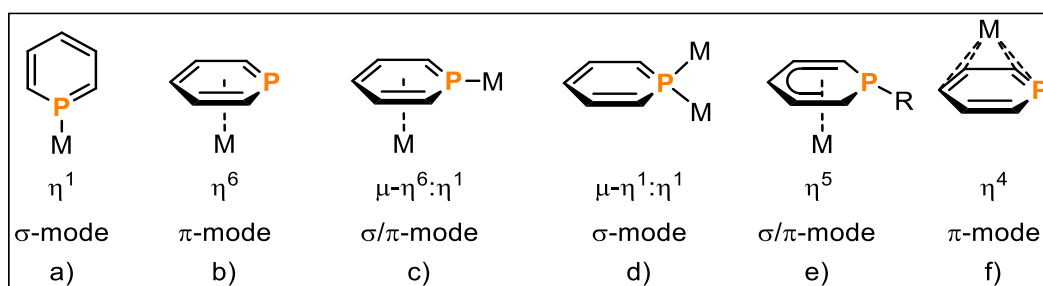


Figure 4. Range of coordination modes of phosphine transition metal complexes.

In general, the strong π -accepting capacity of phosphines enables the stabilization of electron-rich transition metal complexes. Late transition metals in low oxidation states undergo η^1 -coordination with phosphines. This was observed for a range of homoleptic complexes by Elschenbroich who used the parent phosphine as a ligand (Figure 5). Tetrahedral Ni(0)^[40] (**1**), octahedral group 6 (Cr(0), Mo(0), W(0))^[41] (**2**) and trigonal bipyramidal Fe(0)^[42] (**3**) complexes were prepared and structurally characterized, showing σ -coordination of the parent phosphine to the metal center exclusively.

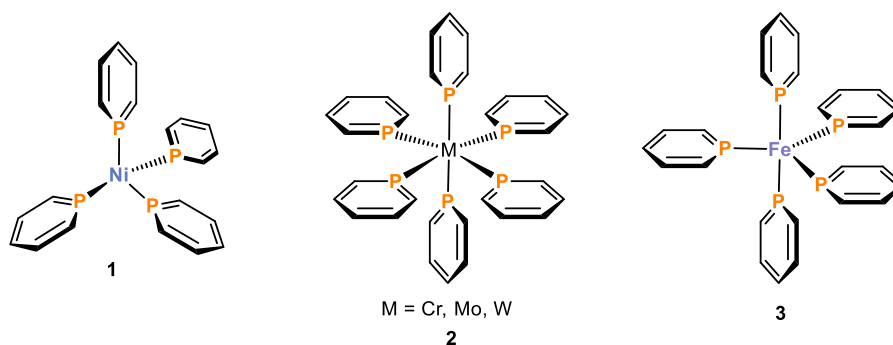


Figure 5. Examples for σ -coordinated transition metal phosphine complexes in η^1 -mode.

Another common motif is coordination through the π -system of the phosphinine, which results in the formation of η^6 -phosphinine complexes (Figure 6). Bulky substituents on the phosphinine ligand in compound **4** prevent the formation of σ -complexes as shown in Figure 5, above, for the parent phosphinine.^[43] In addition, group 8 metals are also able to form π -complexes with phosphinines. The η^6 -phosphinine complex **5** was synthesized by reacting $[\text{Fe}(\text{cod})_2]$ (cod = 1,5-cyclooctadiene) with free phosphinine at low temperatures.^[44] Compound **5** can also be utilized in catalytic reactions which will be discussed in section 1.6. Compound **6** is an example of a cationic ruthenium phosphinine complex in the η^6 -coordination mode. It is formed by the reaction of free ligand with $[\text{Cp}^*\text{Ru}(\eta^4\text{-C}_6\text{H}_{10})\text{Cl}]$ ($\text{Cp}^* = 1,2,3,4,5$ -pentamethylcyclopentadiene) in the presence of AgBF_4 .^[45] Again, bulky tris-trimethylsilyl substituents prevents σ -coordination from the phosphinine.

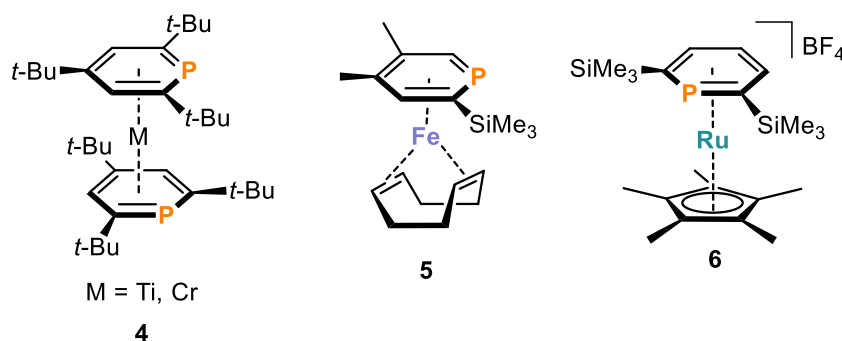


Figure 6. Examples for π -coordinated transition metal phosphinine complexes in η^6 -mode.

Dinuclear or even trinuclear phosphinine complexes are rather scarce.^[46–53] So far, such species have not been utilized in catalytic applications. In contrast, η^5 -phosphinine complexes have found several catalytic applications.^[54] The η^5 -coordination mode in phosphinine complexes can be achieved by reacting a λ^4 -phosphinine, also known as a phosphacyclohexadienyl anion, with transition metal precursors (Figure 7). The first step of this method is to react a free phosphinine ligand with a nucleophile, e.g. organolithium agents. The addition of the nucleophile occurs at the P atom due to the low-lying LUMO which is mainly localized at the P atom.^[55] The resulting λ^4 -phosphinine can further react with metal precursors such as $[\text{Rh}(\text{cod})\text{Cl}]_2$ to form η^5 -complexes **7** (Figure 7).^[56]

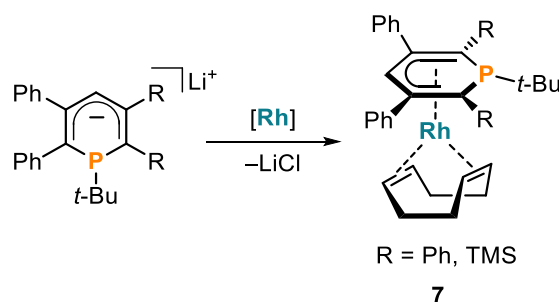


Figure 7. Example for π -coordinated transition metal phosphinine complex in η^5 -mode; $[\text{Rh}] = \text{Rh}(\text{cod})\text{Cl}_2$.

There are only a few examples of the η^4 -mode in the literature, for example the dinuclear phosphinine iron(0) complex **8** (Figure 8).^[53] The phosphinine ligand in **8** is η^4 coordinated to an $\text{Fe}(\text{CO})_3$ fragment and η^1 coordinated *via* the P-lone pair of electrons to an $\text{Fe}(\text{CO})_4$ moiety.^[53] The anionic iron(0) complex **9** possesses an η^4 -coordinated TPP ligand and is generated by the ligand exchange of TPP with naphthalene (C_{10}H_8) in $[\text{K}([\text{18}]\text{crown-6})][\text{Cp}^*\text{Fe}(\eta^4\text{-C}_{10}\text{H}_8)]$ (Figure 8).^[52]

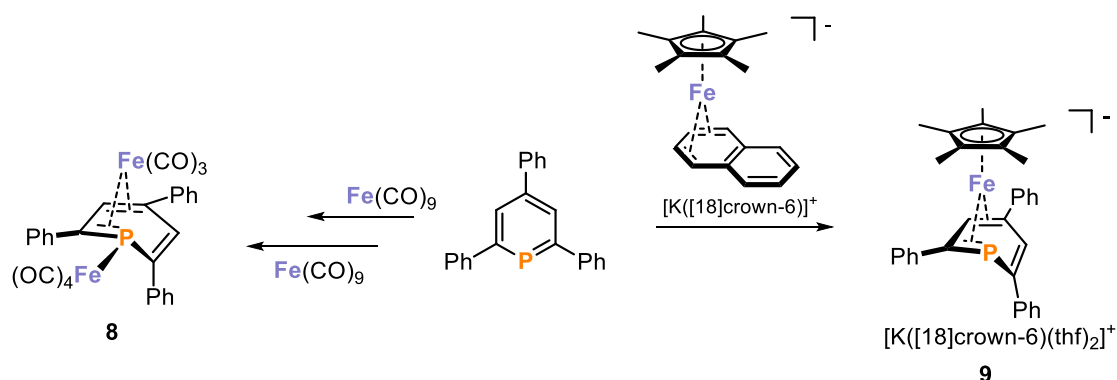


Figure 8. Examples for π -coordinated transition metal phosphinine complexes in η^4 mode and their syntheses.

Due to the multitude of coordination modes available, phosphinines are highly versatile ligands. The examples given in this section illustrate the flexibility of phosphinines resulting from their characteristic electronic and steric properties. The subsequent phosphinine metal complexes are not only interesting from a coordination chemistry perspective, but also find use in many catalytic transformations. Selected examples for such catalytic applications are discussed in section 1.6, below.

1.5 Synthesis and coordination of donor-functionalized phosphinines

2,2'-Bipyridines (a, Figure 9) have been extensively used as ligands in transition metal complexes for different chemical applications due to their versatile spectroscopic, photochemical and electrochemical properties.^[57] Hence, there was interest in synthesizing the heavier analogue of bipyridines, 2,2'-biphosphinines (b, Figure 9). Donor-functionalized phosphinines provide enhanced stability to metal centers through donation from their substituents, which has an influence on the coordination chemistry and catalysis.

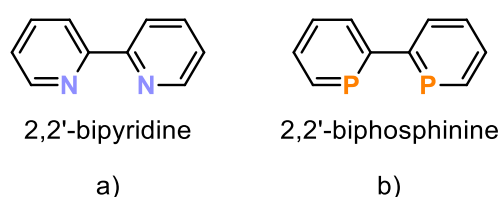
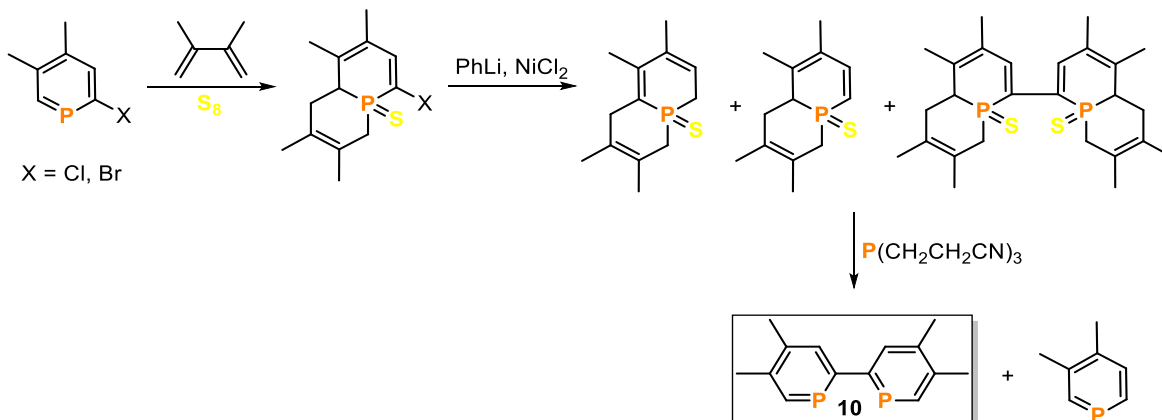


Figure 9. Generic examples for group 15 chelate ligands.

Although the symmetry of the MOs of bipyridines and biphosphinines is very similar, the properties of biphosphinines differ from bipyridines. The LUMO in bipyridines is located at the carbocyclic backbone, whereas the LUMO of biphosphinines is localized at the P atom and is lower in energy.^[58,59] The first biphosphinine was isolated by Le Floch in 1991.^[60] The multi-step synthesis of 3,3',4,4'-tetramethyl-2,2'-biphosphinine **10** is formed from 2-halophosphinines^[61] and involves cycloaddition, dehalogenation combined with homocoupling and reduction reactions (Scheme 9).



Scheme 9. Synthesis of the first 2,2'-biphosphinine.

Biphosphinine **10** can be isolated in only moderate yields (*ca.* 22%), which has limited the study of its reactivity. However, a range of different transition metal complexes with **10**, including neutral and anionic complexes, were synthesized (Figure 10). Le Floch and co-workers reacted **10** with $[\text{Cr}(\text{CO})_5(\text{thf})]$ (thf = tetrahydrofuran) to form chelate complex **11**.^[60] Anionic tetragonal biphosphinine complexes bearing highly reduced metal centers (**12**) were achieved by reducing **10** with an excess of sodium metal and by subsequent reaction with $[\text{M}(\text{acac})_3]$ (M = Co, Rh; acac = acetylacetonate).^[62] The same procedure was applied for group 4 dianionic octahedral biphosphinine complexes (**13**). Neutral biphosphinine complexes **14** could be obtained by reacting group 6 metal salts MCl_n (M = Cr, Mo, W) with **10** in the presence of an excess of magnesium.^[63] Interestingly, complexes **14** showed an unusual trigonal prismatic geometry, rather than octahedral.

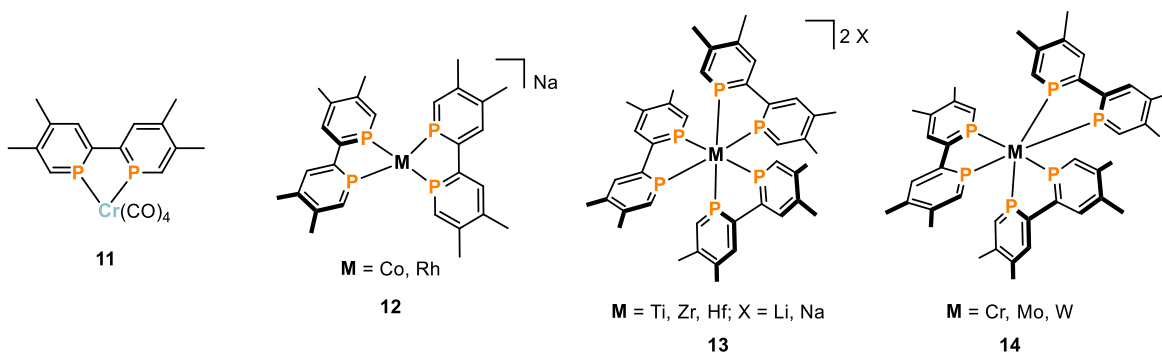


Figure 10. Transition metal biphosphinine complexes.

Apart from bipyridines and biphosphinines, it is also possible to isolate mixed P,N heterodonor compounds in the form of 2-pyridylphosphinines (Figure 11). The first pyridyl-substituted phosphinine – NIPHOS – was synthesized by Mathey and co-workers.^[64] The multi-step synthesis starts from a phosphole and 2-acetylchloride-pyridine (Scheme 10). A ring-expansion reaction is followed by condensation and reduction with metallic nickel at high temperatures, which affords NIPHOS.

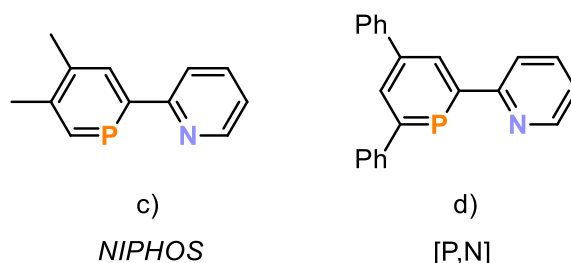
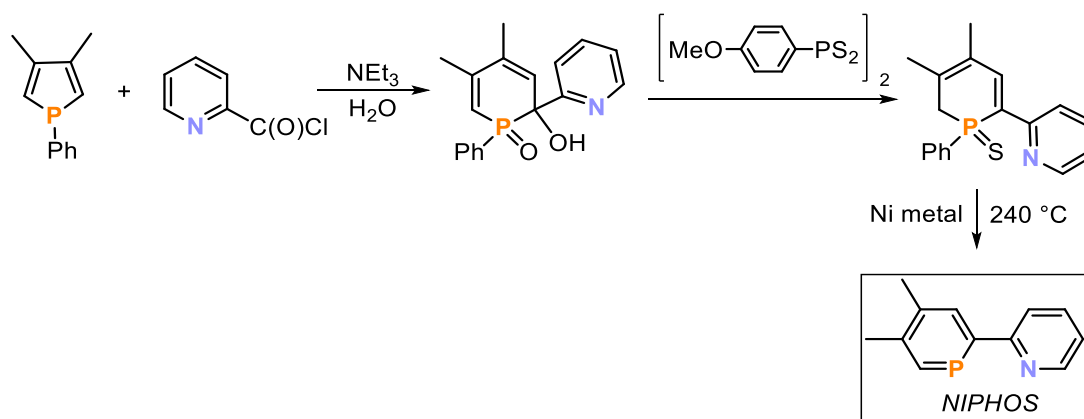


Figure 11. 2-Pyridyl-functionalized phosphinines.



Scheme 10. Synthesis of NIPHOS.

NIPHOS possesses a phosphinine moiety which is sensitive toward bases and nucleophiles, and a pyridyl group which does not tolerate acidic mediums. However, combination of these two opposing properties does not interfere with follow-up chemistry. A range of different neutral and cationic transition metal complexes bearing NIPHOS as a ligand were synthesized (Figure 12). After Mathey and co-workers reported on the synthesis of NIPHOS, they reacted it with group 6 metal precursors $[M(CO)_5(thf)]$ ($M = Cr, W$) in order to generate complexes **15**.^[65] Dinuclear platinum complexes of the general formula $[Pt_2Cl_4L_2]$ ($L = PPh_3, PMePh_2, PMe_2Ph, PMe_3, P(nBu)_3$) were reacted with NIPHOS to afford mononuclear chelate complexes **16a**.^[66] Complexes **16a** are very sensitive toward nucleophilic reagents such as water, causing hydrolysis of the P=C bond in the phosphinine moiety forming complexes **16b**. Another example of NIPHOS-containing compounds are the dimeric group 9 complexes **17**.^[67] Transition metal precursors $[Ir_2Cl_2(cod)_2]$ and $[Rh_2Cl_2(nbd)_2]$ ($cod = 1,5$ -cyclooctadiene; $nbd = 2,5$ -norbornadiene) were reacted with two equivalents NIPHOS in order to generate dinuclear chelate complexes **17** which were isolated as SbF_6 salts in good yields (up to 74%).

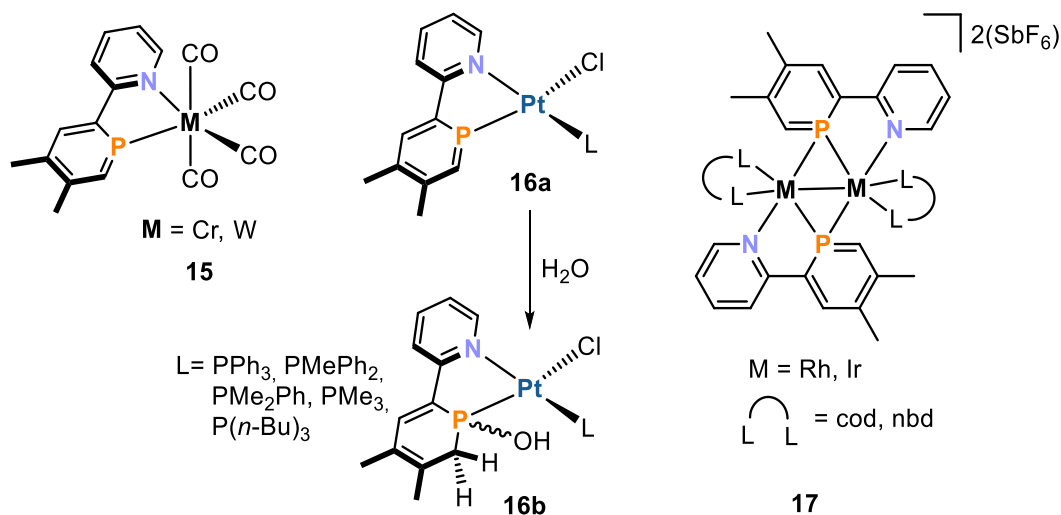
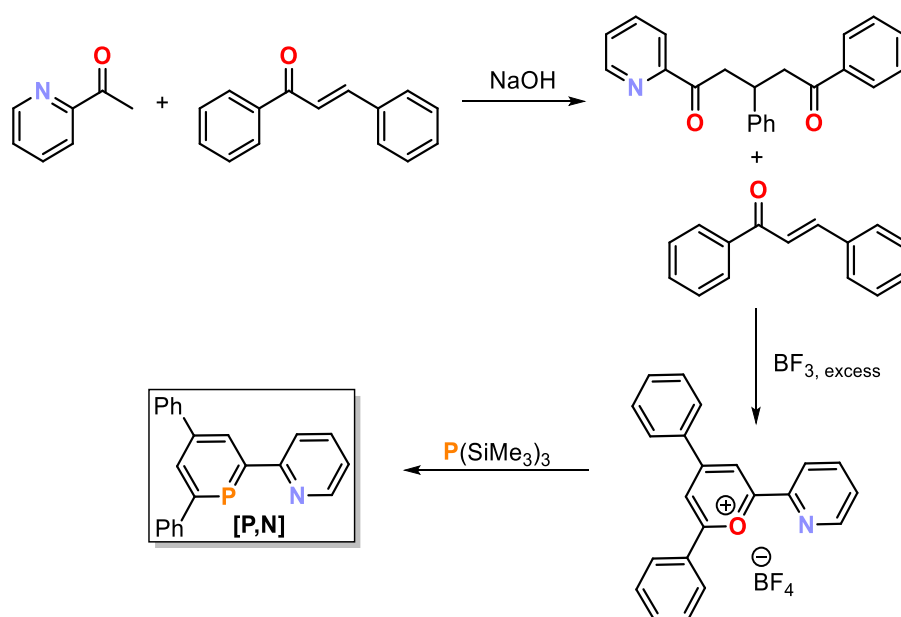


Figure 12. Transition metal complexes of NIPHOS; cod = 1,5-cyclooctadiene, nbd = 2,5-norbornadiene.

Due to the sophisticated ligand synthesis and lability of NIPHOS-containing complexes, the chemistry of pyridylphosphinines is underdeveloped. The group of Müller gave this heterodonor ligand a renaissance by the facile synthesis of the pyridyl-functionalized phosphinine 2-(2'-pyridyl)-4,6-diphenylphosphinine [**P,N**] (d, Figure 11). Müller and co-workers employed the pyrylium salt route for the synthesis of [**P,N**] (Scheme 11).^[68] 2-Acetylpyridine undergoes a condensation reaction with *trans*-chalcone to form a diketone which subsequently is reacted with another equivalent chalcone and BF₃ to afford the pyridyl-substituted pyrylium salt. After reacting the pyrylium salt with P(SiMe₃)₃, 2-(2'-pyridyl)-4,6-diphenylphosphinine [**P,N**] can be isolated in moderate yields (up to 30%). Although the pyrylium salt route delivers [**P,N**] in moderate yield, it is a facile approach compared to the multi-step synthesis of NIPHOS.



Scheme 11. Synthesis of 2-pyridylphosphinine [**P,N**] via pyrylium salt route.

On account of this new synthetic route for pyridylphosphinines, a number of transition metal complexes have been isolated (Figure 13). The general synthesis of such complexes is the reaction of **[P,N]** with group 6 carbonyl complexes.^[69] The transition metal precursors $[\text{Cr}(\text{CO})_6]$, $[\text{Mo}(\text{nbd})(\text{CO})_4]$ and $[\text{W}(\text{CO})_6]$ were reacted with one equivalent of **[P,N]** to afford mononuclear complexes **18** in which **[P,N]** acts as a bidentate chelating ligand. Cationic complexes **19a** were synthesized by the reaction of **[P,N]** with $[\text{Cp}^*\text{M}(\text{Cl}_2)_2]$ ($\text{M} = \text{Rh}, \text{Ir}$) and they react with H_2O regio- and diastereo-selectively at the external $\text{P}=\text{C}$ double bond (**19b**).^[70] Finally, neutral group 10 complexes **20a**, were generated from ligand exchange reaction of **[P,N]** and $[\text{M}(\text{cod})\text{Cl}_2]$ ($\text{M} = \text{Pd}, \text{Pt}$).^[71] Reaction of **20a** with methanol afforded the *syn*-addition to the $\text{P}=\text{C}$ double bond quantitatively (**20b**).

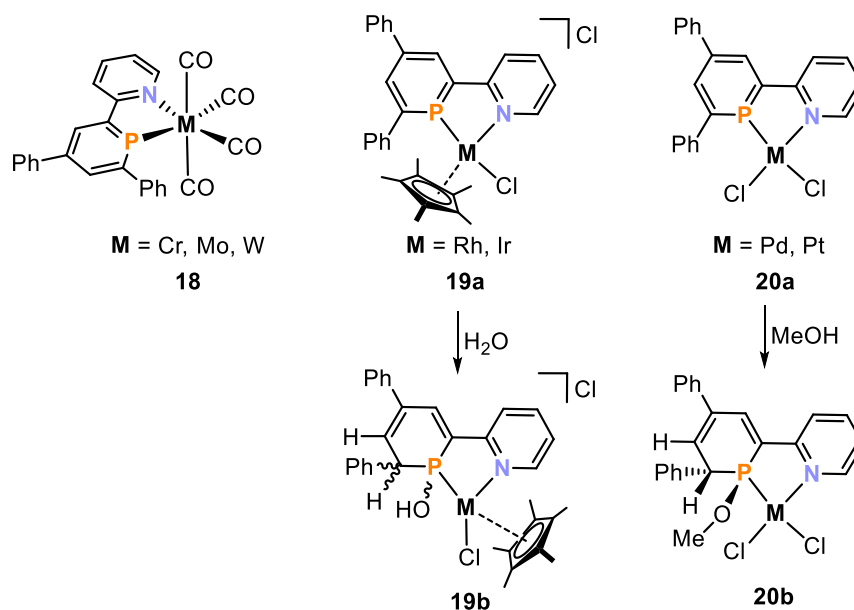
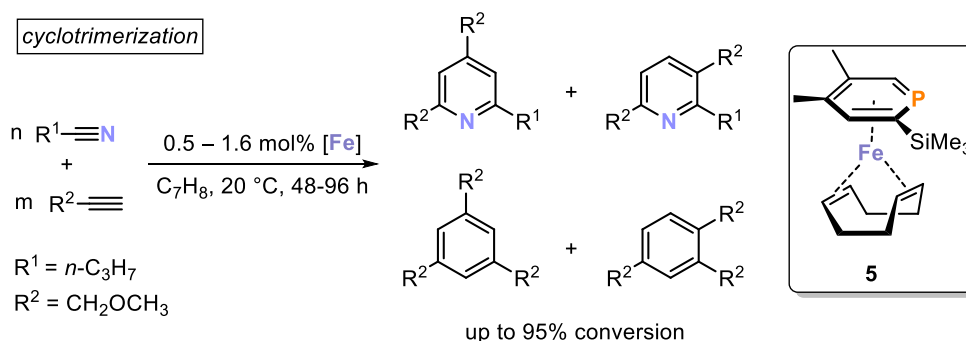


Figure 13. Transition metal complexes of **[P,N]**.

1.6 Phosphanes in homogeneous catalysis

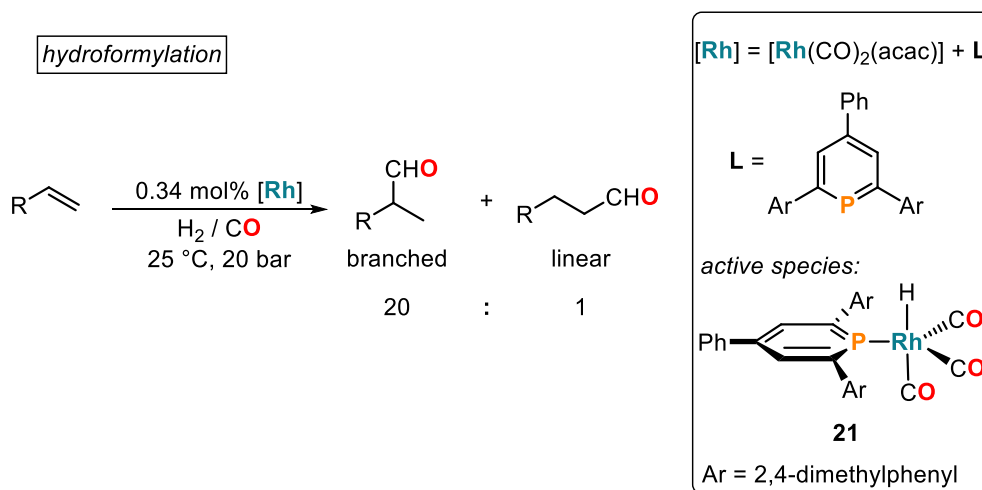
Organometallic catalysis is an important field in modern chemistry because it allows for the selective formation of chemical products under mild conditions. Phosphorus-containing ligands have found various applications in homogenous catalysis.^[72] The field is mostly dominated by phosphines and phosphite ligands, however, phosphinines have garnered more attention in the past three decades.^[58] As mentioned above, phosphinines are electron withdrawing or π -accepting ligands, thus they are able to stabilize metals in low oxidation states and electron-rich transition metal complexes which can be utilized as catalysts. Zenneck and co-workers reported the first example on phosphinine-mediated homogeneous catalysis in 1996. The $[2+2+2]$ cyclotrimerization reaction of electron-poor alkynes with butyronitrile was catalyzed by the η^6 -phosphinine $\text{Fe}(0)$ complex **5**, affording functionalized pyridines and benzenes in high conversions (up to 95 %) under mild conditions (Scheme 12).^[44] Interestingly, complex **5** showed higher catalytic activities in the cyclotrimerization

reaction compared to its toluene equivalent $[\text{Fe}(\eta^6\text{-C}_7\text{H}_8)(\text{cod})]^{[73]}$, however, **5** cannot compete with classical $[\text{CpCo}(\text{L})]$ (Cp = cyclopentadiene; L = cod , $(\text{CO})_2$) catalysts.^[74,75]



Scheme 12. First catalytic application of a phosphinine complex by Zenneck.

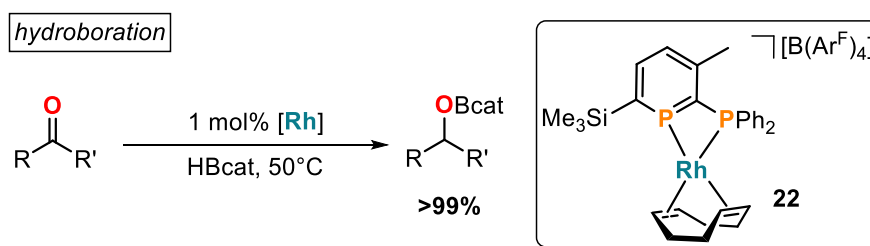
Phosphinine rhodium complexes have also found use in catalytic reactions. Breit and co-workers reported on a novel class of phosphinine-based Rh complexes which are able to catalyze the hydroformylation reaction of alkenes (Scheme 13). Catalyst **21** was generated *in-situ* by treating $[\text{Rh}(\text{CO})_2(\text{acac})]$ (acac = acetylacetonate) with phosphinine ligand **L** (Scheme 13) under a high pressures of H_2 and CO .^[76] The composition of the phosphinine ligand is essential for the reactivity of **21**: α -substituted phosphinines (substitution at P) inhibit the catalytic reactivity, while 2,4,6-substitued ligands possess high activity and regioselectivity, for the formation of the branched product in hydroformylation of styrene.^[77] The high catalytic activity of the phosphinine complexes originates from its high π -accepting ability, which enables the easy dissociation of CO from the metal center, leading to a vacant site for substrates.^[11]



Scheme 13. Hydroformylation of styrene catalyzed by a phosphinine Rh complex **21**; acac = acetylacetonate.

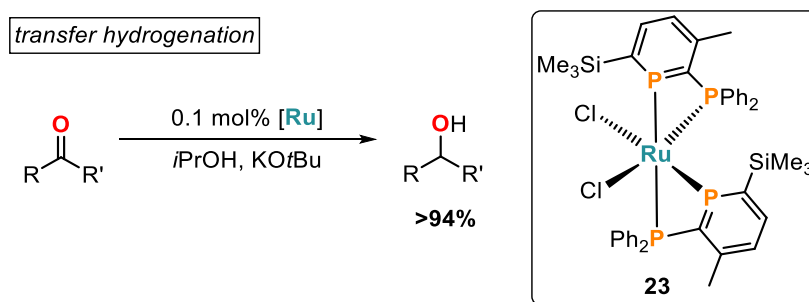
Another prevalent transformation for rhodium-based catalysts is the hydroboration of ketones.^[78] Mansell and co-workers showed that phosphinine complex **22** is a very potent catalyst in the hydroboration of acetophenone derivatives with catecholborane (HBcat)

(Scheme 14). With only 1 mol% catalyst loading the ketone is reduced under mild conditions and yields up to 99% are afforded.



Scheme 14. Hydroboration of ketones mediated by Rh complex **22**; cat = catechol; $\text{BAr}^{\text{F}}_4 = \text{tetrakis}(3,5\text{-bis}(\text{trifluoromethyl})\text{phenyl})\text{borate}$.

Ruthenium also forms catalytically active phosphinine complexes, with Mansell and co-workers reporting on the phosphinine-catalyzed transfer hydrogenation of ketones (Scheme 15).^[79] The combination of donor-functionalized, small bite-angle 2-phosphinophosphinine with $[\text{RuCl}_2(\text{dmsO}_4)]$ (dmsO = dimethoxysulfoxide) leads to the formation of the homoleptic Ru(II) chelate complex **23** in the *cis*-conformation. Compound **23** acts as an excellent pre-catalyst for the transfer hydrogenation of acetophenone derivatives with isopropanol at ambient temperatures. With a catalyst loading of 0.1 mol%, acetophenones could be reduced in high yields of up to 94%. The reduction of substrates with electron withdrawing groups gave good conversions at room temperature, while reduction of substrates with electron donating groups required higher temperatures (up to 82 °C).



Scheme 15. Catalytic transfer hydrogenation of ketones with phosphinine Ru complex **23**.

In summary, this section highlights the versatility of phosphinines in catalytically active transition metal coordination compounds, which can serve as potent catalysts for range of different reactions.

1.7 Conclusion

The pioneering work of Gottfried Märkl initiated the development of a whole new area in phosphorus chemistry with the synthesis of 2,4,6-triphenylphosphinine. These low-valent phosphorus heterocycles act as versatile ligands in coordination chemistry and catalysis due to their special electronic and steric properties. Over the last five decades a range of synthetic routes to substituted phosphinine ligands have been reported with the pyrylium salt route being the most accessible. The six-membered P heterocycles have been utilized as ligands for transition metal complexes. These compounds can possess variable coordination modes depending on the substituents on the phosphinine ligand. The most common mode is the σ -coordination to the metal center *via* the phosphorus lone pair electrons. π -Coordination occurs mostly through η^6 -mode, but also η^4 - and η^5 -coordination compounds are accessible. The implementation of a donor substituent leads to chelating phosphinines. Biphosphinines and pyridylphosphinines proved as effective chelating ligands for transition metals. Phosphinine complexes were successfully utilized as potent catalysts in reactions such as hydroformylation, hydroboration and transfer hydrogenation. Although the chemistry of phosphinines has been intensively investigated over the past decades, they still emerge in modern literature. Several new aspects e.g. the ability of phosphinines to split CO₂ or the application as a Lewis base in FLPs are described in *Chapters 2-6* of this thesis.

1.8 References

- [1] L. D. Tuck, *J. Pharm. Sci.* **1966**, *55*, 993–993.
- [2] P. Jutzi, *Angew. Chem. Int. Ed.* **1975**, *14*, 232–245.
- [3] P. Le Floch, F. Mathey, *Coord. Chem. Rev.* **1998**, *178–180*, 771–791.
- [4] N. Inamoto, M. Yoshifuji, *J. Am. Chem. Soc.*, **1981**, *103*, 4587.
- [5] M. J. Fink, R. West, *Science*, **1981**, *214*, 1343.
- [6] F. Mathey, *Acc. Chem. Res.* **1992**, *25*, 90–96.
- [7] K. B. Dillon, F. Mathey, J. F. Nixon, *Phosphorus: The Carbon Copy: From Organophosphorus to Phospha-Organic Chemistry*, Wiley-VCH, New York, **1998**.
- [8] G. Märkl, *Angew. Chem. Int. Ed.* **1966**, *78*, 907–908.
- [9] T. E. Gier, *J. Am. Chem. Soc.* **1961**, *83*, 1769–1770.
- [10] K. Dimroth, P. Hoffmann, *Angew. Chem. Int. Ed.* **1964**, *76*, 433–433.
- [11] C. Müller, D. Vogt, *Dalton Trans.* **2007**, 5505–5523.
- [12] R. Awartani, K. Sakizadeh, B. Gabrielsen, *J. Chem. Educ.* **1986**, *63*, 172.
- [13] A. R. Katritzky, S. S. Thind, *J. Chem. Soc. Perkin 1* **1980**, 1895–1900.
- [14] K. Dimroth, N. Greif, W. Städe, F. W. Steuber, *Angew. Chem. Int. Ed.* **1967**, *6*, 711–712.
- [15] G. Märkl, F. Lieb, A. Merz, *Angew. Chem. Int. Ed.* **1967**, *6*, 458–459.
- [16] A. J. Ashe, *J. Am. Chem. Soc.* **1971**, *93*, 3293–3295.
- [17] P. L. Floch, F. Mathey, *J. Chem. Soc. Chem. Commun.* **1993**, 1295–1296.
- [18] B. Wrackmeyer, U. Klaus, *J. Organomet. Chem.* **1996**, *520*, 211–226.
- [19] W. Rösch, M. Regitz, *Z. Naturforsch. B* **1986**, *41B(7)*, 931–933.
- [20] W. Rösch, M. Regitz, *Z. Naturforsch. B* **2014**, *41*, 931–934.
- [21] M. Regitz, P. Binger, *Angew. Chem. Int. Ed.* **1988**, *27*, 1484–1508.
- [22] F. Mathey, *Chem. Rev.* **1988**, *88*, 429–453.
- [23] F. Mathey, *Tetrahedron Lett.* **1979**, *20*, 1753–1756.
- [24] N. Avarvari, P. Le Floch, F. Mathey, *J. Am. Chem. Soc.* **1996**, *118*, 11978–11979.
- [25] N. Avarvari, P. L. Floch, C. Charrier, F. Mathey, *ChemInform* **1997**, 28.
- [26] N. Avarvari, P. Le Floch, L. Ricard, F. Mathey, *Organometallics* **1997**, *16*, 4089–4098.
- [27] K. H. Dötz, A. Tiriliomis, K. Harms, *Tetrahedron* **1993**, *49*, 5577–5597.
- [28] D. Böhm, F. Knoch, S. Kummer, U. Schmidt, U. Zenneck, *Angew. Chem. Int. Ed.* **1995**, *34*, 198–201.
- [29] P. Binger, J. Stannek, B. Gabor, R. Mynott, J. Bruckmann, C. Krüger, S. Leininger, *Angew. Chem. Int. Ed.* **1995**, *34*, 2227–2230.
- [30] S. A. Sullivan, H. Sandford, J. L. Beauchamp, A. J. Ashe III, *J. Am. Chem. Soc.* **1978**, *100*, 3737–3742.
- [31] F. Mathey, *Angew. Chem. Int. Ed.* **2003**, *42*, 1578–1604.
- [32] P. D. Burrow, A. J. Ashe, D. J. Bellville, K. D. Jordan, *J. Am. Chem. Soc.* **1982**, *104*, 425–429.
- [33] E. F. DiMauro, M. C. Kozlowski, *J. Chem. Soc. Perkin 1* **2002**, 439–444.
- [34] A. Modelli, B. Hajgató, J. F. Nixon, L. Nyulászi, *J. Phys. Chem. A* **2004**, *108*, 7440–7447.
- [35] L. Nyulászi, T. Veszprémi, *J. Phys. Chem.* **1996**, *100*, 6456–6462.
- [36] N.-N. Pham-Tran, G. Bouchoux, D. Delaere, M. T. Nguyen, *J. Phys. Chem. A* **2005**, *109*, 2957–2963.
- [37] C. A. Tolman, *Chem. Rev.* **1977**, *77*, 313–348.
- [38] M. Rigo, M. Weber, C. Müller, *Chem. Commun.* **2016**, *52*, 7090–7093.
- [39] M. Rigo, E. R. M. Habraken, K. Bhattacharyya, M. Weber, A. W. Ehlers, N. Mézailles, J. C. Sloatweg, C. Müller, *Chem. Eur. J.* **2019**, *25*, 8769–8779.

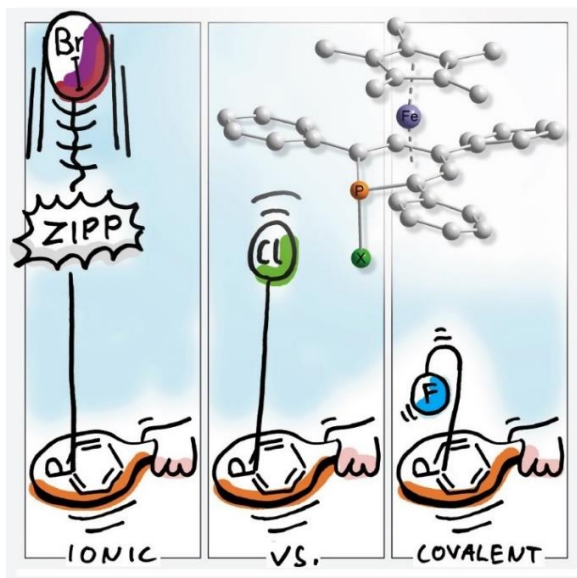
- [40] C. Elschenbroich, M. Nowotny, A. Behrendt, W. Massa, S. Wocadlo, *Angew. Chem. Int. Ed.* **1992**, *104*, 1388–1390.
- [41] C. Elschenbroich, S. Voss, O. Schiemann, A. Lippek, K. Harms, *Organometallics* **1998**, *17*, 4417–4424.
- [42] C. Elschenbroich, M. Nowotny, A. Behrendt, K. Harms, S. Wocadlo, J. Pebler, *J. Am. Chem. Soc.* **1994**, *116*, 6217–6219.
- [43] P. L. Arnold, F. G. N. Cloke, K. Khan, P. Scott, *J. Organomet. Chem.* **1997**, *528*, 77–81.
- [44] F. Knoch, F. Kremer, U. Schmidt, U. Zenneck, P. Le Floch, F. Mathey, *Organometallics* **1996**, *15*, 2713–2719.
- [45] N. Mézailles, L. Ricard, F. Mathey, P. Le Floch, *Organometallics* **2001**, *20*, 3304–3307.
- [46] B. Schmid, L. M. Venanzi, T. Gerfin, V. Gramlich, F. Mathey, *Inorg. Chem.* **1992**, *31*, 5117–5122.
- [47] K. C. Nainan, C. T. Sears, *J. Organomet. Chem.* **1978**, *148*, C31–C34.
- [48] C. Elschenbroich, J. Six, K. Harms, *Chem. Commun.* **2006**, 3429–3431.
- [49] P. L. Floch, N. Maigrot, L. Ricard, C. Charrier, F. Mathey, *Inorg. Chem.* **1995**, *34*, 5070–5072.
- [50] Francois. Nief, Jean. Fischer, *Organometallics* **1986**, *5*, 877–883.
- [51] A. Moores, N. Mézailles, L. Ricard, Y. Jean, P. le Floch, *Organometallics* **2004**, *23*, 2870–2875.
- [52] B. Rezaei Rad, U. Chakraborty, B. Mühldorf, J. A. W. Sklorz, M. Bodensteiner, C. Müller, R. Wolf, *Organometallics* **2015**, *34*, 622–635.
- [53] K. Eggers, F. W. Heinemann, M. Hennemann, T. Clark, P. Binger, U. Zenneck, *Comptes Rendus Chim.* **2010**, *13*, 1203–1212.
- [54] A. Moores, N. Mézailles, L. Ricard, P. Le Floch, *Organometallics* **2005**, *24*, 508–513.
- [55] G. Märkl, F. Lieb, A. Merz, *Angew. Chem. Int. Ed.* **1967**, *6*, 87–88.
- [56] K. Eggers, F. W. Heinemann, M. Hennemann, T. Clark, P. Binger, U. Zenneck, *Comptes Rendus Chim.* **2010**, *13*, 1203–1212.
- [57] C. Kaes, A. Katz, M. W. Hosseini, *Chem. Rev.* **2000**, *100*, 3553–3590.
- [58] P. L. Floch, *Coord. Chem. Rev.* **2006**, *250*, 627–681.
- [59] P. Le Floch, D. Carmichael, L. Ricard, F. Mathey, A. Jutand, C. Amatore, *Organometallics* **1992**, *11*, 2475–2479.
- [60] P. Le Floch, D. Carmichael, L. Ricard, F. Mathey, *J. Am. Chem. Soc.* **1991**, *113*, 667–669.
- [61] P. Le Floch, L. Ricard, F. Mathey, *Polyhedron* **1990**, *9*, 991–997.
- [62] N. Mézailles, P. Rosa, L. Ricard, F. Mathey, P. Le Floch, *Organometallics* **2000**, *19*, 2941–2943.
- [63] P. Rosa, L. Ricard, P. Le Floch, F. Mathey, G. Sini, O. Eisenstein, *Inorg. Chem.* **1998**, *37*, 3154–3158.
- [64] J.-M. Alcaraz, A. Breque, F. Mathey, *Tetrahedron Lett.* **1982**, *23*, 1565–1568.
- [65] A. Breque, C. C. Santini, F. Mathey, J. Fischer, A. Mitschler, *Inorg. Chem.* **1984**, *23*, 3463–3467.
- [66] Bruno. Schmid, L. M. Venanzi, Alberto. Albinati, Francois. Mathey, *Inorg. Chem.* **1991**, *30*, 4693–4699.
- [67] B. Schmid, L. M. Venanzi, T. Gerfin, V. Gramlich, F. Mathey, *Inorg. Chem.* **1992**, *31*, 5117–5122.
- [68] C. Müller, D. Wasserberg, J. J. M. Weemers, E. A. Pidko, S. Hoffmann, M. Lutz, A. L. Spek, S. C. J. Meskers, R. A. J. Janssen, R. A. van Santen, et al., *Chem. Eur. J.* **2007**, *13*, 4548–4559.

- [69] I. de Krom, M. Lutz, C. Müller, *Dalton Trans.* **2015**, *44*, 10304–10314.
- [70] I. deKrom, L. E. E. Broeckx, M. Lutz, C. Müller, *Chem. Eur. J.* **2013**, *19*, 3676–3684.
- [71] A. Campos-Carrasco, L. E. E. Broeckx, J. J. M. Weemers, E. A. Pidko, M. Lutz, A. M. Masdeu-Bultó, D. Vogt, C. Müller, *Chem. Eur. J.* **2011**, *17*, 2510–2517.
- [72] P.C. J. Kamer, P. W. N. M. van Leeuwen, *PhosphorusIII Ligands Homogeneous Catalysis – Design and Synthesis*, Wiley-VCH, New York, **2012**.
- [73] U. Zenneck, U. Schmidt, *J Organomet Chem* **1992**, *440*, 187–90.
- [74] B. Heller, G. Oehme, *J. Chem. Soc. Chem. Commun.* **1995**, 179–180.
- [75] H. Bönemann, *Angew. Chem. Int. Ed.* **1985**, *97*, 264–279.
- [76] B. Breit, R. Winde, T. Mackewitz, R. Paciello, K. Harms, *Chem. Eur. J.* **2001**, *7*, 3106–3121.
- [77] B. Breit, R. Winde, K. Harms, *J. Chem. Soc. Perkin Trans. 1* **1997**, 2681–2682.
- [78] R. J. Newland, J. M. Lynam, S. M. Mansell, *Chem. Commun.* **2018**, *54*, 5482–5485.
- [79] R. J. Newland, M. F. Wyatt, R. L. Wingad, S. M. Mansell, *Dalton Trans.* **2017**, *46*, 6172–6176.

Chapter 2

Halide-Substituted Phosphacyclohexadienyl Iron Complexes: Covalent Structures vs. Ion Pairs

Abstract: The coordination chemistry of phosphinines (phosphabenzenes) has been intensively investigated over the last decades, but metal complexes of halophosphinines and related halide-substituted phosphacyclohexadienyls have remained scarce. Here, we describe the synthesis of a series of complexes $[\text{Cp}^*\text{Fe}(1\text{-F-PC}_5\text{Ph}_3\text{H}_2)]$ (**2-F**, $\text{Cp}^* = \text{C}_5\text{Me}_5$), $[\text{Cp}^*\text{Fe}(1\text{-Cl-PC}_5\text{Ph}_3\text{H}_2)]$ (**2-Cl**), $[\text{Cp}^*\text{Fe}(\text{PC}_5\text{Ph}_3\text{H}_2)]\text{Br}$ (**2-Br**) and $[\text{Cp}^*\text{Fe}(\text{PC}_5\text{Ph}_3\text{H}_2)]\text{I}$ (**2-I**), which were obtained by reacting the previously reported 2,4,6-triphenylphosphinine iron complex $[\text{K}(\text{[18]crown-6})(\text{thf})_2][\text{Cp}^*\text{Fe}(\text{PC}_5\text{Ph}_3\text{H}_2)]$ (**1**) with electrophilic halogenating agents. To the best of our knowledge, **2-F** and **2-Cl** are the first π -coordinated λ^3 -halophosphacyclohexadienyl complexes with covalent P–X bonds (X = halogen). In the solid state **2-Br** and **2-I** show ionic structures with $[\text{Cp}^*\text{Fe}(\text{PC}_5\text{Ph}_3\text{H}_2)]^+$ cations and separated X^- anions. Anion exchange of I^- in **2-I** for $[\text{BAr}^{\text{F}}_4]^-$ ($\text{Ar}^{\text{F}} = 3,5\text{-(CF}_3)_2\text{C}_6\text{H}_3$) affords $[\text{Cp}^*\text{Fe}(\text{PC}_5\text{Ph}_3\text{H}_2)][\text{BAr}^{\text{F}}_4]$ (**2-[BAr^F]₄**), which also displays an ionic structure. These new complexes were further characterized by solid-state and solution ^{31}P NMR spectroscopy, UV-vis spectroscopy, elemental analyses, electrical conductivity measurements in solution, and DFT calculations. The resulting data indicate that **2-F** retains its covalent P–F bond in THF, fluorobenzene, and acetonitrile solution, while the remaining **2-X** complexes containing heavier halogen atoms (X = Cl, Br, and I) apparently form ion pairs in such solvents.



Reproduced with permission from C. M. Hoidn, J. Leitl, C. G. P. Ziegler, I. Shenderovich, R. Wolf, *Eur. J Inorg. Chem.* **2019**, 1567–1574.

C. M. Hoidn performed initial experiments and, characterized compounds **2-Cl**, **2-Br** and **2-[BAr^F]₄** by single crystal X-ray analysis. J. Leitl fully characterized **2-F**, **2-Cl**, **2-Br** and **2-[BAr^F]₄** by NMR and UV-Vis spectroscopy, elemental analysis, cyclic voltammetry, mass spectrometry and conductance measurements. C. G. P. Ziegler performed all DFT calculations. I. Shenderovich performed ^{31}P CP-MAS NMR spectroscopic measurements. C. M. Hoidn and J. Leitl wrote the manuscript with contribution from all authors. R. Wolf supervised and directed the project.

2.1 Introduction

Phosphinines are six-membered aromatic phosphorus heterocycles with distinct properties compared to both related arenes (e.g. pyridines) and other trivalent phosphorus species.^[1–3] The presence of a phosphorus atom in the aromatic π -system enables versatile coordination behavior, which can be attributed to their special electronic structure.^[4] Both the lone pair on phosphorus and the conjugated π -system may interact with metal-based orbitals, resulting in ambidentate ligand properties evident in numerous transition metal complexes.^[1,4] In such complexes, phosphinines can adopt various coordination modes such as η^1 , η^2 , η^4 , η^5 , and η^6 -coordination to single metal atoms and bridging coordination between two metal atoms.^[4–26] This highly versatile coordination behavior forms the basis for successful applications in homogeneous catalysis.^[27–34] Derivatization reactions of free phosphinines are also well-established.^[1,4] In particular, reactions with nucleophiles afford λ^3 -phosphacyclohexadienide anions (commonly referred to as λ^4 -phosphine anions),^[4,35] which can be converted into λ^5 -phosphinines by reaction with electrophiles.^[36,37] Reactions of neutral phosphinines with electrophiles give λ^3 -phosphinium cations.^[38] Halophosphinines are of interest because they enable a broad spectrum of further modifications.^[39,40] 1,1-Dihalo- λ^5 -phosphinines (type **A**, Figure 1) can be prepared by the oxidation of phosphinines with elemental halogens for $X = \text{Cl}, \text{Br}$.^[39–42] The synthesis of fluoro-substituted phosphinines was achieved by halide, alkoxide or amide substituent metathesis of certain λ^5 -phosphinines and 1,1-dibromo-2,4,6-triphenylphosphinine with SbF_3 .^[39] While metal complexes of halogenated phosphinines are scarce, Lückoff and Dimroth synthesized π -coordinated 1,1-difluoro- λ^5 -phosphine chromium complexes **B** (Figure 1) by exchanging three acetonitrile ligands in $[\text{Cr}(\text{CH}_3\text{CN})_3(\text{CO})_3]$ with λ^5 -difluorophosphinine.^[41,43] Pincer complexes **C** published by Le Floch and co-workers were the first σ -coordinated λ^3 -halophosphacyclohexadienyl complexes.^[44,45] To our knowledge, π -complexes of such ligands are unknown.

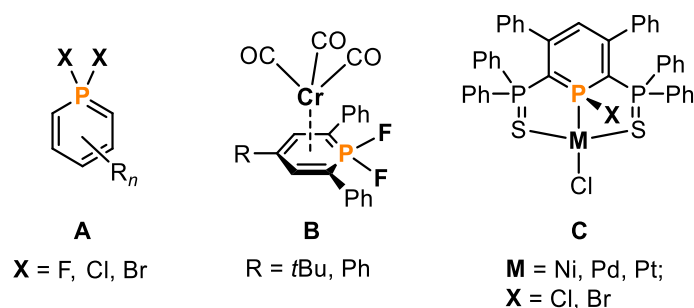
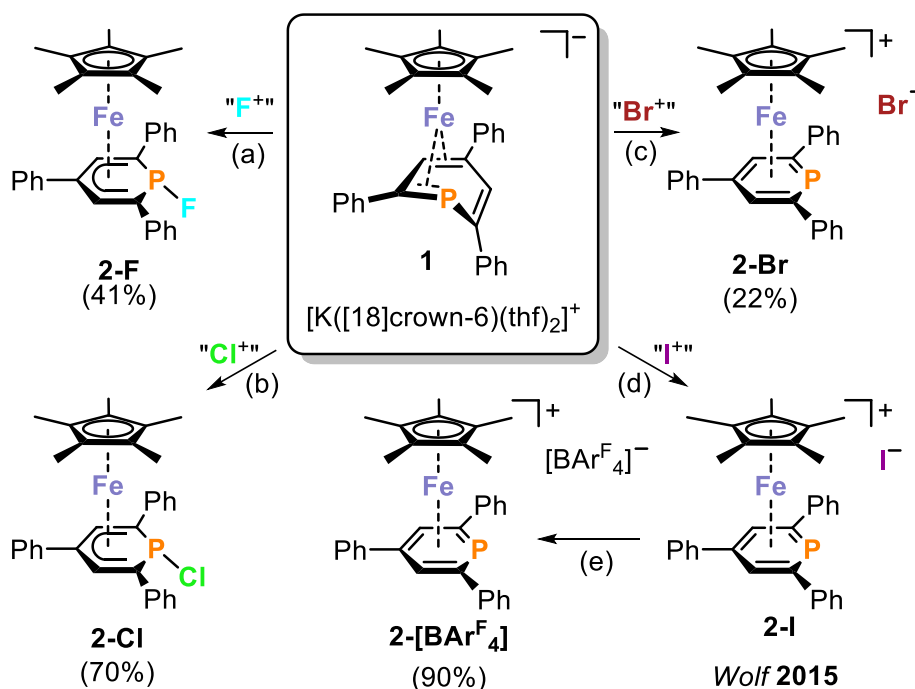


Figure 1. Known halophosphinines and halophosphinine metal complexes.^[39–45]

2.2 Results and Discussion

We recently reported the synthesis of the 2,4,6-triphenylphosphinine ferrate anion **1** (Scheme 1).^[9] Various P-substituted phosphacyclohexadienyl complexes can be obtained by reacting **1** with electrophiles.^[9,10] Similarly, reaction of **1** with elemental iodine afforded [Cp*Fe(PC₅Ph₃H₂)]I (**2-I**), which shows an essentially ionic structure in the solid state with a P–I distance of 3.639(1) Å.^[9] Inspired by this promising result, we have now synthesized a series of new 1-halophosphacyclohexadienyl complexes [Cp*Fe-(1-F-PC₅Ph₃H₂)] (**2-F**), [Cp*Fe(1-Cl-PC₅Ph₃H₂)] (**2-Cl**), [Cp*Fe(PC₅Ph₃H₂)]Br (**2-Br**), and the reference compound [Cp*Fe(PC₅Ph₃H₂)][BAr^F₄] (**2-[BAr^F₄]**, Ar^F = 3,5-(CF₃)₂C₆H₃). Single crystal X-ray diffraction studies revealed pronounced structure differences in the solid-state. While covalent P–X bonds are present in the structures of **2-F** and **2-Cl**, ion-separated structures were found for **2-Br**, **2-I**, and **2-[BAr^F₄]**. To investigate this dichotomy and to gain insight into the behavior of these molecules in solution, we have gathered spectroscopic, electrochemical, electrical conductivity and quantum chemical data. By analyzing these results, we arrive at a comprehensive view of the structural behavior of the complexes **2-X** in the solid state and in solution.



Scheme 1. Synthesis of complexes **2-F**, **2-Cl**, **2-Br**, **2-I**^[9] and **2-[BAr^F₄]** (Ar^F = 3,5-(CF₃)₂C₆H₃); reagents and by-products: (a) +*N*-fluoropyridinium tetrafluoroborate/–KBF₄, –[18]crown-6, –pyridine; (b) +C₂Cl₆/–KCl, –C₂Cl₄, –[18]crown-6; (c) +Br₂/–KBr, –[18]crown-6; (d) +I₂/–KI, –[18]crown-6; (e) +Na[BAr^F₄]/–NaI; isolated yields are given in parentheses.

In an initial experiment, we investigated the reaction of **1** with the well-known fluorinating agent *N*-fluoropyridinium tetrafluoroborate (Scheme 1). The formation of a deep red reaction mixture was observed, from which the unprecedented P-fluorinated complex [Cp*Fe(1-F-PC₅Ph₃H₂)] (**2-F**) could be isolated in 41% yield. We subsequently prepared

[Cp*Fe(1-Cl-PC₅Ph₃H₂)] (**2-Cl**) in 70% yield in a similar manner by reacting **1** with hexachloroethane in THF. **2-F** and **2-Cl** both dissolve well in toluene and THF and are highly moisture sensitive: the compounds hydrolyze in the presence of traces of water to the hydrophosphinine oxide complex Cp*Fe(1-H-1-O-PC₅Ph₃H₂)] (**2-OH**). The brominated derivative [Cp*Fe(PC₅Ph₃H₂)]Br (**2-Br**) can be prepared in 22% yield by reacting **1** with elemental bromine. The preparation of [Cp*Fe(PC₅Ph₃H₂)]I (**2-I**) by reaction of **1** with elemental iodine (61% yield) was previously reported by us.^[9] Additionally, we can now report that the iodide anion of **2-I** can be exchanged with the weakly coordinating tetraaryl borate anion [BAR^F₄]⁻ to give [Cp*Fe(PC₅Ph₃H₂)] [BAR^F₄] (**2-[BAR^F₄]**), which was isolated in 90% yield by crystallization from *n*-hexane/THF. **2-Br**, **2-I** and **2-[BAR^F₄]** are less moisture sensitive than **2-F** and **2-Cl** and dissolve only sparsely in toluene and moderately in THF, while the solubility is high in MeCN.

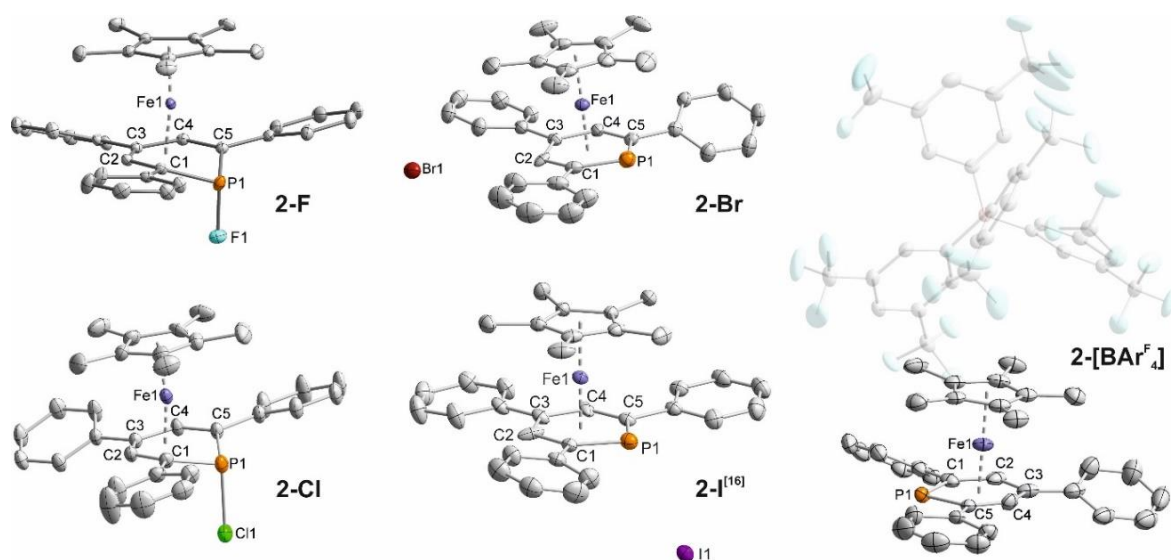


Figure 2. Solid-state molecular structures of complexes **2-X** (X = F, Cl, Br, I, and [BAR^F₄]). Ellipsoids are drawn at the 40% probability level; H atoms, solvent molecules and disorder in the *para*-phenyl substituent and the Cp* ligand of **2-Cl**, and in the CF₃ groups of **2-[BAR^F₄]** are omitted for clarity. The crystal of **2-F** contained a second crystallographically independent molecules with very similar structural parameters; only one of these molecules is shown. Selected bond lengths (Å) and angles (°) for **2-F** P1–F1 1.658(4), 1.663(4), C1–P1–F1 104.4(3), 103.6(2), C5–P1–F1 103.8(2), 103.8(8); for **2-Cl** P1–Cl1 2.295(1), C1–P1–Cl1 102.87(9), C5–P1–Cl1 101.9(1); for **2-Br** P1–Br1 6.730(1), for **2-I** P1–I1 3.639(1), see Table 1 for additional structural data.

Table 1. Selected bond lengths (Å) and angles (°) of **2-X** (X = F, Cl, Br, I, and [BAr^F₄]); P1–X distances are given in the caption of Figure 2 and Table 3 below.

	2-F ^[a]	2-Cl	2-Br	2-I ^[9]	2-[BAr^F₄]
Fe1–P1	2.736(2); 2.737(2)	2.670(1)	2.340(1)	2.392(1)	2.433(1)
Fe1–C1	2.135(6); 2.141(6)	2.153(3)	2.147(3)	2.157(3)	2.166(3)
Fe1–C2	2.067(6); 2.058(6)	2.055(2)	2.200(3)	2.074(4)	2.133(3)
Fe1–C3	2.111(6); 2.108(6)	2.102(3)	2.132(3)	2.147(3)	2.160(3)
Fe1–C4	2.056(6); 2.056(6)	2.066(3)	2.117(3)	2.095(4)	2.007(6)
Fe1–C5	2.169(6); 2.155(6)	2.145(3)	2.183(3)	2.146(3)	2.145(2)
P1–C1	1.786(7); 1.795(6)	1.772(3)	1.736(4)	1.765(2)	1.761(3)
C1–C2	1.422(8); 1.424(8)	1.414(3)	1.450(5)	1.416(5)	1.437(4)
C2–C3	1.410(8); 1.402(8)	1.416(4)	1.504(4)	1.414(5)	1.430(4)
C3–C4	1.415(9); 1.417(8)	1.420(3)	1.427(4)	1.419(5)	1.470(7)
C4–C5	1.427(8); 1.434(8)	1.421(3)	1.410(5)	1.408(5)	1.348(6)
P1–C5	1.787(6); 1.768(7)	1.772(3)	1.765(3)	1.774(3)	1.787(3)
C1–P1–C5	96.5(3); 96.3(3)	97.6(1)	101.0(2)	98.8(1)	97.6(1)

[a] Data for two crystallographically independent molecules

Single-crystal X-ray diffraction studies on **2-F** and **2-Cl** revealed sandwich structures with η^5 -coordinated cyclopentadienyl and halogenated η^5 -phosphacyclohexadienyl ligands (Figure 2, Table 1). While the P–F distances in **2-F** (1.663(4) Å and 1.658(4) Å for two crystallographically independent molecules) are close to P–F single bonds in other three-coordinate phosphorus species, the P–Cl bond in **2-Cl** (2.295(1) Å) is remarkably elongated compared to other three-coordinate phosphorus compounds bearing P–Cl single bonds.^[46] It is noteworthy that long P–Cl bonds were observed by *Gudat et al.* in *P*-chloro-1,3,2-diazaphospholenes (from 2.3241(4) up to 2.759(2) Å),^[47] while the phosphanyl-substituted phosphacyclohexadienyl complex [Cp*Fe(1-PPh₂-PC₅Ph₃H₂)] and P-phosphanyldiazaphospholenes display elongated P–P bonds.^[10,48] By analogy with these previous observations, the elongated P–Cl bond in **2-Cl** suggests a polarized P–Cl interaction with significant ionic character. Consistent with this interpretation, compound **2-Br**, which contains a superior leaving group, shows a fully ionic solid-state structure with a [Cp*Fe(η^6 -PC₅Ph₃H₂)]⁺ cation well separated from the bromide counterion (the shortest P–Br distance being 6.730(1) Å). A similar ionic structure bearing a planar η^6 -coordinated phosphinine

ligand was found for **2**-[BAr^F₄] and for **2**-**I**,^[9] where the iodide counterion is separated by 3.639(1) Å from the next P atom. This P–I distance in **2**-**I** is in fact little shorter than the sum of van der Waals radii ($\sum r_{\text{vdW}} = 3.90$ Å).^[49]

Table 2. Comparison of ³¹P NMR shifts of compounds **2**-**X** (X = F, Cl, Br, I, [BAr^F₄]) in MAS ³¹P, ³¹P{¹H} NMR spectra and calculated shieldings.

	MAS ³¹ P NMR (ppm)	³¹ P{ ¹ H} NMR shifts (ppm) in solution			calculated ³¹ P shieldings (ppm) ^[c]	
		[D ₈]THF	FB ^[a]	[D ₃]MeCN	covalent	ionic
2 - F	31.8 (¹ J _{PF} = 930 Hz)	33.2 (¹ J _{PF} = 916 Hz)	33.0 (¹ J _{PF} = 905 Hz)	33.0 (¹ J _{PF} = 830 Hz) ^[b]	48.6	−10.0
2 - Cl	3.8	−11.9	−9.9	−1.5	9.9	−7.2
2 - Br	−12.2	−11.8	−8.0	−1.2	8.6	−8.7
2 - I	4.1	−5.2	−4.9	−1.2	−3.5	−6.2
2 -[BAr ^F ₄]	−8.9	−2.4	−4.6	−1.2	-	-

[a] Solvent fluorobenzene/C₆D₆ capillary.

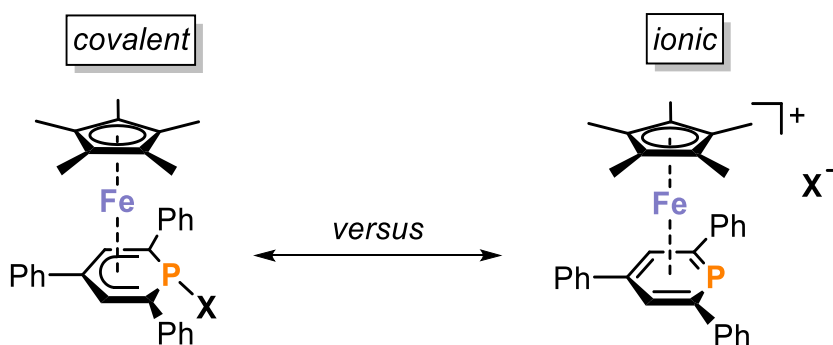
[b] Partial hydrolysis of **2**-**F** to [Cp*Fe(1-H-1-O-PC₃Ph₃H₂)] (**2**-**OH**, singlet at −30.7 ppm) was observed (see Figure S7, SI).

[c] Calculated at the ZORA-OPBE/def2-TZVP level of theory; the calculated chemical shielding of the [Cp*Fe(PC₅Ph₃H₂)]⁺ ion **2**⁺ ($\sigma_{\text{calc}} = 365.7$) was referenced to the MAS ³¹P NMR shift of **2**-[BAr^F₄] ($\delta_{\text{exp}} = -8.9$ ppm), see the SI for further details.

In order to analyze the covalent vs. ionic nature of the phosphorus-halogen bonds in **2**-**X** further, we performed ³¹P NMR spectroscopic studies in the solid state and in solution (Table 2; see the SI for further details). The solid-state ³¹P MAS spectrum of **2**-**F** shows a strongly downfield shifted doublet at 31.8 ppm. The large ¹J_{PF} coupling constant of 930 Hz is consistent with the presence of a covalent P–F bond.^[50] ¹⁹F{¹H} and ³¹P{¹H} NMR spectra of **2**-**F** in [D₈]THF, fluorobenzene (FB) and [D₃]MeCN (Table 2) show a very similar picture as the ³¹P MAS spectrum recorded in the solid with very similar chemical shifts for the observed doublets and a high ¹J_{PF} coupling constant. In particular, the large P–F coupling strongly indicates that the covalent P–F-bonded structure is retained in solution. Significantly, the isotropic ³¹P MAS signals for **2**-**Cl**, **2**-**Br**, **2**-**I**, and **2**-[BAr^F₄] are shifted to high field compared to that of **2**-**F**, but there are slight variations: The signals of **2**-**Cl** (+3.8 ppm) and **2**-**I** (+4.1 ppm) are deshielded compared to those of **2**-**Br** (−12.2 ppm) and **2**-[BAr^F₄] (−8.9 ppm). It is noteworthy that the isotropic ³¹P NMR shift of **2**-**Cl** significantly changes when this compound is dissolved in [D₈]THF or FB ($\Delta\delta = 15.7$ ppm for [D₈]THF), while the shift of **2**-**Br** in these solvents is very similar to the chemical shift recorded for the solid ($\Delta\delta = 0.4$ ppm for [D₈]THF). Considering these data, it seems plausible that the chloride ion in **2**-**Cl** dissociates in THF due to the polarized nature of the P–Cl bond. As a consequence, the solution ³¹P NMR chemical shift of **2**-**Cl** is close to the values detected for

the ionic species **2-Br**, **2-I** and **2-[BAr^F₄]**, but distinct from the ³¹P MAS chemical shift recorded for solid **2-Cl**. The chemical shifts recorded for **2-X** (X = F, Cl, Br, I and BAr^F₄) in FB show the same trend as those recorded for the same compounds in [D₈]THF. Notably, the values for **2-Cl**, **2-Br**, **2-I**, and **2-[BAr^F₄]** in [D₃]MeCN are different from those recorded in FB and [D₈]THF; moreover, they are in a very close range. This observation might indicate that genuine ion-separated species (solvent separated ion-pairs) are formed by these species in [D₃]MeCN. Larger deviations of the chemical shifts for **2-Cl** and **2-Br** in FB and [D₈]THF from those observed in [D₃]MeCN seem to suggest that **2-Cl**, **2-Br** and perhaps also **2-I** form contact ion pairs in the former two solvents. In contrast, **2-[BAr^F₄]** likely exist as solvent-separated ion pairs in all three solvents.

Table 3. Comparison of P–X distances (Å) of **2-X** (X = F, Cl, Br, I) determined by XRD and DFT geometry optimization (OPBE/TZ2P level), and calculated relative thermal enthalpies (ΔH at 298 K) of the geometry optimized covalent and ionic structures; the relative free enthalpies (ΔG at 298 K) are given in parentheses; see the SI for details.



2-X	XRD (Å)	geometry optimization (Å)		relative thermal enthalpies (kcal·mol ⁻¹)	
		covalent	ionic	covalent	ionic
2-F	1.658(4); 1.663(4) ^[a]	1.659	5.334	0	+32.8 (+30.9)
2-Cl	2.295(1)	2.150	6.177	0	+19.6 (+17.9)
2-Br	6.730(1)	2.340	6.318	0	+18.2 (+15.9)
2-I	3.639(1)	2.588	6.834	0	+15.5 (+13.5)

[a] Data for two crystallographically independent molecules.

Using DFT methods (OPBE/TZ2P level, see the SI for details), both a structure featuring a covalent phosphorus-halogen bond and an ionic structure with the halide anion located between two phenyl substituents of the η^6 -coordinated phosphinone ligand were successfully optimized for **2-X** (X = F, Cl, Br, I, Table 3, see also the SI). The calculated covalently-bonded structures are all energetically favored over the ionic ones based on the calculated thermal enthalpies in the gas phase. In the case of **2-F**, the ion-separated structure

is +32.8 kcal mol⁻¹ less stable than the covalent one. The enthalpy differences are significantly reduced for **2-Cl** (+19.6 kcal mol⁻¹), **2-Br** (+18.2 kcal mol⁻¹), and **2-I** (+15.5 kcal mol⁻¹) though. These calculated enthalpies qualitatively mirror the trend observed in solution, where the P–X bond in **2-F** is retained, whereas in **2-Cl**, **2-Br** and **2-I** dissociation can occur. The optimized covalent structures of **2-F** and **2-Cl** are in good agreement with the crystallographically determined data (*vide supra*). For **2-Br** and **2-I**, it is noteworthy that the P–X bonds in the optimized covalent structures (**2-Br**: 2.340 Å, **2-I**: 2.588 Å) are considerably longer than the sum of covalent radii for P–Br ($\sum r_{\text{cov}} = 2.25$ Å) and P–I ($\sum r_{\text{cov}} = 2.44$ Å).^[51] In this regard, it is remarkable that the molecular ion of the bromine compound **2-Br** was indeed detected at 594.00 *m/z* by mass spectrometric measurements (LIFDI-MS). The molecular ion of **2-I** was not observed.

We also calculated ³¹P NMR shieldings for the covalent and ionic forms of **2-X** at the ZORA-OPBE/def2-TZVP level (X = F, Cl, Br, I, Table 2, see also the SI). The results of these calculations are in good agreement with the ³¹P MAS data (also displayed in Table 2). The covalently P–X-bonded isomers feature more strongly deshielded ³¹P nuclei compared to the ionic ones. For the covalent forms of **2-F** and the ionic forms of **2-Cl**, **2-Br** and **2-I**, the calculated ³¹P{¹H} NMR shifts are in good agreement with the actual experimental values recorded in THF and FB solution.

Table 4. Molar conductivities (Λ_m) in $\Omega^{-1} \text{ cm}^2 \text{ mol}^{-1}$ of **2-X** (X = F, Cl, Br, I, and [BAr^F₄]). Concentration of all solutions: c = 9 mM in THF or MeCN, 300 K.

2-X	molar conductivities Λ_m ($\Omega^{-1} \text{ cm}^2 \text{ mol}^{-1}$) in	
	THF	MeCN
2-F	0.23	10.5
2-Cl	0.51	64.1
2-Br	0.24	74.0
2-I	0.24	81.6
2-[BAr^F₄]	20.9	48.2

Considering that the proposed dissociation of the polarized phosphorus–halogen bonds should also influence the electric conductivity in solution, we performed molar conductivity measurements for **2-X** (X = F, Cl, Br, I, and BAr^F₄) in THF and MeCN (Table 4).^[47] The molar conductivities (Λ_m) are low for **2-X** (X = F, Cl, Br and I) in THF, but drastically higher for **2-[BAr^F₄]**. In good agreement with the ³¹P NMR spectroscopic data (*vide supra*), this indicates the presence of either covalent structures or strongly associated contact ion pairs for **2-X** (X = F, Cl, Br and I) in THF. Significantly, high molar conductivities were measured for **2-X** (X = Cl, Br, I and BAr^F₄) in acetonitrile. Consistent with the NMR data, the high molar conductivities suggest that ion-separated structures are present in this case, whereas the relatively low Λ_m value for **2-F** supports the notion that the covalent P–F bond is retained in solution.

The formation of covalent molecular structures vs. ion pairs is also reflected by the colors observed for **2-X**. **2-F** is orange-colored as a crystalline solid and in solution (THF, FB and MeCN). By contrast, **2-[BAr^F₄]** shows a distinct yellow color. **2-Cl**, **2-Br** and **2-I** are orange solids, but they give yellow MeCN solutions consistent with the proposed presence of ion-separated structures in this solvent. **2-X** (X = F, Cl, Br, and I) are orange in THF and FB, while **2-[BAr^F₄]** remains yellow in these solvents. These visual observations are in line with the UV-vis spectra. The spectra of **2-X** (X = F, Cl, and Br) recorded in THF are very similar, showing strong peaks in the UV and weak absorptions in the visible range at 370 to 380, 455 and 525 nm (see the SI for graphical representations of the spectra). The UV-vis spectrum of **2-I** in THF is distinct showing stronger bands at 390 and 480 nm; absorptions at higher wavelength are not observed for this compound. The UV-vis spectrum of **2-[BAr^F₄]** in THF features further hypsochromically shifted absorptions as shoulders at 350 and 420 nm. Interestingly, the UV-vis spectra of **2-F** and **2-[BAr^F₄]** in THF are essentially identical to those recorded in MeCN, while compounds **2-X** (X = Cl, Br and I) in MeCN show the same absorption pattern as **2-[BAr^F₄]**, which is in line with the proposed presence of solvent separated ion pairs in that solvent.

Finally we studied the redox properties of **2-F**, **2-Cl**, and **2-Br** by cyclic voltammetry, in order to gain further insight into the redox behavior of these complexes and to compare it to the previously published data for **2-I**.^[9] Interestingly, the cyclic voltammogram (CV) of **2-F** recorded in THF/[*n*Bu₄N](PF₆) features a clean reversible one-electron oxidation process at $E_{1/2} = 0.110$ V vs. Fc/Fc⁺ (Figures 3, S38 and S39, SI). In comparison, the CVs of **2-X** (X = Cl, Br, and I) are distinct and feature several (quasi-reversible or irreversible) oxidation and reduction processes (Figures S40 and S41, SI, see also ref. ^[9]). This simpler electrochemical behavior for **2-F** is again qualitatively consistent with a strong, persistent P–F interaction, whereas reversible P–X bonding in either the oxidized or reduced forms of **2-X** (X = Cl, Br, and I) would be expected to give the complex behavior observed experimentally.

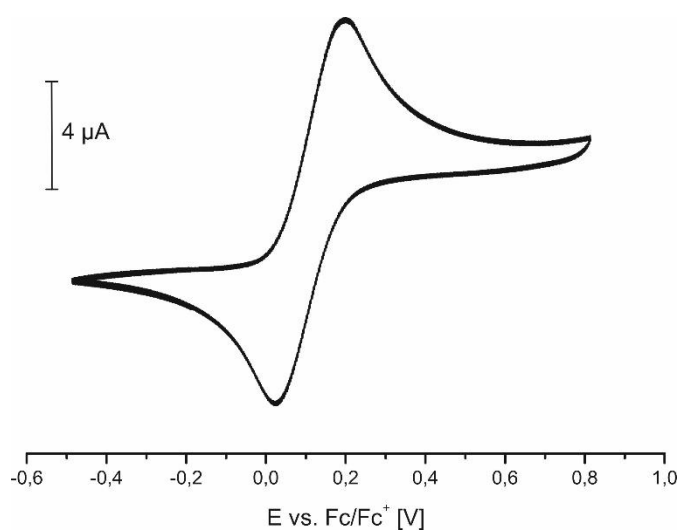


Figure 3. Cyclic voltammogram of **2-F**, $E_{1/2} = 0.110$ V vs. Fc/Fc⁺.

2.3 Conclusion

Rare halide-substituted phosphacyclohexadienyl complexes **2-X** (X = F, Cl, Br, and I) can be synthesized in varying yields by reacting the anionic iron phosphinine complex **1** with electrophilic halogenating agents. The related complex [Cp*Fe(PC₅Ph₃H₂)] [BAr^F₄] (**2-BAr^F₄**), Ar^F = 3,5-(CF₃)₂C₆H₃), which contains a more weakly coordinating anion, is likewise accessible in high yield by salt metathesis from **2-I**. The properties of **2-X** were studied comprehensively by crystallographic, spectroscopic, analytical and quantum chemical techniques. The solid-state molecular structures show covalent P–X bonds for **2-F** and **2-Cl**. To our knowledge, these compounds represent the first structurally authenticated transition metal complexes with π -coordinated λ^3 -halophosphacyclohexadienyl ligands. By contrast, ionic structures with dissociated halide anions were observed for **2-Br** and **2-I**. While our DFT calculations suggest that the covalent isomers are favored in the gas phase independent of the halogen substituent, the P–X bonds are cleaved for X = Br and I probably due to the weaker P–X bonds and packing effects in the solid-state. For **2-Cl**, **2-Br**, and **2-I**, ³¹P NMR, UV-vis, CV and computational data indicate that ionic structures are present in THF, fluorobenzene and acetonitrile, while only **2-F** apparently retains its covalent P–F bond in solution. This interesting structural dichotomy has significant implications for further functionalization reactions and potential applications in homogeneous catalysis. Investigations in these directions are currently ongoing in our laboratory.

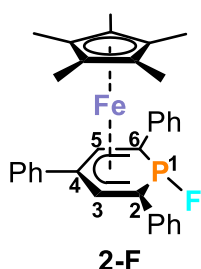
2.4 Experimental Details

2.4.1 General Considerations

All experiments were performed under an atmosphere of dry argon by using standard Schlenk and glovebox techniques. THF, toluene, Et₂O and *n*-hexane were purified, dried, and degassed with an MBraun SPS800 solvent purification system. MeCN, fluorobenzene (FB) and *ortho*-difluorobenzene (DFB) were dried and degassed over CaH₂; benzene was dried and degassed over Na. NMR spectra were recorded on Bruker Avance 300 and Avance 400 spectrometers at 300 K and internally referenced to residual solvent resonances. The assignment of the ¹H and ¹³C NMR signals was confirmed by two-dimensional (COSY, HSQC, and HMBC) experiments. Solid state ³¹P MAS-NMR spectra were recorded with a Bruker 400 MHz spectrometer. Melting points were measured on samples in sealed capillaries on a Stuart SMP10 melting point apparatus. UV/vis spectra were recorded on a Varian Cary 50 spectrometer. Cyclic voltammograms were recorded with a CH Instruments Electrochemical Analyzer. Elemental analyses were determined by the analytical department of Regensburg University. Mass spectra were performed with Jeol AccuTOF GCX LIFDI-MS by the analytical Department of Regensburg University. Conductance measurements were performed in THF and MeCN at ambient temperature (300 K) with a Mettler Toledo Seven Compact conductometer and an InLab 710 sensor. [K([18]crown-6)(thf)₂][Cp*Fe(η⁴-PC₃Ph₃H₂)] (**1**)^[9] and Na[BAr^F₄]^[52] were prepared according to literature procedures. N-fluoropyridinium tetrafluoroborate, hexachloroethane and bromine were purchased from Sigma-Aldrich and used as received.

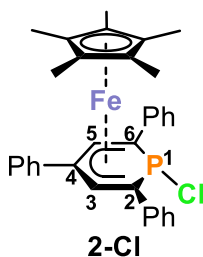
X-ray Crystallography: The single-crystal X-ray diffraction data were recorded on an Agilent Technologies SuperNova, an Agilent Technologies Gemini Ultra R and a GV1000, TitanS2 diffractometer with Cu-K_α radiation (λ = 1.54184 Å). Either semi-empirical multi-scan absorption corrections^[53] or analytical ones^[54] were applied to the data. The structures were solved with SHELXT^[55] and least-square refinements on *F*² were carried out with SHELXL.^[56] The hydrogen atoms were located in idealized positions and refined isotropically with a riding model.

CCDC 1866340 (for **2-Br**), CCDC 1866341 (for **2-Cl**), CCDC 1866342 (for **2-F**) and CCDC 1866343 (for **2-[BAr^F₄]**) contain the supplementary crystallographic data for this paper. These data can be obtained free of charge from The Cambridge Crystallographic Data Centre.

2.4.2 Synthesis of $[\text{Cp}^*\text{Fe}(1\text{-F-PC}_5\text{Ph}_3\text{H}_2)]$ (**2-F**)

A solution of *N*-fluoropyridinium tetrafluoroborate (0.42 mmol, 77 mg, 1 eq.) in THF (6 mL) was added to a solution of **1** (0.415 mmol, 400 mg, 1 eq.) in THF (6 mL) at room temperature. After stirring overnight (during which time the brown reaction mixture turned deep red), the solvent was removed under vacuum and the dark red residue was washed with *n*-hexane (9 x 2 mL), before being extracted into Et₂O (10 x 2 mL). The solvent was removed under vacuum and the residue was dissolved in toluene (2 mL).

Red crystals were obtained by layering this toluene solution with *n*-hexane (20 mL). The product was isolated by decanting the solution, washing with *n*-hexane and drying *in vacuo*. Yield: 90 mg, 41%. M.p. 235 °C (decomposition to a black oil). UV/vis: (THF, λ_{max} / nm, ϵ_{max} / L·mol⁻¹·cm⁻¹): 290 (22000), 370sh (4000), 455 (1400), 525sh (1000); (MeCN, λ_{max} / nm, ϵ_{max} / L·mol⁻¹·cm⁻¹): 295 (19000), 370sh (4000), 450 (2000), 520sh (1000); (fluorobenzene, λ_{max} / nm, ϵ_{max} / L·mol⁻¹·cm⁻¹): 290 (18000), 370sh (3000), 450 (800), 520sh (300). ¹H NMR (400.13 MHz, 300 K, [D₈]THF): δ = 1.11 (s, 15H, C₅(CH₃)₅), 6.28 (d, ³J_{PH} = 3.0 Hz, 2H, C^{3,5}-H of TPP), 7.23 – 7.25 (m, 2H, C⁴-H of C^{2,6}-Ph), 7.37 – 7.41 (m, 4H, C^{3,5}-H of C^{2,6}-Ph), 7.45 – 7.49 (m, 1H, C⁴-H of C⁴-Ph), 7.55 – 7.58 (m, 2H, C^{3,5}-H of C⁴-Ph), 8.26 – 8.28 (m, 6H, C^{2,6}-H of C^{2,6}-Ph and C^{2,6}-H of C⁴-Ph). ¹³C{¹H} NMR (100.61 MHz, 300 K, [D₈]THF): δ = 9.0 (s, C₅(CH₃)₅), 65.1 (m, C^{2,6} of TPP), 78.9 (d, ²J_{CP} = 4.5 Hz, C^{3,5}-H of TPP), 85.5 (s, C₅(CH₃)₅), 94.2 (m, C⁴ of TPP), 126.2 (s, C⁴-H of C^{2,6}-Ph), 128.3 (s, C^{2,6}-H of C⁴-Ph), 128.4 (s, C⁴-H of C⁴-Ph), 128.6 (m, C^{2,6}-H of C^{2,6}-Ph), 128.9 (s, C^{3,5}-H of C^{2,6}-Ph), 129.5 (s, C^{3,5}-H of C⁴-Ph), 139.7 (s, C¹ of C⁴-Ph), 143.5 (d, ²J_{CP} = 27.7 Hz, C¹ of C^{2,6}-Ph). ¹⁹F{¹H} NMR (376.50 MHz, 300 K, [D₈]THF): δ = -60.0 (d, ¹J_{FP} = 918 Hz). ¹⁹F NMR (376.50 MHz, 300 K, [D₈]THF): δ = -60.0 (d, ¹J_{FP} = 918 Hz). ³¹P{¹H} NMR (161.98 MHz, 300 K, [D₈]THF): δ = 33.2 (d, ¹J_{PF} = 918 Hz). ³¹P NMR (161.98 MHz, 300 K, [D₈]THF): δ = 33.2 (d, ¹J_{PF} = 918 Hz). ³¹P CPMAS (5 kHz/6 kHz, 300 K): δ = 31.5 (d, ¹J_{PF} = 930 Hz). Elemental analysis calcd. for C₃₃H₃₂FePF (M_w = 534.44 g·mol⁻¹) C 74.16, H 6.04; found C 74.78, H 6.06. MS (LIFDI, THF): *m/z* (%) = 534.14 (100) M⁺, 515.15 (3) [Cp*Fe(PC₅Ph₃H₂)]⁺.

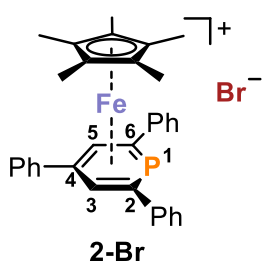
2.4.3 Synthesis of $[\text{Cp}^*\text{Fe}(1\text{-Cl-PC}_5\text{Ph}_3\text{H}_2)]$ (**2-Cl**)

A solution of hexachloroethane (0.31 mmol, 74 mg, 1 eq.) in THF (4 mL) was added to a solution of **1** (0.312 mmol, 300 mg, 1 eq.) in THF (3 mL) at -30 °C. After stirring overnight, the reaction mixture turned dark red and was evaporated to dryness. The residue was washed with *n*-hexane (7 x 2 mL) and Et₂O (7 x 2 mL). The remained residue was extracted into toluene (7 x 2 mL) and the solution was reduced (4 mL). Red crystals were obtained by layering this toluene solution with *n*-hexane (20 mL).

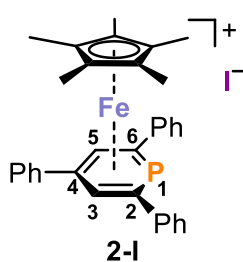
The product was isolated by decanting the solution, washing with *n*-hexane and drying *in vacuo*. Yield: 120 mg, 70%. M.p. 242 °C (decomposition to a black oil). UV/vis: (THF, λ_{max} / nm, ϵ_{max} / L·mol⁻¹·cm⁻¹): 295 (37000), 370sh (6000), 455 (2000), 530sh (1000); (MeCN,

λ_{\max} / nm, ϵ_{\max} / L·mol⁻¹·cm⁻¹): 290 (34000), 355sh (4700), 430sh (1000). ¹H NMR (400.13 MHz, 300 K, [D₈]THF): δ = 1.13 (s, 15H, C₅(CH₃)₅), 6.47 (d, ³J_{PH} = 2.5 Hz, 2H, C^{3,5}-H of TPP), 7.28 – 7.32 (m, 2H, C⁴-H of C^{2,6}-Ph), 7.40 – 7.43 (m, 4H, C^{3,5}-H of C^{2,6}-Ph), 7.49 – 7.52 (m, 1H, C⁴-H of C⁴-Ph), 7.57 – 7.61 (m, 2H, C^{3,5}-H of C⁴-Ph), 8.24 – 8.26 (m, 4H, C^{2,6}-H of C^{2,6}-Ph), 8.24 – 8.26 (m, 2H, C^{2,6}-H of C⁴-Ph). ¹³C{¹H} NMR (100.61 MHz, 300 K, [D₈]THF): δ = 9.2 (s, C₅(CH₃)₅), 70.7 (d, ²J_{CP} = 34.7 Hz, C^{2,6} of TPP), 80.6 (d, ²J_{CP} = 9.4 Hz, C^{3,5}-H of TPP), 86.5 (s, C₅(CH₃)₅), 96.5 (d, ²J_{CP} = 6.7 Hz, C⁴ of TPP), 127.1 (d, ²J_{CP} = 3.5 Hz, C⁴-H of C^{2,6}-Ph), 128.7 (d, ²J_{CP} = 7.2 Hz, C^{2,6}-H of C⁴-Ph), 128.9 (s, C⁴-H of C⁴-Ph), 129.2 (s, C^{2,6}-H of C^{2,6}-Ph), 129.2 (s, C^{3,5}-H of C^{2,6}-Ph), 129.7 (s, C^{3,5}-H of C⁴-Ph), 138.8 (s, C¹ of C⁴-Ph), 141.4 (d, ²J_{CP} = 26.2 Hz, C¹ of C^{2,6}-Ph). ³¹P{¹H} NMR (161.98 MHz, 300 K, [D₈]THF): δ = -12.4. ³¹P NMR (161.98 MHz, 300 K, [D₈]THF): δ = -11.5. ³¹P CPMAS (5 kHz/6 kHz, 300 K): δ = 3.8. Elemental analysis calcd. for C₃₃H₃₂FePCl (Mw = 550.88 g·mol⁻¹) C 71.95, H 5.86; found C 72.39, H 5.85. MS (LIFDI, THF): m/z (%) = 550.11 (100) M⁺, 515.14 (72) [Cp*Fe(PC₅Ph₃H₂)]⁺.

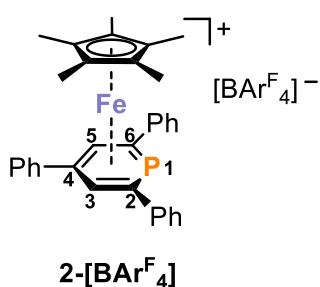
2.4.4 Synthesis of [Cp*Fe(PC₅Ph₃H₂)]Br (**2-Br**)



A freshly prepared stock solution ($c = 0.193$ mmol·mL⁻¹, 0.1 mL Br₂ in 10 mL benzene) of bromine (0.727 mmol, 3.77 mL, 1 eq.) was added to a solution of **1** (0.727 mmol, 700 mg, 1 eq.) in THF (10 mL) at room temperature and in the absence of light. An orange precipitate was formed immediately and the reaction mixture was stirred overnight. The solution was decanted, and the remaining orange solid was dissolved in THF (10 mL). The product was obtained as an orange powder after filtration through silica (in order to remove [18]crown-6), and subsequent crystallization from a saturated THF solution. Yield: 96 mg, 22%. M.p. 180 °C. UV-Vis: (THF, λ_{\max} / nm, ϵ_{\max} / L·mol⁻¹·cm⁻¹): 290 (25000), 380sh (4000), 455 (1400), 520sh (800); (MeCN, λ_{\max} / nm, ϵ_{\max} / L·mol⁻¹·cm⁻¹): 290 (36000), 360sh (5000), 430sh (1200). ¹H NMR (400.13 MHz, 300 K, [D₈]THF): δ = 1.16 (s, 15H, C₅(CH₃)₅), 6.62 (d, ³J_{PH} = 3.8 Hz, 2H, C^{3,5}-H of TPP), 7.34 – 7.737 (m, 2H, C⁴-H of C^{2,6}-Ph), 7.43 – 7.47 (m, 4H, C^{3,5}-H of C^{2,6}-Ph), 7.51 – 7.55 (m, 1H, C⁴-H of C⁴-Ph), 7.60 – 7.64 (m, 2H, C^{3,5}-H of C⁴-Ph), 8.27 – 8.30 (m, 4H, C^{2,6}-H of C^{2,6}-Ph), 8.36 – 8.37 (m, 2H, C^{2,6}-H of C⁴-Ph). ¹³C{¹H} NMR (100.61 MHz, 300 K, [D₈]THF): δ = 9.0 (s, C₅(CH₃)₅), 77.3 – 76.9 (s, C^{2,6} of TPP), 81.7 (d, ²J_{CP} = 9.4 Hz, C^{3,5}-H of TPP), 87.2 (s, C₅(CH₃)₅), 97.03 (s, C⁴ of TPP), 127.7 (d, ²J_{CP} = 3 Hz, C⁴-H of C^{2,6}-Ph), 128.7 (d, ²J_{CP} = 7.2 Hz, C^{2,6}-H of C⁴-Ph), 128.9 (s, C⁴-H of C⁴-Ph), 129.2 (s, C^{2,6}-H of C^{2,6}-Ph), 129.4 (s, C^{3,5}-H of C^{2,6}-Ph), 129.7 (s, C^{3,5}-H of C⁴-Ph), 138.3 (s, C¹ of C⁴-Ph), 140.4 (d, ²J_{CP} = 26 Hz, C¹ of C^{2,6}-Ph). ³¹P{¹H} NMR (161.98 MHz, 300 K, [D₈]THF): δ = -11.9. ³¹P NMR (161.98 MHz, 300 K, [D₈]THF): δ = -11.9. ³¹P CPMAS (5 kHz/6 kHz, 300 K): δ = -12.2. Elemental analysis calcd. for C₃₃H₃₂FePBr (Mw = 595.34 g·mol⁻¹) C 66.58, H 5.42; found C 66.64, H 6.10. MS (LIFDI, THF): m/z (%) = 594.00 (1) M⁺, 515.14 (100) [Cp*Fe(PC₅Ph₃H₂)]⁺.

2.4.5 Synthesis of $[\text{Cp}^*\text{Fe}(\text{PC}_5\text{Ph}_3\text{H}_2)]\text{I}$ (**2-I**).^[9]

Iodine (0.15 g, 0.61 mmol) was added to a solution of **1** (0.5 g, 0.61 mmol) in THF (50 mL) at room temperature. An orange solid precipitated after a few minutes. The reaction mixture was stirred overnight, and the solution was then removed by filtration. The solid residue was dissolved in hot MeCN. Orange crystals formed after slow cooling of this solution to room temperature. Yield: 0.24 g 0.37 mmol, 61%; UV/vis: (THF, λ_{max} / nm, ϵ_{max} / $\text{L}\cdot\text{mol}^{-1}\cdot\text{cm}^{-1}$): 290 (34000), 340 (22000), 390sh (13000), 480sh (4000); (MeCN, λ_{max} / nm, ϵ_{max} / $\text{L}\cdot\text{mol}^{-1}\cdot\text{cm}^{-1}$): 290 (40000), 360sh (7000), 430sh (1400). ^1H NMR (400.13 MHz, 300 K, CD_3CN): δ = 1.26 (s, 15H, $\text{C}_5(\text{CH}_3)_5$), 7.16 (d, $^3J_{\text{PH}} = 4.7$ Hz, 2H, $\text{C}^{3,5}\text{-H}$, TPP), 7.60 (m, 6H, $\text{C}^{3,4,5}\text{-H}$ of $\text{C}^{2,6}\text{-Ph}$), 7.71 (m, 3H, $\text{C}^{3,4,5}\text{-H}$ of $\text{C}^4\text{-Ph}$), 8.14 (m, 4H, $\text{C}^{2,6}\text{-H}$ of $\text{C}^{2,6}\text{-Ph}$), 8.34 (m, 2H, $\text{C}^{2,6}\text{-H}$ of $\text{C}^4\text{-Ph}$); $^{31}\text{P}\{^1\text{H}\}$ NMR (161.98 MHz, 300 K, CD_3CN): δ = -0.9 (s). MS (LIFDI, THF): m/z (%) = 515.13 (100) $[\text{Cp}^*\text{Fe}(\text{PC}_5\text{Ph}_3\text{H}_2)]^+$.

2.4.6 Synthesis of $[\text{Cp}^*\text{Fe}(\text{PC}_6\text{Ph}_3\text{H}_2)][\text{BAr}^{\text{F}_4}]$ (**2-[BAr^F₄]**)

A solution of $\text{Na}[\text{BAr}^{\text{F}_4}]$ (0.425 mmol, 376 mg, 1 eq.) in *ortho*-difluorobenzene (DFB, 5 mL) was added dropwise to a solution of **2-I** (0.0425 mmol, 273 mg, 1 eq.) in DFB (5 mL) at room temperature. An orange suspension formed and a white precipitate was observed. Another 5 mL of DFB was added for complete dissolution. The suspension was stirred overnight and filtered for the removal of solid NaI. The deep orange solution was evaporated under vacuum and the remaining residue was extracted into THF (3 mL). After layering with *n*-hexane (4 mL) and storage at -35 °C, the product was isolated as an orange solid. Yield: 526 mg, 90%. M.p. 182 °C. UV-Vis: (THF, λ_{max} / nm, ϵ_{max} / $\text{L}\cdot\text{mol}^{-1}\cdot\text{cm}^{-1}$): 265 (43000), 290sh (30000), 350sh (4000), 420sh (1000); (MeCN, λ_{max} / nm, ϵ_{max} / $\text{L}\cdot\text{mol}^{-1}\cdot\text{cm}^{-1}$): 290sh (28000), 360sh (4600), 430sh (1000). ^1H NMR (400.13 MHz, 300 K, $[\text{D}_8]\text{THF}$): δ = 1.34 (s, 15H, $\text{C}_5(\text{CH}_3)_5$), 7.32 (d, $^3J_{\text{PH}} = 4.6$ Hz, 2H, $\text{C}^{3,5}\text{-H}$ of TPP), 7.57 (bs, 4H, BAr^{F_4}), 7.60 – 7.75 (m, 9H, $\text{C}^{3,4,5}\text{-H}$ of $\text{C}^{2,4,6}\text{-Ph}$), 7.79 (m, 8H, BAr^{F_4}), 8.22 – 8.24 (m, 4H, $\text{C}^{2,6}\text{-H}$ of $\text{C}^{2,6}\text{-Ph}$), 8.42 – 8.45 (m, 2H, $\text{C}^{2,6}\text{-H}$ of $\text{C}^4\text{-Ph}$). $^{13}\text{C}\{^1\text{H}\}$ NMR (100.61 MHz, 300 K, $[\text{D}_8]\text{THF}$): δ = 9.3 (s, $\text{C}_5(\text{CH}_3)_5$), 86.72 (d, $^2J_{\text{CP}} = 6.8$ Hz, $\text{C}^{3,5}\text{-H}$ of TPP), 94.1 (s, $\text{C}_5(\text{CH}_3)_5$), 103.6 (d, $^2J_{\text{CP}} = 3$ Hz, C^4 of TPP), 116.2 (s), 118.2 (m, $\text{C}^4\text{-Ph}$ of BAr^{F_4}), 124.2 (s, $\text{C}^{1,3,5}$ of BAr^{F_4}), 126.9 (s, $\text{C}^{1,3,5}$ of BAr^{F_4}), 128.9 (s, $\text{C}^{2,6}\text{-H}$ of $\text{C}^{2,6}\text{-Ph}$), 129.6 (m, $\text{C}^{2,6}\text{-H}$ of $\text{C}^4\text{-Ph}$), 130.5 (s, $\text{C}^{3,4,5}\text{-H}$ of $\text{C}^{2,4,6}$), 130.7 (s, $\text{C}^{3,4,5}\text{-H}$ of $\text{C}^{2,4,6}$), 134.4 (s, C^1 of $\text{C}^4\text{-Ph}$), 135.6 (bs, $\text{C}^{2,6}\text{-Ph}$ of BAr^{F_4}), 136.7 (d, $^2J_{\text{CP}} = 22$ Hz, C^1 of $\text{C}^{2,6}\text{-Ph}$), 162.8 (m, CF_3 of BAr^{F_4}). $^{31}\text{P}\{^1\text{H}\}$ NMR (161.98 MHz, 300 K, $[\text{D}_8]\text{THF}$): δ = -2.40. $^{11}\text{B}\{^1\text{H}\}$ NMR (128.38 MHz, 300 K, $[\text{D}_8]\text{THF}$): δ = -6.43. $^{19}\text{F}\{^1\text{H}\}$ NMR (376.66 MHz, 300 K, $[\text{D}_8]\text{THF}$): δ = -62.47. ^{31}P CPMAS (5 kHz/6 kHz, 300 K): δ = -8.9. Elemental analysis calcd. for $\text{C}_{65}\text{H}_{44}\text{BF}_{24}\text{FeP}$

(Mw = 1378.22 g·mol⁻¹) C 56.63, H 3.22; found C 57.05, H 3.41. MS (LIFDI, THF): *m/z* (%) = 515.16 (100) [Cp*Fe(PC₅Ph₃H₂)]⁺.

2.5 References

- [1] P. L. Floch, *Coord. Chem. Rev.* **2006**, *250*, 627–681.
- [2] G. Märkl, *Angew. Chem.* **1966**, *78*, 907–908.
- [3] A. J. Ashe, *J. Am. Chem. Soc.* **1971**, *93*, 3293–3295.
- [4] C. Müller, L. E. E. Broeckx, I. de Krom, J. J. M. Weemers, *Eur. J. Inorg. Chem.* **2013**, *2013*, 187–202.
- [5] C. Elschenbroich, S. Voss, O. Schiemann, A. Lippek, K. Harms, *Organometallics* **1998**, *17*, 4417–4424.
- [6] C. Elschenbroich, M. Nowotny, A. Behrendt, W. Massa, S. Wocadlo, *Angew. Chem. Int. Ed. Engl.* **1992**, *31*, 1343–1345.
- [7] C. Elschenbroich, M. Nowotny, A. Behrendt, K. Harms, S. Wocadlo, J. Pebler, *J. Am. Chem. Soc.* **1994**, *116*, 6217–6219.
- [8] P. Le Floch, L. Ricard, F. Mathey, *Polyhedron* **1990**, *9*, 991–997.
- [9] B. Rezaei Rad, U. Chakraborty, B. Mühldorf, J. A. W. Sklorz, M. Bodensteiner, C. Müller, R. Wolf, *Organometallics* **2015**, *34*, 622–635.
- [10] C. M. Hoidn, R. Wolf, *Dalton Trans.* **2016**, *45*, 8875–8884.
- [11] C. Elschenbroich, M. Nowotny, B. Metz, W. Massa, J. Graulich, K. Biehler, W. Sauer, *Angew. Chem. Int. Ed. Engl.* **1991**, *30*, 547–550.
- [12] F. Knoch, F. Kremer, U. Schmidt, U. Zenneck, P. Le Floch, F. Mathey, *Organometallics* **1996**, *15*, 2713–2719.
- [13] M. Doux, L. Ricard, F. Mathey, P. L. Floch, N. Mézailles, *Eur. J. Inorg. Chem.* **2003**, *2003*, 687–698.
- [14] B. Schmid, L. M. Venanzi, T. Gerfin, V. Gramlich, F. Mathey, *Inorg. Chem.* **1992**, *31*, 5117–5122.
- [15] K. C. Nainan, C. T. Sears, *J. Organomet. Chem.* **1978**, *148*, C31–C34.
- [16] C. Elschenbroich, J. Six, K. Harms, *Chem. Commun.* **2006**, 3429–3431.
- [17] P. L. Floch, N. Maigrot, L. Ricard, C. Charrier, F. Mathey, *Inorg. Chem.* **1995**, *34*, 5070–5072.
- [18] Francois. Nief, Jean. Fischer, *Organometallics* **1986**, *5*, 877–883.
- [19] H. Lehmkuhl, R. Paul, C. Krüger, Y.-H. Tsay, R. Benn, R. Mynott, *Liebigs Ann. Chem.* **1981**, *1981*, 1147–1161.
- [20] A. Moores, N. Mézailles, L. Ricard, Y. Jean, P. le Floch, *Organometallics* **2004**, *23*, 2870–2875.
- [21] K. Eggers, F. W. Heinemann, M. Hennemann, T. Clark, P. Binger, U. Zenneck, *Comptes Rendus Chim.* **2010**, *13*, 1203–1212.
- [22] B. Schmid, L. M. Venanzi, T. Gerfin, V. Gramlich, F. Mathey, *Inorg. Chem.* **1992**, *31*, 5117–5122.

- [23] M. T. Reetz, E. Bohres, R. Goddard, M. C. Holthausen, W. Thiel, *Chem. – Eur. J.* **1999**, *5*, 2101–2108.
- [24] Y. Mao, K. M. H. Lim, Y. Li, R. Ganguly, F. Mathey, *Organometallics* **2013**, *32*, 3562–3565.
- [25] X. Chen, Z. Li, F. Yanan, H. Grützmacher, *Eur. J. Inorg. Chem.* **2016**, *2016*, 633–638.
- [26] M. H. Habicht, F. Wossidlo, T. Bens, E. A. Pidko, C. Müller, *Chem. – Eur. J.* **2018**, *24*, 944–952.
- [27] C. Müller, in *PhosphorusIII Ligands Homog. Catal. Des. Synth.*, Wiley-Blackwell, **2012**, pp. 287–307.
- [28] R. J. Newland, M. F. Wyatt, R. L. Wingad, S. M. Mansell, *Dalton Trans.* **2017**, *46*, 6172–6176.
- [29] R. J. Newland, J. M. Lynam, S. M. Mansell, *Chem. Commun.* **2018**, *54*, 5482–5485.
- [30] M. Rigo, L. Hettmanczyk, F. J. L. Heutz, S. Hohloch, M. Lutz, B. Sarkar, C. Müller, *Dalton Trans.* **2016**, *46*, 86–95.
- [31] L. E. E. Broeckx, A. Bucci, C. Zuccaccia, M. Lutz, A. Macchioni, C. Müller, *Organometallics* **2015**, *34*, 2943–2952.
- [32] C. Müller, D. Vogt, *Dalton Trans.* **2007**, *0*, 5505–5523.
- [33] L. Kollár, G. Keglevich, *Chem. Rev.* **2010**, *110*, 4257–4302.
- [34] J. J. M. Weemers, W. N. P. van der Graaff, E. A. Pidko, M. Lutz, C. Müller, *Chem. Eur. J.* **2013**, *19*, 8991–9004.
- [35] A. Moores, L. Ricard, P. Le Floch, N. Mézailles, *Organometallics* **2003**, *22*, 1960–1966.
- [36] G. Märkl, F. Lieb, A. Merz, *Angew. Chem. Int. Ed. Engl.* **1967**, *6*, 87–88.
- [37] G. Märkl, A. Merz, *Tetrahedron Lett.* **1968**, *9*, 3611–3614.
- [38] Y. Zhang, F. S. Tham, J. F. Nixon, C. Taylor, J. C. Green, C. A. Reed, *Angew. Chem. Int. Ed.* **2008**, *47*, 3801–3804.
- [39] H. Kanter, K. Dimroth, *Angew. Chem. Int. Ed. Engl.* **1972**, *11*, 1090–1091.
- [40] T. N. Dave, H. Kaletsch, K. Dimroth, *Angew. Chem.* **1984**, *96*, 984–985.
- [41] In *Categ. 2 Hetarenes Relat. Ring Syst.*, Thieme Verlag, **2005**.
- [42] K. Dimroth, S. Berger, H. Kaletsch, *Phosphorus Sulfur Relat. Elem.* **1981**, *10*, 305–315.
- [43] M. Lückoff, K. Dimroth, *Angew. Chem.* **1976**, *88*, 543–544.
- [44] M. Doux, C. Bouet, N. Mézailles, L. Ricard, P. Le Floch, *Organometallics* **2002**, *21*, 2785–2788.
- [45] M. Doux, N. Mézailles, L. Ricard, P. Le Floch, *Eur. J. Inorg. Chem.* **2003**, *2003*, 3878–3894.
- [46] A survey in the Cambridge Crystal Structure Database (CCSD, version 5.39 update 4, 31/08/2018, revealed 30 three-coordinate P–F compounds with a mean P–F distance of 1.587 Å (median 1.581 Å) and 394 three-coordinate P–Cl compounds with a mean P–Cl distance of 2.114 Å (median 2.095 Å).
- [47] D. Gudat, A. Haghverdi, H. Hupfer, M. Nieger, *Chem. – Eur. J.* **2000**, *6*, 3414–3425.
- [48] S. Burck, D. Gudat, M. Nieger, *Angew. Chem.* **2004**, *116*, 4905–4908.
- [49] A. Bondi, *J. Phys. Chem.* **1964**, *68*, 441–451.

- [50] S. Berger, S. Braun, H.-O. Kalinowski, *NMR-Spektroskopie von Nichtmetallen*, Georg Thieme Verlag, Stuttgart; New York, **1993**.
- [51] P. Pyykkö, M. Atsumi, *Chem. – Eur. J.* **2009**, *15*, 12770–12779.
- [52] N. A. Yakelis, R. G. Bergman, *Organometallics* **2005**, *24*, 3579–3581.
- [53] a) SCALE3ABS, CrysAlisPro, Aglient Technologies Inc., Oxford, GB, **2012**. b) G. M. Sheldrick, SADABS, Bruker AXS, Madison, USA, **2007**.
- [54] R. C. Clark, J. S. Reid, *Acta Crystallogr. A* **1995**, *51*, 887–897.
- [55] G. M. Sheldrick, *Acta Crystallogr. Sect. Found. Adv.* **2015**, *71*, 3–8.
- [56] G. M. Sheldrick, *Acta Crystallogr. A* **2008**, *64*, 112–122.

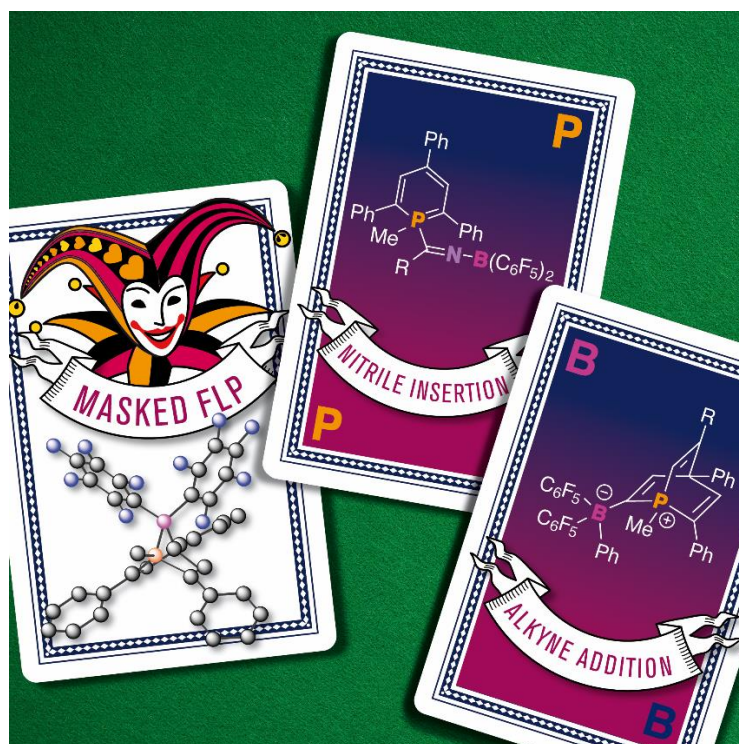
2.6 Supporting Information

The supporting information of *Chapter 2* can be found on the supplied CD-ROM and on <https://doi.org/10.1002/ejic.201801135>. The supporting information contains: NMR and UV-vis spectra, X-ray crystallography details, cyclic voltammograms and results of quantum chemical calculations including Cartesian coordinates of all optimized structures.

Chapter 3

A Phosphinine-Derived 1-Phospha-7-Bora-Norbornadiene: Frustrated Lewis Pair Type Activation of Triple Bonds

Abstract: Salt metathesis of 1-methyl-2,4,6-triphenylphosphacyclohexadienyl lithium and chlorobis(pentafluorophenyl)borane affords a 1-phospha-7-bora-norbornadiene derivative **2**. The C≡N triple bonds of nitriles insert into the P–B bond of **2** with concomitant C–B bond cleavage, while the C≡C bonds of phenylacetylenes react with **2** to form λ^4 -phosphabarrelenes. Even though **2** must formally be regarded as a classical Lewis adduct, the C≡N and C≡C activation processes observed (and the mild conditions under which they occur) are reminiscent of the reactivity of frustrated Lewis pairs. Indeed, NMR and computational studies give insight into the mechanism of the reactions and reveal the labile nature of the phosphorus-boron bond in **2**, which is also suggested by detailed NMR spectroscopic studies on this compound. Nitrile insertion is thus preceded by ring opening of the bicycle of **2** through P–B bond splitting with a low energy barrier. By contrast, the reaction with alkynes involves formation of a reactive zwitterionic methylphosphinium borate intermediate, which readily undergoes alkyne 1,4-addition.



Reproduced with permission from J. Leidl, A. R. Jupp, E. R. M. Habraken, V. Streitferdt, P. Coburger, D. J. Scott, R. M. Gschwind, C. Müller, J. C. Sloatweg and R. Wolf, *Chem. Eur. J.* **2020**, *26*, 7788–7800.

J. Leidl performed all reactions and fully characterized compounds **2**, **3a-3e**, **4**, **5a-5c** and **6** by single crystal X-ray analysis, NMR and UV-Vis spectroscopy and elemental analysis. J. Leidl wrote the manuscript with contributions from all authors. A. R. Jupp performed DFT calculations (all mechanisms and NMR shifts) and prepared the manuscript and supporting information. E. R. M. Habraken supplied $(\text{C}_6\text{F}_5)_2\text{BCl}$ and was involved in the initial reaction of **2**. V. Streitferdt performed NMR monitoring experiments and was involved in the preparation of the manuscript. P. Coburger performed DFT calculations for NMR shifts. D. J. Scott was involved in the preparation of the manuscript. R. M. Gschwind, C. Müller, J. C. Sloatweg and R. Wolf supervised and directed the project.

3.1 Introduction

1-*R*-Phosphacyclohexadienyl anions (**A**, Figure 1, also sometimes referred to as λ^4 -phosphinine anions) present a promising, yet underutilized platform for accessing diverse functionalized organophosphorus molecules.^[1–4] Anions **A** can easily be prepared from organolithium or Grignard reagents and aromatic λ^3, σ^2 -phosphinines and show ambidentate character toward various electrophiles, including transition metal centers. With “soft” alkylating agents, such as CH₃I, an S_N2 reaction with the phosphorus atom lone pair typically results in formation of a 1,1-disubstituted λ^5 -phosphinine (type **B**). On the other hand, with “hard” electrophiles such as acylium ions or protons, alkylation usually occurs at the more electron-rich C4- or C2-positions of the heterocycle (type **C** and **D**, respectively), affording the corresponding 1,2- or 1,4-dihydrophosphacyclohexadienes.^[5–7]

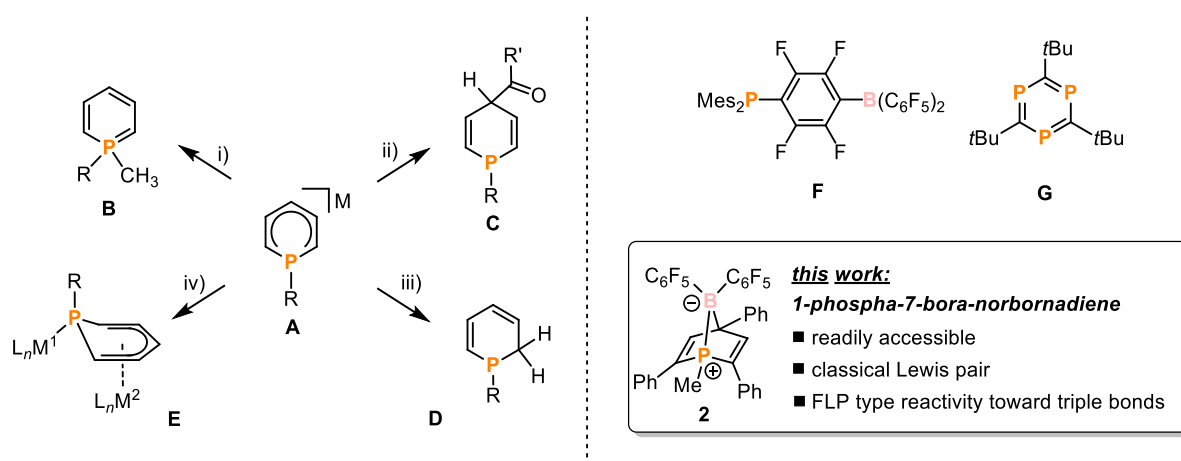


Figure 1. A generic 1-*R*-phosphacyclohexadienyl anion **A** and its reactivity toward various electrophiles; the first reported P/B FLP (**F**); a triphosphabenzene derivative that displays FLP-like reactivity (**G**). Reagents: i) CH₃I, ii) R'COCl, iii) H⁺, iv) MⁿL_n = M²L_n = Rh(1,5-cod), cod = cycloocta-1,5-diene; R = aryl or alkyl substituents.

For example, protonation (type **D**) usually proceeds exclusively at the C2-position of the λ^4 -phosphinine anion.^[8,9] It has been proposed that typically 1,1-products (**B**) are thermodynamically favoured, while 1,2- and 1,4-products (**C** and **D**) arise through kinetically controlled alkylation.^[6] λ^4 -Phosphinines can also serve as anionic ligands for transition metal complexes. Depending on the nature of the ring-substitution pattern and the metal fragment, η^1 -, η^2 -, η^5 - or even $\eta^1:\eta^5$ -coordination (type **E**) can be observed.^[10–14] Some of these coordination compounds have found applications in homogeneous catalysis, such as [(1,5-cod)Rh(η^5 -1-*t*Bu-2,4,5,6-Ph-PC₅H)] for the Rh-catalysed hydroformylation of olefins.^[11–14]

As part of our programme to study the chemistry of reactive and catalytically active phosphinine and phosphacyclohexadienyl complexes,^[15–17] we anticipated that the reaction of λ^4 -phosphinine anions **A** with chloroboranes would lead to neutral, phosphinine-based

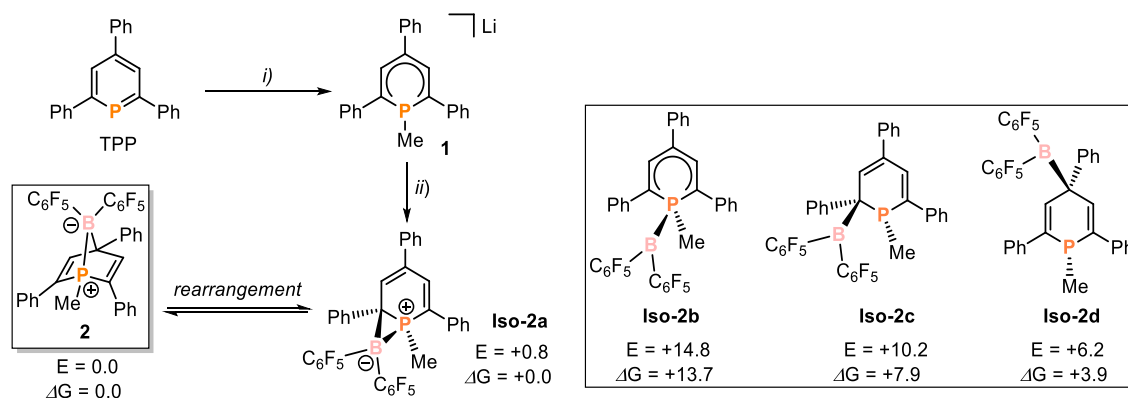
heterocycles that exhibit both a Lewis basic phosphorus atom moiety and an additional Lewis acidic boryl site.^[16] Related systems have attracted much attention lately as so-called “frustrated Lewis pairs” (FLPs), which typically consist of trivalent alkyl or aryl phosphine and borane units.^[18] For example, Stephan’s groundbreaking intramolecular FLP $\text{Mes}_2\text{PC}_6\text{F}_4\text{B}(\text{C}_6\text{F}_5)_2$ (**F**, Figure 1) displays unquenched reactivity at the Lewis acidic borane and basic phosphine moieties, allowing it to split dihydrogen reversibly,^[19] and similar systems also react with other small molecules such as CO_2 .^[20,21]

Despite the ubiquity of sp^3 -hybridised λ^3, σ^3 -phosphorus Lewis bases in FLP chemistry, the use of phosphorus bases in other coordination environments remains essentially unexplored, except for one recent example reported by Stephan and co-workers who showed that 2,4,6-tri-*tert*-butyl-1,3,5-triphosphinine (**G**, Figure 1) is able to activate dihydrogen in an FLP type manner.^[22] Herein we describe the synthesis, thorough characterisation and reactivity of a bicyclic 1-phospha-7-boranorbornadiene **2**, which possesses a direct, polar P–B bond. Despite formally being a classical Lewis adduct, compound **2** displays characteristic FLP-like behavior due to the presence of easily thermally-accessible ring-opened isomers, which contain unquenched Lewis acidic and Lewis basic sites. As a result, **2** behaves as a masked FLP and readily activates the strong $\text{C}\equiv\text{N}$ and $\text{C}\equiv\text{C}$ triple bonds of nitriles and phenylacetylenes, forming unusual nitrile insertion and alkyne addition products.

3.2 Results and Discussion

3.2.1 Synthesis, characterisation and mechanism of formation of 1-phospha-7-boranorbornadiene **2**

Taking the known reactivity of **A** with electrophiles into account (Figure 1), it was anticipated that a chloroborane could be used to install a strongly electrophilic boron center onto a phosphacyclohexadienyl scaffold by salt elimination. On this basis, the simple salt $\text{Li}[1\text{-Me-PC}_5\text{H}_2\text{Ph}_3]$ (**1**) was chosen as a starting material, which is easily prepared from methyl lithium and 2,4,6-triphenylphosphinine (TPP, Scheme 1).^[7] Upon treatment of **1** with $(\text{C}_6\text{F}_5)_2\text{BCl}$ at $T = -35\text{ }^\circ\text{C}$ in *n*-hexane, a colour change from deep pink to orange was observed, with concomitant precipitation of an orange solid. Following filtration, dissolution of the remaining solid in diethyl ether, refiltration (to remove LiCl) and removal of solvent, a new compound **2** was isolated as a bright orange solid in 35% yield. Compound **2** was characterized by single crystal X-ray diffraction, NMR and UV-Vis spectroscopy as well as elemental analysis, all of which provided data that are consistent with the molecular structure depicted in Scheme 1 (*vide infra*). In particular, single crystals of **2**, suitable for X-ray diffraction, were obtained by slow evaporation of the solvent from a solution of **2** in *n*-hexane at room temperature. Crystallographic characterization revealed a hitherto unknown heteronorbornadiene structure (Figure 2), in which the boron atom has adopted a bridging position between the P1 and C4 positions of the phosphorus heterocycle.



Scheme 1. Synthesis of **2** via **1** and **Iso-2a**; reagents and conditions: i) +MeLi (Et₂O, -78 °C), ii) +(C₆F₅)₂BCl/LiCl (r.t., *n*-hexane). Relative wb97X-D/6-311+G** electronic energies (ΔE in kcal mol⁻¹) and free energies (ΔG in kcal mol⁻¹) for possible isomers of **2** (**Iso-2a** – **Iso-2d**).

This unusual structure (c.f. **B** – **D**) can be attributed to the doubly electrophilic nature of the chloroborane, which allows the formation of a second, bridging interaction that is not available to most other main group electrophiles. It is worth noting that hetero-norbornadienes have received significant attention as ligands in homogeneous catalytic reactions, e.g. the hydrogenation and hydroformylation of alkenes as well as Heck reactions.^[23,24] Furthermore, compound **2** is a rare example of a hetero-norbornadiene based on both phosphorus *and* boron.^[25,26] Derivatives with phosphorus and another additional heteroatom in the norbornadiene scaffold are scarce, although Streubel and co-workers have described a 7-aza-1-phospha-norbornadiene and group 13 7-metalla-1,4-diphospha-norbornadienes (mechanistic and reactivity studies of which have unfortunately not been reported).^[27,28] Also of note are the very mild conditions used for the preparation of **2**, which contrasts with the much more forcing conditions required to prepare many other 1-phospha-norbornadiene derivatives.^[29]

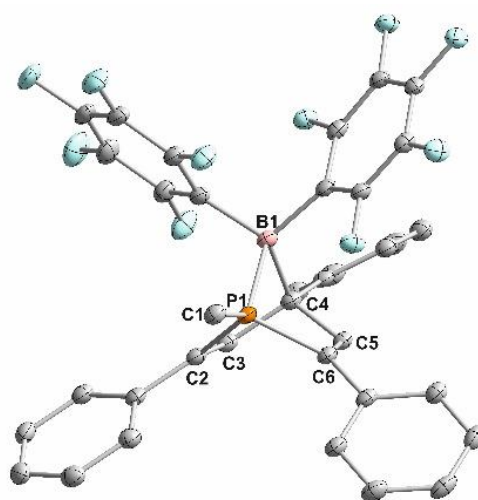


Figure 2. Molecular structure of **2** in the crystal. Displacement ellipsoids are shown at the 40% probability level; H atoms are omitted for clarity; selected bond lengths [Å] and angles [°]: P1–B1 1.9894(19); P1–C1 1.8025(17); B1–C4 1.721(2); P1–C2 1.8146(17); P1–C6 1.8081(17); C2–C3 1.344(3); C6–C5 1.336(2); C1–P1–B1 129.51(8); C2–P1–C6 101.44(8); P1–B1–C4 84.58(10).

While the P1–B1 distance of 1.9894(19) Å in **2** is in the range of phosphorus boron single bonds (sum of covalent radii = 1.96 Å),^[30] the B1–C4 bond is slightly elongated compared both to the sum of the covalent radii (1.721(2) Å vs. 1.60 Å)^[30] and to previously reported 7-bora-norbornadienes (ca. 1.641 Å),^[31–33] suggesting significant strain in the bicyclic structure.^[34,35] A similar phenomenon was observed by Braunschweig and co-workers for a heptaphenyl-7-borabicyclohepta-2,5-diene N-heterocyclic carbene adduct (B–C: 1.743 Å), in which the boron atom is also four-coordinate.^[36] Also of note are the C2–C3 and C5–C6 distances within the phosphorus heterocycle, which are characteristic of C=C double bonds (1.344(3) and 1.336(3) Å, respectively).^[37] The ³¹P{¹H} NMR spectrum of **2** shows a poorly resolved signal at $\delta(\text{ppm}) = +18.6$ at r.t. (see Figures S3 and S79), while the ¹¹B spectrum reveals a resonance at $\delta(\text{ppm}) = +14.1$ consistent with four-coordinate boron (see Figures S5, S82 and S84).

In order to elucidate the pathway for the formation of **2**, variable temperature (VT) ¹¹B and ³¹P{¹H} NMR reaction monitoring was performed, alongside DFT calculations. ¹¹B NMR spectra recorded during the reaction of **1** and (C₆F₅)₂BCl revealed not only the formation of product **2** ($\delta(\text{ppm}) = +13$) but also of an additional species, **Iso-2a**, characterised by a resonance at $\delta(\text{ppm}) = -25$ (Figure S82). Further information on the reaction was obtained by ³¹P{¹H} NMR monitoring (see Figure 3a; see SI for experimental details and Figure S79 for further spectra) which showed that **1** ($\delta(\text{ppm}) = -72.5$) is fully converted even at low temperature. The signal of product **2** appears within minutes even at 193 K (see Figure 3a). However, another intense and broad signal can be observed at $\delta(\text{ppm}) = -102$ (**Iso-2a** in Figure 3a), which converts into **2** as the temperature is increased, suggesting an intermediate species. Calculations at the TPSS/IGLO-III CPCM(THF) level of theory showed that the experimental ³¹P shift of -102 ppm and the ¹¹B shift of -25 ppm both fit well to a proposed three-membered B–C–P ring species, and this structure is consequently assigned to **Iso-2a** (see Table 1 and Scheme 1). Calculations also suggested that this structure should be very similar in energy to **2**, and indeed, NMR analysis of even authentic samples of crystalline **2** showed the presence of minor amounts of **Iso-2a**, consistent with reversible isomerisation in solution. Given the known reactivity of λ^4 -phosphinine anions with electrophiles shown in Scheme 1, other plausible structures **Iso-2b** – **Iso-2d** were also investigated as possible intermediates. DFT calculations at the ω B97X-D/6-311+G** level showed that isomers with a tricoordinate boryl substituent in the 1-, 2- or 4-position are all higher in energy than **2** or **Iso-2a** (see Scheme 1), and therefore less likely to accumulate during the course of the reaction. This is corroborated by a chemical shift analysis of these structures (Table 1), which predicts significantly different NMR shifts for the isomers **Iso-2b** – **Iso-2d** than those observed experimentally. Nevertheless, it should be noted that structure **Iso-2d** in particular is predicted to be thermally accessible at even modest temperatures on the basis of the above calculations.

3.2.2 Variable temperature NMR characterisation of isomers **2** and **Iso-2a**

During VT NMR monitoring of the formation of **2** it was noted that the $^{31}\text{P}\{^1\text{H}\}$ resonances for both **2** and **Iso-2a** show complex temperature-dependent behaviour. In order to understand these observations (and also further support the structural assignment of **Iso-2a**) an in-depth analysis of the relevant multinuclear VT NMR spectra was carried out. In the $^{31}\text{P}\{^1\text{H}\}$ NMR spectra, the multiplicities of the $^{31}\text{P}\{^1\text{H}\}$ signals of both **2** and **Iso-2a** change upon warming from 193 K (see Figure 3a). Over the entire temperature range examined, the signal of **2** is dominated by scalar couplings to ^{11}B and the quadrupolar relaxation of ^{11}B . This was proven by simultaneously ^{11}B and ^1H decoupled ^{31}P spectra (see $^{31}\text{P}\{^{11}\text{B}, ^1\text{H}\}$ spectrum in Figure 3b), which show a clear collapse of the triplet with a coupling constant of $^1J_{\text{PB}} = 84$ Hz at 193 K. Additional $^{31}\text{P}\{^{19}\text{F}, ^1\text{H}\}$ experiments did not change the signal of **2** (Figure S80), which is reasonable for scalar couplings being significantly smaller than the half line width ($\nu_{1/2} = 90$ Hz). With increasing temperature, the $^{31}\text{P}\{^1\text{H}\}$ signal of **2** becomes first a singlet and then a very broad doublet from 300 K upwards (for a temperature row between 193 K and 333 K of **2**, see Figure S83). The corresponding ^{11}B signal changes from a very broad singlet to a sharper doublet at 300 K corroborating the large scalar coupling constant between ^{11}B and ^{31}P ($^1J_{\text{PB}} = 90$ Hz, see Figure S82), which is accompanied by a downfield shift. Similar behaviour was observed in a temperature screening of a solution containing exclusively **2** in which the ^{11}B signal of **2** started out as being relatively sharp at 193 K (see Figure S84), then first broadened and subsequently narrowed during a steady temperature increase. Again, this went along with a downfield shift (around 1.4 ppm, see Figure S84). The line broadening associated with a downfield shift is probably related to a coalescence of **2** with another species downfield shifted relative to **2**. Given the relatively low energy predicted for isomer **Iso-2d** (*vide supra*) this is likely to be the relevant species, and these variable temperature measurements therefore further hint at the labile nature of the B–P bond in **2** (a ^{11}B shift of 1.4 ppm for **2** would correspond to the presence of around 4% of **Iso-2d**; see SI for calculation). Within this exchange the P–B bond is broken and re-established, which may alter $^1J_{\text{PB}}$ and could therefore give rise to the observed change in shape of the $^{31}\text{P}\{^1\text{H}\}$ signal of **2** during temperature increase (see Figure 3a). The $^{31}\text{P}\{^1\text{H}\}$ signal of **Iso-2a** at $\delta(\text{ppm}) = -102$ exhibits a significantly different response upon temperature increase. At 193 K quadrupolar relaxation seems to dominate producing a broad singlet ($\nu_{1/2} = 98$ Hz). During warm-up, this signal becomes sharper (Figure S79) and develops a quartet splitting which at higher temperatures converts into a quintet (see Figure 3a and Figure S79). ^{31}P NMR with simultaneous ^{19}F and ^1H decoupling revealed that the splitting results from coupling to ^{19}F (see $^{31}\text{P}\{^{19}\text{F}, ^1\text{H}\}$ in Figure 3d). The fact that different multiplets are observed at altered temperatures may be attributed to the presence of two chemically-distinct, hindered C_6F_5 rings, each of which may independently suffer from hindered rotation about its B–C bond (of the structures proposed in Scheme 1 this is only the case for **Iso-2a**). While the ortho (and meta) fluorines of a freely rotating ring would have identical scalar couplings to phosphorus, those in a hindered ring may have different

couplings. Thus, similar coupling of ^{31}P to both fluorines of one freely-rotating C_6F_5 ($^5J_{\text{PF}} = 22.5$ Hz) and only one fluorine of a hindered C_6F_5 ($^5J_{\text{PF}} = 23.5$ Hz) would give rise to the observed quartet (see Figure 3e). At elevated temperatures, stronger rotation of the fluoroaryls and/or rapid P–B-bond opening and closing presumably results in a similar scalar coupling of ^{31}P to all four ortho fluorines, creating a quintet coupling pattern. $^{31}\text{P}\{^{11}\text{B}, ^1\text{H}\}$ measurements at 193 K showed a small reduction in line width (see Figure 3c) while at 233 K no change in line width or multiplet structure was observed (see Figure 3e). This implies that at 193 K the ^{31}P signal of **Iso-2a** is dominated by the quadrupolar relaxation effects of ^{11}B . In contrast, at higher temperatures there is an apparently smaller influence of ^{11}B on the line width which is now mainly dominated by coupling to ^{19}F . Calculations at the TPSS/IGLO-III CPCM(THF) level of theory revealed a $^1J_{\text{PB}}$ of 6 Hz for **Iso-2a** (see Table 1) which fits well to the observation of a small change in line width at 193 K and no change at 233 K. Verifying the P–B bond in **Iso-2a** via ^{31}P - ^{11}B -HMQC was not successful due to the extremely broad ^{11}B signals associated with very short transverse relaxation times (T_2). A ^1H - ^{31}P -HSQC spectrum revealed the expected break in symmetry of the heterocycle in **Iso-2a** compared to **2** since the protons bound to the P-heterocycle exhibit different shifts and ^1H - ^{31}P coupling constants (Figure S81). Taken collectively, these NMR observations therefore strongly support the proposed structure of **Iso-2a**.

Table 1. Calculated (calcd.) ^{31}P and ^{11}B NMR shifts (ppm) and coupling constants $J_{\text{P-B}}$ (Hz) at the TPSS/IGLO-III CPCM(THF) level of theory. The calculated absolute shieldings of compound **2** served as reference for the other compounds. Experimental (exp.) chemical shifts of **2** and **Iso-2a** are also given.

	2	Iso-2a	Iso-2b	Iso-2c	Iso-2d
$\delta(^{31}\text{P})$	+18 (exp.)	-102 (exp.) -98 (calcd.)	-16	-38	-43
$\delta(^{11}\text{B})$	+14 (exp.)	-25 (exp.) -26 (calcd.)	+32	+66	+47
$J_{\text{P-B}}$	87	6			

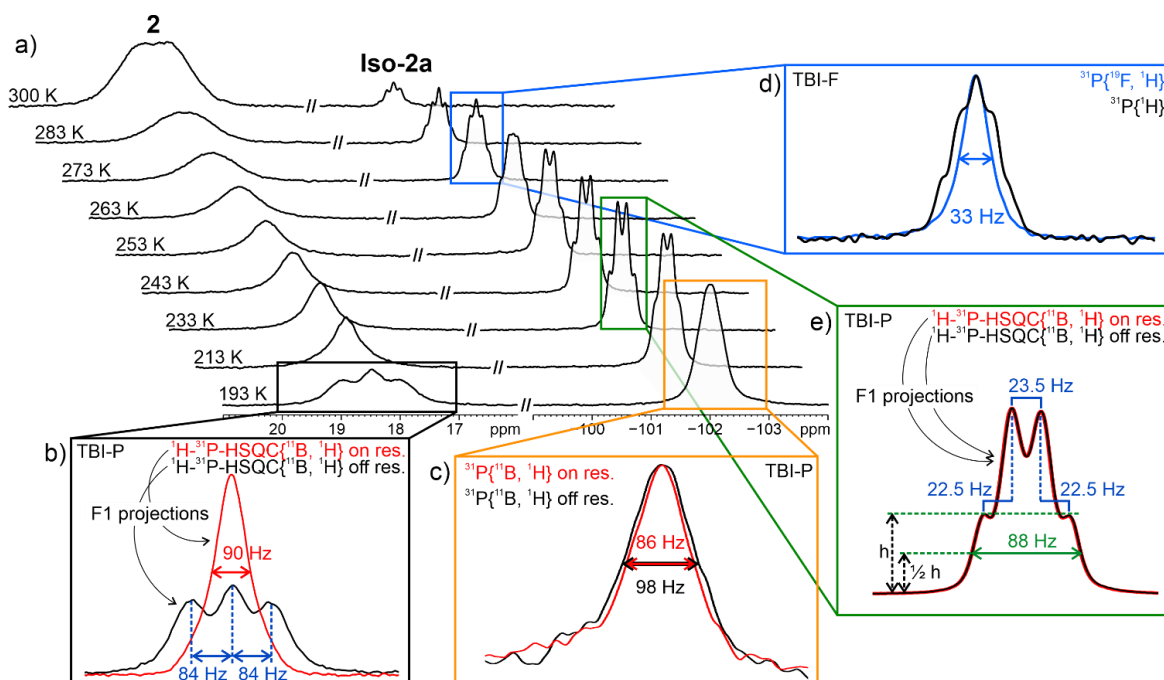
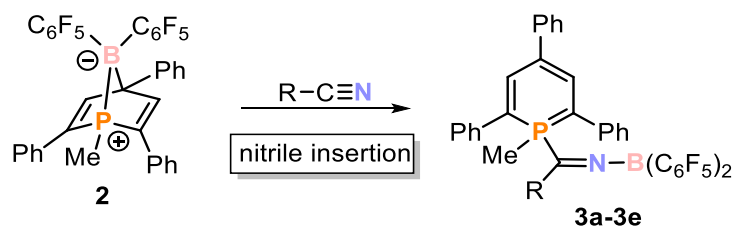


Figure 3. a) $^{31}\text{P}\{^1\text{H}\}$ NMR monitoring (starting from 193 K and warming up to 300 K) of the reaction of **1** with $(\text{C}_6\text{F}_5)_2\text{BCl}$ (see SI for full spectra, Figure S79). The spectral regions of **2** and **Iso-2a** are displayed with the same expansion and intensity scaling. b) Overlaid F1 (indirect dimension) projections of a ^1H - ^{31}P -HSQC with simultaneous ^{11}B and ^1H decoupling in F1 and ^{31}P decoupling in F2 (direct dimension) acquired in the region of **2** (better signal/noise compared to 1d ^{31}P spectrum, see S81 in SI for pulse program). ^{11}B decoupling was applied on resonance (red) and off resonance (black). The spectra were acquired on a TBI-P probe. c) Overlaid 1d ^{31}P spectra with simultaneous ^{11}B and ^1H decoupling. ^{11}B decoupling was applied on resonance (red) and off resonance (black). The spectra were adjusted to same height for a better comparison of line widths. The spectra were acquired on a TBI-P probe. d) Overlaid 1d ^{31}P spectra with ^1H decoupling only (black) and simultaneous ^{19}F and ^1H decoupling (blue). The spectra were adjusted to same height for a better comparison of line widths (see also S80 in SI). The spectra were acquired on a TBI-F probe. e) Overlaid F1 projections of a ^1H - ^{31}P -HSQC with simultaneous ^{11}B and ^1H decoupling in F1 and ^{31}P decoupling in F2 acquired in the region of **Iso-2a**. The spectra were acquired on a TBI-P probe.

3.2.3 Reactivity of **2** toward nitriles

Although the solid-state structure of **2** clearly indicated the formation of a classical P/B Lewis acid/base adduct, XRD, DFT and VT NMR analyses all suggested that reversible, thermal P–B bond cleavage could plausibly provide access to a ring-opened isomer **Iso-2d** possessing unquenched acidic and basic sites. It was thus anticipated that FLP-type behaviour might still be observable for compound **2**, in line with both our initial predictions and results reported previously for some other boron-based Lewis adducts.^[38–41] Indeed, more direct evidence that such reactivity is possible was observed during attempts to dissolve samples of **2** in deuterated acetonitrile for NMR purposes, which led to a clear colour change from orange to deep green. Although activation of other unsaturated C=X bonds by FLPs is very well established, reports of nitrile activation are remarkably scarce, with this having been achieved only for a family of geminal phosphinoboranes reported by Wagner and Sloatweg, which reacted to generate five-membered cyclic structures, and a single, more elaborate enamine/borane system reported by Erker *et al.*^[42–44]



Scheme 2. Synthesis of nitrile insertion products **3a-3e** (yields of isolated compounds are given in parentheses in this caption): **3a**: R = Me (33%), **3b**: R = Ph (64%), **3c**: R = 3,5-Br₂C₆H₃ (43%), **3d**: R = CH₂Cl (39%), **3e**: R = Et (41%).

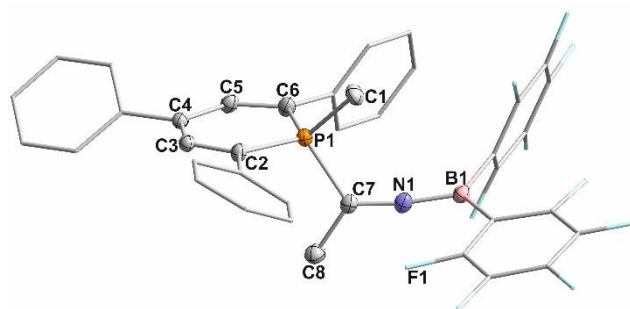
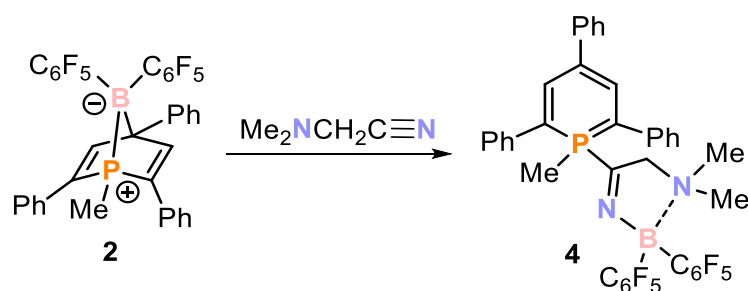


Figure 4. Molecular structure of **3a** in the crystal. Displacement ellipsoids are shown at the 40% probability level; H atoms are omitted for clarity; phenyl and C₆F₅ groups were shown in wireframe for clarity; selected bond lengths [Å] and angles [°]: P1–C1 1.8036(18); P1–C7 1.8822(17); P1–C2 1.7475(16); P1–C6 1.7431(17); C2–C3 1.397(2); C3–C4 1.399(2); C5–C6 1.378(2); C7–N1 1.251(2); N1–B1 1.367(2); C7–C8 1.492(2); C1–P1–C7 102.58(8); P1–C7–N1 120.29(13); C7–N1–B1 172.06(18); C8–C7–N1 124.56(16).

Nevertheless, addition of acetonitrile to a solution of **2** in diethyl ether at room temperature resulted in an immediate colour change to deep green and the ³¹P{¹H} NMR spectrum of the reaction mixture indicated the selective formation of a single new species **3a** (Scheme 2), as evidenced by a sharp singlet resonance at $\delta(\text{ppm}) = +0.6$, that is shifted to higher field relative to **2** (Figure S11). In the proton-coupled ³¹P NMR spectrum this signal appears as a complex multiplet (Figure S12). Additionally, the ¹¹B{¹H} NMR spectrum shows a broad signal at $\delta(\text{ppm}) = +21.9$ that is shifted to lower field relative to **2**, which is qualitatively consistent with a change from four- to three-coordinate boron. Single crystals were grown by slow evaporation of an *n*-hexane solution of **3a** at room temperature. Gratifyingly, the crystallographic characterization confirmed activation of the nitrile triple bond, although this was unexpectedly accompanied by cleavage of not just the P–B bond but also the C–B bond of **2** (Figure 4) with the nitrile having formally inserted into the former. The resulting BCN moiety is almost linear (C7–N1–B1 172°), and the N1–B1 distance is significantly shortened (1.367(2) Å) compared to common N–B single bonds (1.57 Å),^[30] suggesting some multiple bond character due to donation of electron density from the nitrogen lone pair into the empty p orbital on boron. The nitrile-derived C7–N1 distance is in the range of typical C–N double bonds (1.251(2) Å),^[37] and the P1–C7 separation (1.8822(17) Å) is in the range of single bonds according to the sum of the covalent radii (P–C 1.86 Å).^[30]

Other substituted nitriles were subsequently employed in similar reactions, yielding compounds **3b-3e** (Scheme 2) as deep green crystals in moderate yields (33–64 %). The crystallographic characterization of **3b** and **3c** revealed structures similar to that already discussed for **3a**, with essentially linear C–N–B arrangements and short B–N distances (for more details, see SI). Multinuclear NMR data of all compounds were also in line with those found for **3a**.

A slightly different outcome was observed using 2-(dimethylamino)acetonitrile (Scheme 3), which contains an additional pendant donor functionality, as was indicated by an immediate colour change from orange to deep pink (*c.f.* deep green for compounds **3a-3e**) upon addition of the substrate to a solution of **2** in diethyl ether. NMR analysis indicated the clean formation of a new product **4** that features a $^{31}\text{P}\{\text{^1H}\}$ resonance at $\delta(\text{ppm}) = -9.2$, which is shifted to higher field relative to **3a-3e** ($\delta(\text{ppm}) = -1.0$ to $+0.6$). The $^{11}\text{B}\{\text{^1H}\}$ signal (11.5 ppm for **4** vs. *ca.* 22–26 ppm for **3a-3e**) is also shifted to higher field, suggesting a different product structure, which was confirmed by single crystal X-ray diffraction (Figure 5). The molecular structure of **4** in the crystal reveals insertion of the nitrile into the P–B bond of **2** analogously to **3a-3e**. However, instead of a linear CNB moiety a five-membered Lewis adduct is formed in which the boron moiety interacts with both available nitrogen atoms. The rather elongated B1–N2 bond (1.7322(16) Å) of **4** is consistent with a dative interaction between B1 and the lone pair of N2. This interaction has a significant influence on the solid-state structure and spectroscopic properties of **4**. The crystallographic characterization further shows that the C–N–B fragment is no longer linear ($111.27(10)^\circ$) and the B1–N1 bond distance (1.5237(16) Å) is elongated compared to **3a** (1.367(2) Å). The UV-Vis spectrum of **4** shows an additional absorbance at $\lambda = 523$ nm, which explains the apparent colour change from green (for **3a-3e**) to pink.



Scheme 3. Reaction of **2** with 2-(dimethylamino)acetonitrile.

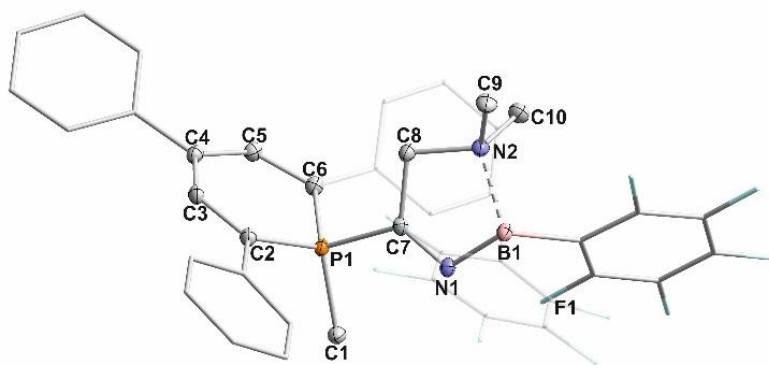


Figure 5. Molecular structure of **4** in the crystal. Displacement ellipsoids are shown at the 40% probability level; H atoms are omitted for clarity; phenyl and C₆F₅ groups were shown in wireframe for clarity; selected bond lengths [Å] and angles [°]: P1–C7 1.8435(12); P1–C2 1.7631(12); P1–C6 1.7612(12); P1–C1 1.8231(12); C2–C3 1.3916(17); C3–C4 1.3985(18); C4–C5 1.4070(17); C5–C6 1.3822(17); C7–C8 1.5084(16); N2–B1 1.7322(16); B1–N1 1.5237(16); N1–C7 1.2578(16); C7–N1–B1 111.27(10); N1–B1–N2 100.38(9); P1–C7–N1 125.34(9); C8–N2–B1 103.

To analyse the reaction course of **2** with nitriles in more detail, DFT calculations were again performed at the ω B97X-D/6-311+G** level of theory (all energy values discussed are ΔG values in kcal·mol⁻¹; see Figure 6 and *vide supra*). As already discussed, an initial ring opening of **2** forms isomer **Iso-2d**, which can act as an FLP for the activation of nitriles, modelled here using acetonitrile. This first step is consistent with the chemical exchange between **2** and **Iso-2d** suggested by ¹¹B NMR (Figure S84 and *vide supra*). Nitrile binding to the boron centre of **Iso-2d** then gives an adduct **Int-A** with almost identical energy. The subsequent rate-determining step involves cyclisation to give the high-energy bridged intermediate **Int-B** (this proceeds over an energy barrier of +21.5 kcal·mol⁻¹, which is slightly higher than expected given the rapid reactivity observed at room temperature, but is nevertheless in satisfactory agreement with the experimental result, given the errors typically associated with the computational methods employed). This compound is highly unstable and rapidly rearranges with cleavage of the B–C bond. Flattening of the six-membered λ^5 -phosphinine-derived ring gives initially **Int-C**, which readily isomerises through P–C bond rotation to the slightly more stable conformer **3a**, as is observed in the solid-state structure.

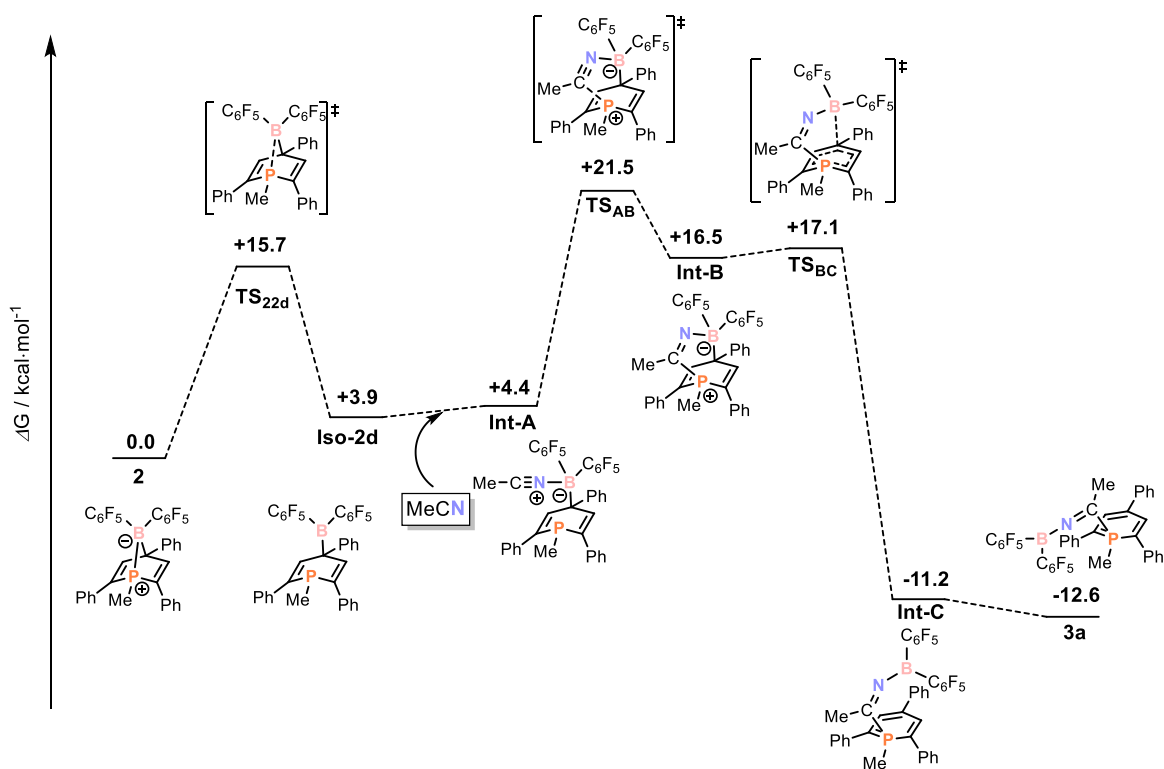
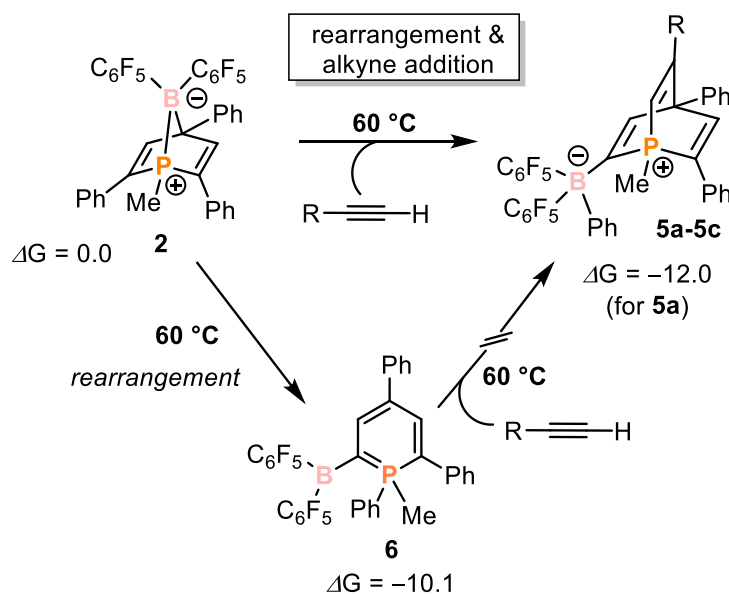


Figure 6. Relative ω B97X-D/6-311+G** energies (calculated free energies ΔG in kcal·mol⁻¹) for the conversion of **2** into **3**.

3.2.4 Reactivity of **2** toward alkynes

Encouraged by the high reactivity of **2** toward the strong, polar triple bond of nitriles, we were motivated to also test the reactivity of **2** toward the similarly strong, but apolar triple bonds of simple alkynes. The combination of **2** with one equivalent of phenylacetylene in benzene did not show any significant reactivity at room temperature. However, when heating this mixture to $T = 60\text{ }^{\circ}\text{C}$ overnight, the selective formation of a new product **5a** was observed (Scheme 4), indicated by the detection of a single new resonance in the $^{31}\text{P}\{^1\text{H}\}$ NMR spectrum at $\delta(\text{ppm}) = 1.7$ (Figure S53 and Figure S54). This signal appears within the range observed for the nitrile activation products **3a-3e**, which suggests the formation of a similar tetracoordinate phosphorus environment. In contrast, the $^{11}\text{B}\{^1\text{H}\}$ NMR signal of **5a** is shifted to significantly higher field relative to **3a-3e** (-11.2 ppm for **5a** vs. *ca.* 22-26 ppm for **3a-3e**), and suggests a tetracoordinate rather than tricoordinate boron moiety (Figure S55). The reactions of **2** with 4-(trifluoromethyl)- and 4-bromophenylacetylene led to analogous results, as the selective formation of the corresponding new compounds **5b** and **5c** was observed, which show very similar heteroatom NMR resonances ($^{31}\text{P}\{^1\text{H}\}$ $\delta(\text{ppm}) = 2.1$ (**5b**), 1.9 (**5c**); $^{11}\text{B}\{^1\text{H}\}$ $\delta(\text{ppm}) = -11.2$ (**5b**), -11.1 (**5c**)). Compounds **5a-5c** could be isolated as light red powders in good yields (up to 72%) by treatment of the crude product with *n*-hexane and thorough drying of the resulting precipitate under vacuum.



Scheme 4. Reaction of **2** with phenylacetylene derivatives, leading to the formation of **5a-5c**, thermal rearrangement of **2** to **6**, and relative ω B97X-D/6-311+G** energies (calculated free energies ΔG in kcal·mol⁻¹); **5a**: R = Ph (61%); **5b**: R = 4-CF₃-C₆H₄ (62%); **5c**: R = 4-Br-C₆H₄ (72%).

Single crystals of **5b** and **5c** were grown by slow evaporation of *n*-hexane solutions. The single crystal X-ray structures reveal the formation of a λ^4 -1-phosphabarrelenium moiety, in which the alkyne bridges between P1 and C4 of the phosphinine-derived heterocycle. As with nitriles, alkyne addition is accompanied by cleavage of both the P–B and C–B bonds of **2**. Remarkably, this is accompanied by migration of the B(C₆F₅)₂ moiety *via* formal insertion into the C2–Ph bond of **2**. Due to the modest quality of the structural data of **5c** (Figure S106 and Table S2), only the structural data of **5b** is discussed in detail here. The P1–C8 bond length (1.783(4) Å) is in the range of common P–C single bonds, while the C4–C7 bond (1.577(5) Å) is in the range of C–C single bonds.^[37] The C2–C3, C5–C6 and C8–C7 distances are typical for C=C double bonds.^[37] The bond lengths and angles of **5b** are consistent with other reported 1-phosphabarrelenes, except for P1–C8, which is slightly shortened (1.783(4) Å *vs.* average 1.836 Å).^[45–47] As a corollary, the angle C2–P1–C6 is also widened by roughly 8° compared to other 1-phosphabarrelenes (103.36(17)° *vs.* average 95.351°). These changes can be attributed to the tetracoordinate nature of the P atom, and were also observed for a selenium-substituted phosphabarrelene.^[45] Finally, the B1–C2 bond length in **5b** (1.636(5) Å) is consistent with typical B–C single bonds.^[30]

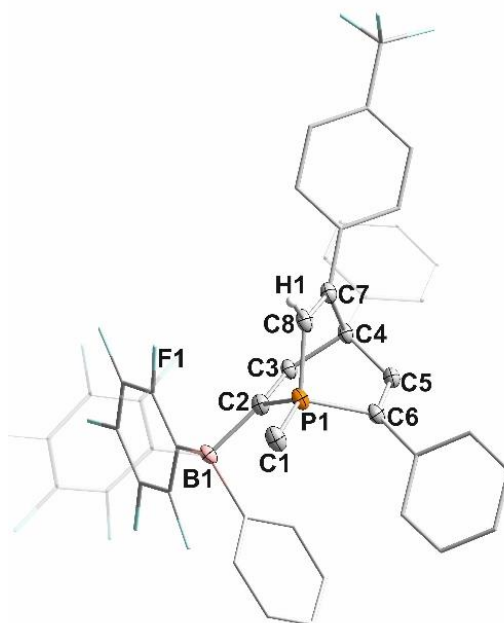


Figure 7. Molecular structure of **5b** in the crystal. Displacement ellipsoids are drawn at the 40% probability level; H atoms are omitted for clarity; phenyl; C₆H₄CF₃ and C₆F₅ groups were shown in wireframe for clarity; a disordered *n*-hexane molecule is omitted for clarity; selected bond lengths [Å] and angles [°]: P1–C8: 1.783(4); C4–C7: 1.577(5); P1–C2: 1.799(4); P1–C6: 1.816(4); P1–C1: 1.781(4); C2–C3: 1.335(5); C3–C4: 1.560(5); C4–C5: 1.541(5); C5–C6: 1.335(5); C7–C8: 1.334(5); C2–B1: 1.636(5); P1–C8–C7: 112.1(3); C8–C7–C4: 116.4(3); C2–P1–C6: 103.36(17); C3–C4–C5: 107.2(3).

Typically, Diels-Alder type [4+2] cycloaddition of alkynes to neutral phosphinines to form 1-phospha-barrelenes must be performed using highly reactive arynes or activated alkynes (such as F₃CC≡CCF₃) as dienophiles.^[48,45,46,49,50,47] That phospha-norbornadiene **2** reacts with simple phenylacetylenes under modest reaction conditions is therefore significant, and is reminiscent of the *cationic* 1-methyl-phosphinium salt [1-Me-2,6-(SiMe₃)₂-3,5-Ph₂-PC₃H][GaCl₄]^[51] that upon reaction with 4-octyne affords a 1-methyl-phospha-barrelenium tetrachlorogallate which was characterized by NMR spectroscopy.

While activation of alkynes is known to occur for other FLP systems, the concomitant B(C₆F₅)₂ migration observed in this case suggests an atypical activation mechanism.^[42,43,52–60] To gain more insight, a solution of **2** was monitored by ³¹P{¹H} NMR spectroscopy at 60 °C in the absence of alkyne, which resulted in the slow formation of a new species observed as a sharp singlet at δ(ppm) = +1.3 ppm (no analogous transformation was observed at r.t.). The chemical shift of this species is quite similar to those of **5a-5c** (δ(ppm) = 1.7–2.0), suggesting a similar environment at P. The structure of this species could not be determined by single crystal X-ray diffractometry; however, LIFDI-MS spectrometry, elemental analysis and NMR observations are consistent with the structure **6** depicted in Scheme 4. In particular, the calculated ³¹P (δ(ppm) = +5 vs. +1.3 observed) and ¹¹B NMR (δ(ppm) = +43 vs. +54 observed) shifts of **6** are in agreement with the observed shifts (Table S5). Additionally, the calculated and observed UV-Vis spectrum of **6** are in reasonable agreement (Figure S104 and S115).

VT $^{31}\text{P}\{^1\text{H}\}$ NMR monitoring of **2** was also carried out in the presence of an alkyne substrate. When 4-(trifluoromethyl)phenylacetylene was added to **2** at room temperature only a small singlet in the ^{31}P NMR spectrum at $\delta(\text{ppm}) = 1.4$ ppm corresponding to the product **5b** could be observed next to the signals of **2** and **Iso-2a** (Figure S89). $^{31}\text{P}\{^1\text{H}\}$ NMR monitoring at 60 °C showed that **2** and **Iso-2a** convert quite selectively to the product **5b** (accompanied by generation of only 5% of **6**) within three hours (Figure S89), with no other observable intermediates. Notably, when the same alkyne was added to compound **6** at room temperature no reaction occurred, even upon heating to 60 °C. Thus, **6** does not appear to be an intermediate during the formation of **5a-5c**, but rather a competitive side-product that forms selectively in the absence of alkyne (Scheme 4, see Figure S114, SI, and the discussion in section S5.4 of the SI for further details).

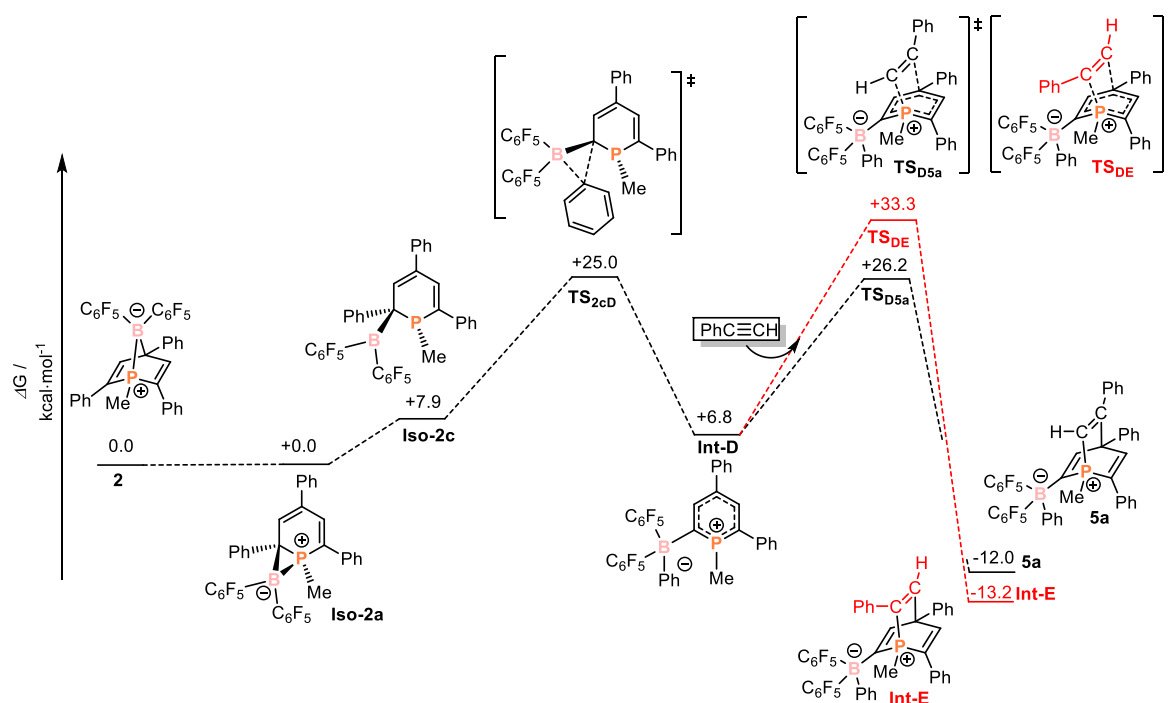


Figure 8. Relative $\omega\text{B97X-D/6-311+G}^{**}$ energies (calculated free energies ΔG in $\text{kcal}\cdot\text{mol}^{-1}$) for the conversion of **2** into **5a**.

Based on the structures of products **5** and **6**, it was anticipated that the observed reactivity might be proceeding through the isomeric form of **2**, **Iso-2c** (*vide supra*), in which the $\text{B}(\text{C}_6\text{F}_5)_2$ has migrated fully to the ‘ortho’ position of the phosphorus heterocycle. This proposal is supported by DFT calculations which show that, following isomerization to this ‘open’ form, a subsequent 1,2-phenyl migration can occur *via* **TS_{2cD}** ($\Delta G = 25$ $\text{kcal}\cdot\text{mol}^{-1}$), which is accessible at elevated temperatures. This results in a zwitterionic methylphosphinium borate species **Int-D**. The alkyne subsequently adds to **Int-D** in a 1,4-manner forming **5a**,^[51] in a step that can formally be considered as a hetero-Diels-Alder reaction. Alternatively, this step can be viewed as another FLP type reaction, in which the conjugated phosphorus heterocycle provides both the Lewis acidic and basic sites (*c.f.* **G**,

Scheme 1) needed to activate the alkyne. In this interpretation it is expected that the aryl-substituted carbon atom from the phenylacetylene derivative should end up bound to the formally Lewis basic fragment of the FLP,^[24g] due to better stabilisation of the positive charge that will accumulate on this carbon atom during the interaction of the alkyne with the Lewis acidic centre. Indeed, an alternative reaction pathway between **Int-D** and phenylacetylene to generate regioisomer **Int-E** was also calculated and it was found that although **Int-E** is thermodynamically slightly favoured over **5a**, the associated transition state **TS_{DE}** is significantly higher in energy than **TS_{D5a}** (+33.3 vs. +26.2 kcal·mol⁻¹, see Figure 8). This implies that the phosphorus centre is the Lewis acidic site in this system, and “*para-C4*” is the Lewis basic site, which is consistent with the FLP type activation of dihydrogen by 1,3,5-triphosphinine derivatives.^[9] Thus, the phenyl migration that transforms **Iso-2c** into **Int-D** results in an *umpolung* effect, where the phosphorus centre changes in reactivity from nucleophilic (as observed in the activation of nitriles) to electrophilic (as observed in the activation of alkynes).

3.3 Conclusion

The unusual compound **2** incorporating a boron atom in a phospha-norbornadiene scaffold is readily accessible by reaction of a λ^4 -phosphinine anion and a chloroborane. Even though **2** is nominally a classical Lewis acid/base adduct it shows FLP type reactivity due to its strained bicyclic structure, readily activating the C \equiv N triple bonds of various nitriles. These nitriles formally insert into the P–B bond, with concomitant splitting of the B–C bond, and ultimately connect to the resulting B(C₆F₅)₂ moiety in a linear fashion (**3a-3e**) unless an additional donor functionality is also present (as in **4**). DFT calculations revealed that these reactions proceed *via* a low energy ring-opening of the bridging norbornadiene P–B bond. Conversely, reactions of **2** with phenylacetylene derivatives afford phosphabarrelenes **5a-5c** *via* a mechanism that involves initial migration of “(C₆F₅)₂B”, through formal insertion into a C–C bond. This work highlights the ability of seemingly classical Lewis pairs to form reactive intermediates by reversible heterolytic element-element bond dissociation, while also illustrating the ability of phosphinine-derived Lewis bases to engage in interesting FLP reactivity that is not easily accessible using more conventional λ^3, σ^3 -phosphines. The application of these principles to the activation of further small molecules is a worthwhile subject for future investigations.

3.4 Experimental Details

3.4.1 General Considerations

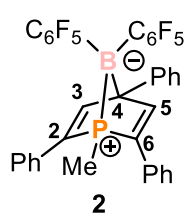
All experiments were performed under an atmosphere of dry argon by using standard glovebox techniques. Diethyl ether and *n*-hexane were purified, dried, and degassed with an MBraun SPS800 solvent purification system. NMR spectra were recorded on Bruker Avance 300 MHz and Avance 400 MHz spectrometer equipped with a BBF-H-D probe at 300 K. Temperature screening were performed at a Bruker Avance 400 MHz spectrometer equipped with a BB-H-D probe and a Bruker Avance III HD 600 MHz spectrometer with a fluorine selective TBIF probe and a phosphorus selective TBIP probe. ^1H and ^{13}C spectra were referenced externally to TMS and calibrated on the corresponding residual solvent signals. ^{11}B spectra were reference externally to $\text{Et}_2\text{O}\times\text{BF}_3$. ^{19}F spectra were referenced externally to CFCl_3 . ^{31}P spectra were referenced externally to 85% H_3PO_4 (aq.). The assignment of ^1H and ^{13}C NMR signals was confirmed by two-dimensional (COSY, HSQC, and HMBC) experiments. For the chemical assignment 2,4,6-triphenylphosphinine will be referred to as TPP. UV/Vis spectra were recorded on a Varian Cary 50 spectrometer. Elemental analyses were determined by the analytical department of Regensburg University. Mass spectra were performed with Jeol AccuTOF GCX LIFDI-MS by the analytical Department of Regensburg University. **1** was synthesized according to a literature procedure and $(\text{C}_6\text{F}_5)_2\text{B-Cl}$ was synthesized by an unpublished procedure.^[7] Nitriles and alkynes were purchased from Sigma-Aldrich and used as received.

X-ray Crystallography: The single-crystal X-ray diffraction data were recorded on an Agilent Technologies SuperNova and a GV1000, TitanS2 diffractometer with $\text{Cu-}K_\alpha$ radiation ($\lambda = 1.54184 \text{ \AA}$). Either semi-empirical multi-scan absorption corrections^[61] or analytical ones^[62] were applied to the data. The structures were solved with SHELXT^[63] and least-square refinements on F^2 were carried out with SHELXL.^[64] The hydrogen atoms were located in idealized positions and refined isotropically with a riding model.

CCDC 1946109 (for **2**), CCDC 1946111 (for **3a**), CCDC 1946112 (for **3b**), CCDC 1946114 (for **3c**), CCDC 1946115 (for **4**), CCDC 1946116 (for **5b**) and CCDC 1946118 (for **5c**), contain the supplementary crystallographic data for this paper. These data can be obtained free of charge from The Cambridge Crystallographic Data Centre.

3.4.2 Synthesis of **2**

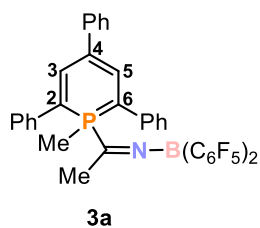
Compound 2 was prepared in an MBraun argon glove box. 2 is sensitive toward moisture and air. 2 is soluble and stable in diethyl ether, benzene and toluene, it is not stable in tetrahydrofuran.



(C₆F₅)₂B-Cl (171 mg, 0.45 mmol, 1 equiv.) was dissolved in *n*-hexane (2 mL), cooled to -35 °C and slowly added to a suspension of **1** (200 mg, 0.45 mmol, 1 equiv.) cooled to -35 °C in *n*-hexane (2 mL). An immediate colour change from deep pink to orange was observed. The orange suspension was stirred for 15 minutes and the precipitate was separated from the solution. The bright orange solid was extracted into diethyl ether (3 x 2 mL) and the solution was reduced in volume by half. After storage at -35 °C, **2** was isolated as a light orange powder. Yield 107 mg, 35%. Elemental analysis calcd. for C₃₆H₂₀BF₁₀P (Mw = 684.32 g·mol⁻¹) C 63.19, H 2.95; found C 63.12, H 3.17. UV-Vis: (*n*-hexane, λ_{max} / nm, ε_{max} / L·mol⁻¹·cm⁻¹): 221 (18278), 229 (15854), 290 (5399). ¹H NMR (400.13 MHz, 300 K, C₆D₆): δ = 1.47 (d, 3H, *Me*, ²J_{PH} = 12.5 Hz), 6.91 (m, 4H, C^{2,6}-*H* of C^{2,6}-Ph), 7.04 (m, 6H, C^{3,4,5}-*H* of C^{2,6}-Ph), 7.20 (m, 3H, C^{2,4,6}-*H* of C⁴-Ph), 7.27 (m, 2H, C^{3,5}-*H* of C⁴-Ph), 7.56 (d, 2H, C^{3,5}-*H* of TPP, ³J_{PH} = 35 Hz). ¹³C{¹H} NMR (100.61 MHz, 300 K, C₆D₆): δ = 1.51 (d, *Me*-TPP, ¹J_{CP} = 25 Hz), 64.28 (br, C⁴ of TPP), 117.02 (br, C¹ of C₆F₅), 126.25 (s, C⁴ of C⁴-Ph), 127.19 (d, C^{2,6} of C^{2,6}-Ph, ³J_{CP} = 4 Hz), 127.39 (m, C^{2,6} of C⁴-Ph), 128.29 (s, C^{3,5} of C^{2,6}-Ph), 129.26 (s, C⁴ of C^{2,6}-Ph), 134.63 (d, C¹ of C^{2,6}-Ph, ²J_{CP} = 5 Hz), 137.48 (br d, C₆F₅, ¹J_{FC} = 250 Hz), 137.91 (m, C^{2,6} of TPP, ¹J_{CB} = 48 Hz), 140.12 (br d, C₆F₅, ¹J_{FC} = 260 Hz), 143.38 (d, C¹ of C⁴-Ph, J_{CF} or J_{CB} = 14 Hz), 147.46 (br d, C₆F₅, ¹J_{FC} = 244 Hz), 156.62 (d, C³ and C⁵ of TPP, ²J_{CP} = 17 Hz). ³¹P{¹H} NMR (161.98 MHz, 300 K, C₆D₆): δ = 18.7 (broad unresolved multiplet, the ¹J_{PB} could not be exactly determined to the line broadening *ca.* ¹J_{PB} = 60 Hz; minor **iso-2a** is also observed). ³¹P NMR (161.98 MHz, 300 K, C₆D₆): δ = 18.6 (br m). ¹¹B{¹H} NMR (128.38 MHz, 300 K, THF-d₈): δ = 14.71 (br d, ¹J_{BP} = 90 Hz). ¹¹B NMR (128.38 MHz, 300 K, C₆D₆): δ = 14.1 (bs). ¹⁹F NMR (376.66 MHz, 300 K, C₆D₆): δ = -129.40 (br, 4F), -156.39 (t, ³J_{FF} = 21 Hz, 2F), -163.01 (m, 4F). MS (LIFDI, toluene): *m/z* (%) = 684.10 M⁺ (**2**); 339.12 ([1-Me-P(C₅H₂Ph₃)]).

3.4.3 Synthesis of **3a**

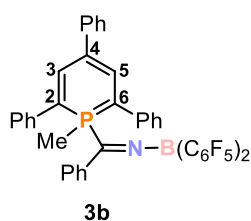
Compounds **3a-3e** were prepared in an MBraun argon glove box. **3a-3e** are sensitive toward moisture and air. **3a-3e** are soluble and stable in hexane, diethyl ether, benzene.



Acetonitrile (4 μL, 0.059 mmol, 1 equiv.) was added to a solution of **2** (40 mg, 0.059 mmol, 1 equiv.) in diethyl ether (1 mL) at room temperature. An immediate colour change from orange to deep green was observed. The reaction mixture was stirred for 15 minutes, the solvent was completely removed, and the dark green oily residue was extracted with *n*-pentane (2 x 2 mL). After reducing the solution to half and storage at room temperature for 1 hour, **3a** could be isolated as dark green needles. Yield: 14 mg (33%). Elemental analysis calcd. for C₃₈H₂₀BF₁₀NP (Mw = 725.38 g·mol⁻¹) C 62.92, H 3.20, N 1.93; found: C 63.28, H 3.31, N 1.42. UV-Vis: (*n*-hexane, λ_{max} / nm, ε_{max} / L·mol⁻¹·cm⁻¹): 224 (41862), 253 (33000), 320sh (11060). ¹H NMR (400.13 MHz, 300 K, C₆D₆): δ = 1.74 (d, 3H, ²J_{PH} = 13 Hz, *Me*-TPP), 2.09 (d, 3H, ³J_{PH} = 8 Hz, *Me*CN), 6.94 –

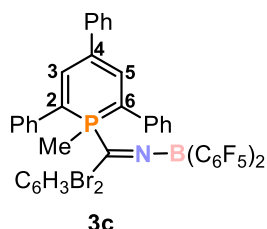
7.13 (m, 11H, H_{aromatic}), 7.27 (m, 2H, H_{aromatic}), 7.41 (m, 2H, H_{aromatic}), 7.63 (s, 1H, H_{aromatic}), 7.70 (s, 1H, H_{aromatic}). $^{13}\text{C}\{^1\text{H}\}$ NMR (100.61 MHz, 300 K, C_6D_6): $\delta = 9.00, 24.43, 82.00, 114.39, 124.50, 125.74, 126.97, 128.59, 128.68, 137.30, 139.36, 140.15, 142.75, 147.50, 156.87$; due to the low S/N, not all of the ^{13}C signals could be resolved. $^{31}\text{P}\{^1\text{H}\}$ NMR (161.98 MHz, 300 K, C_6D_6): $\delta = 0.6$ (s). ^{31}P NMR (161.98 MHz, 300 K, C_6D_6): $\delta = 0.6$ (m). $^{11}\text{B}\{^1\text{H}\}$ NMR (128.38 MHz, 300 K, C_6D_6): $\delta = 21.92$ (br). ^{11}B NMR (128.38 MHz, 300 K, C_6D_6): $\delta = 21.4$ (br s). $^{19}\text{F}\{^1\text{H}\}$ NMR (376.66 MHz, 300 K, C_6D_6): $\delta = -131.81$ (m, 4F), -151.07 (m, 2 F), -161.51 (m, 4F).

3.4.4 Synthesis of **3b**



Benzonitrile (7.5 μL , 0.073 mmol, 1 equiv.) was added to a solution of **2** (50 mg, 0.073 mmol, 1 equiv.) in diethyl ether (1 mL) at room temperature. An immediate colour change from orange to deep green was observed. The reaction mixture was stirred for 15 minutes, the solvent was completely removed, and the dark green oily residue was extracted with *n*-pentane (3 x 2 mL). After reducing the solution to half and storage at $-35\text{ }^\circ\text{C}$ for 1 hour, **3b** could be isolated as dark green needles. Yield: 37 mg (64%). Elemental analysis calcd. for $\text{C}_{43}\text{H}_{25}\text{BF}_{10}\text{NP}$ ($M_w = 787.45\text{ g}\cdot\text{mol}^{-1}$) C 65.59, H 3.20, N 1.78; found: C 65.33, H 3.34, N 1.80. UV-Vis: (*n*-hexane, λ_{max} / nm, ϵ_{max} / $\text{L}\cdot\text{mol}^{-1}\cdot\text{cm}^{-1}$): 259 (12766), 320sh (3979). ^1H NMR (400.13 MHz, 300 K, C_6D_6): $\delta = 2.00$ (d, 3H, $^2J_{\text{PH}} = 13\text{ Hz}$, *Me*-TPP), 6.89 – 7.11 (m, 15H, H_{aromatic}), 7.26 (m, 2H, H_{aromatic}), 7.38 (m, 2H, H_{aromatic}), 7.50 (s, 1H, H_{aromatic}), 7.59 (s, 1H, H_{aromatic}), 7.94 (d, 1H, H_{aromatic}). $^{13}\text{C}\{^1\text{H}\}$ NMR (100.61 MHz, 300 K, C_6D_6): $\delta = 12.10, 85.55, 108.11, 115.10, 124.89, 125.10, 126.37, 128.82, 128.99, 129.44, 129.69, 131.95, 132.39, 132.65, 132.96, 137.65, 139.69, 140.16, 140.29, 147.96, 151.26$; due to the low S/N, not all of the ^{13}C signals could be resolved. $^{31}\text{P}\{^1\text{H}\}$ NMR (161.98 MHz, 300 K, C_6D_6): $\delta = -0.1$ (s). ^{31}P NMR (161.98 MHz, 300 K, C_6D_6): $\delta = -0.1$ (m). $^{11}\text{B}\{^1\text{H}\}$ NMR (128.38 MHz, 300 K, C_6D_6): $\delta = 23.02$ (bs). ^{11}B NMR (128.38 MHz, 300 K, C_6D_6): $\delta = 23.18$ (br s). $^{19}\text{F}\{^1\text{H}\}$ NMR (376.66 MHz, 300 K, C_6D_6): $\delta = -131.26$ (m, 4F), -151.01 (m, 2 F), -161.19 (m, 4F).

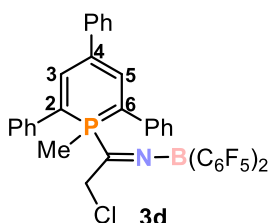
3.4.5 Synthesis of **3c**



3,5-Dibromobenzonitrile (19 mg, 0.073 mmol, 1 equiv.) was added to a solution of **2** (50 mg, 0.073 mmol, 1 equiv.) in diethyl ether (1 mL) at room temperature. An immediate colour change from orange to deep green was observed. The reaction mixture was stirred for 15 minutes, the solvent was completely removed, and the dark green oily residue was extracted with *n*-hexane (2 mL). After reducing the solution to half and storage at room temperature, **3c** could be isolated as dark green crystals. Yield: 30 mg (43%). Elemental analysis calcd. for $\text{C}_{43}\text{H}_{23}\text{BBr}_2\text{F}_{10}\text{NP}$ ($M_w = 945.24\text{ g}\cdot\text{mol}^{-1}$) C 54.64, H 2.45, N 1.48; found: C 53.99, H 2.58, N 1.39. UV-Vis: (*n*-hexane, λ_{max} / nm,

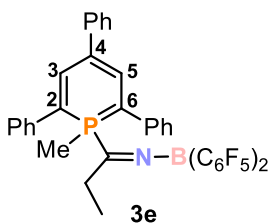
$\epsilon_{\max} / \text{L} \cdot \text{mol}^{-1} \cdot \text{cm}^{-1}$): 260 (14990), 310sh (7040), 432 (2230). ^1H NMR (400.13 MHz, 300 K, C_6D_6): $\delta = 2.12$ (d, 3H, $^2J_{\text{PH}} = 13$ Hz, *Me*-TPP), 7.08 – 7.13 (m, 2H, H_{aromatic}), 7.15 (s, 4H, H_{aromatic}), 7.31 – 7.34 (m, 3H, H_{aromatic}), 7.45 – 7.50 (m, 3H, H_{aromatic}), 7.68 (m, 2H, H_{aromatic}), 7.73 (s, 1H, H_{aromatic}), 7.81 (s, 1H, H_{aromatic}), 8.19 (s, 1H, H_{aromatic}). $^{13}\text{C}\{^1\text{H}\}$ NMR (100.61 MHz, 300 K, C_6D_6): $\delta = 11.54, 84.93, 115.74, 124.15, 124.89, 125.33, 126.28, 128.56, 128.61, 130.93, 137.26, 137.94, 138.94, 142.24, 140.14, 147.52, 148.24$; due to the low S/N, not all of the ^{13}C signals could be resolved. $^{31}\text{P}\{^1\text{H}\}$ NMR (161.98 MHz, 300 K, C_6D_6): $\delta = 0.6$ (s). ^{31}P NMR (161.98 MHz, 300 K, C_6D_6): $\delta = 0.6$ (m). $^{11}\text{B}\{^1\text{H}\}$ NMR (128.38 MHz, 300 K, C_6D_6): $\delta = 23.3$ (br s). ^{11}B NMR (128.38 MHz, 300 K, C_6D_6): $\delta = 23.6$ (br s). $^{19}\text{F}\{^1\text{H}\}$ NMR (376.66 MHz, 300 K, C_6D_6): $\delta = -131.29$ (m, 4F), -150.18 (m, 2F), -160.82 (m, 4F).

3.4.6 Synthesis of **3d**



2-Chloroacetonitrile (4.6 μL , 0.073 mmol, 1 equiv.) was added to a solution of **2** (50 mg, 0.073 mmol, 1 equiv.) in diethyl ether (1 mL) at room temperature. An immediate colour change from orange to deep green was observed. The reaction mixture was stirred for 15 minutes, the solvent was completely removed, and the dark green oily residue was extracted with *n*-hexane (3 x 2 mL). After reducing the solution to half and storage at room temperature, **3d** could be isolated as dark green solid. Yield: 22 mg (39%). Elemental analysis calcd. for $\text{C}_{38}\text{H}_{22}\text{BClF}_{10}\text{NP}$ ($M_w = 759.82 \text{ g} \cdot \text{mol}^{-1}$) C 60.07, H 2.92, N 1.84; found: C 60.46, H 3.27, N 1.23. UV-Vis: (*n*-hexane, $\lambda_{\max} / \text{nm}$, $\epsilon_{\max} / \text{L} \cdot \text{mol}^{-1} \cdot \text{cm}^{-1}$): 248 (22550), 307 (13470), 416 (6130). ^1H NMR (400.13 MHz, 300 K, C_6D_6): $\delta = 1.78$ (d, 3H, $^2J_{\text{PH}} = 13$ Hz, *Me*-TPP), 4.25 (s, CH_2CN), 6.97 – 7.13 (m, 11H, H_{aromatic}), 7.28 (m, 2H, H_{aromatic}), 7.36 (m, 2H, H_{aromatic}), 7.55 (s, 1H, H_{aromatic}), 7.63 (s, 1H, H_{aromatic}). $^{13}\text{C}\{^1\text{H}\}$ NMR (100.61 MHz, 300 K, C_6D_6): $\delta = 10.05, 45.78, 81.91, 114.97, 124.63, 124.75, 126.08, 126.91, 128.73, 137.19, 138.76, 139.86, 140.13, 147.80, 153.86$; due to the low S/N, not all of the ^{13}C signals could be resolved. $^{31}\text{P}\{^1\text{H}\}$ NMR (161.98 MHz, 300 K, C_6D_6): $\delta = -1.0$ (s). ^{31}P NMR (161.98 MHz, 300 K, C_6D_6): $\delta = -1.0$ (m). $^{11}\text{B}\{^1\text{H}\}$ NMR (128.38 MHz, 300 K, C_6D_6): $\delta = 25.8$ (br s). ^{11}B NMR (128.38 MHz, 300 K, C_6D_6): $\delta = 25.8$ (br s). $^{19}\text{F}\{^1\text{H}\}$ NMR (376.66 MHz, 300 K, C_6D_6): $\delta = -131.13$ (m, 4F), -150.22 (m, 2 F), -161.29 (m, 4F).

3.4.7 Synthesis of **3e**

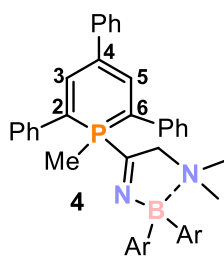


Propionitrile (5.1 μL , 0.073 mmol, 1 equiv.) was added to a solution of **2** (50 mg, 0.073 mmol, 1 equiv.) in diethyl ether (1 mL) at room temperature. An immediate colour change from orange to deep green was observed. The reaction mixture was stirred for 15 minutes, the solvent was completely removed, and the dark green oily residue was extracted with *n*-hexane (2 mL). After reducing the solution to half

and storage at room temperature, **3e** was isolated as dark green crystals. Yield: 22 mg (41%). Elemental analysis calcd. for $C_{39}H_{25}BF_{10}NP$ ($M_w = 739.40 \text{ g}\cdot\text{mol}^{-1}$) C 63.35, H 3.41, N 1.89; found: C 62.43, H 3.41, N 1.39. UV-Vis: (*n*-hexane, $\lambda_{\text{max}} / \text{nm}$, $\epsilon_{\text{max}} / \text{L}\cdot\text{mol}^{-1}\cdot\text{cm}^{-1}$): 259 (12766), 320sh (3979). ^1H NMR (400.13 MHz, 300 K, C_6D_6): $\delta = 0.93$ (t, 3H, CH_2CH_3 , $^3J_{\text{HH}} = 7 \text{ Hz}$), 1.89 (d, 3H, $^2J_{\text{PH}} = 13 \text{ Hz}$, *Me*-TPP), 2.65 (dq, 2H, CH_2CH_3 , $^3J_{\text{HH}} = 7 \text{ Hz}$, $^3J_{\text{PH}} = 2.7 \text{ Hz}$), 7.06 – 7.23 (m, 11H, H_{aromatic}), 7.38 (m, 2H, H_{aromatic}), 7.53 (m, 2H, H_{aromatic}), 7.76 (s, 1H, H_{aromatic}), 7.84 (s, 1H, H_{aromatic}). $^{13}\text{C}\{^1\text{H}\}$ NMR (100.61 MHz, 300 K, C_6D_6): $\delta = 7.95, 8.84, 29.56, 82.22, 107.9, 114.22, 124.45, 124.48, 125.78, 126.99, 128.59, 128.69, 137.24, 139.35, 139.94, 142.00, 142.76, 147.55, 161.49$; due to the low S/N, not all of the ^{13}C signals could be resolved. $^{31}\text{P}\{^1\text{H}\}$ NMR (161.98 MHz, 300 K, C_6D_6): $\delta = 0.1$ (s). ^{31}P NMR (161.98 MHz, 300 K, C_6D_6): $\delta = 0.1$ (m). $^{11}\text{B}\{^1\text{H}\}$ NMR (128.38 MHz, 300 K, C_6D_6): $\delta = 23.2$ (br s). ^{11}B NMR (128.38 MHz, 300 K, C_6D_6): $\delta = 23.2$ (br s). $^{19}\text{F}\{^1\text{H}\}$ NMR (376.66MHz, 300 K, C_6D_6): $\delta = -131.71$ (m, 4F), -151.15 (m, 2 F), -161.43 (m, 4F).

3.4.8 Synthesis of **4**

Compound **4** was prepared in an MBraun argon glove box. **4** is sensitive toward moisture and air. **4** is soluble and stable in diethyl ether, benzene.

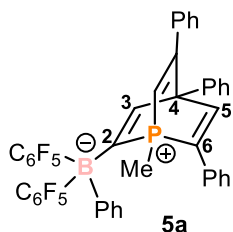


2-(dimethylamino)acetonitrile (7.1 μL , 0.073 mmol, 1 equiv.) was added to a solution of **2** (50 mg, 0.073 mmol, 1 equiv.) in diethyl ether (1 mL) at room temperature. An immediate colour change from orange to deep pink was observed. The reaction mixture was stirred for 15 minutes, while a suspension with a pink solid was formed. The solution was decanted and the pink solid was washed with *n*-hexane (2 x 2 mL). **4** was

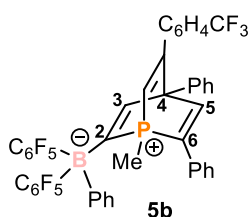
isolated as a pink crystalline powder after drying under vacuum. Yield: 28 mg (50%). Elemental analysis calcd. for $C_{40}H_{28}BF_{10}N_2P$ ($M_w = 768.45 \text{ g}\cdot\text{mol}^{-1}$) C 62.52, H 3.67, N 3.65; found: C 62.41, H 3.60, N 3.49. UV-Vis: (diethyl ether, $\lambda_{\text{max}} / \text{nm}$, $\epsilon_{\text{max}} / \text{L}\cdot\text{mol}^{-1}\cdot\text{cm}^{-1}$): 260sh (17060), 316 (17420), 411 (4100), 523 (6644). ^1H NMR (400.13 MHz, 300 K, C_6D_6): $\delta = 1.39$ (s, 6H, Me_2NCH_2CN), 2.05 (d, 3H, $^2J_{\text{PH}} = 13 \text{ Hz}$, *Me*-TPP), 3.43 (s, 2H, Me_2NCH_2CN), 6.97 – 7.00 (m, 2H, H_{aromatic}), 7.13 (m, 1H, H_{aromatic}), 7.17 (m, 4H, H_{aromatic}), 7.34 – 7.39 (m, 6H, H_{aromatic}), 7.67 (m, 2H, H_{aromatic}), 7.96 (s, 1H, H_{aromatic}), 8.03 (s, 1H, H_{aromatic}). $^{13}\text{C}\{^1\text{H}\}$ NMR (100.61 MHz, 300 K, C_6D_6): $\delta = 12.68, 48.80, 73.10, 82.08, 113.76, 124.25, 124.43, 124.98, 125.61, 128.59, 128.81, 137.40, 137.47, 140.38, 143.45, 147.95, 165.69$; due to the low S/N, not all of the ^{13}C signals could be resolved. $^{31}\text{P}\{^1\text{H}\}$ NMR (161.98 MHz, 300 K, C_6D_6): $\delta = -9.2$ (s). ^{31}P NMR (161.98 MHz, 300 K, C_6D_6): $\delta = -9.2$ (m). $^{11}\text{B}\{^1\text{H}\}$ NMR (128.38 MHz, 300 K, C_6D_6): $\delta = 11.5$ (br s). ^{11}B NMR (128.38 MHz, 300 K, C_6D_6): $\delta = 11.3$ (br s). $^{19}\text{F}\{^1\text{H}\}$ NMR (376.66MHz, 300 K, C_6D_6): $\delta = -128.79$ (m, 4F), -154.91 (m, 2 F), -162.45 (m, 4F).

3.4.9 Synthesis of **5a**

Compounds **5a-5c** were prepared in an MBraun argon glove box. **5a-5c** are sensitive toward moisture and air. **5a-5c** are soluble and stable in diethyl ether, toluene and benzene.



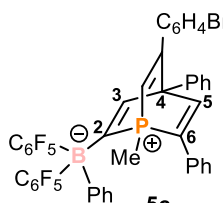
Phenylacetylene (16 μL , 0.146 mmol, 1 equiv.) was added to a solution of **2** (100 mg, 0.146 mmol, 1 equiv.) in benzene (2 mL), the mixture was warmed up to 60 $^{\circ}\text{C}$ overnight. A colour change from orange to deep red was observed. After cooling down to room temperature, the solvent was completely removed. The remaining oily residue was triturated with *n*-hexane (2 mL). After drying under vacuum, **5a** was isolated as a light red powder. Yield: 70 mg (61%). Elemental analysis calcd. for $\text{C}_{44}\text{H}_{26}\text{BF}_{10}\text{P}$ ($M_w = 786.46 \text{ g}\cdot\text{mol}^{-1}$) C 67.20, H 3.33; found: C 66.52, H 3.51. UV-Vis: (diethyl ether, $\lambda_{\text{max}} / \text{nm}$, $\epsilon_{\text{max}} / \text{L}\cdot\text{mol}^{-1}\cdot\text{cm}^{-1}$): 451 (414). ^1H NMR (400.13 MHz, 300 K, C_6D_6): $\delta = 1.20$ (d, 3H, $^2J_{\text{PH}} = 15 \text{ Hz}$, *Me*-TPP), 6.05 (d, 1H, $^2J_{\text{PH}} = 22 \text{ Hz}$, *HCCPh*), 6.36 (m, 2H, H_{aromatic}), 6.58 (m, 2H, H_{aromatic}), 6.76–6.87 (m, 5H, H_{aromatic}), 7.02–7.18 (m, 7H, H_{aromatic}), 7.36 (m, 2H, H_{aromatic}), 7.58 (s, 1H, H_{aromatic}), 7.65 (s, 1H, H_{aromatic}). $^{13}\text{C}\{^1\text{H}\}$ NMR (100.61 MHz, 300 K, C_6D_6): $\delta = -0.33$, 66.35, 120.78, 125.09, 127.20, 128.14, 128.53, 128.70, 128.76, 128.96, 132.05, 134.99, 136.90, 139.46, 148.25, 150.38; due to the low S/N, not all of the ^{13}C signals could be resolved. $^{31}\text{P}\{^1\text{H}\}$ NMR (161.98 MHz, 300 K, C_6D_6): $\delta = 1.70$ (s). ^{31}P NMR (161.98 MHz, 300 K, C_6D_6): $\delta = 1.67$ (s). $^{11}\text{B}\{^1\text{H}\}$ NMR (128.38 MHz, 300 K, C_6D_6): $\delta = -11.16$ (s). ^{11}B NMR (128.38 MHz, 300 K, C_6D_6): $\delta = -11.18$ (s). $^{19}\text{F}\{^1\text{H}\}$ NMR (376.66 MHz, 300 K, C_6D_6): $\delta = -128.18$ (m, 4F), -159.44 (m, 2 F), -164.02 (m, 4F).

3.4.10 Synthesis of **5b**

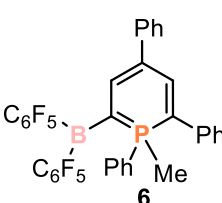
4-(Trifluoromethyl)phenylacetylene (24 μL , 0.146 mmol, 1 equiv.) was added to a solution of **2** (100 mg, 0.146 mmol, 1 equiv.) in benzene (2 mL), the mixture was warmed up to 60 $^{\circ}\text{C}$ overnight. A colour change from orange to deep red was observed. After cooling down to room temperature, the solvent was completely removed. The remaining oily residue was triturated with *n*-hexane (2 mL). After drying under vacuum, **5b** was isolated as a light red powder. Yield: 77 mg (62%). Elemental analysis calcd. for $\text{C}_{45}\text{H}_{25}\text{BF}_{13}\text{P}$ ($M_w = 854.46 \text{ g}\cdot\text{mol}^{-1}$) C 63.26, H 2.95; found: C 63.58, H 3.30. UV-Vis: (diethyl ether, $\lambda_{\text{max}} / \text{nm}$, $\epsilon_{\text{max}} / \text{L}\cdot\text{mol}^{-1}\cdot\text{cm}^{-1}$): 467 (431). ^1H NMR (400.13 MHz, 300 K, C_6D_6): $\delta = 1.19$ (s, 3H, *Me*-TPP), 6.00 (d, 1H, $^2J_{\text{PH}} = 23 \text{ Hz}$, *HCCC* $_6\text{H}_4\text{CF}_3$), 6.35 (m, 2H, H_{aromatic}), 6.46 (m, 2H, H_{aromatic}), 6.74–6.82 (m, 3H, H_{aromatic}), 6.98–7.17 (m, 9H, H_{aromatic}), 7.33 (m, 2H, H_{aromatic}), 7.50 (s, 1H, H_{aromatic}), 7.58 (s, 1H, H_{aromatic}). $^{13}\text{C}\{^1\text{H}\}$ NMR (100.61 MHz, 300 K, C_6D_6): $\delta = -0.33$, 66.01, 122.37, 124.51, 125.19, 125.40, 128.49, 128.69, 128.84, 129.15, 129.92, 130.25, 131.77, 135.00, 138.79, 140.34, 141.25, 148.27, 150.00, 171.76; due to the low S/N, not all of the ^{13}C signals could be resolved.

$^{31}\text{P}\{^1\text{H}\}$ NMR (161.98 MHz, 300 K, C_6D_6): $\delta = 2.07$ (s). ^{31}P NMR (161.98 MHz, 300 K, C_6D_6): $\delta = 2.07$ (s). $^{11}\text{B}\{^1\text{H}\}$ NMR (128.38 MHz, 300 K, C_6D_6): $\delta = -11.16$ (s). ^{11}B NMR (128.38 MHz, 300 K, C_6D_6): $\delta = -11.17$ (s). $^{19}\text{F}\{^1\text{H}\}$ NMR (376.66 MHz, 300 K, C_6D_6): $\delta = -62.68$ (s, 3F, CF_3), -128.39 (m, 2F, C_6F_5), -159.12 (m, 2 F, C_6F_5), -163.94 (m, 4F, C_6F_5).

3.4.11 Synthesis of **5c**

 **5c** 4-Bromophenylacetylene (26 mg, 0.146 mmol, 1 equiv.) was added to a solution of **2** (100 mg, 0.146 mmol, 1 equiv.) in benzene (2 mL), the mixture was warmed up to 60 °C overnight. A colour change from orange to deep red was observed. After cooling down to room temperature, the solvent was completely removed. The remaining oily residue was triturated with *n*-hexane (2 mL). After drying under vacuum, **5c** was isolated as a light red powder. Yield: 91 mg (72%). Elemental analysis calcd. for $\text{C}_{44}\text{H}_{25}\text{BBrF}_{10}\text{P}$ (Mw = 865.36 $\text{g}\cdot\text{mol}^{-1}$) C 61.07, H 2.91; found: C 64.45, H 3.42. UV-Vis: (diethyl ether, λ_{max} / nm, ϵ_{max} / $\text{L}\cdot\text{mol}^{-1}\cdot\text{cm}^{-1}$): 470 (500). ^1H NMR (400.13 MHz, 300 K, C_6D_6): $\delta = 1.19$ (s, 3H, *Me*-TPP), 5.98 (d, 1H, $^2J_{\text{PH}} = 23$ Hz, $\text{H}_{\text{CCCC}_6\text{H}_4\text{Br}}$), 6.27 (m, 2H, H_{aromatic}), 6.34 (m, 2H, H_{aromatic}), 6.77–6.82 (m, 3H, H_{aromatic}), 6.95 (m, 3H, H_{aromatic}), 7.00–7.08 (m, 6H, H_{aromatic}), 7.33 (m, 2H, H_{aromatic}), 7.51 (s, 1H, H_{aromatic}), 7.58 (s, 1H, H_{aromatic}). $^{13}\text{C}\{^1\text{H}\}$ NMR (100.61 MHz, 300 K, C_6D_6): $\delta = -0.31$, 66.03, 121.26, 122.75, 125.15, 128.59, 128.69, 128.80, 129.07, 130.86, 131.46, 131.87, 133.38, 135.00, 135.58, 135.71, 139.05, 148.36, 150.00, 172.24; due to the low S/N, not all of the ^{13}C signals could be resolved. $^{31}\text{P}\{^1\text{H}\}$ NMR (161.98 MHz, 300 K, C_6D_6): $\delta = 1.92$ (s). ^{31}P NMR (161.98 MHz, 300 K, C_6D_6): $\delta = 1.94$ (s). $^{11}\text{B}\{^1\text{H}\}$ NMR (128.38 MHz, 300 K, C_6D_6): $\delta = -11.15$ (s). ^{11}B NMR (128.38 MHz, 300 K, C_6D_6): $\delta = -11.16$ (s). $^{19}\text{F}\{^1\text{H}\}$ NMR (376.66 MHz, 300 K, C_6D_6): $\delta = -128.09$ (m, 2F), -159.25 (m, 2 F), -164.01 (m, 4F).

3.4.12 Synthesis of **6**

 **6** **2** (50 mg, 0.073 mmol) was dissolved in benzene (0.5 mL) and heated to 60 °C over two days. The solvent of the deep red reaction mixture was completely evaporated, and the remaining red oily residue was extracted with *n*-hexane (2 x 2 mL). After slow evaporation at room temperature and recrystallization from *n*-hexane, **6** could be isolated as deep red crystalline solid. Yield 18 mg, 36%. Elemental analysis calcd. for $\text{C}_{36}\text{H}_{20}\text{BF}_{10}\text{P}$ (Mw = 684.32 $\text{g}\cdot\text{mol}^{-1}$) C 63.19, H 2.95; found C 63.54, H 3.17. UV-Vis: (diethyl ether, λ_{max} / nm, ϵ_{max} / $\text{L}\cdot\text{mol}^{-1}\cdot\text{cm}^{-1}$): 270 (22251), 490 (9017). ^1H NMR (400.13 MHz, 300 K, C_6D_6): $\delta = 1.65$ (d, 3H, $^2J_{\text{PH}} = 14$ Hz), 6.96 (m, 9H, H_{aromatic}), 7.11 (m, 2H, H_{aromatic}), 7.33 (m, 2H, H_{aromatic}), 7.54 (m, 3H, H_{aromatic}), 8.04 (bd, 1H, H_{aromatic}). $^{13}\text{C}\{^1\text{H}\}$ NMR (100.61 MHz, 300 K, C_6D_6): $\delta = 125.37$, 125.72, 126.84, 126.88, 128.73, 128.88, 128.94, 137.72, 137.74, 142.25, 146.42, 146.49, 146.60; due to the low S/N, not all of the ^{13}C signals could be resolved. $^{31}\text{P}\{^1\text{H}\}$ NMR (161.98 MHz, 300 K, C_6D_6): $\delta = 1.7$ (s). ^{31}P NMR (161.98 MHz, 300 K,

C₆D₆): $\delta = 1.8$. ¹¹B{¹H} NMR (128.38 MHz, 300 K, C₆D₆): $\delta = 54.2$ (br s). ¹¹B NMR (128.38 MHz, 300 K, C₆D₆): $\delta = 54.4$ (br s). ¹⁹F{¹H} NMR (376.66 MHz, 300 K, C₆D₆): $\delta = -129.3$ (m), -130.3 (s), -133 (m), -144.7 (m), -154.8 (m), -159.5 (s), -160.8 (s), -161.9 (s), -162.7 (s). MS (LIFDI, toluene): m/z (%) = 684.14 M⁺ (**6**).

3.5 References

- [1] G. Märkl, *Angew. Chem.* **1966**, *78*, 907–908.
- [2] A. Moores, L. Ricard, P. Le Floch, N. Mézailles, *Organometallics* **2003**, *22*, 1960–1966.
- [3] A. J. Ashe, *Acc. Chem. Res.* **1978**, *11*, 153–157.
- [4] A. J. Ashe, T. W. Smith, *Tetrahedron Lett.* **1977**, *18*, 407–410.
- [5] G. Märkl, A. Merz, *Tetrahedron Lett.* **1968**, *9*, 3611–3614.
- [6] G. Märkl, A. Merz, *Tetrahedron Lett.* **1971**, *12*, 1215–1218.
- [7] G. Märkl, F. Lieb, A. Merz, *Angew. Chem. Int. Ed.* **1967**, *6*, 87–88.
- [8] G. Märkl, C. Martin, W. Weber, *Tetrahedron Lett.* **1981**, *22*, 1207–1210.
- [9] M. Bruce, G. Meissner, M. Weber, J. Wiecko, C. Müller, *Eur. J. Inorg. Chem.* **2014**, 1719–1726.
- [10] A. Moores, N. Mézailles, L. Ricard, Y. Jean, P. le Floch, *Organometallics* **2004**, *23*, 2870–2875.
- [11] A. Moores, N. Mézailles, L. Ricard, P. Le Floch, *Organometallics* **2005**, *24*, 508–513.
- [12] M. Dochnahl, M. Doux, E. Faillard, L. Ricard, P. L. Floch, *Eur. J. Inorg. Chem.* **2005**, 125–134.
- [13] M. Bruce, *Doctoral Thesis*, Freie Universität Berlin, Berlin, **2016**.
- [14] M. Doux, N. Mézailles, M. Melaimi, L. Ricard, P. Le Floch, *Chem. Commun.* **2002**, 1566–1567.
- [15] B. Rezaei Rad, U. Chakraborty, B. Mühldorf, J. A. W. Sklorz, M. Bodensteiner, C. Müller, R. Wolf, *Organometallics* **2015**, *34*, 622–635.
- [16] C. M. Hoidn, R. Wolf, *Dalton Trans.* **2016**, *45*, 8875–8884.
- [17] C. M. Hoidn, J. Leitl, C. G. P. Ziegler, I. G. Shenderovich, R. Wolf, *Eur. J. Inorg. Chem.* **2019**, 1567–1574.
- [18] D. W. Stephan, *J. Am. Chem. Soc.* **2015**, *137*, 10018–10032.
- [19] G. C. Welch, R. R. San Juan, J. D. Masuda, D. W. Stephan, *Science* **2006**, *314*, 1124–1126.
- [20] R. Liu, X. Liu, K. Ouyang, Q. Yan, *ACS Macro Lett.* **2019**, *8*, 200–204.
- [21] C. M. Mömming, E. Otten, G. Kehr, R. Fröhlich, S. Grimme, D. W. Stephan, G. Erker, *Angew. Chem. Int. Ed.* **2009**, *48*, 6643–6646.
- [22] L. E. Longobardi, C. A. Russell, M. Green, N. S. Townsend, K. Wang, A. J. Holmes, S. B. Duckett, J. E. McGrady, D. W. Stephan, *J. Am. Chem. Soc.* **2014**, *136*, 13453–13457.
- [23] D. Neibecker, R. Réau, *Angew. Chem. Int. Ed.* **1989**, *28*, 500–501.
- [24] M. Siutkowski, F. Mercier, L. Ricard, F. Mathey, *Organometallics* **2006**, *25*, 2585–2589.

- [25] J. H. Barnard, S. Yruegas, S. A. Couchman, D. J. D. Wilson, J. L. Dutton, C. D. Martin, *Organometallics* **2016**, *35*, 929–931.
- [26] S. Dong, L. Wang, T. Wang, C. G. Daniliuc, M. Brinkkötter, H. Eckert, G. Kehr, G. Erker, *Dalton Trans.* **2018**, *47*, 4449–4454.
- [27] U. Rohde, F. Ruthe, P. G. Jones, R. Streubel, *Angew. Chem. Int. Ed.* **1999**, *38*, 215–217.
- [28] A. Koner, B. M. Gabidullin, Z. Kelemen, L. Nyulászi, G. I. Nikonov, R. Streubel, *Dalton Trans.* **2019**, *48*, 8248–8253.
- [29] F. Mathey, *Chem. Rev.* **1988**, *88*, 429–453.
- [30] P. Pyykkö, M. Atsumi, *Chem. Eur. J.* **2009**, *15*, 186–197.
- [31] F. Ge, G. Kehr, C. G. Daniliuc, G. Erker, *Organometallics* **2015**, *34*, 229–235.
- [32] C. Fan, W. E. Piers, M. Parvez, R. McDonald, *Organometallics* **2010**, *29*, 5132–5139.
- [33] F. Ge, G. Kehr, C. G. Daniliuc, G. Erker, *J. Am. Chem. Soc.* **2014**, *136*, 68–71.
- [34] C. P. Sindlinger, F. S. W. Aicher, H. Schubert, L. Wesemann, *Angew. Chem. Int. Ed.* **2017**, *56*, 2198–2202.
- [35] J. Schneider, C. P. Sindlinger, S. M. Freitag, H. Schubert, L. Wesemann, *Angew. Chem.* **2017**, *129*, 339–343.
- [36] H. Braunschweig, J. Maier, K. Radacki, J. Wahler, *Organometallics* **2013**, *32*, 6353–6359.
- [37] P. Pyykkö, M. Atsumi, *Chem. – Eur. J.* **2009**, *15*, 12770–12779.
- [38] L. J. Hounjet, C. Bannwarth, C. N. Garon, C. B. Caputo, S. Grimme, D. W. Stephan, *Angew. Chem. Int. Ed.* **2013**, *52*, 7492–7495.
- [39] R. Dobrovetsky, K. Takeuchi, D. W. Stephan, *Chem. Commun.* **2015**, *51*, 2396–2398.
- [40] L. Wu, S. S. Chitnis, H. Jiao, V. T. Annibale, I. Manners, *J. Am. Chem. Soc.* **2017**, *139*, 16780–16790.
- [41] R. Dobrovetsky, D. W. Stephan, *J. Am. Chem. Soc.* **2013**, *135*, 4974–4977.
- [42] K. Samigullin, I. Georg, M. Bolte, H.-W. Lerner, M. Wagner, *Chem. Eur. J.* **2016**, *22*, 3478–3484.
- [43] E. R. M. Habraken, L. C. Mens, M. Nieger, M. Lutz, A. W. Ehlers, J. C. Slootweg, *Dalton Trans.* **2017**, *46*, 12284–12292.
- [44] J. Möricke, B. Wibbeling, C. G. Daniliuc, G. Kehr, G. Erker, *Philos. Trans. R. Soc. Math. Phys. Eng. Sci.* **2017**, *375*, 20170015.
- [45] M. Rigo, J. a. W. Sklorz, N. Hatje, F. Noack, M. Weber, J. Wiecko, C. Müller, *Dalton Trans.* **2016**, *45*, 2218–2226.
- [46] B. Breit, E. Fuchs, *Chem. Commun.* **2004**, 694–695.
- [47] M. Blug, C. Guibert, X.-F. Le Goff, N. Mézailles, P. Le Floch, *Chem Commun* **2008**, 201–203.
- [48] G. Märkl, F. Lieb, C. Martin, *Tetrahedron Lett.* **1971**, *12*, 1249–1252.
- [49] E. Fuchs, M. Keller, B. Breit, *Chem. Eur. J.* **2006**, *12*, 6930–6939.
- [50] M. Rigo, E. R. M. Habraken, K. Bhattacharyya, M. Weber, A. W. Ehlers, N. Mézailles, J. C. Slootweg, C. Müller, *Chem. Eur. J.* **2019**, *25*, 8769–8779.
- [51] A. Moores, L. Ricard, P. L. Floch, *Angew. Chem. Int. Ed.* **2003**, *42*, 4940–4944.
- [52] K. Chernichenko, Á. Madarász, I. Pápai, M. Nieger, M. Leskelä, T. Repo, *Nat. Chem.* **2013**, *5*, 718–723.
- [53] C. Jiang, O. Blacque, H. Berke, *Organometallics* **2010**, *29*, 125–133.
- [54] M. A. Dureen, C. C. Brown, D. W. Stephan, *Organometallics* **2010**, *29*, 6594–6607.
- [55] R. L. Melen, L. C. Wilkins, B. M. Kariuki, H. Wadepohl, L. H. Gade, A. S. K. Hashmi, D. W. Stephan, M. M. Hansmann, *Organometallics* **2015**, *34*, 4127–4137.
- [56] V. Fasano, L. D. Curless, J. E. Radcliffe, M. J. Ingleson, *Angew. Chem. Int. Ed.* **2017**, *56*, 9202–9206.

- [57] C. Chen, R. Fröhlich, G. Kehr, G. Erker, *Chem. Commun.* **2010**, 46, 3580–3582.
- [58] J. Li, C. G. Daniliuc, G. Kehr, G. Erker, *Chem. Commun.* **2018**, 54, 6344–6347.
- [59] M. A. Dureen, D. W. Stephan, *J. Am. Chem. Soc.* **2009**, 131, 8396–8397.
- [60] T. Wang, X. Jentgens, C. G. Daniliuc, G. Kehr, G. Erker, *ChemCatChem* **2017**, 9, 651–658.
- [61] a) SCALE3ABS, CrysAlisPro, Aglient Technologies Inc., Oxford, GB, **2012**. b) G. M. Sheldrick, SADABS, Bruker AXS, Madison, USA, **2007**.
- [62] R. C. Clark, J. S. Reid, *Acta Crystallogr. A* **1995**, 51, 887–897.
- [63] G. M. Sheldrick, *Acta Crystallogr. Sect. Found. Adv.* **2015**, 71, 3–8.
- [64] G. M. Sheldrick, *Acta Crystallogr. A* **2008**, 64, 112–122.

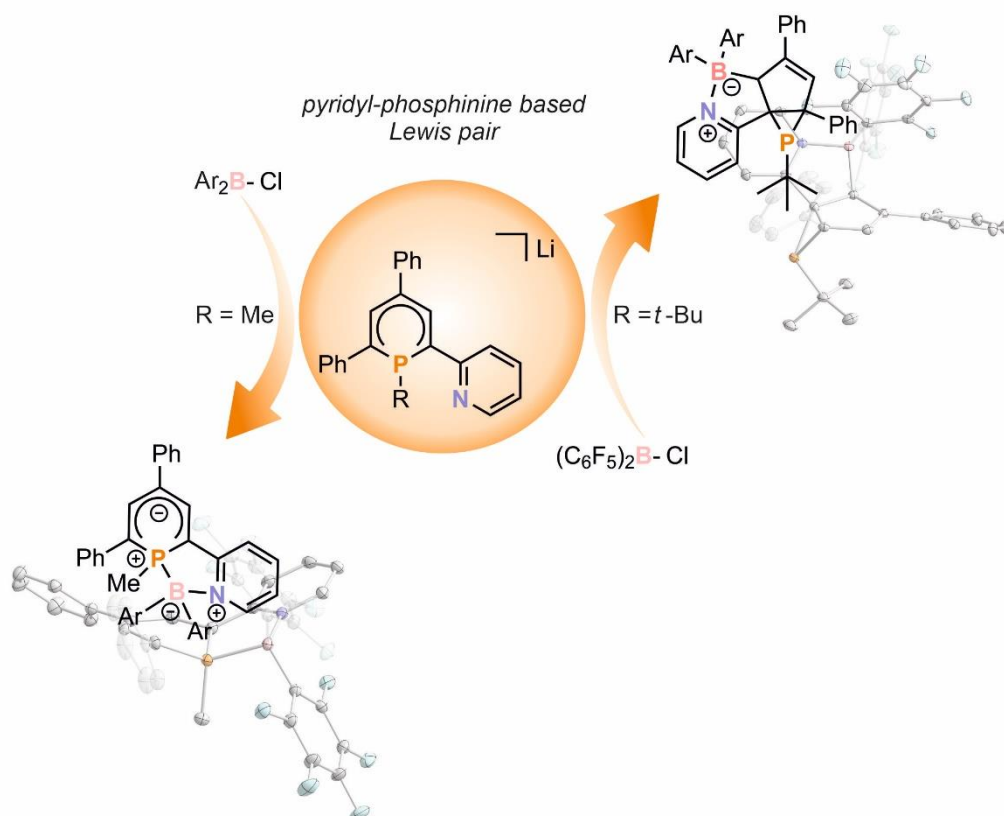
3.6 Supporting Information

The supporting information of *Chapter 3* can be found on the supplied CD-ROM and on <https://chemistry-europe.onlinelibrary.wiley.com/doi/full/10.1002/chem.202001175>. The supporting information contains: NMR and UV-vis spectra, X-ray crystallography details and results of quantum chemical calculations including Cartesian coordinates of all optimized structures.

Chapter 4

2-(2'-Pyridyl)-4,6-Diphenylphosphinine as Platform for the Synthesis of Phosphorus/Boron-Based Lewis Pairs

Abstract: Herein, we present the synthesis of novel phosphorus/boron-based Lewis pairs generated from 2-(2'-pyridyl)-4,6-diphenylphosphinine [**P,N**]. *Chapter 3* reported that the reaction of a 1-methyl-2,4,6-triphenylphosphacyclohexadienyl anion derived from 2,4,6-triphenylphosphinine with $(\text{C}_6\text{F}_5)_2\text{BCl}$ affords a phospho-bora-norbornadiene with frustrated Lewis pair like reactivity. In this work, we investigated if the introduction of an auxiliary donor on the phosphinine has an impact on the coordination chemistry. Addition of MeLi to [**P,N**] and subsequent salt metathesis with chloroboranes affords λ^5 -phosphinines containing a P/B/N-heterocycle (**2-BC₆F₅**, **2-BCF₃**, **2-Bcat** and **2-BPh**). All of these compounds possess the same structural motif, where the boron moiety is chelated by the P and N atoms. Variation of the substituents on the chloroborane has little impact on the reaction outcome. The implementation of the more sterically demanding *tert*-butyl group on the P atom results in the formation of a mixture of a P/B/N-heterocycle **3-BC₆F₅** and a phosphirane **4**. The unusual structure of **4** differs significantly from compounds **3-X** (X = **BC₆F₅**, **BCF₃**, **Bcat** and **BPh**), highlighting how steric hindrance can affect the reaction behavior of the P atom.



All reactions and characterizations were performed by J. Leitl. P. Coburger performed all DFT calculations. R. Wolf conceived and supervised the project.

4.1 Introduction

Early in the last century, Gilbert N. Lewis propelled our understanding of chemical bonding by defining a new acid base concept.^[1] He stated that acids can be considered as electron-pair acceptors and bases as electron donors. The former are now termed *Lewis acids* (LA) and the latter *Lewis bases* (LB).^[2] *Lewis pairs* are formed *via* donation of the lone pair electrons of the LB into an empty orbital of the LA (a, Figure 1). When a LB and a LA cannot form a Lewis pair (generally due to steric constraints) unexpected reactivity occurs. In 1942, H. C. Brown reported that Lewis pair formation does not occur for combination of lutidine and BMe₃.^[3] However 85 years later Geier and Stephan reported that a related Lewis pair consisting of lutidine and the triarylborane B(C₆F₅)₃ is able to split dihydrogen.^[4] The observed reactivity can be ascribed to the formation of a frustrated Lewis pair (FLP) in solution, which is in an equilibrium with the classical LA/LB adduct according to multinuclear NMR studies.^[5] The combination of a bulky LA and a bulky LB inhibits the formation of a donor-acceptor or a dative bond. This leads to the formation of an FLP (b, Figure 1), which has increased reactivity compared to classical LA/LB pairs, allowing the activation of inert small molecules.^[6] A similar phenomenon was observed by Wittig and Benz, who described the formation of zwitterionic alkyne addition products with PPh₃ and BPh₃.^[7] Tochtermann also observed alkene addition to a combination of trityl anion and BPh₃.^[8]

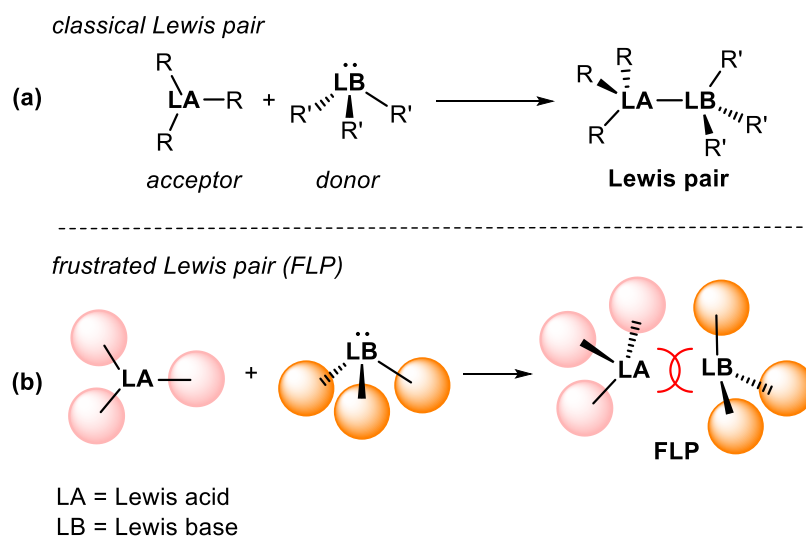


Figure 1. Schematic illustration of classical Lewis pair and frustrated Lewis pair (FLP) formation.

Activation of small molecules was also observed for Stephan's original main-group-based intramolecular FLP Mes₂PC₆F₄B(C₆F₅)₂, which is capable of splitting dihydrogen reversibly (A, Figure 2).^[9] Phosphorus/boron-based FLPs have been especially prominent in the field.^[5] Intramolecular FLPs are well-known, such as the ethylene-bridged (Mes₂P)C₂H₄(B(C₆F₅)₂) (B, Figure 2), while intermolecular FLP systems were also found to split H₂ under ambient

conditions such as the combination of bulky P-donors *t*Bu₃P and Mes₃P with B(C₆F₅)₃ (C, Figure 2).^[10,11]

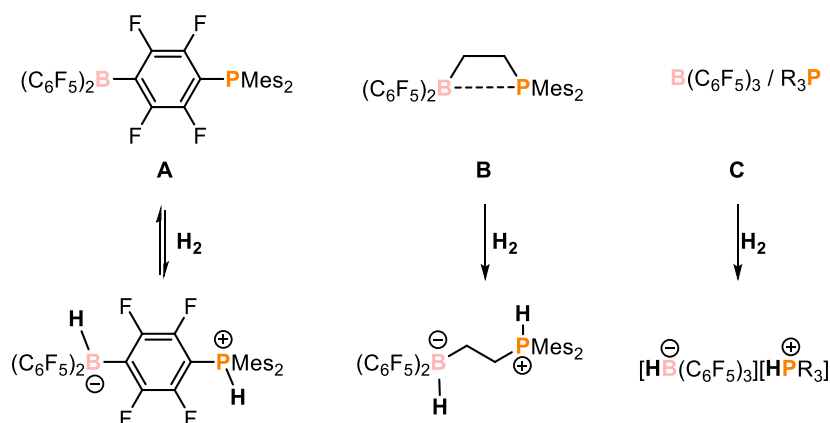
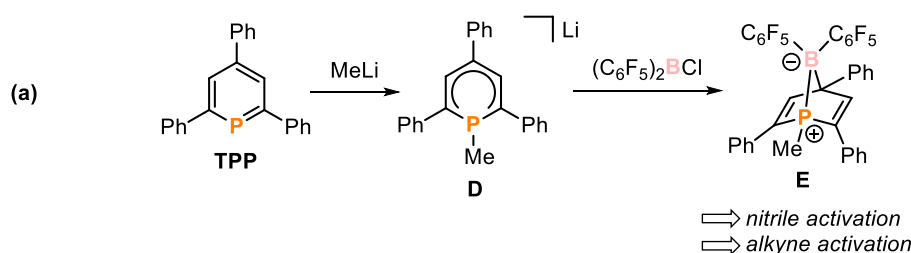


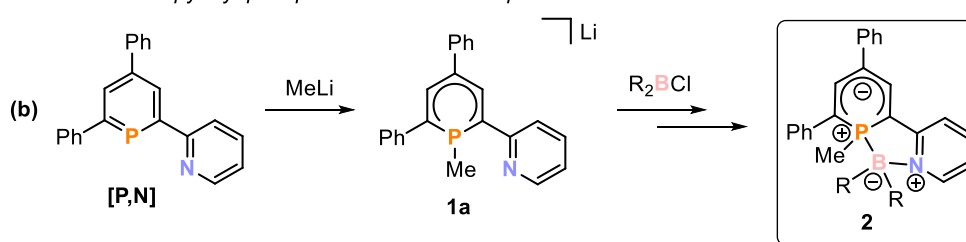
Figure 2. Examples for dihydrogen activation by different P/B-based FLP's.

The utilization of phosphinines as the Lewis basic moiety in FLPs remains mostly unexplored except for one example by Stephan and co-workers, who reported on the splitting of H₂ with 2,4,6-tri-*tert*-butyl-1,3,5-triphosphine.^[12] To test the potential of phosphinines in FLP chemistry, we decided to treat the λ⁴-phosphinine anion **D** with the chloroborane (C₆F₅)₂BCl in order to generate a neutral phosphinoborane with a Lewis basic phosphinine and a Lewis acidic boron site (a, Scheme 1 or see *Chapter 3*). The reaction of **D** with (C₆F₅)₂BCl affords the 1-phospha-7-bora-norbornadiene **E**, which possesses a direct, strained and polar P–B-bond. Although **E** is considered as a classical LA/LB pair, it shows FLP type reactivity toward triple bonds.^[13] The reaction of **E** with nitriles leads to the formation of insertion products, whereas the reaction with phenylacetylene derivatives affords phosphabarrelenes (for details see *Chapter 3*).

2,4,6-triphenylphosphinine based Lewis pair: FLP type reactivity



this work: 2-pyridyl-phosphinine-based Lewis pair



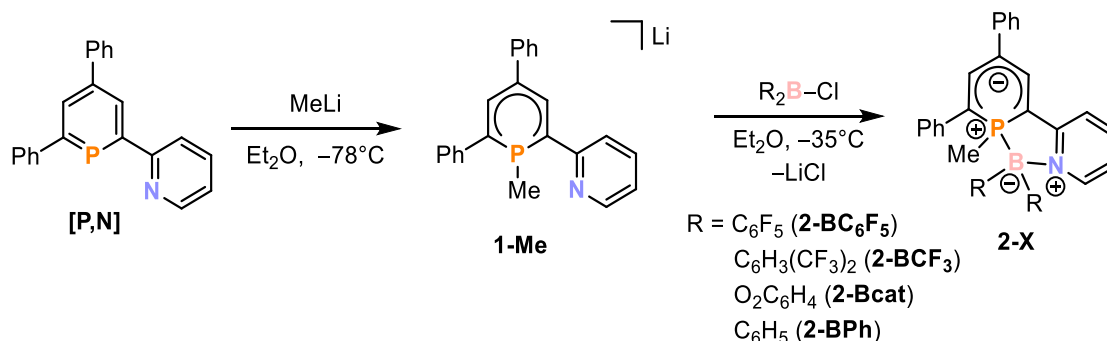
Scheme 1. Synthesis of TPP-based Lewis pair **E** (a, *Chapter 3*) and analogue reaction with 2-(2'-pyridyl)-4,6-diphenylphosphinine [P,N] (b); TPP = 2,4,6-triphenylphosphinine.

In this context, we subsequently sought to investigate the synthesis of different phosphinoboranes *via* the reaction of 2-(2'-pyridyl)-4,6-diphenylphosphinine [**P,N**] with chloroboranes (b, Scheme 2). The introduction of an auxiliary donor group in [**P,N**] should have an effect on the reactivity toward chloroboranes. The pyridyl-phosphinine ligand can be considered as a bidentate hybrid ligand because it possesses, according to the HSAB concept, a “hard” σ -donating N and a “soft” π -accepting P donor.^[14] A range of novel transition metal complexes have been synthesized due to the chelate effect of the ligand. It was possible to isolate metal complexes bearing [**P,N**] where the metal centers can possess both, low *and* high oxidation states, which was not possible with monodentate phosphinine complexes thus far.^[15-19] Additionally, activation of small molecules (CH₃OH, H₂O, NH₃, CO₂) is possible with [**P,N**] containing complexes.^[20-23] These preliminary studies on [**P,N**] show that its reactivity stands out from monodentate phosphinines, which should also be reflected by the reactivity with chloroboranes in this chapter.

Here we describe the synthesis of novel phosphorus/boron-based Lewis pairs generated from 2-(2'-pyridyl)-4,6-diphenylphosphinine [**P,N**]. *Chapter 3* reported that the reaction of a 1-methyl-2,4,6-triphenylphosphacyclohexadienyl anion, derived from 2,4,6-triphenylphosphinine, with (C₆F₅)₂BCl affords a phospho-bora-norbornadiene with frustrated Lewis pair like reactivity. In this work, we investigated if the introduction of an auxiliary donor on the phosphinine has an impact on the coordination chemistry. Addition of MeLi to [**P,N**] and subsequent salt metathesis with chloroboranes affords λ^5 -phosphinines containing a P/B/N-heterocycle (**2-BC₆F₅**, **2-BCF₃**, **2-Bcat** and **2-BPh**). All of these compounds possess the same structural motif, where the boron moiety is chelated by the P and N atoms. Variation of the substituents on the chloroborane has little impact on the reaction outcome. The implementation of the more sterically demanding *tert*-butyl group on the P atom results in the formation of a mixture of a P/B/N-heterocycle **3-BC₆F₅** and phosphirane **4**. The unusual structure of **4** differs significantly from compounds **3-X** (X = **BC₆F₅**, **BCF₃**, **Bcat** and **BPh**), highlighting how steric hindrance can affect the reaction behavior of the P atom.

4.2 Results and Discussions

Encouraged by the results presented in *Chapter 3*, it was decided to react the λ^4 -phosphacyclohexadienyl anion **1-Me** with chloroboranes in order to obtain neutral phosphino-borane compounds *via* salt elimination. **1-Me** is readily accessible by reaction of 2-(2'-pyridyl)-4,6-diphenylphosphinine (**[P,N]**) with MeLi at low temperatures (Scheme 2).^[24] Upon addition of R_2BCl ($R = C_6F_5, C_6H_3(CF_3)_2, Ph, O_2C_6H_4$) to a reaction mixture containing **1-Me** in diethyl ether (Et_2O) at $-35^\circ C$, salt elimination of LiCl occurs and a color change from deep blue to red (for $R = C_6F_5$) or purple (for $R = C_6H_3(CF_3)_2, Ph, O_2C_6H_4$) can be observed. Compounds **2-BC₆F₅**, **2-BCF₃**, **2-Bcat** and **2-BPh** can be isolated as red or purple solids in moderate to good yields (18–75%). All compounds were characterized by single crystal X-ray crystallography, NMR and UV-Vis spectroscopy and elemental analysis.



Scheme 2. Synthesis of phosphacyclohexadienyl anion **1-Me** and subsequent reaction with chloroboranes R_2BCl ($R = C_6F_5, C_6H_3(CF_3)_2, Ph, O_2C_6H_4$) leading to the formation of **2-BC₆F₅** (43%), **2-BCF₃** (75%), **2-Bcat** (18%), and **2-BPh**(23%); yields are given in parentheses.

X-ray quality single crystals of compounds **2-X** ($X = BC_6F_5, BCF_3, Bcat$ and **BPh**) were obtained by slow evaporation of an *n*-hexane solution at room temperature. The solid-state molecular structures were determined by single-crystal X-ray diffraction. The structures are analogous to one another and show the formation of a five-membered heterocycle which contains four different types of main group atoms B, C, N and P (Figure 3). The B atom is bound directly to the P atom, forming a P-B Lewis pair, and it is additionally bound to the nitrogen atom of the flanking pyridine ring. Slight variation of the substituents, electronically or sterically, on the B moiety has little effect on the molecular structure. In contrast to **E**, compounds **2-X** do not form a norbornadiene architecture. The lone pair of electrons on the N and the P atoms, donate their electron density to the empty p-orbital of the B atom leading to a ring-closure in **2**. The fold angles of the C2–P1–C6 plane and C–C bond lengths indicate that the λ^5 -phosphinine moiety remains anionic (see Table 1). Calculations at the BP86-D3BJ/def2-TZVP^[25–29] level of theory confirm the presence of a λ^5 -phosphacyclohexadienyl anion in **2-BC₆F₅** (left, Figure 4). The HOMO resembles that of the parent $C_5H_5PMe^-$ anion (right, Figure 4). The distances of the P1 atom to the methyl group are in the range of P–C single bonds (P–C = 1.86; see Table 1).^[30] The P1–B1 as well as the B1–N1 bond lengths

are in the range of single bonds ($P-B = 1.96 \text{ \AA}$; $B-N = 1.56 \text{ \AA}$).^[30] By contrast, $N1-C7$ bond lengths are elongated and $C6-C7$ bond lengths are shortened compared to the sum of the covalent radii (1.27 \AA for $N=C$; for 1.50 \AA $C-C$)^[30], which is also observed for other pyridyl-phosphinines.^[23]

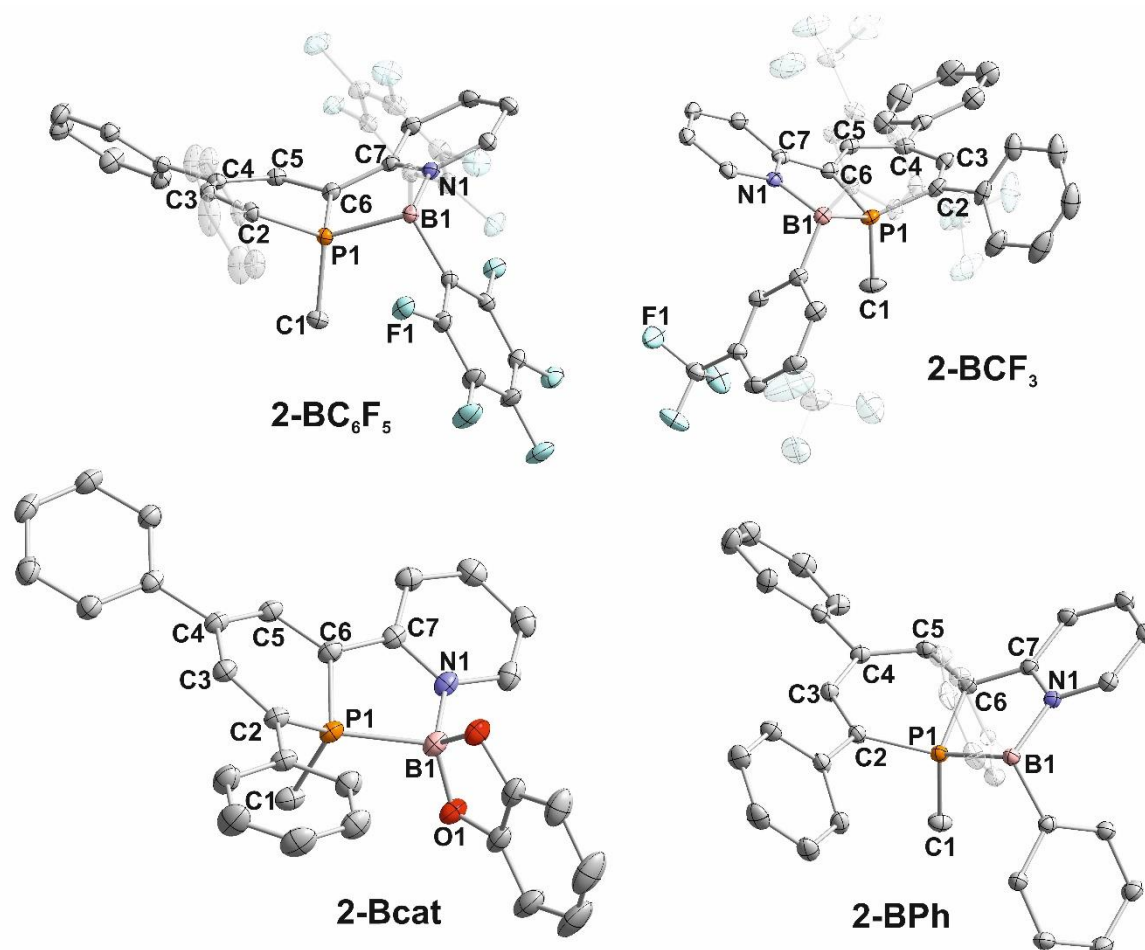


Figure 3. Solid state molecular structures of compounds **2-BC₆F₅**, **2-BCF₃**, **2-Bcat** and **2-BPh**; displacement ellipsoids are shown at the 40% probability level; H atoms are omitted for clarity; C_6F_5 -, mesityl and phenyl-groups are transparent for clarity; the crystal of **2-BCF₃** contained two crystallographically independent molecules with very similar structural parameters, only one of these molecules is shown.

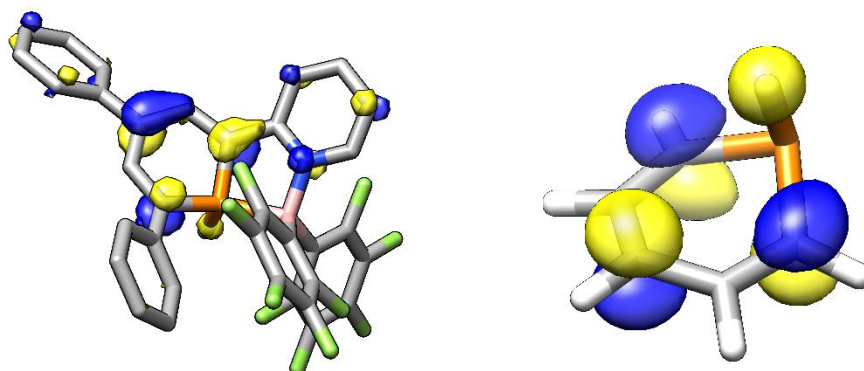
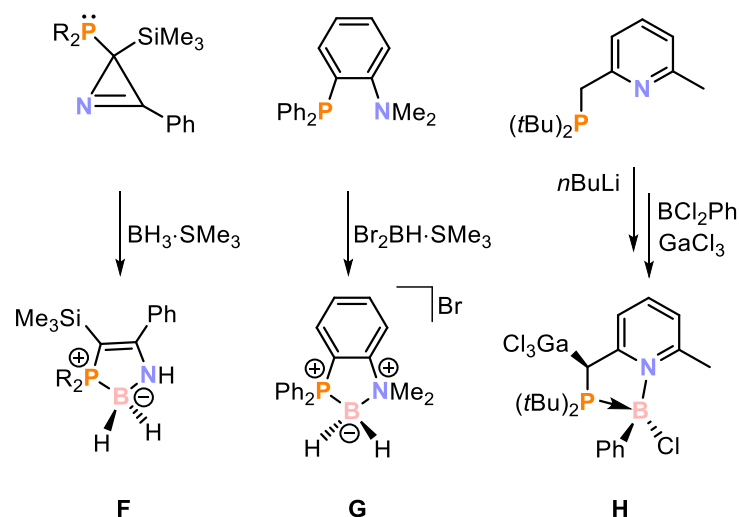


Figure 4. HOMOs of **2-BC₆F₅** (left) and $C_3H_5PMe^-$ anion (right) obtained at the BP86-D3BJ/def2-TZVP level of theory; hydrogen atoms of **2-BC₆F₅** have been omitted for clarity.

Table 1. Selected bond lengths [Å] and angles [°] of **2-BC₆F₅**, **2-BCF₃**, **2-Bcat** and **2-BPh**; the crystal of **2-BCF₃** contained two crystallographically independent molecules with very similar structural parameters, the parameters for only one of the molecules is displayed.

bond type / angle	bond lengths [Å] / angles [°]			
	2-BC₆F₅	2-BCF₃	2-Bcat	2-BPh
P1–C1	1.8146(13)	1.815(3)	1.8221(17)	1.8192(12)
P1–C2	1.7841(12)	1.786(3)	1.7800(15)	1.7925(12)
C2–C3	1.3634(18)	1.377(4)	1.372(2)	1.3704(17)
C3–C4	1.4421(17)	1.437(4)	1.441(2)	1.4391(16)
C4–C5	1.3813(17)	1.374(4)	1.385(2)	1.3834(17)
C5–C6	1.4144(17)	1.405(4)	1.403(2)	1.4079(16)
P1–C6	1.7533(12)	1.757(2)	1.7471(15)	1.7542(11)
P1–B1	2.0112(14)	2.015(3)	2.0295(18)	2.0145(13)
B1–N1	1.5774(16)	1.592(3)	1.581(2)	1.6038(15)
N1–C7	1.3741(16)	1.375(3)	1.3736(19)	1.3759(15)
C6–C7	1.4142(17)	1.414(4)	1.420(2)	1.4173(16)
C2–P1–C6	102.86(6)	100.63(12)	102.80(7)	102.41(6)
C2–P1–B1	127.14(6)	128.51(12)	132.85(7)	127.24(5)
C1–P1–B1	112.33(6)	112.34(13)	107.95(8)	112.63(6)
C6–P1–B1	94.64(6)	94.75(12)	94.28(7)	95.17(5)
P1–B1–N1	97.58(8)	96.92(15)	96.16(9)	96.61(7)
fold angle C2–P1–C6	29.5331(14)	32.7187(4)	29.8619(7)	27.7328(4)
fold angle C6–P1–B1	46.549(2)	43.0167(12)	34.4688(6)	43.6465(7)

A similar heterocycle as for **2-X** is observed for Bertrand's compound **F** (Scheme 3), which is formed by reaction of a phosphino silyl azirine with $\text{BH}_3\cdot\text{SMe}_2$ *via* ring-opening of the azirine and subsequent ring-closure *via* the "B" moiety.^[31] Another example is boronium compound $[\text{HB}(\text{amphos})]\text{Br}$ (**G**) reported by Hill and co-workers. This compound is readily accessible through the reaction of *N,N*-dimethyl-2-(diphenylphosphino)aniline (amphos) with $\text{Br}_2\text{HB}\cdot\text{SMe}_2$ (Scheme 3).^[32] A procedure similar to the synthesis of **2-BC₆F₅** was employed by van der Vlugt with 2-(diphenylphosphinomethyl)-6-methyl-pyridine. After lithiation of the phosphinomethyl-pyridine with *n*BuLi, PhBCl_2 was added to form **H** *via* salt elimination (Scheme 3).^[33] The values of P–B and P–N bond lengths and the P–B–N angles of **F**, **G** and **H** are in a similar range to compounds **2-X**.



Scheme 3. Examples for P/B/N-containing five-membered heterocycles; R = Cy_2N .

The $^{31}\text{P}\{^1\text{H}\}$ NMR spectra of compounds **2-X** show signals which substantiate a direct interaction of the phosphorus and boron nuclei, due to their broadness and multiplicities. The $^{31}\text{P}\{^1\text{H}\}$ NMR spectrum of **2-BC₆F₅** displays a broad quartet in high field at δ (ppm) = -21.5 with a coupling constant of *ca.* $^1J_{\text{PB}} = 80$ Hz indicating the presence of a direct P–B bond (Figure 5). The shape and broadness of the signal resembles that of norbornadiene **E**. Compound **E** shows a broad unresolved doublet at δ (ppm) = +18.6 in the $^{31}\text{P}\{^1\text{H}\}$ NMR spectrum. Usually, a 1:1:1:1 quartet is expected for a compound containing direct 1J P–B coupling due to the nuclear spins (*I*) of the nuclei ^{11}B ($I = 3/2$) and ^{31}P ($I = 1/2$). In the case of compound **E**, P–B bond opening and closure events and effects of the quadrupole relaxation have an impact on the line width and multiplicity of the signal. The five-membered heterocycles **F**, **G** and **H** shown in Scheme 3, which also contain direct P–B bonds show similar signals to **E** in the $^{31}\text{P}\{^1\text{H}\}$ NMR spectrum. Surprisingly, in the case of **2-BC₆F₅**, the quartet arising from 1J P–B coupling is visible, however, the intensities are similar to that of classical quartets. The broadness of the signal (*ca.* $\nu^{1/2} = 300$ Hz) arises conceivably from quadrupolar relaxation effects of the ^{11}B nucleus. The $^{11}\text{B}\{^1\text{H}\}$ NMR spectrum of **2-BC₆F₅** displays a broad doublet at δ (ppm) = -3.9 with a coupling constant of $^1J_{\text{PB}} = 95$ Hz, due to the direct P–B bond. The $^{31}\text{P}\{^1\text{H}\}$ NMR spectra for **2-BCF₃** and **2-BPh** show signals at δ (ppm) = -23.8 and -24.4 in the same region as **2-BC₆F₅** (δ (ppm) = -21.5). In contrast to **2-BC₆F₅**, the quartet structure is not resolved for **2-BCF₃** and **2-BPh** (see Figure 5). Instead, the signal for **2-BCF₃** is a broad doublet with a coupling constant of *ca.* $^1J_{\text{PB}} = 95$ Hz and the signal of **2-BPh** shows as a broad singlet with a line width of *ca.* $\nu^{1/2} = 180$ Hz. The broadness of both signals arises presumably from quadrupolar relaxation effects of the boron atom. Similar to **2-BC₆F₅**, **2-Bcat** gives rise to a quartet signal at δ (ppm) = -51.5 with a coupling constant of $^1J_{\text{PB}} = 153$ Hz in the $^{31}\text{P}\{^1\text{H}\}$ spectrum (Figure 5). **2-Bcat** shows an almost ideal 1:1:1:1 quartet, as expected for the spins of the nuclei (*vide supra*). Compared to the previously mentioned compounds **2-X** ($X = \text{BC}_6\text{F}_5$, **BCF₃** and **BPh**) the signal is high field shifted and the P–B coupling is very well resolved.

The pronounced high-field shift by approximately 30 ppm is likely explained by the electron donating (+M)/shielding effect of the catechol group. As shown in Table 2, similar trend is observed for a range of related diphenyl phosphinoborane compounds. ^{31}P NMR resonances of dioxoboroles^[34,35] generally are strongly shifted to high field compared to diaryl-substituted phosphinoboranes.^[36–38] The different electronic environment of the ^{11}B nucleus also affects the $^{11}\text{B}\{^1\text{H}\}$ NMR spectra. **2-BC₆F₅**, **2-BCF₃** and **2-BPh** give rise to a broad singlet at δ (ppm) = -4.0, 0.6 and 2.2, while the signal for **2-Bcat** is a broad doublet at δ (ppm) = 13.3 with coupling constant of $^1J_{\text{PB}} = 160$ Hz.

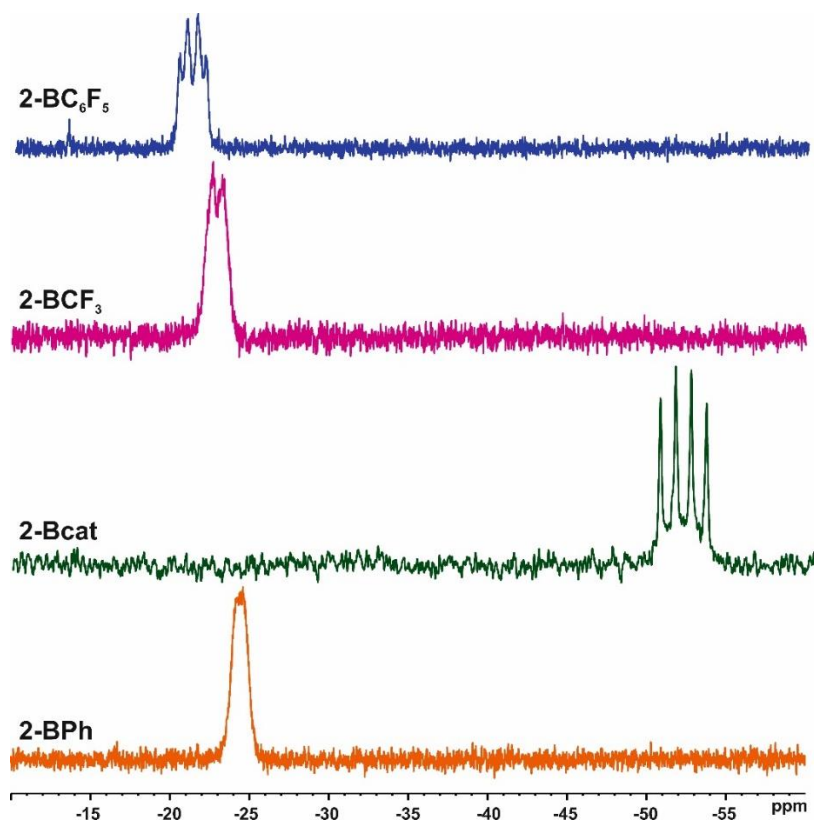
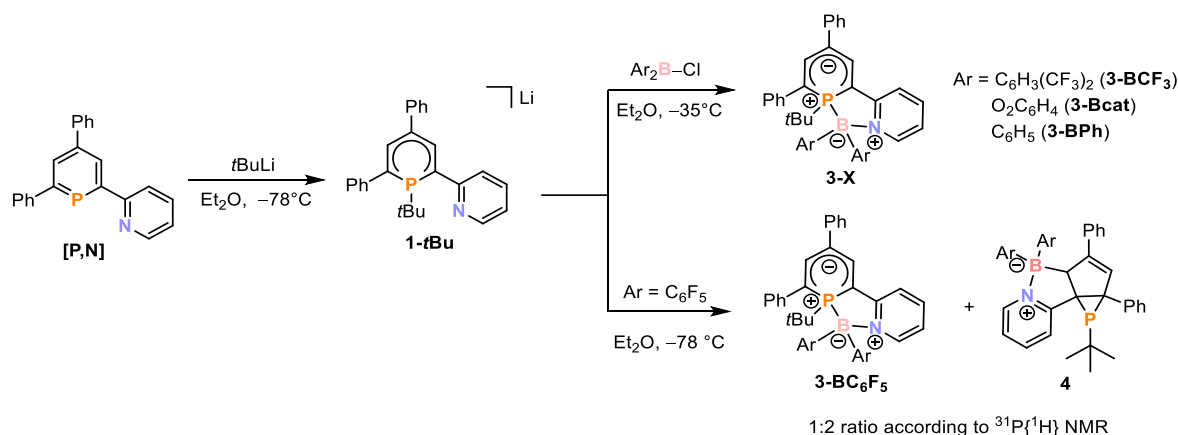


Figure 5. $^{31}\text{P}\{^1\text{H}\}$ NMR spectra (161.98 MHz, 300 K) of compounds **2-BC₆F₅**, **2-BCF₃**, **2-Bcat** and **2-BPh** recorded in C_6D_6 .

Table 2. $^{31}\text{P}\{^1\text{H}\}$ and $^{11}\text{B}\{^1\text{H}\}$ NMR shifts δ [ppm] of different phosphinoboranes; pin = $\text{O}_2\text{C}_6\text{H}_{12}$, cat = $\text{O}_2\text{C}_6\text{H}_4$, quin = $\text{O}_2\text{C}_{14}\text{H}_8$, Mes = mesityl.

compound	$^{31}\text{P}\{^1\text{H}\}$	$^{11}\text{B}\{^1\text{H}\}$
Ph_2PBpin	-63.5	+34.0
Ph_2PBcat	-66.9	+36.0
Ph_2PBquin	-66.1	+37.1
$\text{Ph}_2\text{PBMes}_2$	+26.7	+70.9
$[\text{Ph}_2\text{PBC}_6\text{F}_5]_2$	-0.8	-2.2 (t, $^1J_{\text{PB}} = 66$ Hz)
$\text{Ph}_3\text{PB}(\text{C}_6\text{F}_5)_3$	-5.2	-2.5

Since the variation of the electronic and steric properties on the boron atom has little influence on the molecular structure, the effect of changing the substituent on the P atom in the phosphinine moiety with a bulkier group was explored next. To this end, λ^4 -phosphacyclohexadienyl anion **1-*t*Bu** was prepared by reacting [P,N] with *tert*-butyl lithium (Scheme 4). Compound **1-*t*Bu** was subsequently reacted with chloroboranes {C₆H₃(CF₃)₂}₂BCl, Ph₂BCl, (cat)BCl and (C₆F₅)₂BCl in diethyl ether at low temperature ($T = -35\text{ }^\circ\text{C}$ or $-78\text{ }^\circ\text{C}$, see Scheme 4). An immediate color change from deep blue to purple was observed. The multinuclear NMR data suggest the formation of P/B/N-heterocycles **3-X** ($X = \text{BCF}_3, \text{BPh}, \text{Bcat}$), similar to **2-X** depicted in Scheme 2 above, although the molecular structures could not be determined by single crystal X-ray crystallography. $^{31}\text{P}\{^1\text{H}\}$ NMR investigations of the reaction mixture show that the formation of **3-X** was selective for the first three chloroboranes, while the formation of a mixture of two compounds **3-BC₆F₅** and **4** was observed with (C₆F₅)₂BCl (*vide infra*). For R₂BCl (R = C₆H₃(CF₃)₂, Ph, C₆F₅) broad signals could be observed at similar chemical shifts (**3-BCF₃**: δ (ppm) = -4.2; **3-BPh₂**: δ (ppm) = -5.3; **3-BC₆F₅**: δ (ppm) = -3.2) and in addition they show also large line widths (**3-BCF₃**: $\nu^{1/2} = 216\text{ Hz}$; **3-BPh₂**: $\nu^{1/2} = 90\text{ Hz}$; **3-BC₆F₅**: $\nu^{1/2} = 200\text{ Hz}$). Similar to **2-Bcat** (*vide supra*), the signal of the catecholborate species **3-Bcat** differs from the others. The signal of **3-Bcat** is a well-resolved 1:1:1:1 quartet at δ (ppm) = -30.0 with a coupling constant of $^1J_{\text{PB}} = 150\text{ Hz}$.



Scheme 4. Synthesis of phosphinoborates **3-X** and **4** via *tert*-butyl substituted phosphacyclohexadienyl anion **1-*t*Bu**.

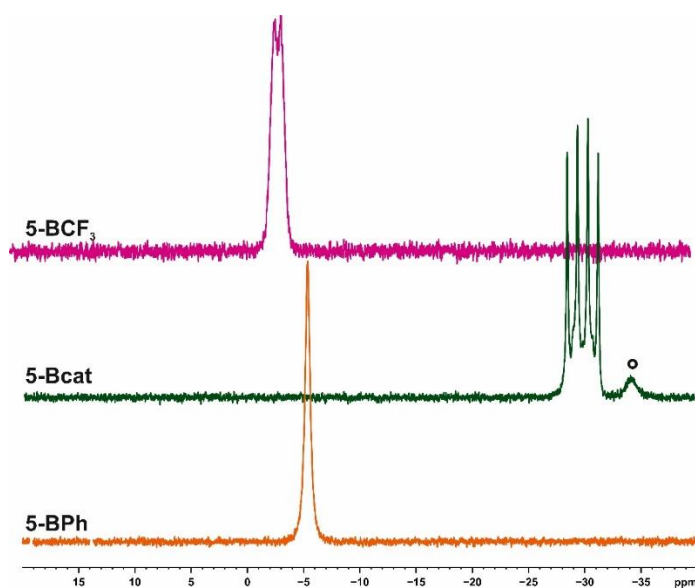


Figure 6. $^{31}\text{P}\{^1\text{H}\}$ reaction NMR spectra (161.98 MHz, 300 K) of the reaction of **1-tBu** with $\{(\text{CF}_3)_2\text{C}_6\text{H}_3\}_2\text{BCl}$, (catechol)BCl and Ph_2BCl recorded in C_6D_6 ; ° unknown impurity.

3-Bcat and **3-BPh** were not isolated as pure compounds as yet. However, compound **3-BCF₃** was synthesized from the reaction of **1-tBu** with $\{\text{C}_6\text{H}_3(\text{CF}_3)_2\}_2\text{BCl}$ and isolated as purple crystals in 22% yield. The analytical data of **3-BCF₃** was compared with the methyl-substituted analogue **2-BCF₃**. The $^{31}\text{P}\{^1\text{H}\}$ signal of **3-BCF₃** arises as a broad singlet and is shifted to low field compared to **2-BCF₃** (δ (ppm) = -4.2 vs. δ (ppm) = -23.8, respectively). Additionally, its signal is less resolved ($\nu^{1/2}$ = 216 Hz) compared to the broad doublet of **2-BCF₃** ($^1J_{\text{PB}}$ = 95 Hz). The $^{11}\text{B}\{^1\text{H}\}$ spectra are similar for both compounds because they display broad singlets at δ (ppm) = 0.6 and δ (ppm) = 0.8 for **2-BCF₃** and **5-BCF₃** respectively. The $^{19}\text{F}\{^1\text{H}\}$ spectrum of **2-BCF₃** displays a multiplet at δ (ppm) = -62.7, which may be the result from coalescence of the ^{19}F signals due to rotation of the aryl substituents around the B–C axis. For **3-BCF₃** the signal arises in the same range but in this case two singlets in 1:1 ratio at δ (ppm) = -62.8 and δ (ppm) = -62.9 are observed. The fact that two singlets are observed may be attributed to the presence of two chemically-distinct $\text{C}_6\text{H}_3(\text{CF}_3)_2$ rings, which may suffer from hindered rotation around its B–C bond. From the comparison of the spectroscopic data, it can be assumed that the molecular structure of **3-BCF₃** is similar to **2-BCF₃**.

For the reaction of **1-tBu** with $(\text{C}_6\text{F}_5)_2\text{BCl}$, $^{31}\text{P}\{^1\text{H}\}$ NMR spectroscopy indicated the presence of two species in the reaction mixture in a 1:2 ratio (Figure 7). One signal appears as a broad multiplet at δ (ppm) = -3.2 with a line width of *ca.* $\nu^{1/2}$ = 200 Hz. This signal is assigned to **3-BC₆F₅** based on the similar habit and chemical shift with the signals of **2-BC₆F₅**. The signal of the second species arises as a high field shifted sharp singlet at δ (ppm) = -86.5 (**4**, see Scheme 4). This indicates that there are no phosphorus boron interactions in this compound.

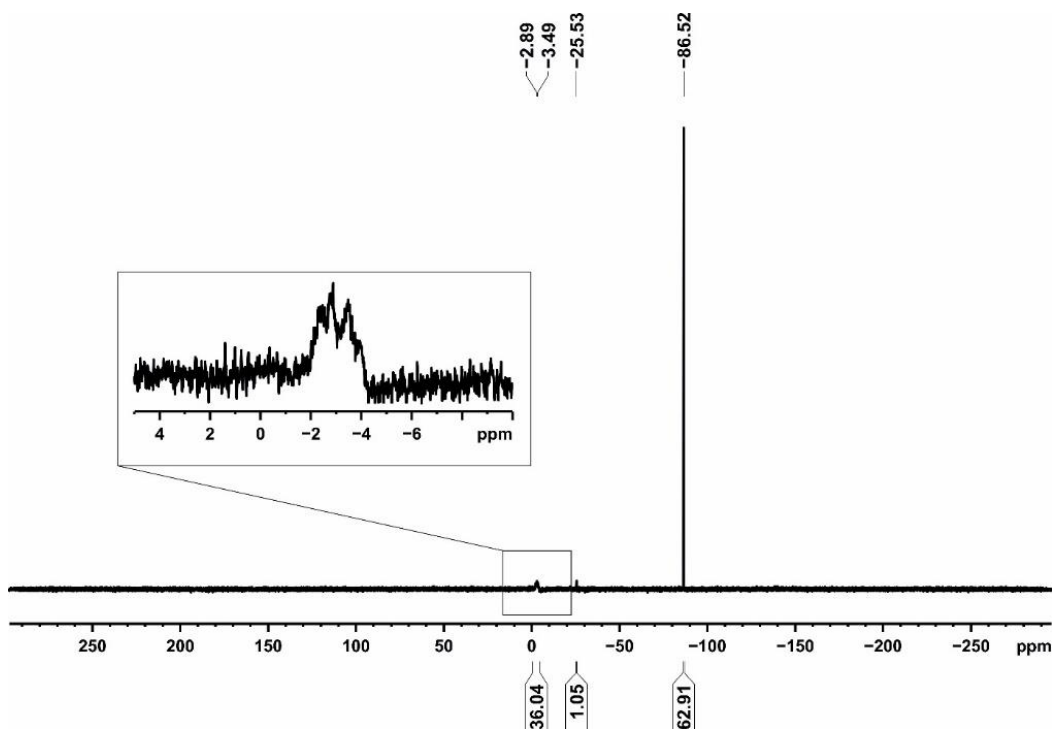


Figure 7. $^{31}\text{P}\{^1\text{H}\}$ NMR spectrum (161.98 MHz, 300 K) of the reaction mixture of **1-*t*Bu** with $(\text{C}_6\text{F}_5)_2\text{BCl}$ recorded in C_6D_6 .

Due to **3-BC₆F₅** and **4** possessing very similar solubility, separation of these compounds in acceptable yields has been unsuccessful as of yet. Nevertheless, single crystals of **4** suitable for X-ray diffraction were obtained in a very low yield from slow evaporation of an *n*-hexane solution of **3-BC₆F₅** and **4**. The solid state molecular structure of **4** reveals the formation of a phosphirane through intramolecular C–C bond formation (Figure 8). It appears that coordination of the P atom to the boron moiety is inhibited due to the steric demand of the *tert*-butyl substituent. Instead, the boron moiety is connected to the N atom of the pyridyl substituent and *meta*-C7 of the phosphinine leading to the formation of a five-membered BNC₃ heterocycle. Compound **4** thus can be described as a concatenation of one six-, two five- and one three-membered rings. All bond lengths in the phosphirane ring (P–C and C–C bonds) are in the range of single bonds (see Table 3).^[30] The short bond length of C8–C9 (1.3419(19) Å) indicates the presence of a C=C double bond.^[39] Distances in the N/B containing heterocycle are in the range of single bonds (see Table).^[30] The formation of **4** from **1-*t*Bu** is the first instance of synthesizing a phosphirane from a phosphinine.

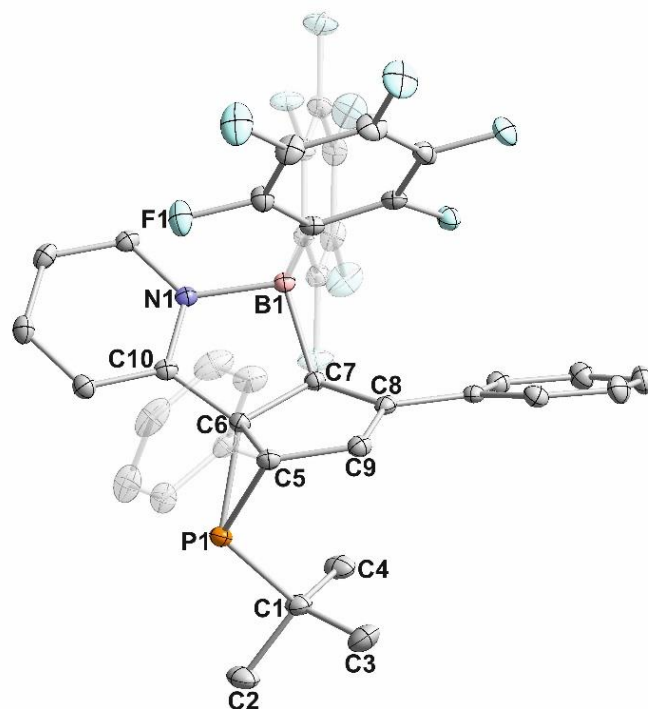


Figure 8. Solid state molecular structure of compound **4**; displacement ellipsoids are shown at the 40% probability level; H atoms are omitted for clarity; C₆F₅- and phenyl-groups are transparent for clarity; the crystal of **4** contained a second crystallographically independent molecule with very similar structural parameters, only one of these molecules is shown.

Table 3. Selected bond lengths [Å] and angles [°] of **4**; the crystal of **4** contained two crystallographically independent molecules with very similar structural parameters, the parameters for only one of the molecules is displayed.

bond type	bond length [Å]	bond angle type	angle [°]
P1–C1	1.8878(15)	C5–P1–C6	49.09(5)
P1–C5	1.8703(14)	N1–B1–C7	98.62(10)
P1–C6	1.8713(13)	C6–C7–B1	103.30(10)
C6–C5	1.5543(18)	C10–C6–P1	116.70(9)
C6–C7	1.5365(18)	C6–C10–N1	111.04(11)
C7–C8	1.5100(18)	P1–C5–C9	119.05(10)
C8–C9	1.3419(19)	fold angle C5–P1–C6	61.297(2)
C9–C5	1.485(2)	fold angle C10–C6–C7–B1 plane	47.6728(16)
C7–B1	1.6634(19)	fold angle C10–N1–B1	16.5605(6)
B1–N1	1.5977(19)		
N1–C10	1.3538(17)		
C10–C6	1.4718(19)		

The formation of two different species in the reaction of **1-*t*Bu** (C_6F_5)₂BCl can likely be attributed to the extra steric encumbrance on the phosphinine moiety. Compound **3-BC₆F₅** is formed by chelation of the chloroborane *via* the P and N atoms of the pyridyl-phosphinine with concomitant salt elimination. However, the formation of **4** is more complex. The λ^5 -phosphacyclohexadienyl anion in **1-*t*Bu** can be depicted in three different resonance structures (**I–III**) (Figure 9a). It is known for phosphinines that not only the P atom can donate electron density *via* its lone pair of electrons, but also the carbocyclic part of the heterocycle can act as nucleophile.^[40] The *ortho*-C atom in **II** is nucleophilic and is able to donate electron density into the empty p-orbital of the boron atom (Figure 9b). Additionally, the nitrogen atom of the pyridyl substituent coordinates *via* its lone pair of electrons. These two nucleophilic attacks on boron lead to the formation of phosphirane **4** with concomitant elimination of LiCl. Calculations at the BP86-D3BJ/def2-TZVP level of theory reveal that isomer **3-BC₆F₅** is energetically favored over **4** by 20.2 kcal·mol⁻¹ (R = *t*Bu) and 17.0 kcal·mol⁻¹ (R = Me) respectively (Figure 9c). Thus, we posit **4** must be the kinetic product and **3-BC₆F₅** the thermodynamic product.

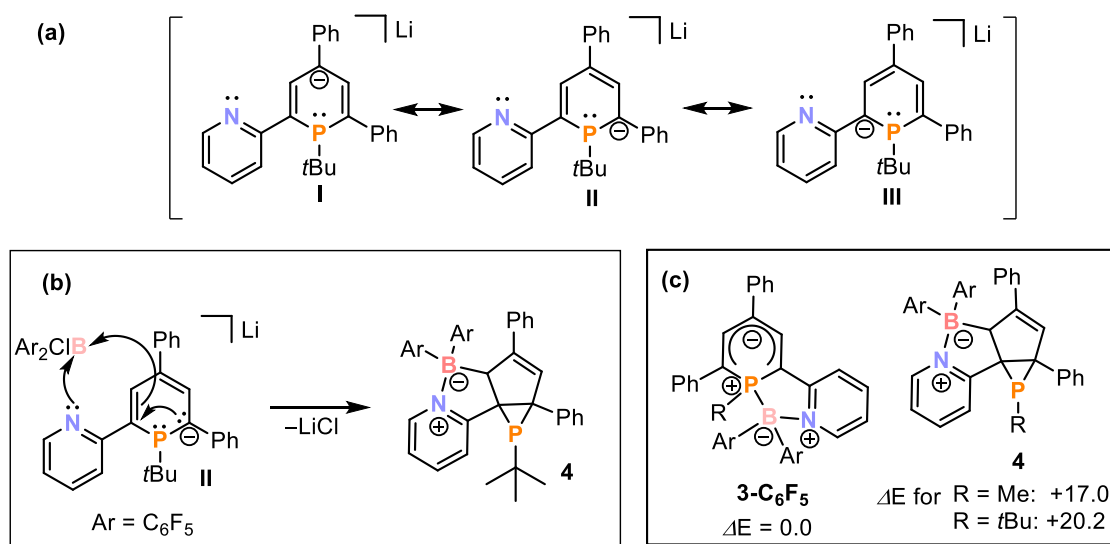


Figure 9. (a) resonance structures of **1-*t*Bu**; (b) proposed mechanism of the formation of **4**; (c) calculated energies at the BP86-D3BJ/def2-TZVP level of theory for **3-BC₆F₅** and **4**; ΔE in kcal·mol⁻¹.

4.3 Conclusion

In summary, a range of pyridyl-phosphinine-based phosphinoborate anions have been synthesized by salt metathesis of phosphacyclohexadienyl anions with chloroboranes. Reactions of the methyl-substituted anion **1-Me** with $(\text{C}_6\text{F}_5)_2\text{BCl}$, $\{\text{C}_6\text{H}_3(\text{CF}_3)_2\}_2\text{BCl}$, (catechol)BCl and Ph_2BCl leads to the formation of **2-BC₆F₅**, **2-BCF₃**, **2-Bcat** and **2-BPh** in moderate to good yields. All of these compounds display the same Lewis pair structure motif

in the solid state: pyridyl-phosphinine anion **1-Me** chelates *via* the lone pair of electrons of the P and N atom to the boron moiety resulting in a five-membered heterocycle. In contrast to the synthesis of the phosphanorbornadiene **E** from a 1-methyl-2,4,6-triphenylphosphacyclohexadienyl anion and chloroborane described in chapter 3 of this thesis, the flanking pyridyl group in [P,N] provides the phosphinine bidentate abilities, which inhibits norbornadiene formation. Altering the substituents on the borane has little effect on the reaction outcome. However, changing the substituent on the P atom to a bulkier group has an effect. The reaction of *tert*-butyl-substituted **1-*t*Bu** with (C₆F₅)₂BCl results in the formation of a mixture of products in a 1:2 ratio. Again, a P/B/N-heterocycle **3-BC₆F₅** is formed, but the major species in this reaction is the unprecedented phosphirane **4**. Compound **4** is energetically disfavoured by +20.2 kcal·mol⁻¹ with respect to **3-BC₆F₅**, and thus appears to be the kinetic product of the reaction. The reaction of **1-*t*Bu** with other chloroboranes possessing different substituents leads to the formation of P/B/N-heterocycles **3-BCF₃**, **3-Bcat** and **3-BPh**. This work showed that the introduction of the substituent on the phosphinine moiety may have a major impact on the reactivity. The implementation of a pyridyl-substituent on the phosphinine leads to phosphinoborate chelate products rather than norbornadienes. Future work should focus on the reactivity of these heterocycles.

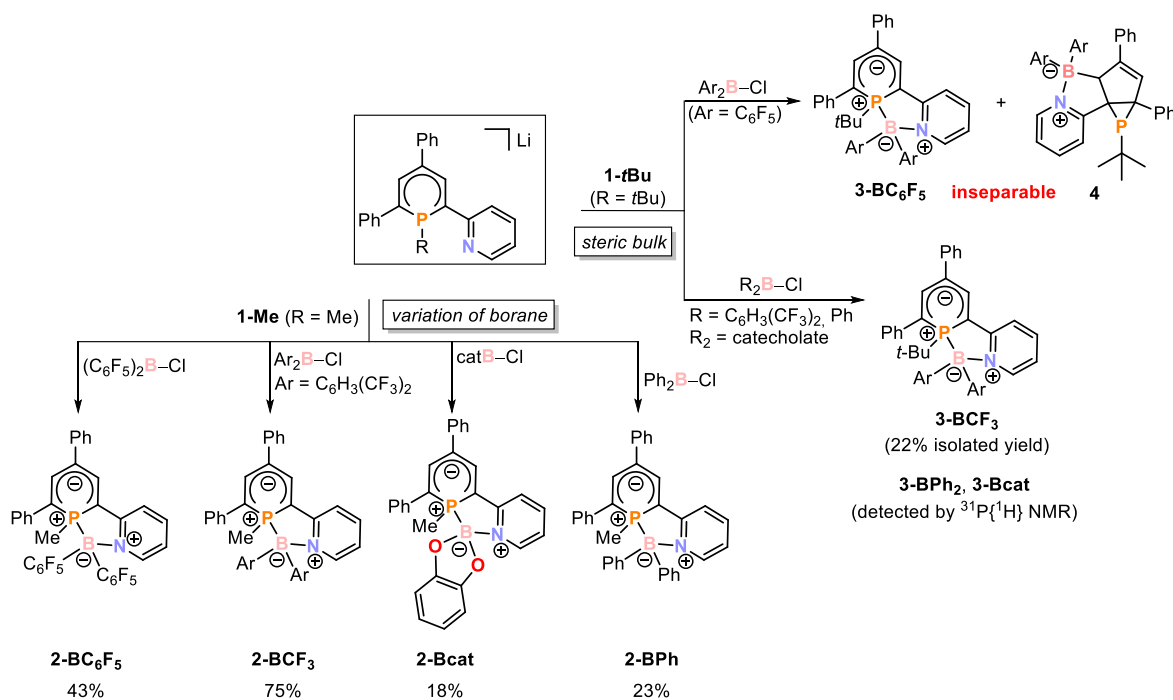


Figure 10. Overview of 2-(2'-pyridyl)-4,6-diphenylphosphinine-based phosphinoborates.

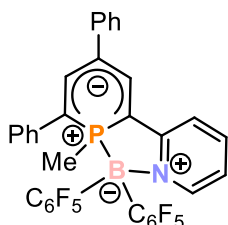
4.4 Experimental Details

4.4.1 General Considerations

All experiments were performed under an atmosphere of dry argon by using standard glovebox techniques. Diethyl ether and *n*-hexane were purified, dried, and degassed with an MBraun SPS800 solvent purification system. NMR spectra were recorded on Bruker Avance 300, Avance 400 and Avance 600 spectrometers at 300 K and internally referenced to residual solvent resonances. The assignment of the ^1H and ^{13}C NMR signals was confirmed by two-dimensional (COSY, HSQC, and HMBC) experiments. UV/vis spectra were recorded on a Varian Cary 50 spectrometer. Elemental analyses were determined by the analytical department of Regensburg University. **1-Me** and **1-*t*Bu** were synthesized according to a literature procedure.^[24] $(\text{C}_6\text{H}_3(3,5\text{-CF}_3)_2)_2\text{BCl}$ was received from J. C. Slootweg, and Ph_2BCl and $(\text{C}_6\text{F}_5)_2\text{BCl}$ were and synthesized by an unpublished procedure from J. C. Slootweg.^[41,42] Chlorocatecholborane was purchased from Sigma Aldrich and used as received.

X-ray Crystallography: The single-crystal X-ray diffraction data were recorded on an Agilent Technologies SuperNova and a GV1000, TitanS2 diffractometer with $\text{Cu-K}\alpha$ radiation ($\lambda = 1.54184 \text{ \AA}$). Either semi-empirical multi-scan absorption corrections^[43] or analytical ones^[44] were applied to the data. The structures were solved with SHELXT^[45] and least-square refinements on F^2 were carried out with SHELXL.^[46] The hydrogen atoms were located in idealized positions and refined isotropically with a riding model.

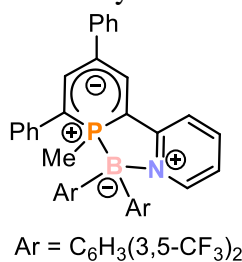
4.4.2 Synthesis of **2-BC₆F₅**



A solution of $(\text{C}_6\text{F}_5)_2\text{BCl}$ (87 mg, 0.23 mmol, 1 equiv.) in diethyl ether (3 mL) was slowly added to a solution of **1-Me** (100 mg, 0.23 mmol, 1 equiv.) in diethyl ether (3 mL) at $-35 \text{ }^\circ\text{C}$. An immediate color change from deep blue to red was observed and a precipitate was formed. The red suspension was stirred overnight and the solid was separated from the solution. The red solution was evaporated to dryness, and the remaining red oil was extracted with *n*-hexane (7 x 2 mL). The solvent was evaporated to half the volume. After storage at $-35 \text{ }^\circ\text{C}$, **2-BC₆F₅** was isolated as a red solid. Yield 67 mg, 43%. Elemental analysis calcd. for $\text{C}_{35}\text{H}_{19}\text{BF}_{10}\text{NP}$ ($M_w = 685.31 \text{ g}\cdot\text{mol}^{-1}$) C 61.34, H 2.79, N 2.04; found C 61.65, H 2.83, N 2.11. UV-Vis: (*n*-hexane, $\lambda_{\text{max}} / \text{nm}$, $\epsilon_{\text{max}} / \text{L}\cdot\text{mol}^{-1}\cdot\text{cm}^{-1}$): 310 (26074), 523 (16519). ^1H NMR (400.13 MHz, 300 K, $[\text{D}_8]\text{THF}$): $\delta = 0.88$ (d, 3H, $^2J_{\text{PH}} = 12 \text{ Hz}$), 6.36–6.39 (m, 1H), 7.08–7.19 (m, 4H), 7.29–7.32 (m, 2H), 7.35–7.45 (m, 5H), 7.54–7.56 (m, 2H), 7.61 (d, 1H, $J = 5 \text{ Hz}$), 7.65 (s, 1H). $^{13}\text{C}\{^1\text{H}\}$ NMR (100.61 MHz, 300 K, $[\text{D}_8]\text{THF}$): $\delta = 11.9$ (d, $J = 50.0 \text{ Hz}$), 74.5 (s), 75.1 (s), 106.3 (s), 106.9 (s), 112.9 (s), 118.7 (d, $J = 10 \text{ Hz}$), 124.9 (s), 125.1 (s), 125.9 (s), 126.0 (s), 127.4 (m), 129.0 (s), 129.5 (s), 133.4 (s), 138.1 (d, $J = 12 \text{ Hz}$), 138.9 (d, $J = 2 \text{ Hz}$), 142.6 (s), 142.7 (s), 143.4 (s), 148.2 (bs), 150.0 (bs), 161.1 (s), 161.4 (s); 27 ^{13}C signals are expected for **2-BC₆F₅**, but due to the low S/N, not all of the ^{13}C signals could be resolved. $^{31}\text{P}\{^1\text{H}\}$ NMR (161.98 MHz, 300 K, $[\text{D}_8]\text{THF}$):

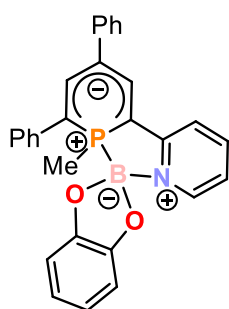
$\delta = -21.5$ (bd, $^1J_{PB} = 113$ Hz). ^{31}P NMR (161.98 MHz, 300 K, $[\text{D}_8]\text{THF}$): $\delta = -21.5$ (bd, $^1J_{PB} = 113$ Hz). $^{11}\text{B}\{^1\text{H}\}$ NMR (128.38 MHz, 300 K, $[\text{D}_8]\text{THF}$): $\delta = -4.0$ (bd, $^1J_{PB} = 95$ Hz). ^{11}B NMR (128.38 MHz, 300 K, $[\text{D}_8]\text{THF}$): $\delta = -4.0$ (bd, $^1J_{PB} = 91$ Hz). $^{19}\text{F}\{^1\text{H}\}$ NMR (376.66 MHz, 300 K, $[\text{D}_8]\text{THF}$): $\delta = -129.4$ (bs, 2F), -131.4 (m, 1F), -156.3 (m, 1F), -157.1 (m, 1F), -163.4 (m, 3F), -164.0 (m, 3F); the integration of the ^{19}F signals is higher than expected due to the low S/N.

4.4.3 Synthesis of **2-BCF₃**



A solution of $(\text{C}_6\text{H}_3(3,5\text{-CF}_3)_2)_2\text{BCl}$ (106 mg, 0.23 mmol, 1 equiv.) in diethyl ether (3 mL) was slowly added to a solution of **1-Me** (100 mg, 0.23 mmol, 1 equiv.) in diethyl ether (3 mL) at -35 °C. An immediate color change from deep blue to deep purple was observed. The purple solution was stirred overnight, filtered and evaporated to dryness. The remaining purple oil was extracted with *n*-hexane (5 mL) and the solvent was evaporated to half the volume. After storage at -35 °C, **2-BCF₃** was isolated as purple crystals. Yield 131 mg, 75%. Elemental analysis calcd. for $\text{C}_{39}\text{H}_{25}\text{BF}_{12}\text{NP}$ ($M_w = 777.4$ g·mol⁻¹) C 60.26, H 3.24, N 1.80; found C 60.25, H 3.29, N 1.81. UV-Vis: (*n*-hexane, λ_{max} / nm, ϵ_{max} / L·mol⁻¹·cm⁻¹): 320 (22030), 558 (14517). ^1H NMR (400.13 MHz, 300 K, $[\text{D}_8]\text{THF}$): $\delta = 0.90$ (d, 3H, $^2J_{\text{PH}} = 11$ Hz), 6.56–6.59 (m, 1H), 7.07–7.23 (m, 6H), 7.29–7.32 (m, 2H), 7.53–7.63 (m, 6H), 7.69 (d, 1H, $J = 19$ Hz), 7.78 (s, 1H), 7.82 (bs, 2H), 8.01 (bs, 2H), 8.04 (bs, 1H). $^{13}\text{C}\{^1\text{H}\}$ NMR (100.61 MHz, 300 K, $[\text{D}_8]\text{THF}$): $\delta = 13.4$ (d, $J = 34$ Hz), 76.1 (s), 76.8 (s), 102.9 (s), 103.7 (s), 114.2 (d, $J = 2$ Hz), 119.3 (d, $J = 10$ Hz), 121.8 (m), 123.2 (s), 123.5 (s), 124.0 (d, $J = 11$ Hz), 125.8 (s), 125.9 (s), 126.2 (s), 126.4 (d, $J = 8$ Hz), 127.4 (s), 127.6 (d, $J = 2$ Hz), 129.0 (s), 129.2 (s), 130.8 (s), 131.1 (s), 131.5 (s), 131.8 (dd, $J = 2$ Hz, 32 Hz), 132.9 (bs), 134.4 (bs), 137.5 (s), 138.7 (d, $J = 13$ Hz), 139.8 (d, $J = 1$ Hz), 142.6 (d, $J = 9$ Hz), 143.3 (d, $J = 1$ Hz), 161.9 (s), 162.1 (s); 29 ^{13}C signals are expected for **2-BCF₃**, but 32 ^{13}C signals were found, which may be attributed to impurities. $^{31}\text{P}\{^1\text{H}\}$ NMR (161.98 MHz, 300 K, $[\text{D}_8]\text{THF}$): $\delta = -23.8$ (bd). ^{31}P NMR (161.98 MHz, 300 K, $[\text{D}_8]\text{THF}$): $\delta = -23.8$ (bs). $^{11}\text{B}\{^1\text{H}\}$ NMR (128.38 MHz, 300 K, $[\text{D}_8]\text{THF}$): $\delta = 0.6$ (bs). ^{11}B NMR (128.38 MHz, 300 K, $[\text{D}_8]\text{THF}$): $\delta = 0.5$ (bs). $^{19}\text{F}\{^1\text{H}\}$ NMR (376.66 MHz, 300 K, $[\text{D}_8]\text{THF}$): $\delta = -62.7$ (m, 12F).

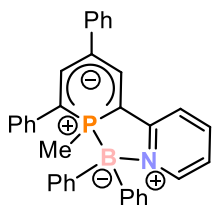
4.4.4 Synthesis of **2-Bcat**



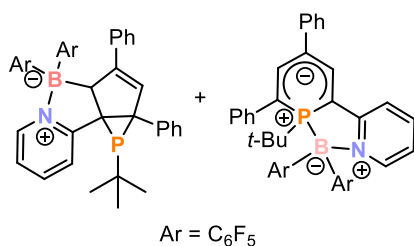
A solution of chlorocatechol borane (17 mg, 0.112 mmol, 1 equiv.) in diethyl ether (3 mL) was slowly added to a solution of **1-Me** (50 mg, 0.112 mmol, 1 equiv.) in diethyl ether (3 mL) at -35 °C. An immediate color change from deep blue to deep purple was observed. The solution was stirred overnight and was evaporated to dryness. The remaining purple oil was extracted with *n*-hexane (7 x 2 mL). The solvent was evaporated to half the volume. After storage at room temperature, **2-Bcat** was isolated as a purple solid. Yield (14 mg, 18%). Sum formula $\text{C}_{30}\text{H}_{24}\text{BO}_2\text{P}$. Molecular weight: 685.31 g·mol⁻¹. Elemental analysis: C 61.34; H 2.79; N 2.04. Found:

C 61.65; H 2.83; N 2.11. UV-Vis: (*n*-hexane, λ_{\max} / nm, ϵ_{\max} / L·mol⁻¹·cm⁻¹): 319 (21051), 556 (13862). ¹H NMR (400.13 MHz, 300 K, C₆D₆): δ = 0.94 (d, 3H, ²J_{PH} = 12 Hz), 5.48–5.52 (m, 1H), 6.28–6.37 (m, 2H), 6.83–7.05 (m, 7H), 7.10 (s, 1H), 7.16–7.18 (m, 2H), 7.29–7.33 (m, 2H), 7.45–7.50 (m, 4H), 7.76 (d, 1H, *J* = 25 Hz); not all ¹H signals could be assigned due to overlapping solvent signal. ¹³C{¹H} NMR (100.61 MHz, 300 K, C₆D₆): δ = 9.5 (d, *J* = 30 Hz), 74.9 (s), 75.6 (s), 104.9 (s), 105.6 (s), 110.7 (s), 111.9 (s), 116.6 (d, *J* = 7 Hz), 120.2 (s), 120.5 (s), 123.7 (d, *J* = 9 Hz), 125.3 (s), 125.4 (s), 125.5 (s), 125.6 (s), 126.4 (s), 128.6 (s), 128.9 (s), 136.1 (s), 137.6 (s), 137.7 (s), 138.9 (d, *J* = 4 Hz), 139.1 (d, *J* = 7 Hz), 143.3 (s), 152.0 (d, *J* = 13 Hz). ³¹P{¹H} NMR (161.98 MHz, 300 K, C₆D₆): δ = -51.5 (m). ³¹P NMR (161.98 MHz, 300 K, C₆D₆): δ = -51.5 (m). ¹¹B{¹H} NMR (128.38 MHz, 300 K, C₆D₆): δ = 13.3 (d, ¹J_{PB} = 160 Hz). ¹¹B NMR (128.38 MHz, 300 K, C₆D₆): δ = 13.1 (m, *J* = 150 Hz).

4.4.5 Synthesis of **2-BPh**

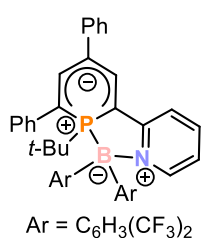


A solution of Ph₂BCl (45 mg, 0.23 mmol, 1 equiv.) in diethyl ether (3 mL) was slowly added to a solution of **1-Me** (100 mg, 0.23 mmol, 1 equiv.) in diethyl ether (3 mL) at -80 °C. An immediate color change from deep blue to deep purple was observed. The purple solution was stirred overnight, filtered and evaporated to dryness. The remaining purple oil was extracted with *n*-hexane (6 x 2 mL). The solvent was evaporated to half the volume. After storage at -35 °C **2-BPh** was isolated as a purple solid. Yield 26 mg, 23%. Elemental analysis calcd. for C₃₅H₂₉BNP (M_w = 505.41 g·mol⁻¹) C 83.18, H 5.78, N 2.77; found: C 83.92, H 5.60, N 2.41. UV-Vis: (*n*-hexane, λ_{\max} / nm, ϵ_{\max} / L·mol⁻¹·cm⁻¹): 322 (61269), 553 (14598). ¹H NMR (400.13 MHz, 300 K, [D₈]THF): δ = 0.59 (d, 3H, ²J_{PH} = 11 Hz), 6.40–6.43 (m, 1H), 6.90–7.04 (m, 4H), 7.07–7.11 (m, 3H), 7.24–7.37 (m, 8H), 7.40–7.44 (m, 4H), 7.46–7.53 (m, 5H), 7.58–7.73 (m, 2H); one additional proton was found according to the integration, this may be attributed to an impurity. ¹³C{¹H} NMR (100.61 MHz, 300 K, [D₈]THF): δ = 13.3 (d, *J* = 36 Hz), 77.7 (s), 78.3 (s), 105.7 (s), 106.3 (s), 113.0 (d, *J* = 2 Hz), 118.1 (d, *J* = 10 Hz), 122.8 (d, *J* = 10 Hz), 125.3 (s), 125.7 (s), 126.4 (s), 126.7 (d, *J* = 7 Hz), 127.0 (d, *J* = 4 Hz), 127.4 (d, *J* = 2 Hz), 127.9 (s), 128.2 (d, *J* = 2 Hz), 128.5 (d, *J* = 3 Hz), 128.9 (d, *J* = 2 Hz), 133.4 (d, *J* = 7 Hz), 134.5 (d, *J* = 4 Hz), 135.4 (s), 138.6 (d, *J* = 1 Hz), 139.2 (d, *J* = 14 Hz), 143.7 (d, *J* = 10 Hz), 144.0 (d, *J* = 1 Hz), 161.4 (s), 161.2 (s). ³¹P{¹H} NMR (161.98 MHz, 300 K, [D₈]THF): δ = -24.4 (bs). ³¹P NMR (161.98 MHz, 300 K, [D₈]THF): δ = -24.4 (bs). ¹¹B{¹H} NMR (128.38 MHz, 300 K, [D₈]THF): δ = 2.2 (bs). ¹¹B NMR (128.38 MHz, 300 K, [D₈]THF): δ = 2.3 (bs).

4.4.6 Synthesis of **3-BC₆F₅** and **4**

A solution of (C₆F₅)₂BCl (35 mg, 0.09 mmol, 1 equiv.) was dissolved in diethyl ether (2 mL) was slowly added to a solution of **1-*t*Bu** (40 mg, 0.09 mmol, 1 equiv.) in diethyl ether (2 mL) at -78 °C. An immediate color change from deep blue to deep purple was observed. The mixture was stirred overnight and was allowed to warm

up to room temperature. The solvent was completely removed and the oily purple residue was extracted with *n*-hexane (2 mL). Slow evaporation of this solution gave crystals of **4** which were suitable for single crystal X-ray crystallography. Due to the very similar solubilities of **3-BC₆F₅** and **4**, it was not possible to separate and isolate these compounds. ³¹P{¹H} NMR (161.98 MHz, 300 K, C₆D₆): δ = -3.2 (bs, **3-BC₆F₅**), -86.5 (s, **4**).

4.4.7 Synthesis of **3-BCF₃**

A solution of (C₆H₃(3,5-CF₃)₂)₂BCl (51 mg, 0.109 mmol, 1 equiv.) in diethyl ether (3 mL) was slowly added to a solution of **1-*t*Bu** (50 mg, 0.109 mmol, 1 equiv.) in diethyl ether (3 mL) at -35 °C. An immediate color change from deep blue to deep purple was observed. The purple solution was stirred overnight, filtered and was evaporated to dryness. The remaining purple oil was extracted with *n*-hexane (2 x 2 mL) and the

solvent was evaporated to half the volume. After storage at room temperature **3-BCF₃** was isolated as purple crystals. Yield 20 mg, 22%. Elemental analysis calcd. for C₄₂H₃₁BF₁₂NP (Mw = 819.48 g·mol⁻¹) C 61.56, H 3.81, N 1.74; found C 61.71, H 3.99, N 1.59. UV-Vis: (*n*-hexane, λ_{max} / nm, ε_{max} / L·mol⁻¹·cm⁻¹): 310 (9843), 560 (5827). ¹H NMR (400.13 MHz, 300 K, C₆D₆): δ = 0.56 (d, 9H, *t*Bu, ³J_{PH} = 15 Hz), 5.49–5.52 (m, 1H), 6.37–6.41 (m, 1H), 6.56–6.59 (m, 1H), 6.67 (d, 1H, *J* = 6 Hz), 6.83–6.87 (m, 1H), 7.05–7.31 (m, 8H), 7.40–7.48 (m, 2H), 7.48 (bs, 1H), 7.74 (d, 1H, *J* = 25 Hz), 7.87 (bs, 1H), 8.07 (bs, 2H), 8.32 (bs, 2H). ¹³C{¹H} NMR (100.61 MHz, 300 K, C₆D₆): δ = 24.1 (m), 40.1 (d, *J* = 28 Hz), 75.2 (s), 75.9 (s), 101.2 (s), 101.8 (s), 112.8 (s), 118.2 (d, *J* = 9 Hz), 120.7 (m), 121.2 (m), 122.5 (s), 122.7 (s), 125.0 (s), 125.1 (s), 125.2 (s), 125.4 (s), 125.5 (s), 125.6 (s), 126.5 (d, *J* = 6 Hz), 126.8 (s), 128.3 (s), 128.7 (s), 130.1 (s), 130.4 (s), 130.7 (s), 131.1 (m), 135.1 (bs), 138.1 (d, *J* = 2 Hz), 139.0 (d, *J* = 12 Hz), 139.5 (s), 140.5 (d, *J* = 8 Hz), 142.8 (s), 163.0 (d, *J* = 18 Hz); 30 ¹³C signals are expected for **3-BCF₃**, but 33 ¹³C signals were found, which may be attributed to an impurity. ³¹P{¹H} NMR (161.98 MHz, 300 K, C₆D₆): δ = -4.2. ³¹P NMR (161.98 MHz, 300 K, C₆D₆): δ = -4.2. ¹¹B{¹H} NMR (128.38 MHz, 300 K, C₆D₆): δ = 0.8. ¹¹B NMR (128.38 MHz, 300 K, C₆D₆): δ = 1.0. ¹⁹F{¹H} NMR (376.66 MHz, 300 K, C₆D₆): δ = -62.8 (s, 6F, B(C₆H₃(CF₃)₂)), -62.9 (s, 6F, B(C₆H₃(CF₃)₂)).

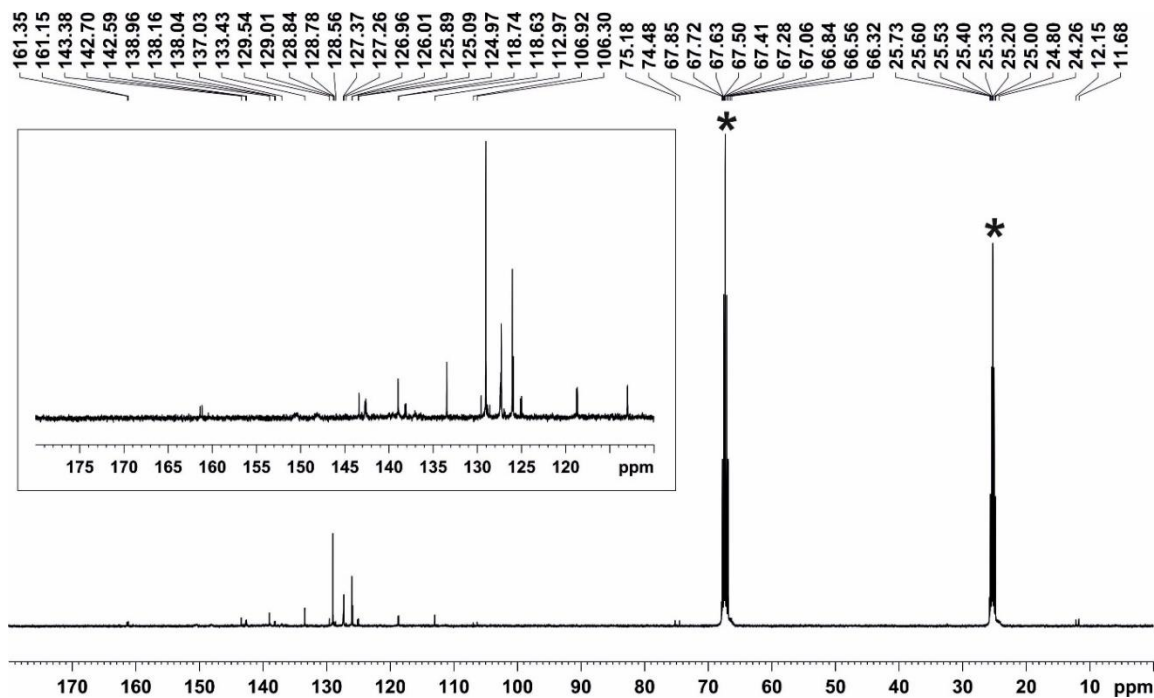
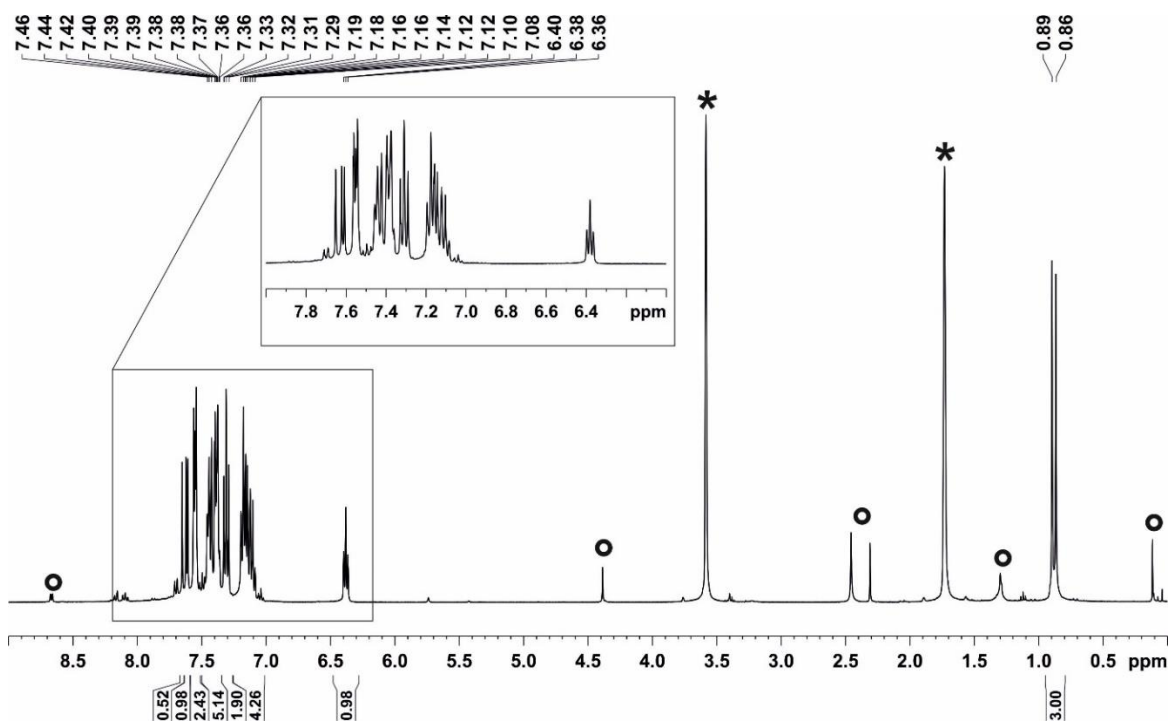
4.5 References

- [1] G. N. Lewis, *J. Am. Chem. Soc.* **1916**, *38*, 762–785.
- [2] G. N. Lewis, *Trans. Faraday Soc.* **1923**, *19*, 452–458.
- [3] H. C. Brown, H. I. Schlesinger, S. Z. Cardon, *J. Am. Chem. Soc.* **1942**, *64*, 325–329.
- [4] S. J. Geier, D. W. Stephan, *J. Am. Chem. Soc.* **2009**, *131*, 3476–3477.
- [5] D. W. Stephan, *J. Am. Chem. Soc.* **2015**, *137*, 10018–10032.
- [6] D. W. Stephan, G. Erker, *Angew. Chem. Int. Ed.* **2010**, *49*, 46–76.
- [7] G. Wittig, E. Benz, *Chem. Ber.* **1959**, *92*, 1999–2013.
- [8] W. Tochtermann, *Angew. Chem. Int. Ed.* **1966**, *5*, 351–371.
- [9] G. C. Welch, R. R. San Juan, J. D. Masuda, D. W. Stephan, *Science* **2006**, *314*, 1124–1126.
- [10] G. C. Welch, D. W. Stephan, *J. Am. Chem. Soc.* **2007**, *129*, 1880–1881.
- [11] P. Spies, G. Erker, G. Kehr, K. Bergander, R. Fröhlich, S. Grimme, D. W. Stephan, *Chem. Commun.* **2007**, *0*, 5072–5074.
- [12] L. E. Longobardi, C. A. Russell, M. Green, N. S. Townsend, K. Wang, A. J. Holmes, S. B. Duckett, J. E. McGrady, D. W. Stephan, *J. Am. Chem. Soc.* **2014**, *136*, 13453–13457.
- [13] J. Leitl, A. R. Jupp, E. R. M. Habraken, V. Streitferdt, P. Coburger, D. J. Scott, R. M. Gschwind, C. Müller, J. C. Sloatweg, R. Wolf, *Chem. Eur. J.* **2020**, *26*, 7788–7800.
- [14] A. Loibl, W. Oschmann, M. Vogler, E. A. Pidko, M. Weber, J. Wiecko, C. Müller, *Dalton Trans.* **2018**, *47*, 9355–9366.
- [15] L. E. E. Broeckx, M. Lutz, D. Vogt, C. Müller, *Chem. Commun.* **2011**, *47*, 2003–2005.
- [16] C. Müller, L. E. E. Broeckx, I. de Krom, J. J. M. Weemers, *Eur. J. Inorg. Chem.* **2013**, 187–202.
- [17] I. de Krom, L. E. E. Broeckx, M. Lutz, C. Müller, *Chem. Eur. J.* **2013**, *19*, 3676–3684.
- [18] L. E. E. Broeckx, S. Güven, F. J. L. Heutz, M. Lutz, D. Vogt, C. Müller, *Chem. Eur. J.* **2013**, *19*, 13087–13098.
- [19] L. E. E. Broeckx, W. Delaunay, C. Latouche, M. Lutz, A. Boucekkine, M. Hissler, C. Müller, *Inorg. Chem.*, **2013**, *52*, 10738–10740.
- [20] A. Campos-Carrasco, L. E. E. Broeckx, J. J. M. Weemers, E. A. Pidko, M. Lutz, A. M. Masdeu-Bultó, D. Vogt, C. Müller, *Chem. Eur. J.* **2011**, *17*, 2510–2517.
- [21] I. de Krom, E. A. Pidko, M. Lutz, C. Müller, *Chem. Eur. J.* **2013**, *19*, 7523–7531.
- [22] L. E. E. Broeckx, A. Bucci, C. Zuccaccia, M. Lutz, A. Macchioni, C. Müller, *Organometallics* **2015**, *34*, 2943–2952.
- [23] J. Leitl, M. Marquardt, P. Coburger, D. J. Scott, V. Streitferdt, R. M. Gschwind, C. Müller, R. Wolf, *Angew. Chem. Int. Ed.* **2019**, *58*, 15407–15411.
- [24] G. Märkl, F. Lieb, A. Merz, *Angew. Chem. Int. Ed. Engl.* **1967**, *6*, 87–88.
- [25] S. Grimme, J. Antony, S. Ehrlich, H. Krieg, *J. Chem. Phys.* **2010**, *132*, 154104.
- [26] F. Weigend, R. Ahlrichs, *Phys. Chem. Chem. Phys.* **2005**, *7*, 3297–3305.
- [27] J. P. Perdew, *Phys. Rev. B* **1986**, *33*, 8822–8824.
- [28] A. D. Becke, *Phys. Rev. A* **1988**, *38*, 3098–3100.
- [29] S. Grimme, S. Ehrlich, L. Goerigk, *J. Comput. Chem.* **2011**, *32*, 1456–1465.
- [30] P. Pyykkö, M. Atsumi, *Chem. Eur. J.* **2009**, *15*, 186–197.
- [31] V. Piquet, A. Baceiredo, H. Gornitzka, F. Dahan, G. Bertrand, *Chem. Eur. J.* **1997**, *3*, 1757–1764.
- [32] A. F. Hill, J. S. Ward, *Dalton Trans.* **2017**, *46*, 7291–7308.

- [33] M. Devillard, C. A. Lamsfus, V. Vreeken, L. Maron, J. I. van der Vlugt, *Dalton Trans.* **2016**, 45, 10989–10998.
- [34] E. N. Daley, C. M. Vogels, S. J. Geier, A. Decken, S. Doherty, S. A. Westcott, *Angew. Chem. Int. Ed.* **2015**, 54, 2121–2125.
- [35] J. H. W. LaFortune, A. Trofimova, H. Cummings S. A. Westcott, D. W. Stephan, *Chem. Eur. J.* **2019**, 25, 12521–12525.
- [36] D. C. Pestana, P. P. Power, *J. Am. Chem. Soc.* **1991**, 113, 8426–8437.
- [37] S. J. Geier, T. M. Gilbert, D. W. Stephan, *Inorg. Chem.* **2011**, 50, 336–344.
- [38] H. Jacobsen, H. Berke, S. Döring, G. Kehr, G. Erker, R. Fröhlich, O. Meyer, *Organometallics* **1999**, 18, 1724–1735.
- [39] P. Pyykkö, M. Atsumi, *Chem. Eur. J.* **2009**, 15, 12770–12779.
- [40] N. Mézailles, P. L. Floch, *Curr. Org. Chem.* **2006**, 10, 3–25.
- [41] D. J. Parks, W. E. Piers, G. P. A. Yap, *Organometallics* **1998**, 17, 25, 5492–5503.
- [42] K. Samigullin, M. Bolte, H. W. Lerner, M. Wagner, *Organometallics* **2014**, 33, 13, 3564–3569.
- [43] a) SCALE3ABS, CrysAlisPro, Aglient Technologies Inc., Oxford, GB, **2012**. b) G. M. Sheldrick, SADABS, Bruker AXS, Madison, USA, **2007**.
- [44] R. C. Clark, J. S. Reid, *Acta Crystallogr. Sect. A* **1995**, 51, 887–897.
- [45] G. M. Sheldrick, *Acta Crystallogr. A* **2008**, 64, 112–122.
- [46] G. M. Sheldrick, *Acta Crystallogr. Sect. C Struct. Chem.* **2015**, 71, 3–8.
- [47] F. Neese, *WIREs Comput. Mol. Sci.* **2018**, 8, 1327.
- [48] F. Neese, *Wiley Interdiscip. Rev. Comput. Mol. Sci.* **2012**, 2, 73–78.

4.6 Supporting Information

4.6.1 NMR Spectra



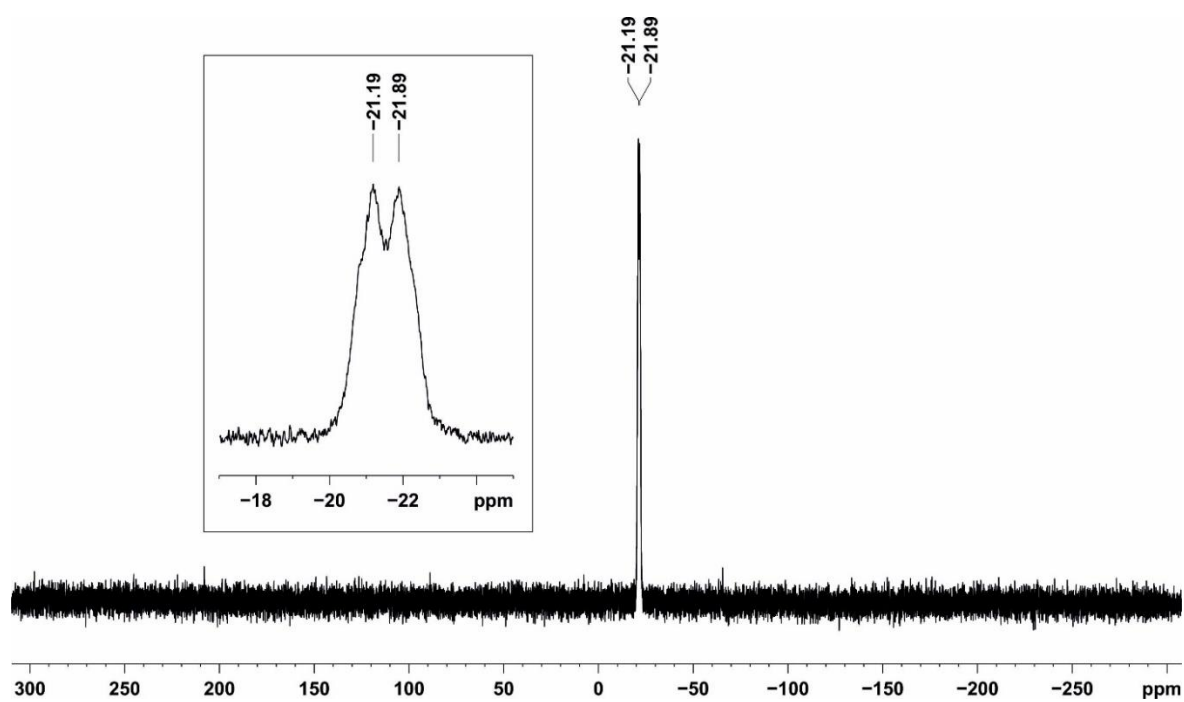


Figure S3. $^{31}\text{P}\{^1\text{H}\}$ NMR spectrum (161.98 MHz, 300 K, d_8 -THF) of 2- BC_6F_5 .

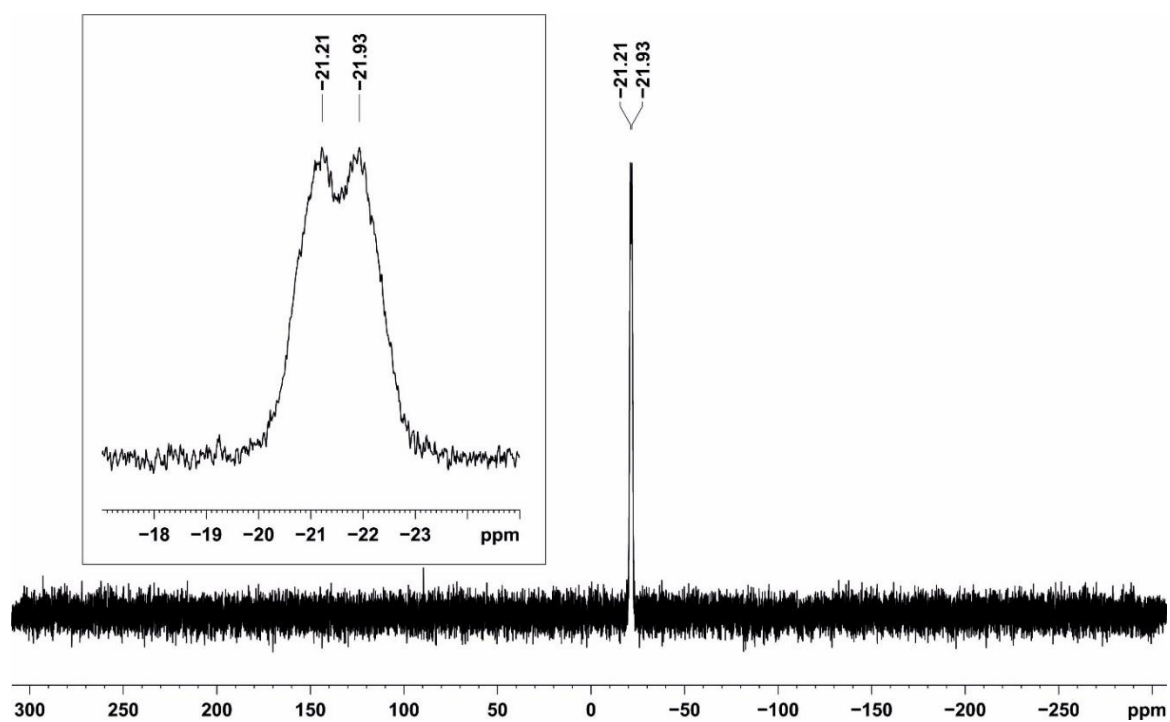


Figure S4. ^{31}P NMR spectrum (161.98 MHz, 300 K, d_8 -THF) of 2- BC_6F_5 .

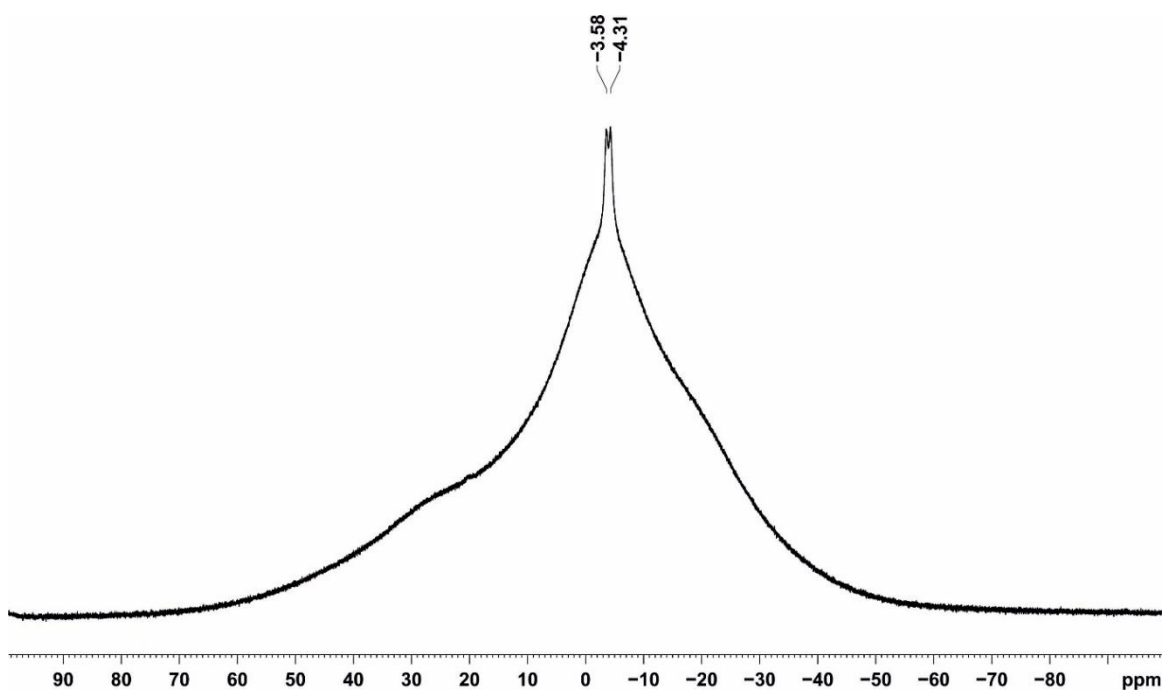


Figure S5. $^{11}\text{B}\{^1\text{H}\}$ NMR spectrum (128.38MHz, 300 K, $\text{d}_8\text{-THF}$) of **2-BC₆F₅**.

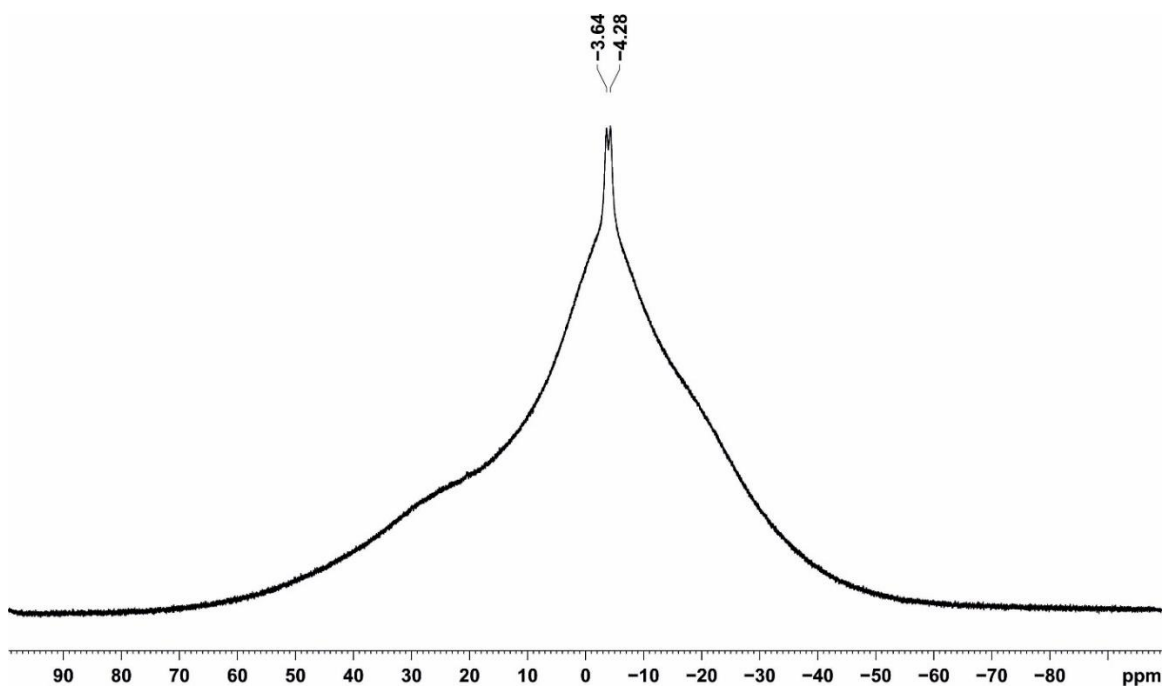


Figure S6. $^{11}\text{B}\{^1\text{H}\}$ NMR spectrum (128.38MHz, 300 K, $\text{d}_8\text{-THF}$) of **2-BC₆F₅**.

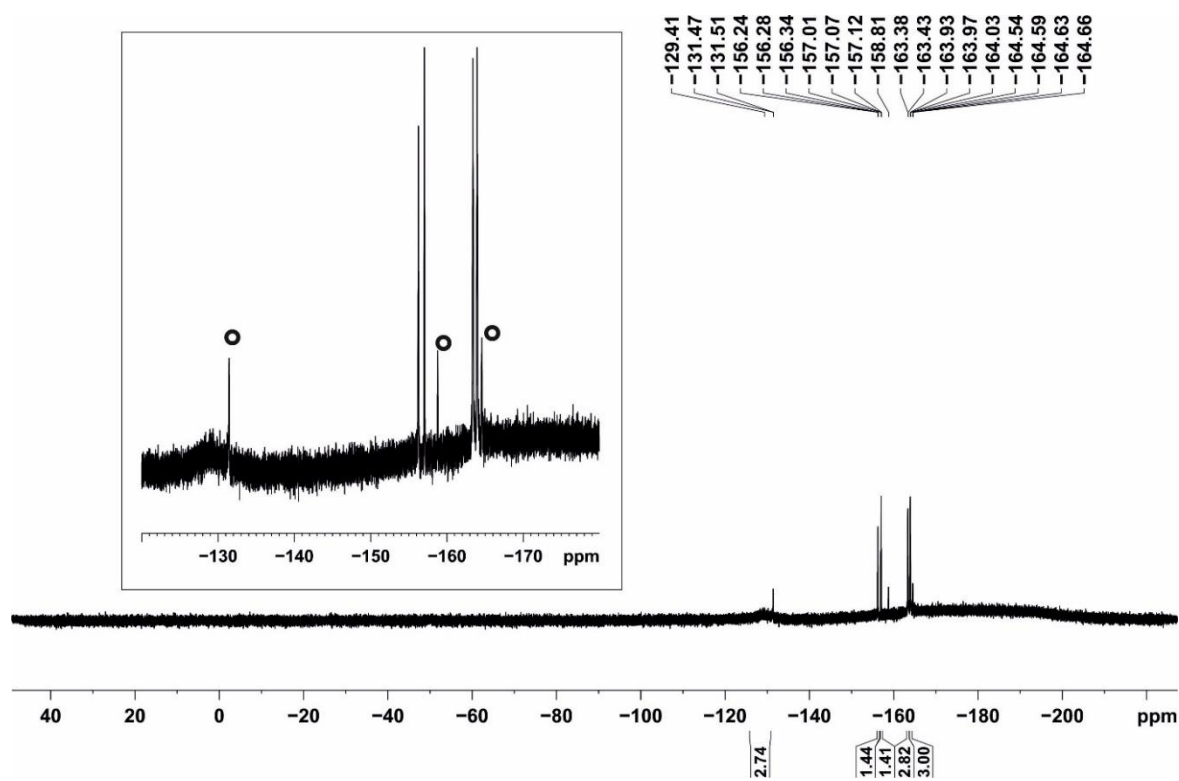


Figure S7. $^{19}\text{F}\{^1\text{H}\}$ NMR spectrum (376.50 MHz, 300 K, d_8 -THF) of **2-BC₆F₅**; °impurities.

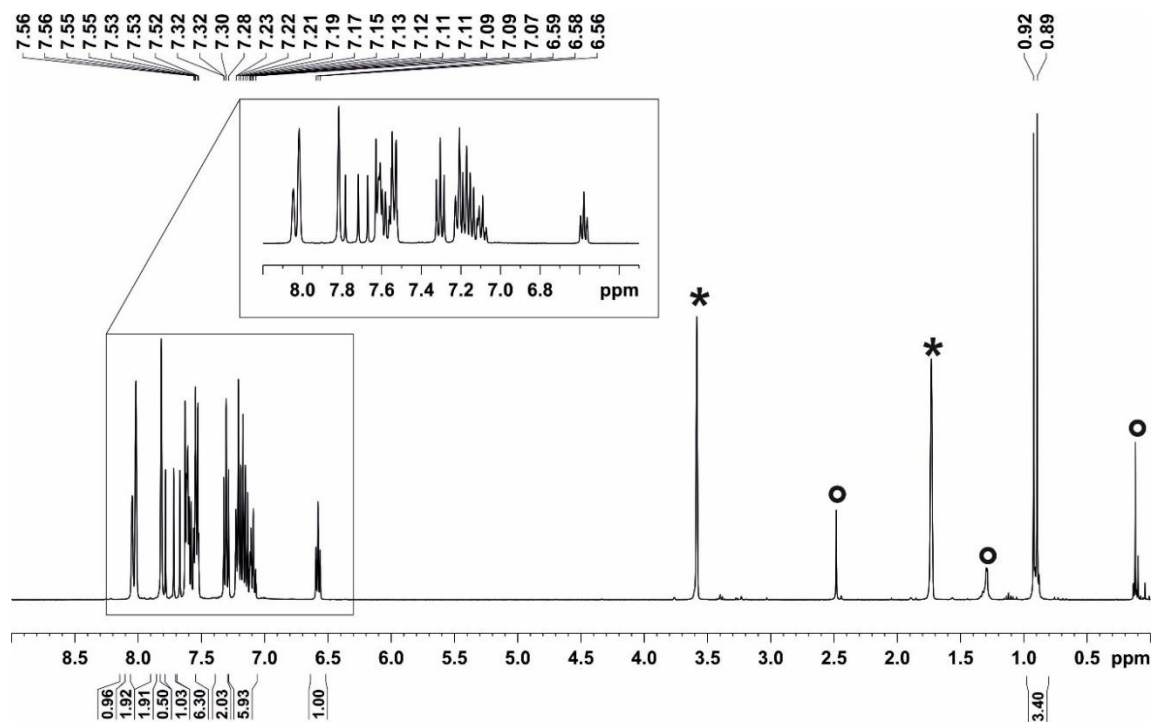


Figure S8. ^1H NMR spectrum (400.13 MHz, 300 K, d_8 -THF) of **2-BCF₃**; * d_8 -THF; °impurities.

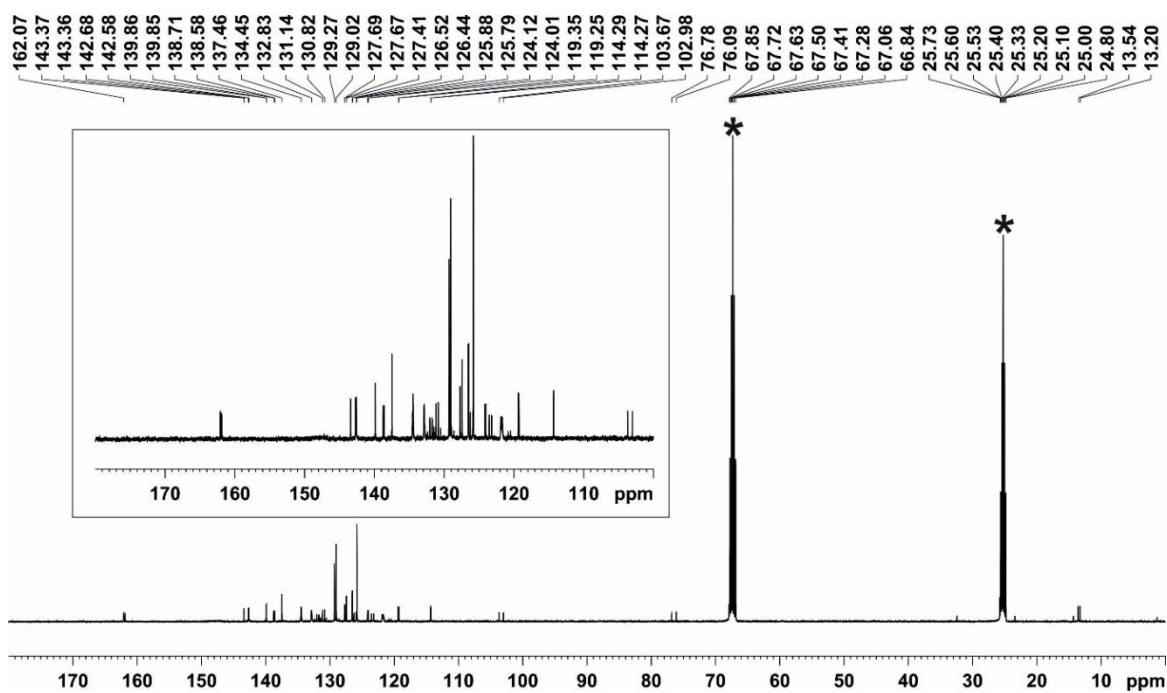


Figure S9. $^{13}\text{C}\{^1\text{H}\}$ NMR spectrum (100.61 MHz, 300 K, d_8 -THF) of **2-BCF₃**; * d_8 -THF.

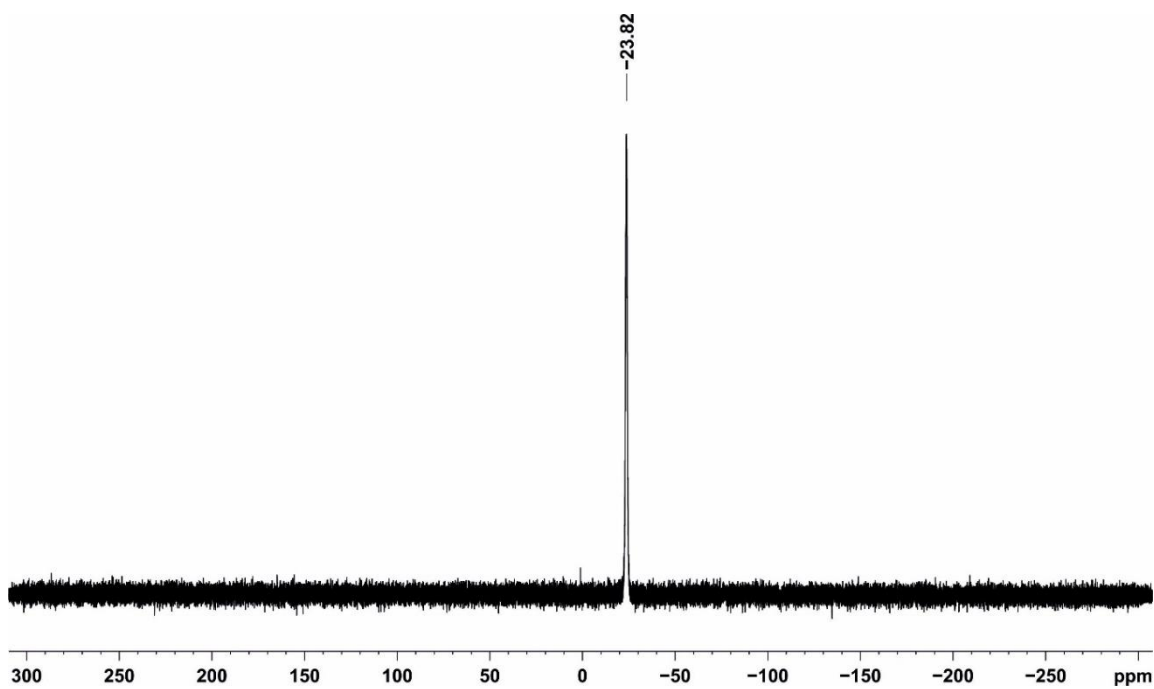


Figure S10. $^{31}\text{P}\{^1\text{H}\}$ NMR spectrum (161.98 MHz, 300 K, d_8 -THF) of **2-BCF₃**.

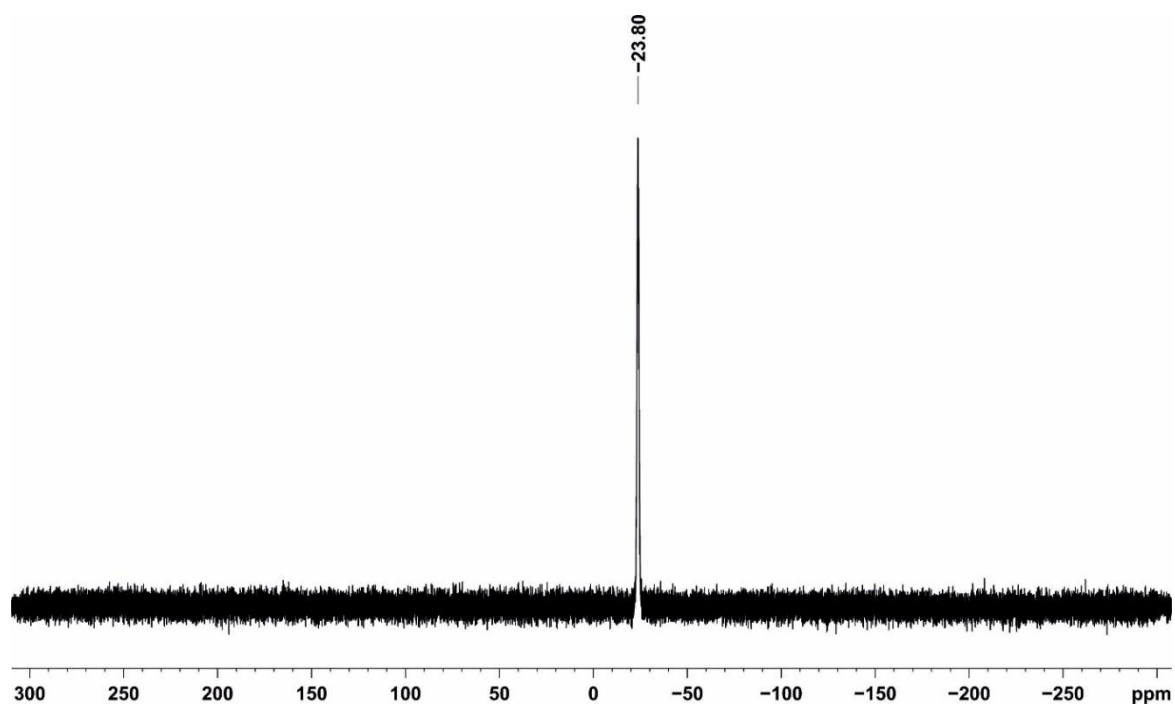


Figure S11. ^{31}P NMR spectrum (161.98 MHz, 300 K, d_8 -THF) of **2-BCF₃**.

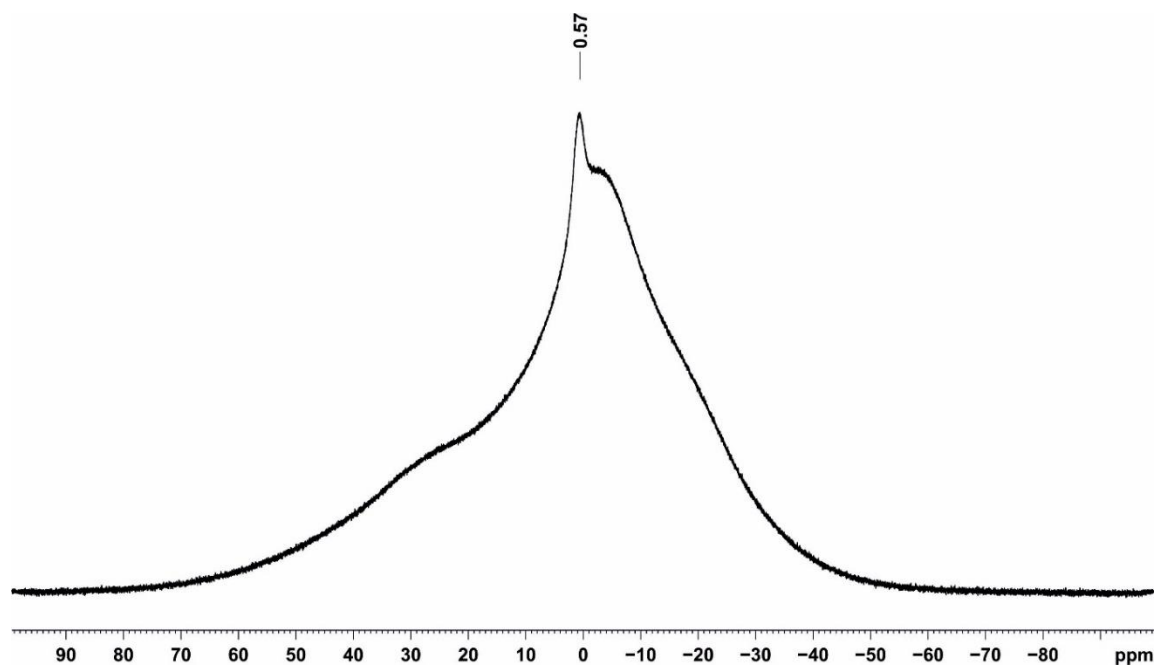


Figure S12. $^{11}\text{B}\{^1\text{H}\}$ NMR spectrum (128.38 MHz, 300 K, d_8 -THF) of **2-BCF₃**.

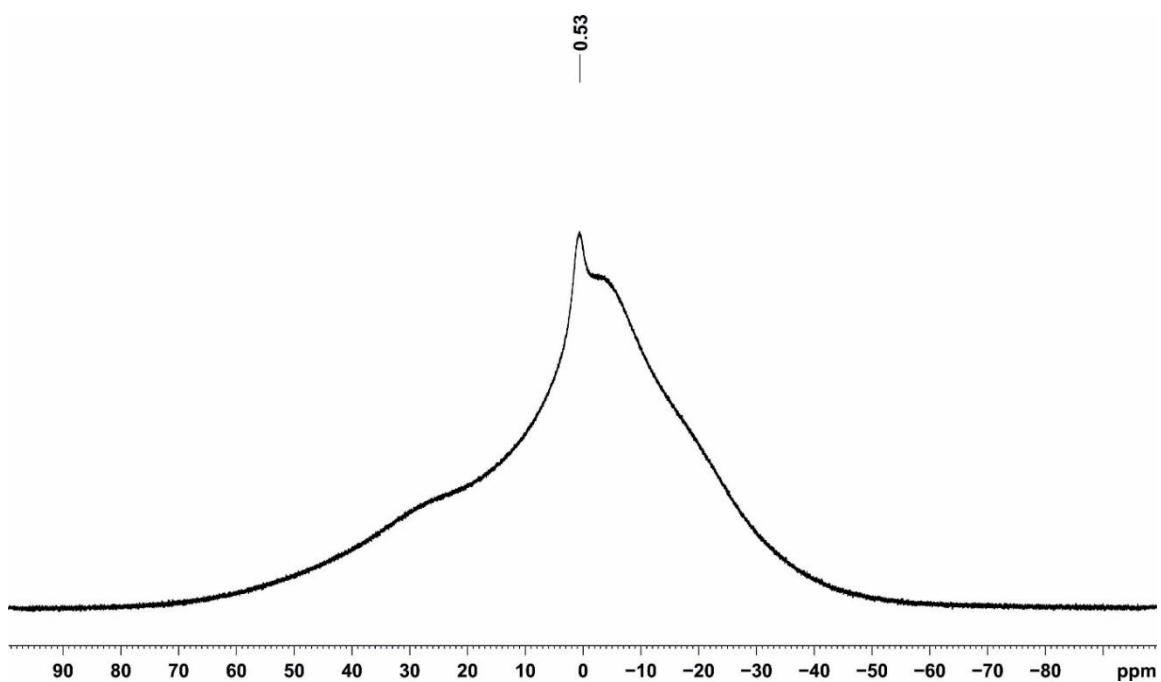


Figure S13. ^{11}B NMR spectrum (128.38MHz, 300 K, $\text{d}_8\text{-THF}$) of **2-BCF₃**.

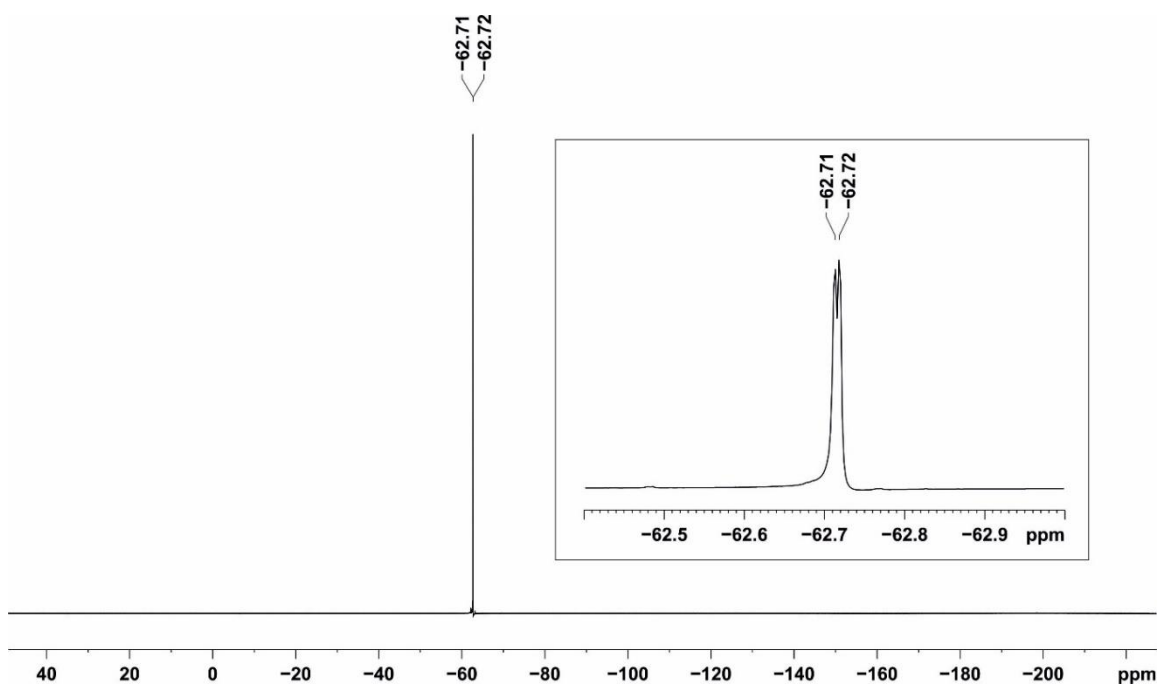


Figure S14. $^{19}\text{F}\{^1\text{H}\}$ NMR spectrum (376.50 MHz, 300 K, $\text{d}_8\text{-THF}$) of **2-BCF₃**.

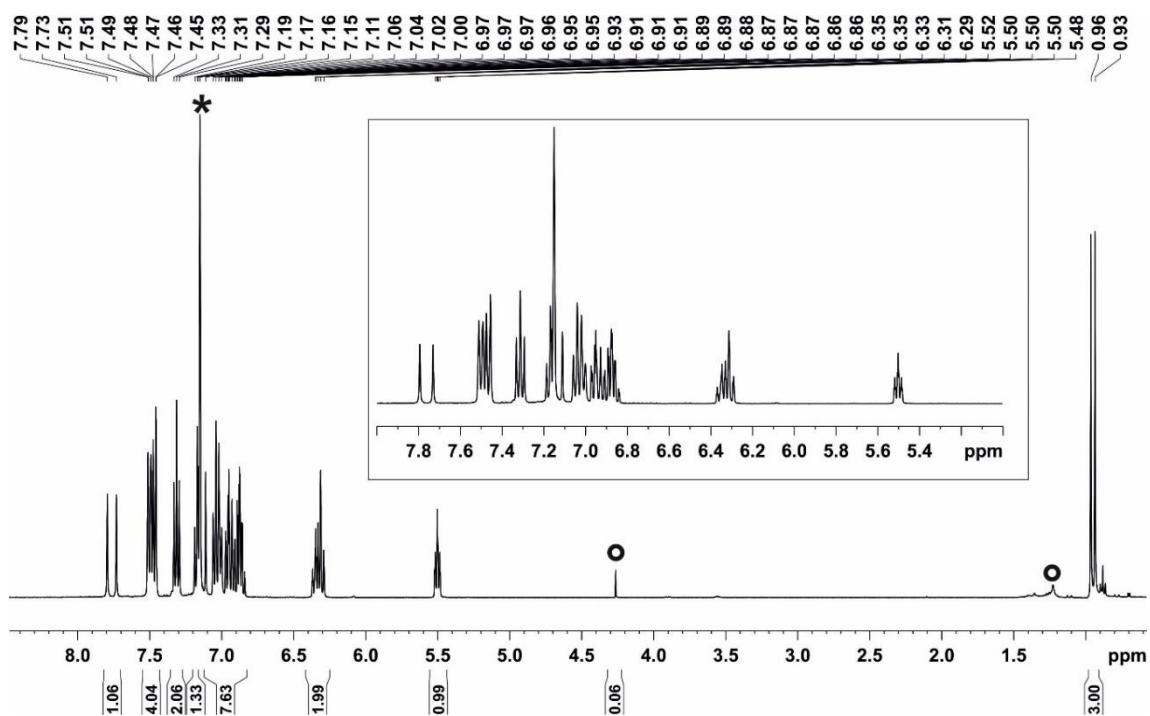


Figure S15. ^1H NMR spectrum (400.13 MHz, 300 K, C_6D_6) of **2-Bcat**; * C_6D_6 ; °impurities.

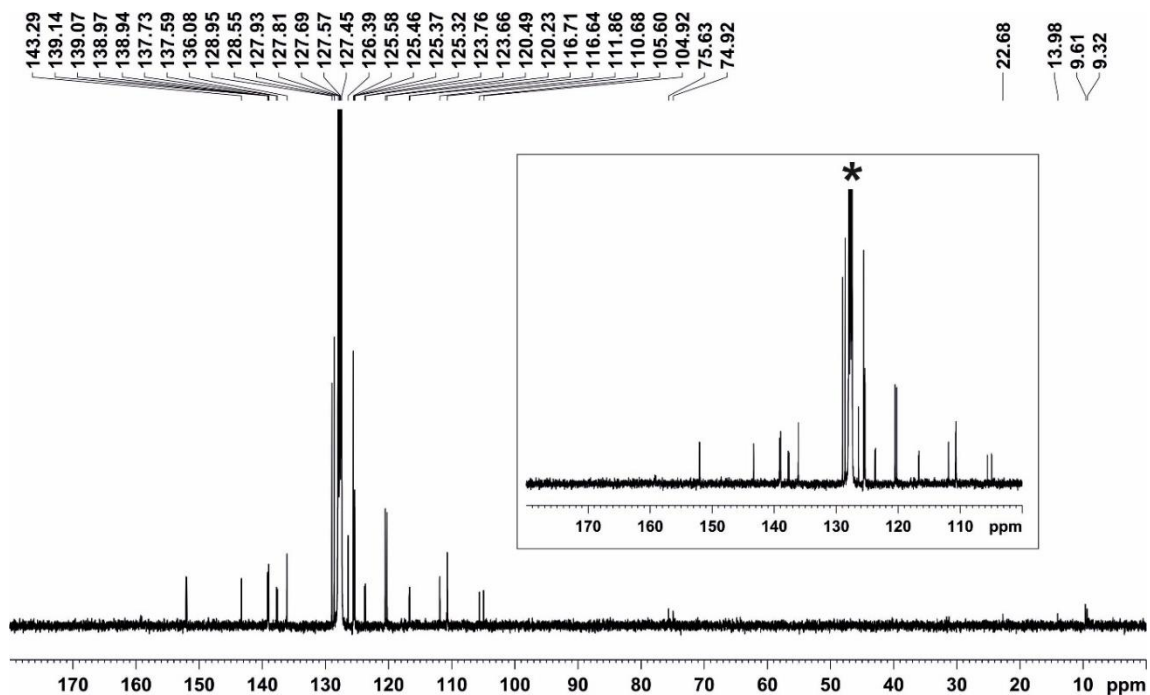


Figure S16. $^{13}\text{C}\{^1\text{H}\}$ NMR spectrum (100.61 MHz, 300 K, C_6D_6) of **2-Bcat**; * C_6D_6 .

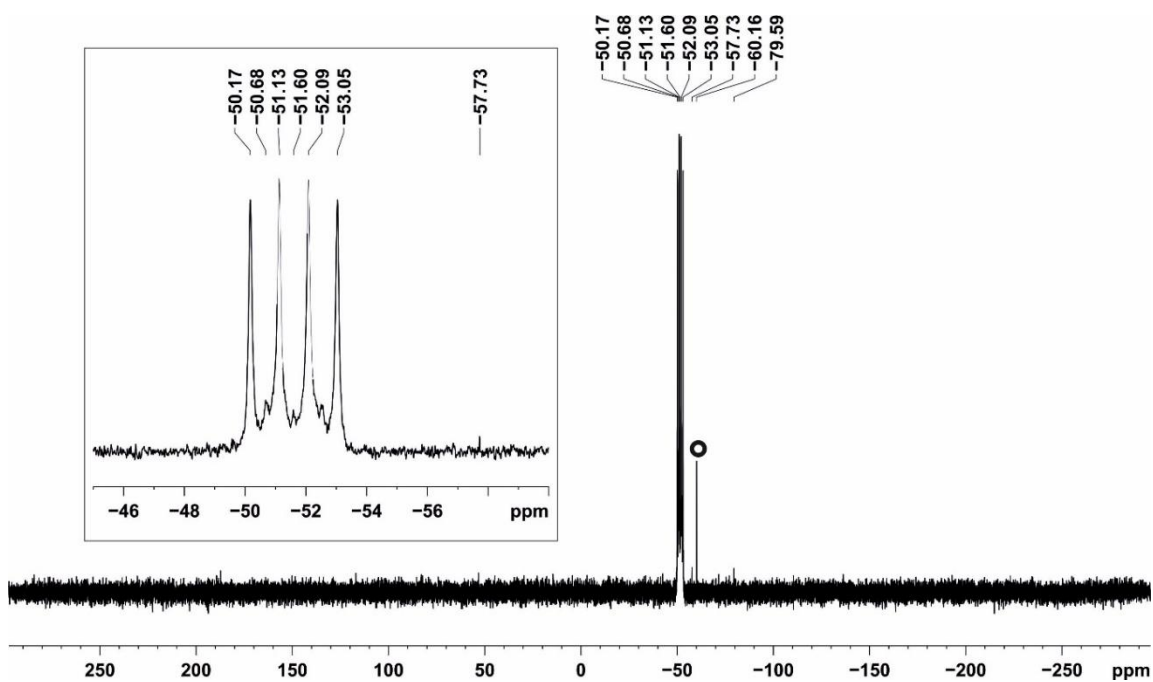


Figure S17. $^{31}\text{P}\{^1\text{H}\}$ NMR spectrum (161.98 MHz, 300 K, C_6D_6) of 2-Bcat; °impurity.

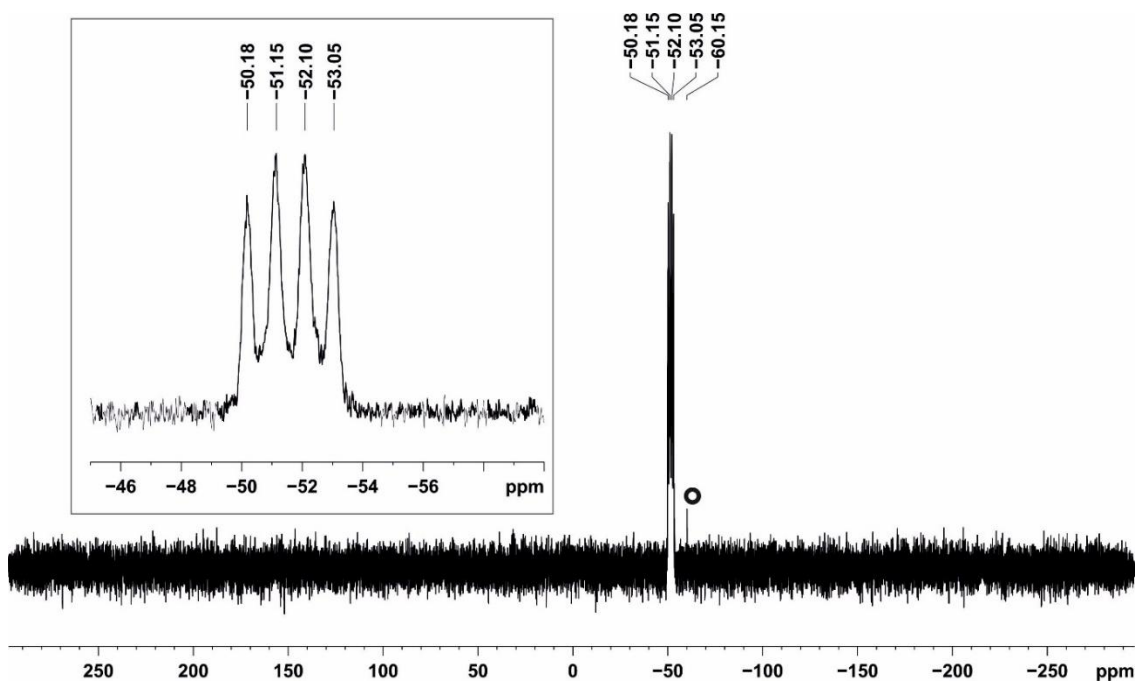


Figure S18. ^{31}P NMR spectrum (161.98 MHz, 300 K, C_6D_6) of 2-Bcat; °impurity.

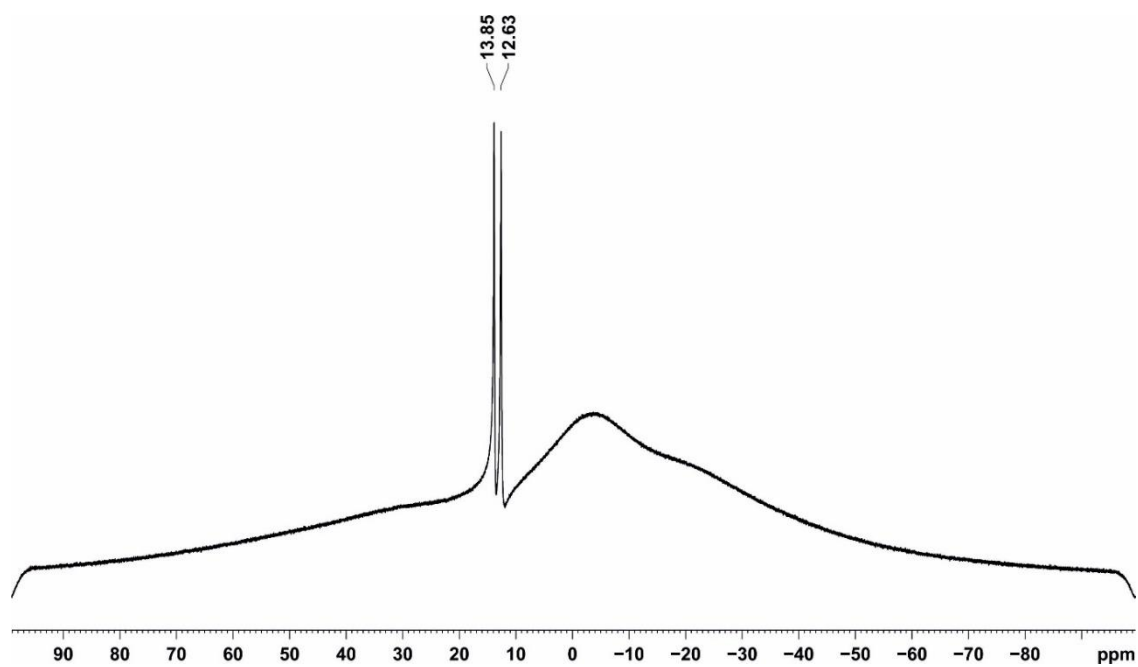


Figure S19. $^{11}\text{B}\{^1\text{H}\}$ NMR spectrum (128.38MHz, 300 K, C_6D_6) of 2-Bcat.

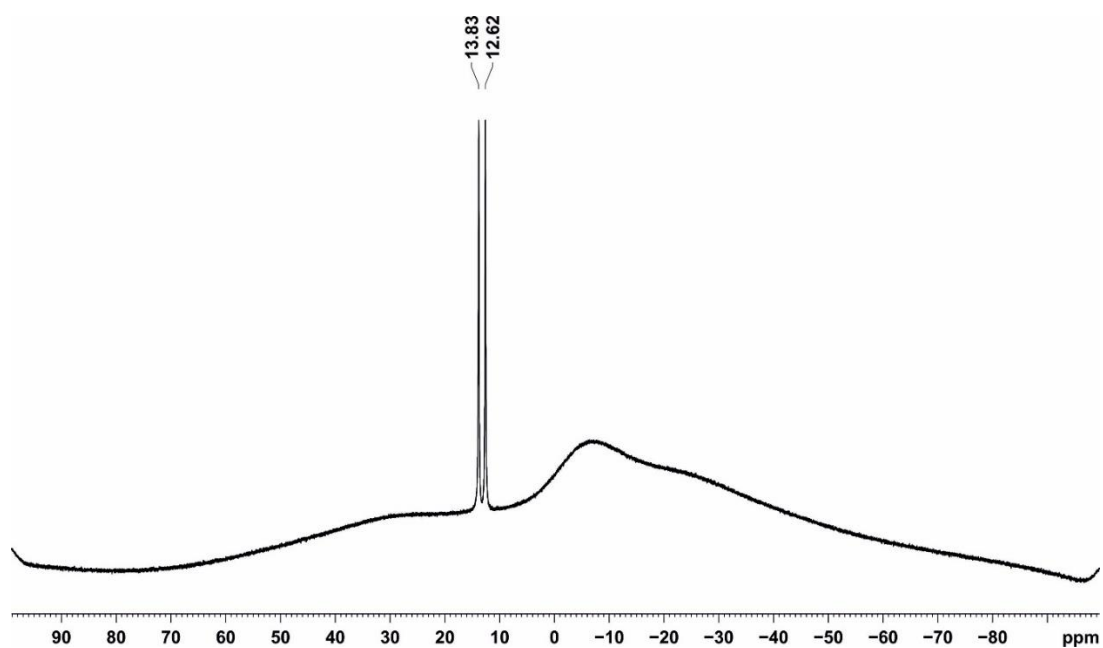


Figure S20. ^{11}B NMR spectrum (128.38MHz, 300 K, C_6D_6) of 2-Bcat.

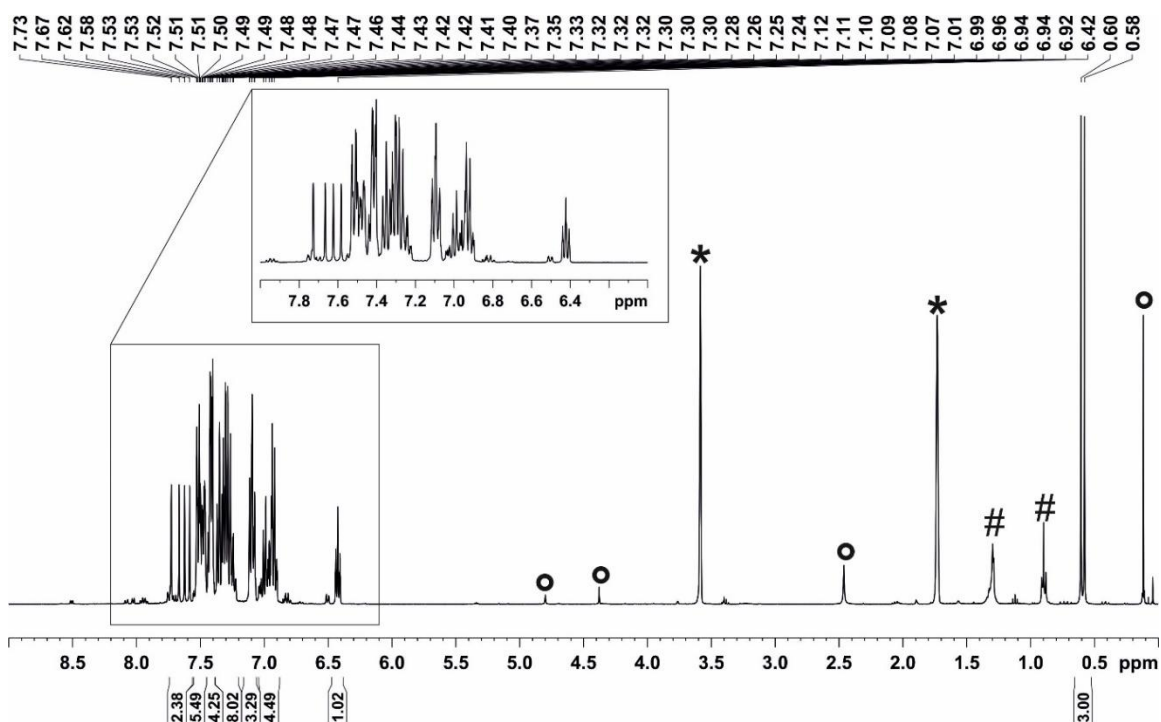


Figure S21. ^1H NMR spectrum (400.13 MHz, 300 K, $\text{d}_8\text{-THF}$) of **2-BPh**; * $\text{d}_8\text{-THF}$; \circ impurities; # *n*-hexane.

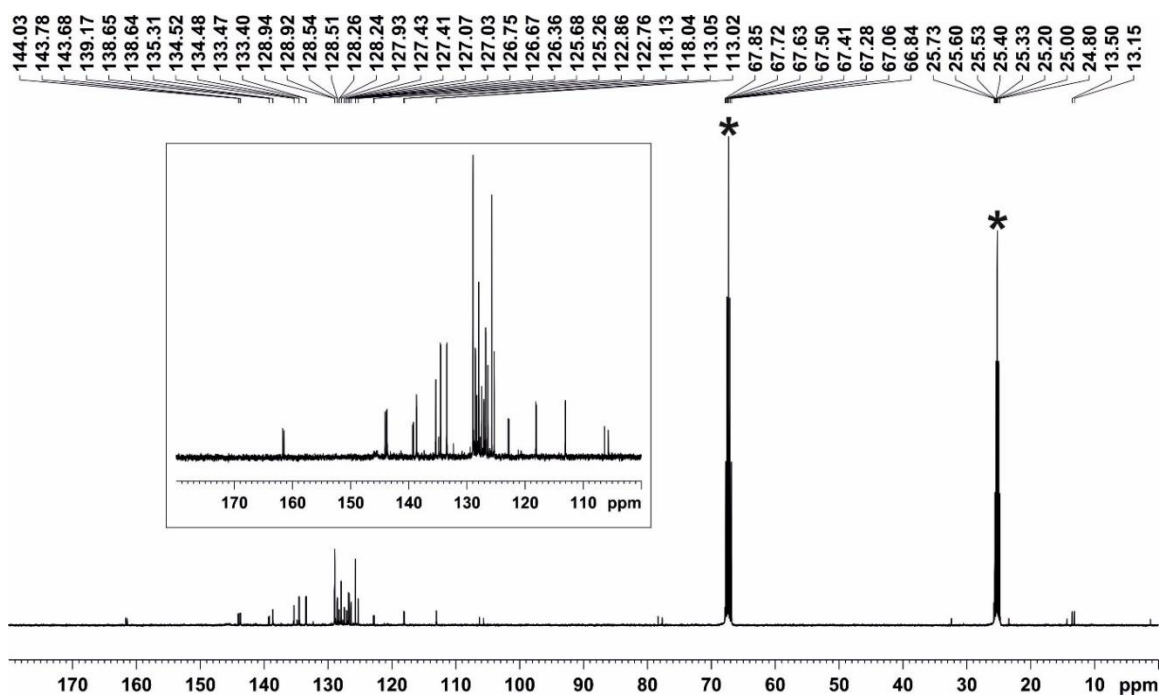


Figure S22. $^{13}\text{C}\{^1\text{H}\}$ NMR spectrum (100.61 MHz, 300 K, $\text{d}_8\text{-THF}$) of **2-BPh**; * $\text{d}_8\text{-THF}$.

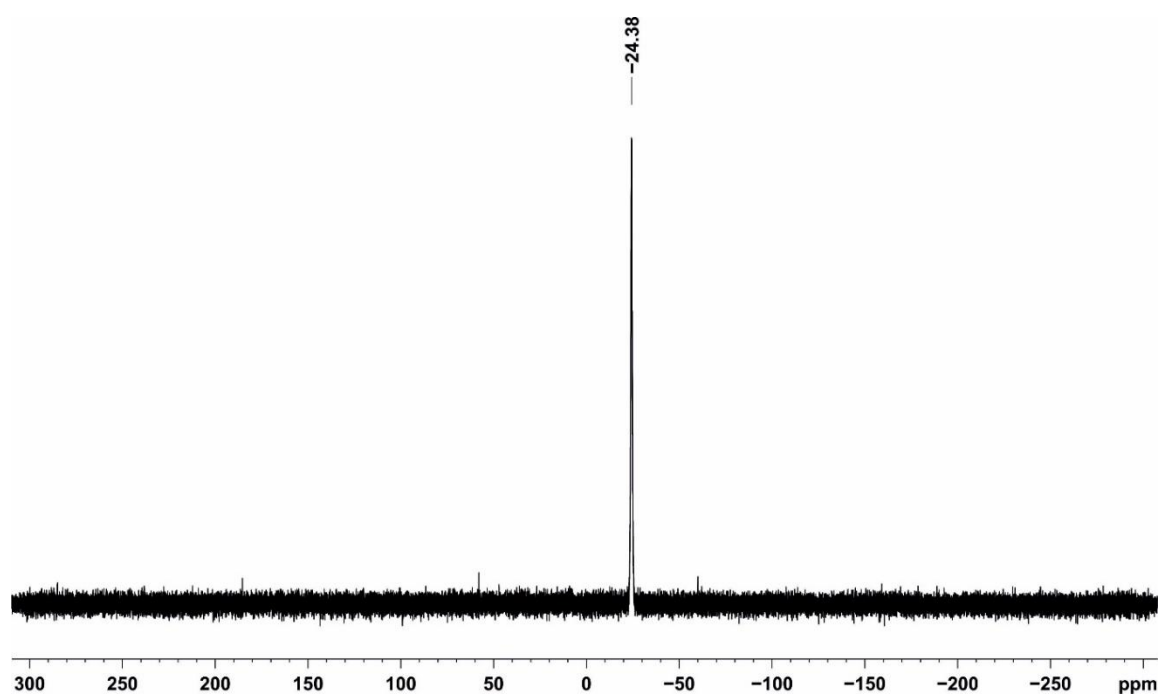


Figure S23. $^{31}\text{P}\{^1\text{H}\}$ NMR spectrum (161.98 MHz, 300 K, d_8 -THF) of **2-BPh**.

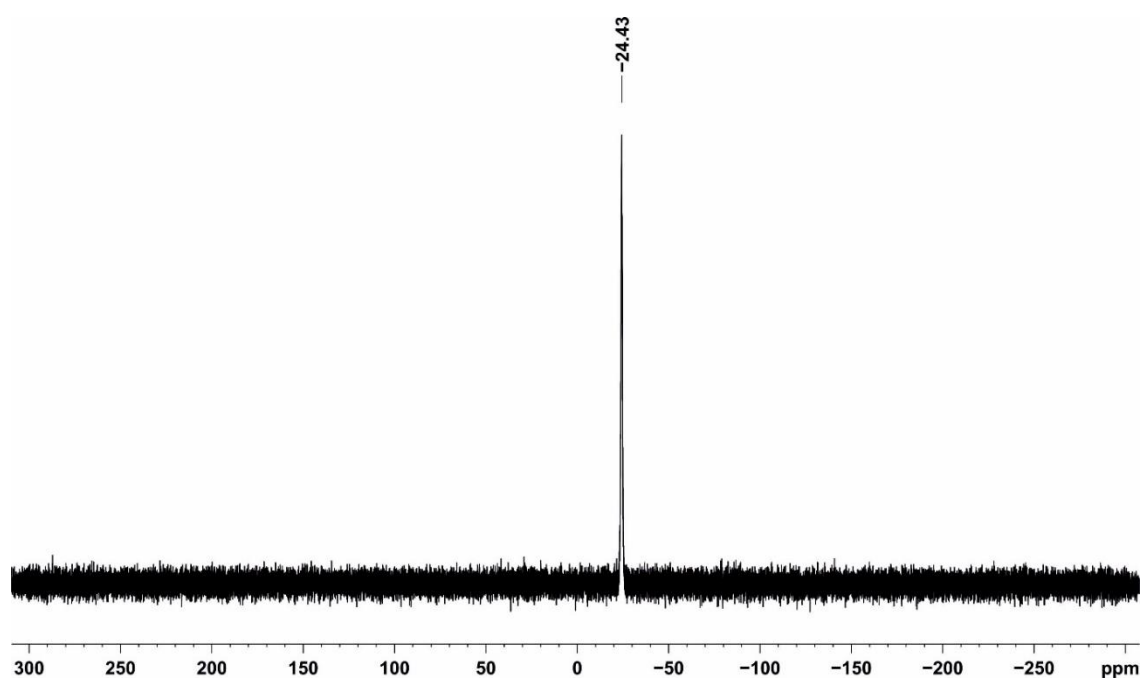


Figure S24. ^{31}P NMR spectrum (161.98 MHz, 300 K, d_8 -THF) of **2-BPh**.

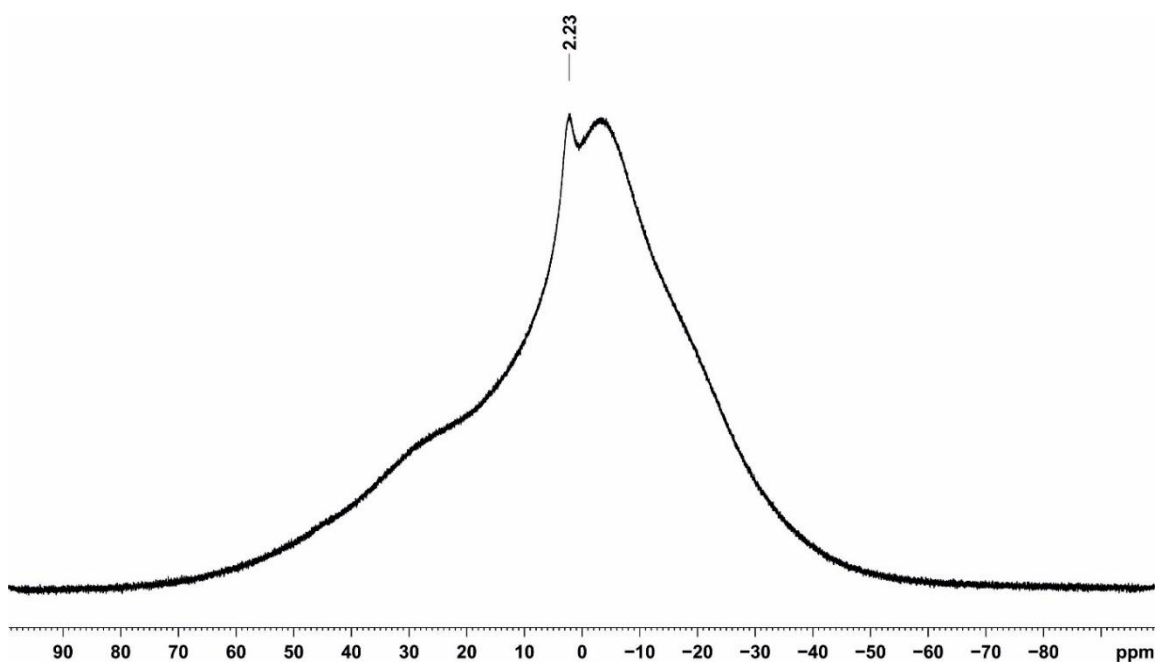


Figure S25. $^{11}\text{B}\{^1\text{H}\}$ NMR spectrum (128.38MHz, 300 K, d_8 -THF) of 2-BPh.

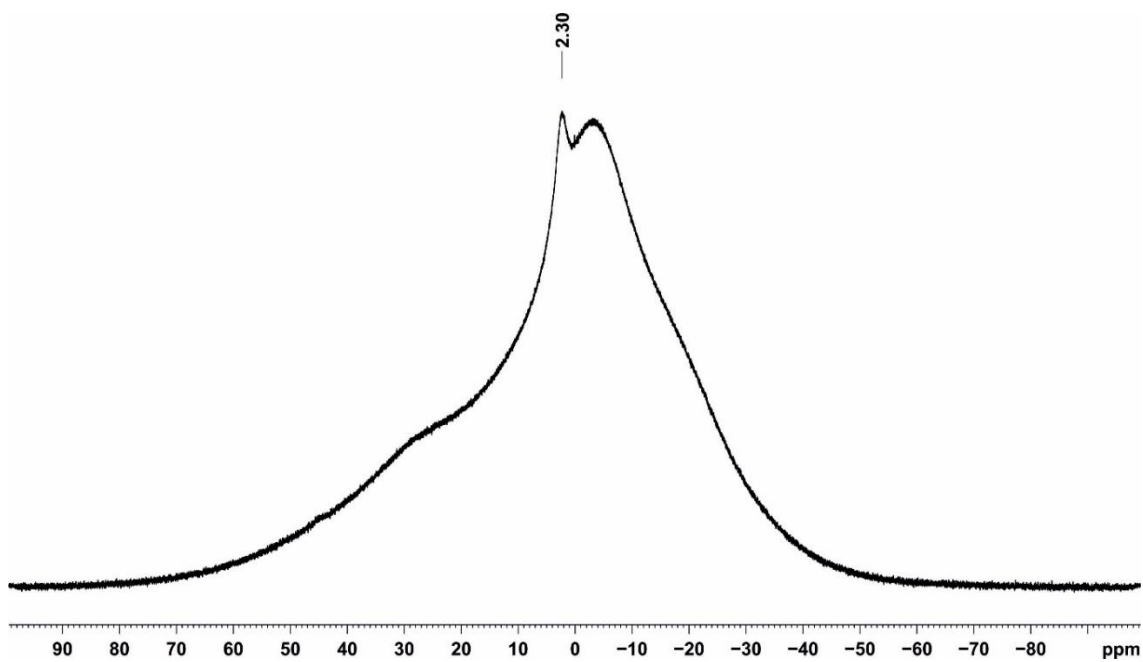


Figure S26. ^{11}B NMR spectrum (128.38MHz, 300 K, d_8 -THF) of 2-BPh.

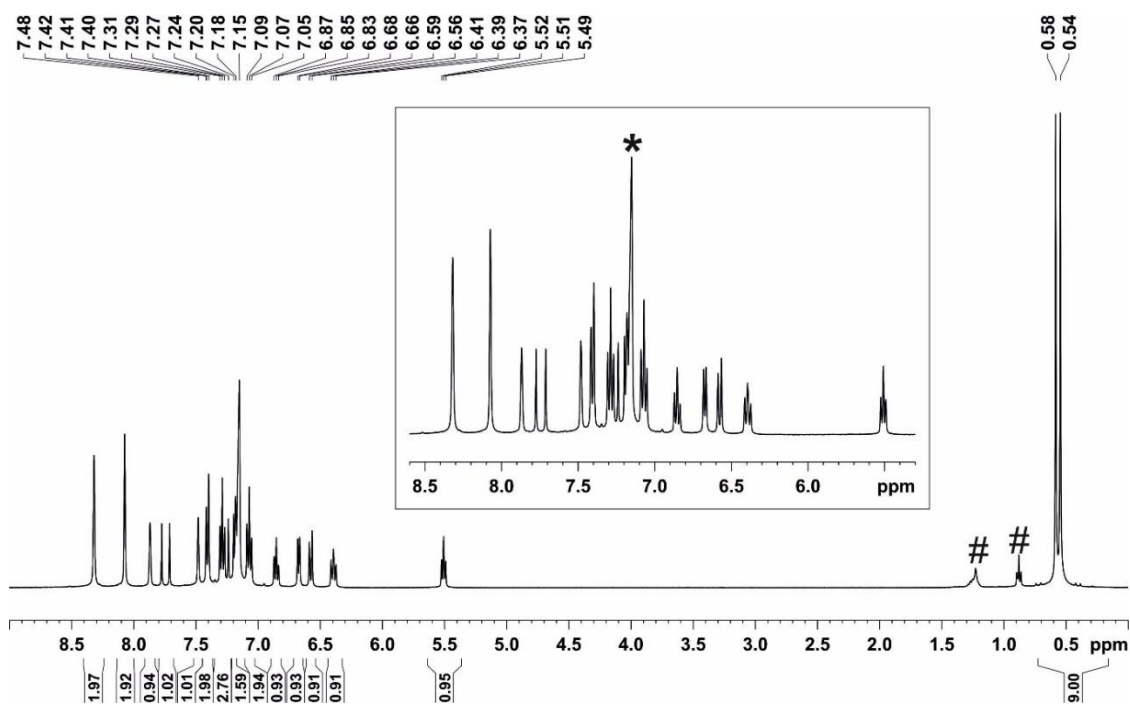


Figure S27. ^1H NMR spectrum (400.13 MHz, 300 K, C_6D_6) of **3-BCF₃**; * C_6D_6 ; °impurities; #*n*-hexane.

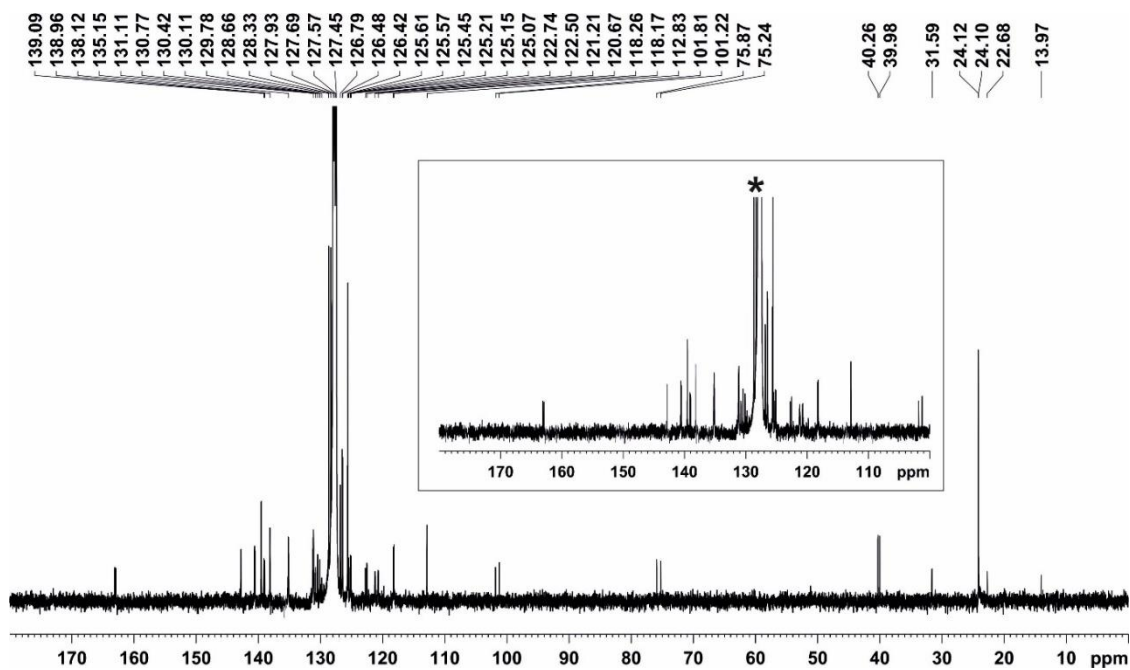


Figure S28. $^{13}\text{C}\{^1\text{H}\}$ NMR spectrum (100.61 MHz, 300 K, C_6D_6) of **3-BCF₃**; * C_6D_6 .

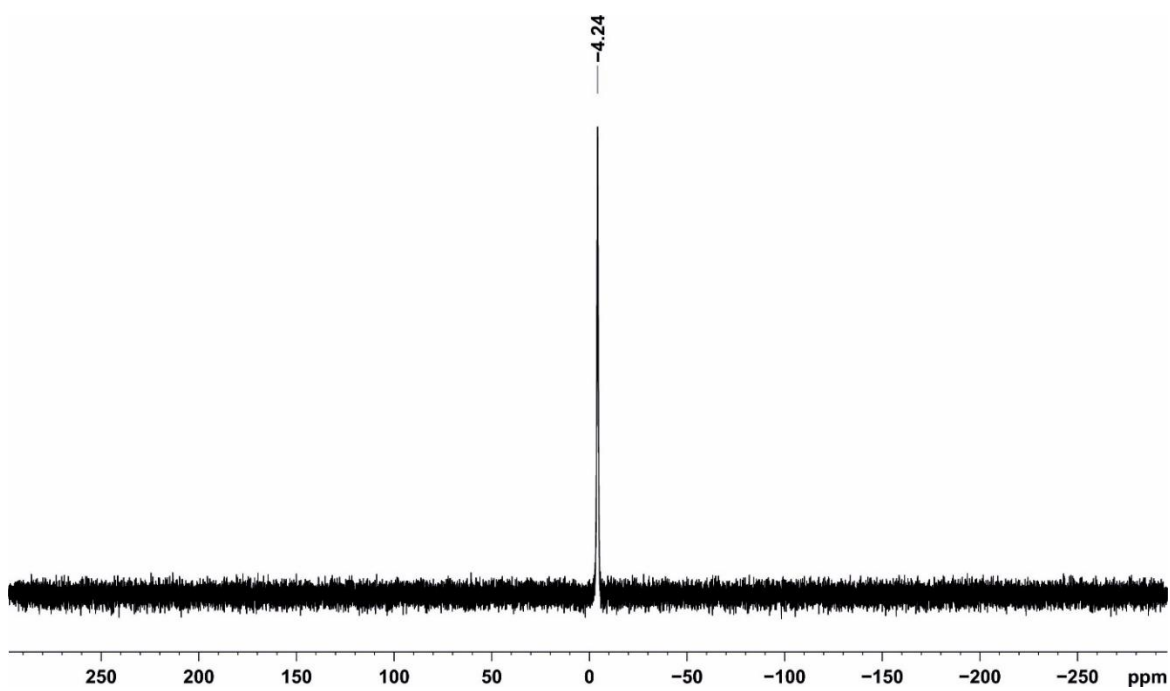


Figure S29. $^{31}\text{P}\{^1\text{H}\}$ NMR spectrum (161.98 MHz, 300 K, C_6D_6) of **3-BCF₃**.

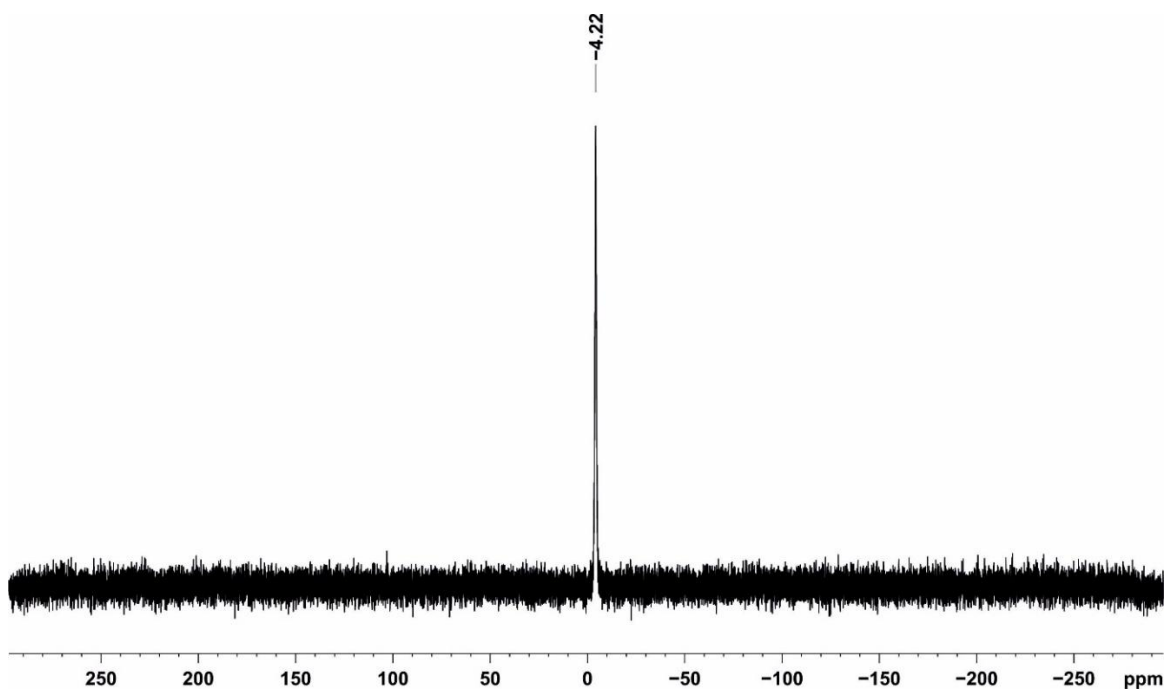


Figure S30. ^{31}P NMR spectrum (161.98 MHz, 300 K, C_6D_6) of **3-BCF₃**.

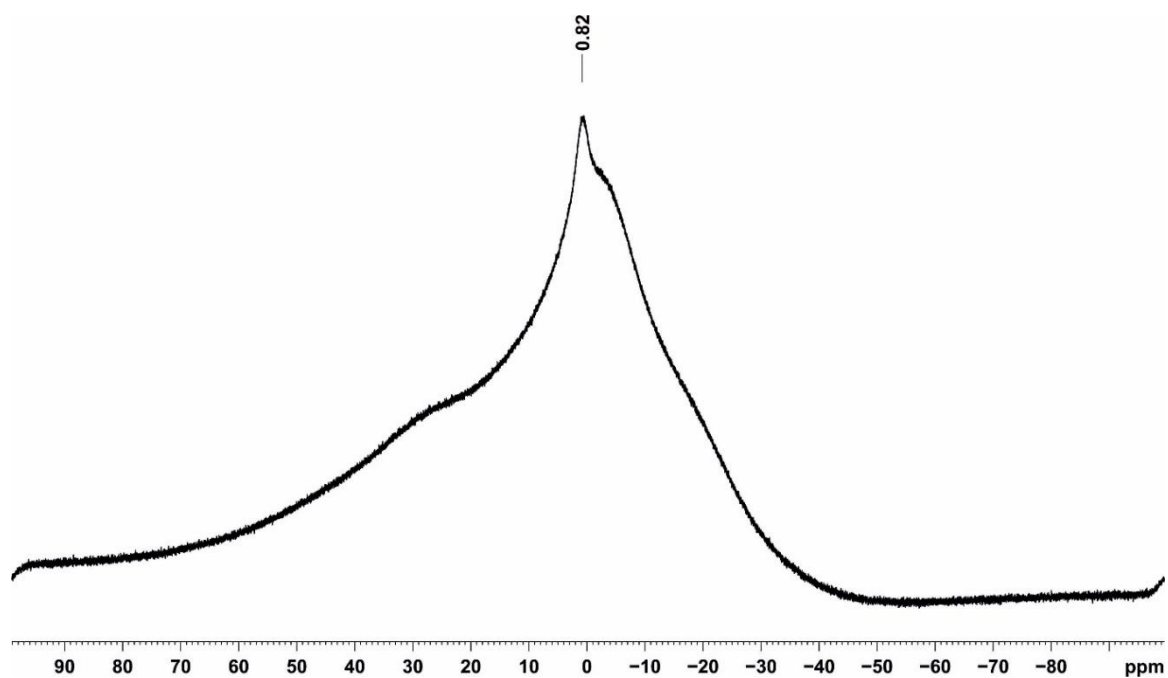


Figure S31. $^{11}\text{B}\{^1\text{H}\}$ NMR spectrum (128.38MHz, 300 K, C_6D_6) of **3-BCF₃**.

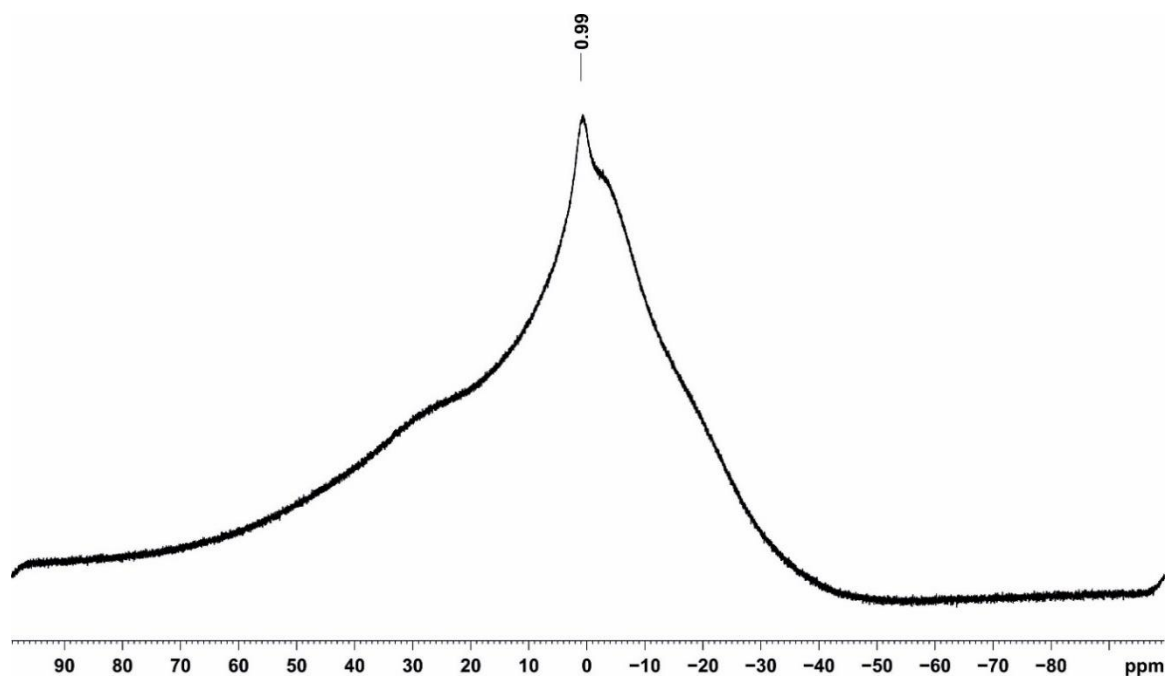


Figure S32. ^{11}B NMR spectrum (128.38MHz, 300 K, C_6D_6) of **3-BCF₃**.

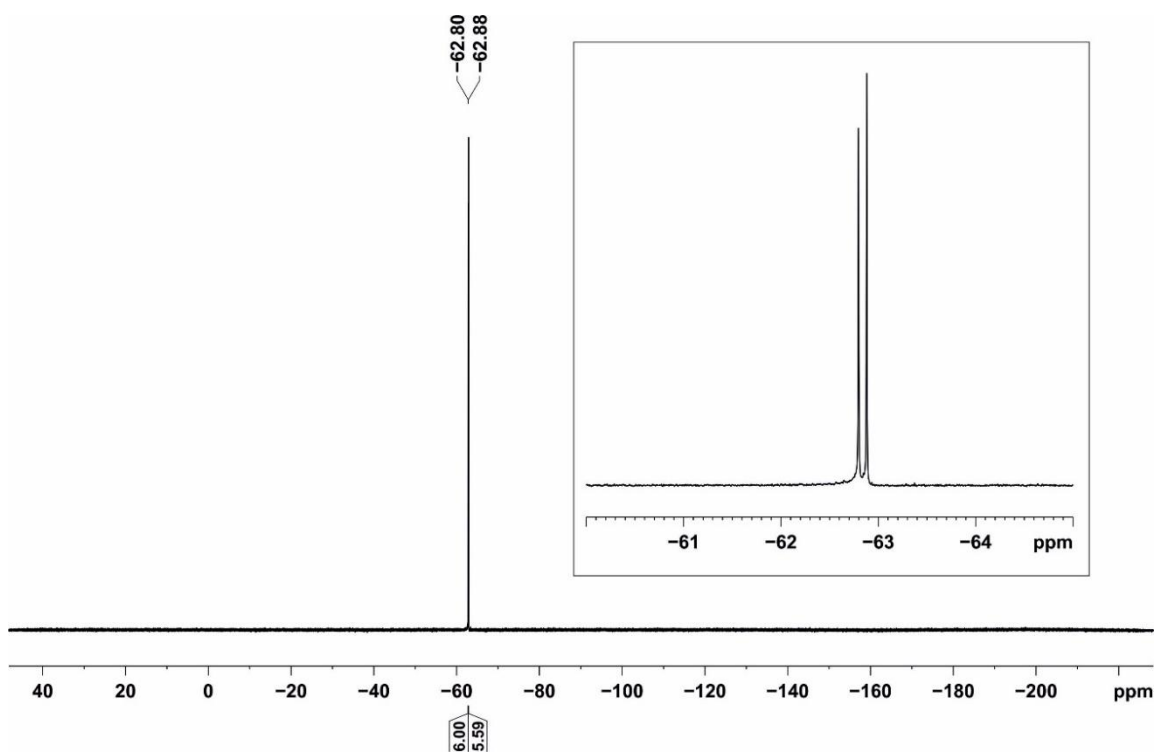


Figure S33. $^{19}\text{F}\{^1\text{H}\}$ NMR spectrum (376.50 MHz, 300 K, C₆D₆) of 3-BCF₃.

4.6.2 UV-Vis Spectra

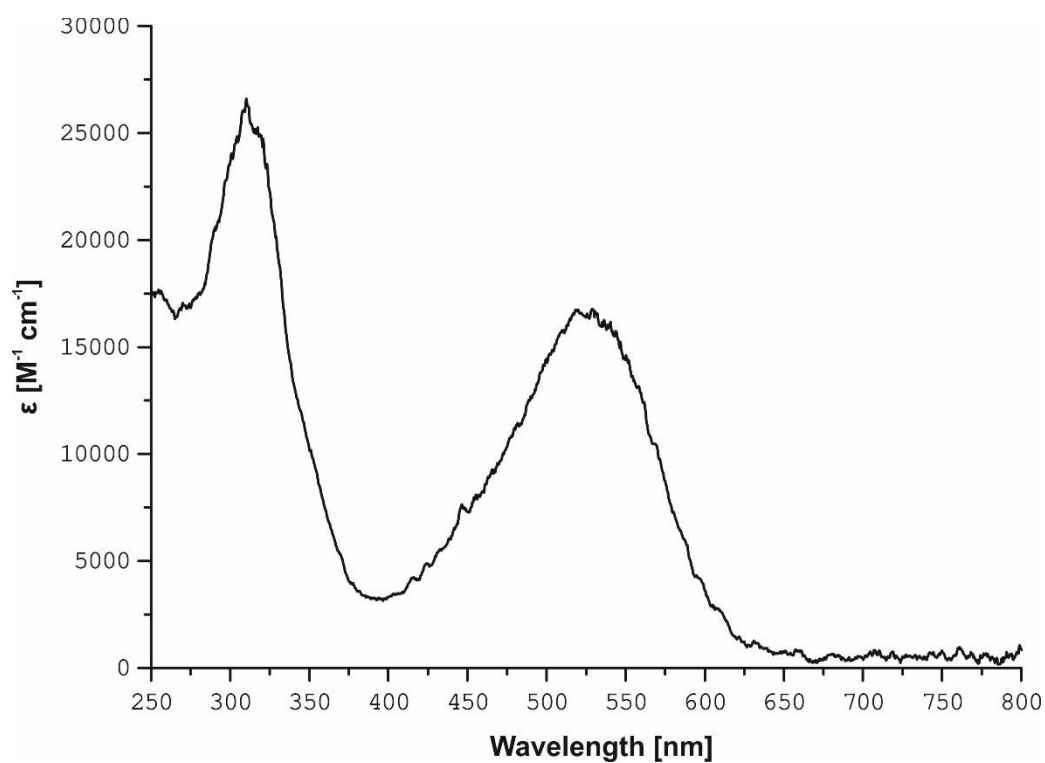


Figure S33. UV-Vis spectrum of 2-BC₆F₅ in *n*-hexane.

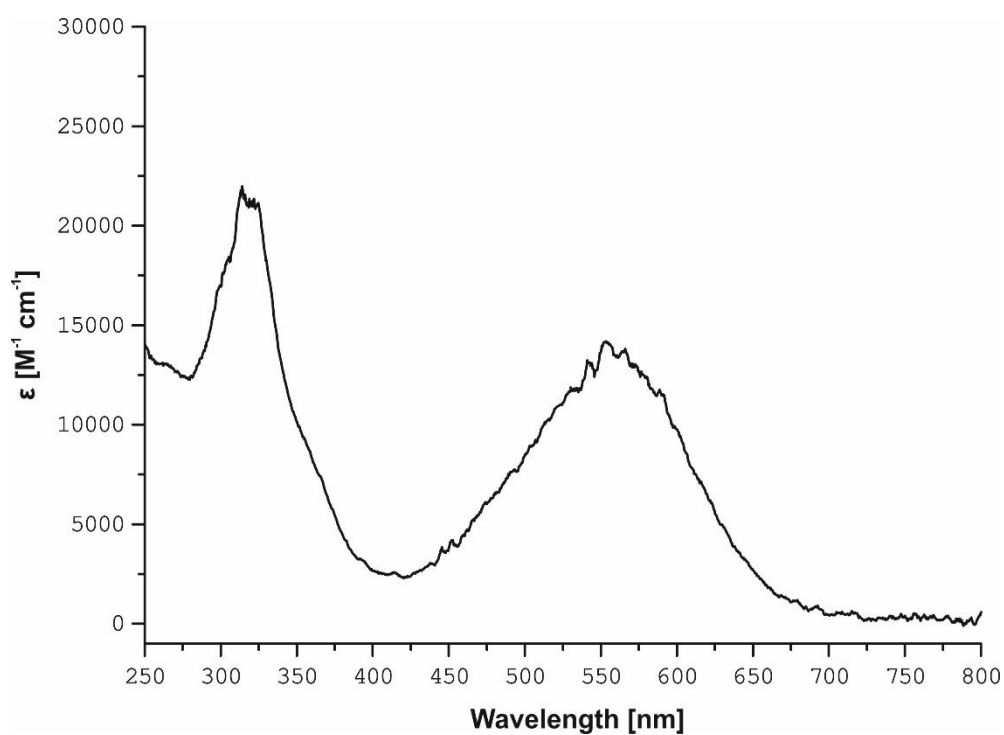


Figure S34. UV-Vis spectrum of 2-BCF₃ in *n*-hexane.

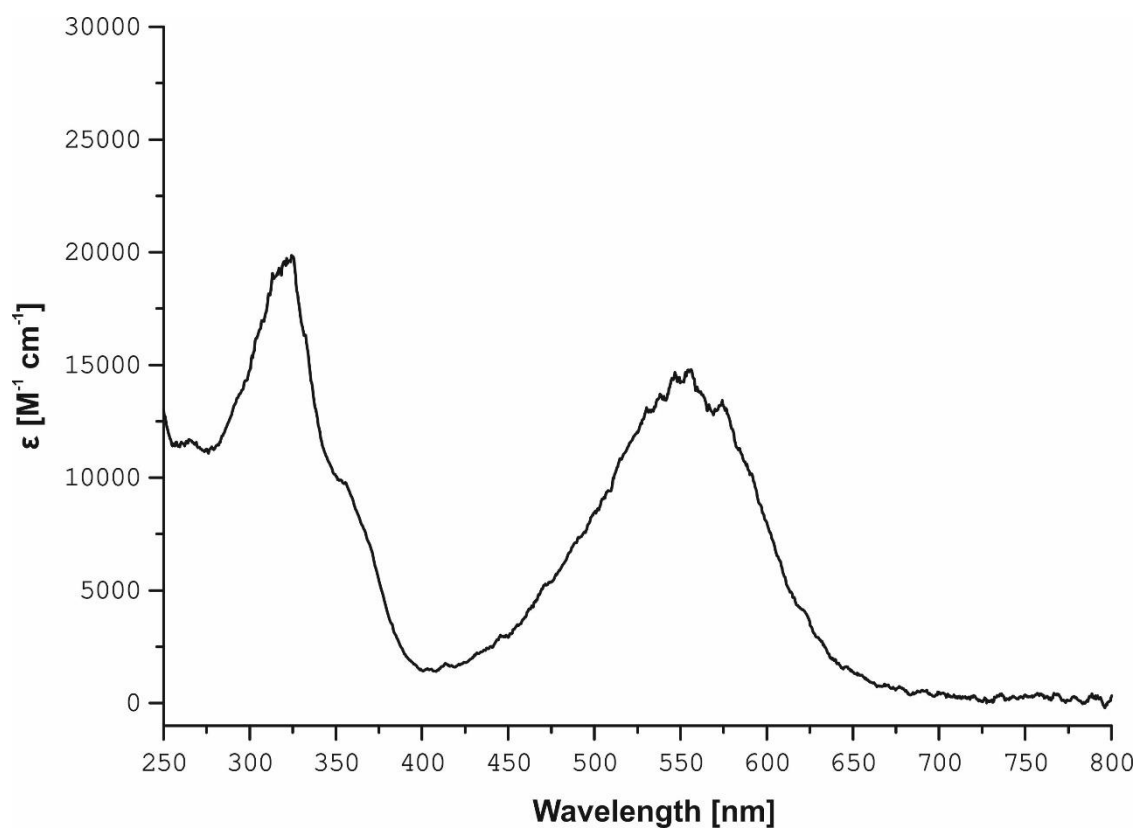


Figure S35. UV-Vis spectrum of 2-Bcat in *n*-hexane.

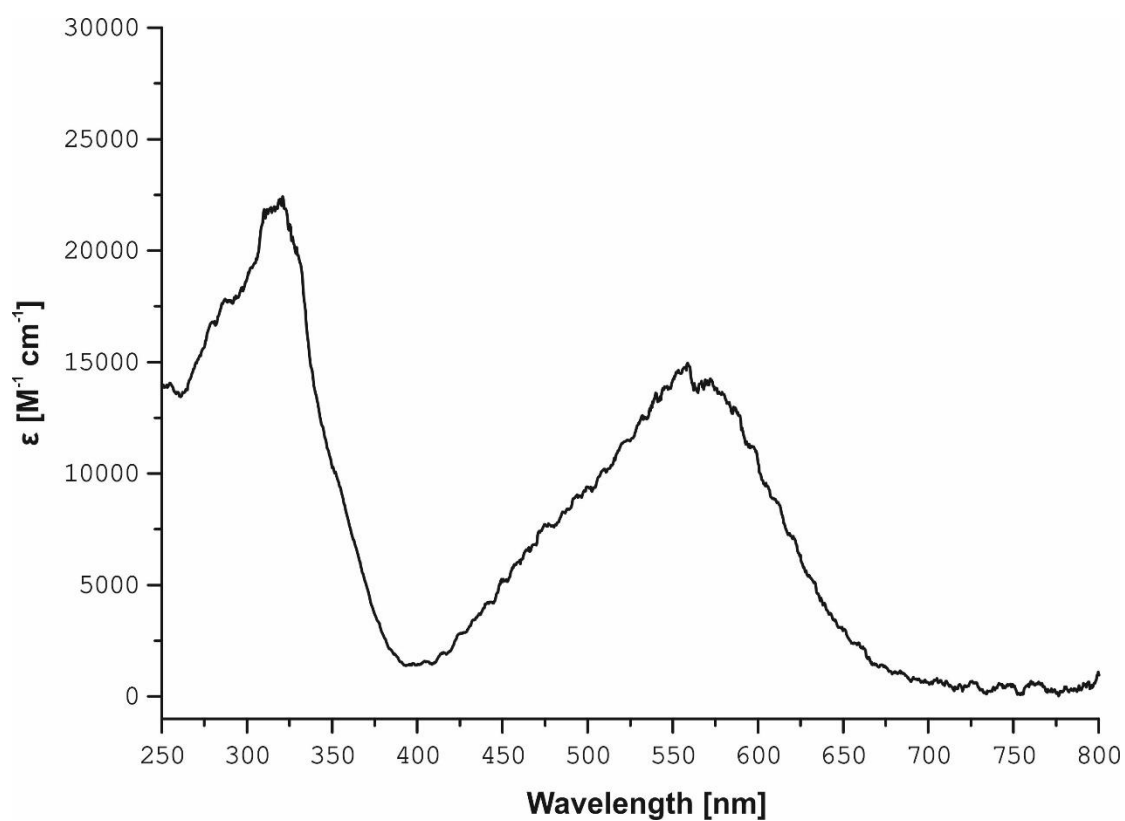


Figure S36. UV-Vis spectrum of 2-BPh in *n*-hexane.

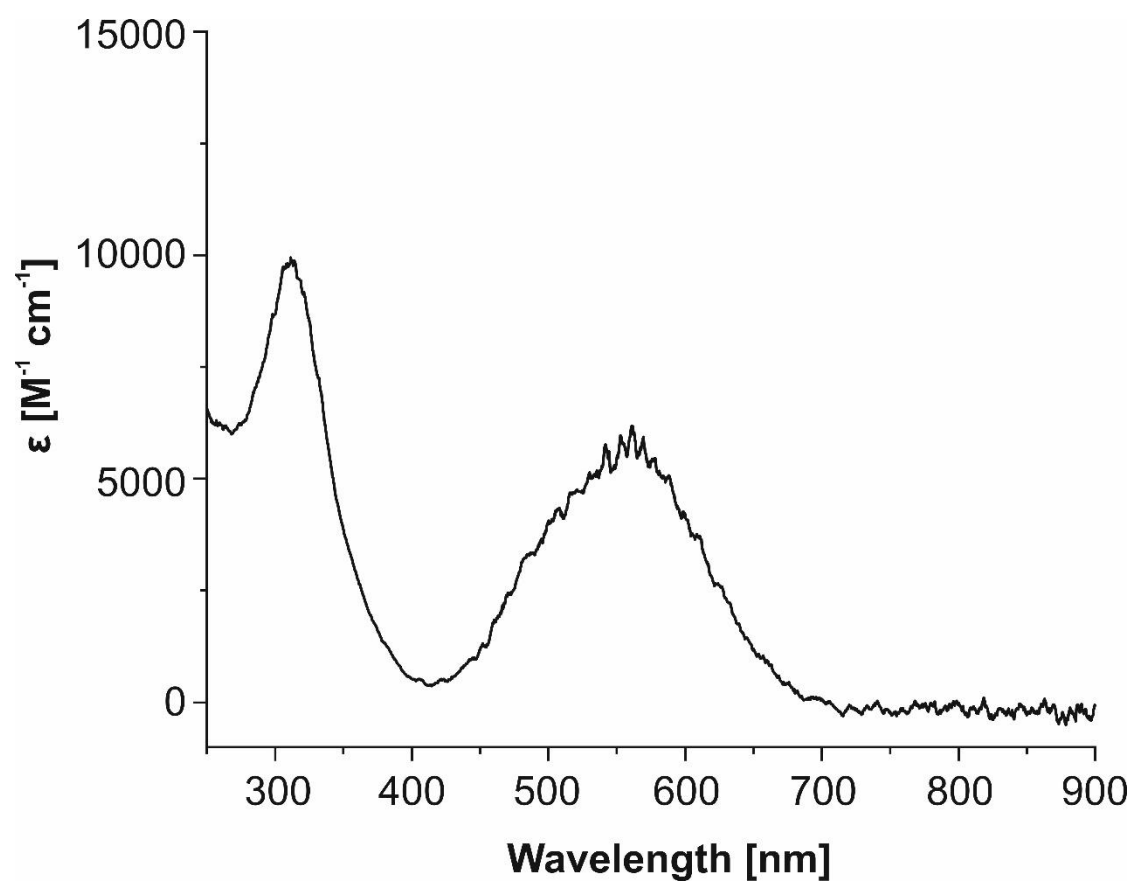


Figure S37. UV-Vis spectrum of 3-BCF₃ in *n*-hexane.

4.6.3 X-ray Crystallography

Table S1. Crystallographic data and structure refinement of **2-BC₆F₅**, **2-BCF₃**, **2-Bcat**, **2-BPh** and **4**.

	2-BC₆F₅	2-BCF₃	2-Bcat	2-BPh	4
Empirical formula	C ₃₅ H ₁₉ BF ₁₀ N P	C _{38.97} H ₂₅ BF ₁₂ N P	C ₂₉ H ₂₃ BNO ₂ P	C ₃₅ H ₂₉ BNP	C ₃₈ H ₂₅ BF ₁₀ N P
Formula weight / g·mol ⁻¹	685.29	777.07	459.26	505.37	727.37
Temperature / K	123.00(10)	123.00(10)	122.9(2)	123.01(10)	123.01(10)
Crystal system	triclinic	monoclinic	monoclinic	monoclinic	triclinic
Space group	P-1	C2/c	P2 ₁ /c	P2 ₁ /n	P-1
<i>a</i> / Å	9.8580(4)	44.6690(9)	7.23010(10)	15.2972(2)	11.0415(2)
<i>b</i> / Å	12.2894(4)	12.8687(2)	19.6816(4)	10.86050(10)	17.6184(3)
<i>c</i> / Å	13.1020(5)	38.7984(9)	17.9632(3)	16.8841(2)	18.7209(4)
<i>α</i> / °	85.388(3)	90	90	90	113.966(2)
<i>β</i> / °	87.082(3)	105.782(3)	96.074(2)	106.6030(10)	95.767(2)
<i>γ</i> / °	71.571(3)	90	90	90	96.533(2)
<i>V</i> / Å ³	1500.47(10)	21461.8(8)	2541.81(8)	2688.09(6)	3262.81(12)
<i>Z</i>	2	24	4	4	4
<i>ρ</i> _{calc} / g cm ⁻³	1.517	1.443	1.200	1.249	1.481
<i>μ</i> / mm ⁻¹	1.631	1.520	1.153	1.080	1.533
F(000)	692.0	9452.0	960.0	1064.0	1480.0
Crystal size / mm ³	0.311 × 0.162 × 0.111	0.653 × 0.139 × 0.111	0.435 × 0.136 × 0.101	0.488 × 0.279 × 0.138	0.225 × 0.17 × 0.121
Radiation / Å	CuKα (λ = 1.54184)	CuKα (λ = 1.54184)	CuKα (λ = 1.54184)	CuKα (λ = 1.54184)	CuKα (λ = 1.54184)
2θ range for data collection / °	6.77 to 147.976	7.066 to 147.888	8.986 to 150.916	6.884 to 147.79	8.168 to 147.572
Diffractometer	SuperNova	SuperNova	SuperNova	SuperNova	SuperNova
Index ranges	-12 ≤ <i>h</i> ≤ 9, -14 ≤ <i>k</i> ≤ 15, -15 ≤ <i>l</i> ≤ 16	-55 ≤ <i>h</i> ≤ 55, -11 ≤ <i>k</i> ≤ 16, -48 ≤ <i>l</i> ≤ 47	-5 ≤ <i>h</i> ≤ 8, -24 ≤ <i>k</i> ≤ 22, -22 ≤ <i>l</i> ≤ 21	-16 ≤ <i>h</i> ≤ 18, -13 ≤ <i>k</i> ≤ 9, -20 ≤ <i>l</i> ≤ 21	-12 ≤ <i>h</i> ≤ 13, -21 ≤ <i>k</i> ≤ 21, -23 ≤ <i>l</i> ≤ 23
Reflections collected	11137	79378	8996	20071	58164
Independent reflections	5909 [R _{int} = 0.0160, R _{sigma} = 0.0199]	21401 [R _{int} = 0.0435, R _{sigma} = 0.0370]	5017 [R _{int} = 0.0242, R _{sigma} = 0.0275]	5360 [R _{int} = 0.0205, R _{sigma} = 0.0165]	13015 [R _{int} = 0.0369, R _{sigma} = 0.0254]
Data/restraints/parameters	5909/0/434	21401/246/1549	5017/0/308	5360/0/344	13015/0/925
Goodness-of-fit on F ²	1.039	1.061	1.048	1.032	1.018
Final R indexes [I ≥ 2σ (I)]	R ₁ = 0.0335, wR ₂ = 0.0916	R ₁ = 0.0652, wR ₂ = 0.1794	R ₁ = 0.0395, wR ₂ = 0.1035	R ₁ = 0.0343, wR ₂ = 0.0904	R ₁ = 0.0327, wR ₂ = 0.0788
Final R indexes [all data]	R ₁ = 0.0352, wR ₂ = 0.0933	R ₁ = 0.0748, wR ₂ = 0.1898	R ₁ = 0.0446, wR ₂ = 0.1071	R ₁ = 0.0353, wR ₂ = 0.0913	R ₁ = 0.0386, wR ₂ = 0.0828
Largest diff. peak/hole / e Å ⁻³	0.41/-0.28	1.49/-0.94	0.32/-0.29	0.33/-0.29	0.30/-0.30

4.6.4 DFT Calculations and Cartesian Coordinates of Optimized Structures

All calculations were carried out with the ORCA^[47,48] program package. All geometry optimisations were performed at the BP86-D3BJ/def2-TZVP^[25-29] level of theory in the gas phase.

For compound **2-B₆F₅** (R = Me)

P	9.96496910147851	7.02365114055747	4.83636691506982
F	6.05070673635707	8.64836040922699	4.33354731050515
F	8.95544679716341	5.66249415311037	1.99305234002927
F	4.00884464782142	7.04809912243154	3.79878936899995
F	11.42965930540115	9.56127639821012	3.81997536271245
F	8.48923193360933	7.89039409707132	0.45700392995440
F	10.32010525773120	8.46038287272308	-1.40182378324959
F	13.21903790803224	10.19639983187664	1.91961285944345
F	12.71021098044263	9.60159240376615	-0.70887925906705
F	6.86699705158054	4.07239582433456	1.46778177258941
F	4.35583693632097	4.73846207410844	2.36406814521127
N	8.64916917018393	9.37583323373109	4.40540958711413
C	7.62634881491492	7.26665725152627	3.14794303142747
C	11.55295236248733	7.18840327323426	7.43544375291650
C	6.32870442384017	7.54408396033247	3.59999081859849
C	9.90838253747195	8.60873658439786	2.25087321294711
C	10.38776123115498	7.95617710914007	7.36941828146135
H	10.09731788965586	8.51065123731399	8.26670218978889
C	8.62983326957542	10.41916540966156	6.56870233367986
H	8.86584506379465	10.37454924107323	7.63046137491978
C	11.73745278287503	6.76425898628611	4.94392305498161
C	8.10865379619523	10.49497851850125	3.86827558285077
H	7.93269838037577	10.45644407598461	2.79392056303848
C	5.22955420590135	6.71669964211463	3.34363752537346
C	12.22814240701084	6.78251772525487	6.23350234819150
H	13.27219019268320	6.47691973384742	6.34915586734818
C	9.67538059355679	8.15057462398931	6.16718372872198
C	8.96518584483237	9.30672827506147	5.75365375160132
C	9.66702614690418	8.39942099792390	0.88872486071896
C	12.06976360038563	9.59227975448905	1.57626412021797
C	8.04808036933563	11.53938531359564	6.01846872809460
H	7.79991830628063	12.39046467475621	6.65383417815738
C	11.12296505211201	9.25092168048571	2.53809659009737
C	9.18589796475378	5.41842941059388	5.22387768930144
H	9.39308411776637	4.69269768172362	4.42723563652557
H	8.10279523652990	5.54158588586892	5.34545865326949
H	9.62882847026188	5.05981190087033	6.16227031737526
C	7.79197699795708	11.59577997419228	4.63020274205673
H	7.35290036281560	12.47377669876746	4.16254036704762
C	11.81061700462800	9.29765152704109	0.23762940615024
C	5.39914347227406	5.54127454924619	2.61583015166856
C	7.73673576392304	6.06442645295505	2.43641065616459
C	10.59559117584299	8.70866560904886	-0.10876448755411
C	6.67530402010765	5.20906669527073	2.15822590007188
B	8.96444446951052	8.13151484152013	3.47819482588929
C	12.19165944701654	6.95536717537157	8.74736000449138
C	13.58987250281714	6.96224983844050	8.91821419051529
C	14.16328854046823	6.75915282463781	10.17247536258946
C	13.35676140320887	6.54581190342448	11.29436934860363
C	11.96785738471450	6.53450811196400	11.14393963753401
C	11.39515974360786	6.72986478508165	9.88734605991762
H	10.31101516485907	6.67947722462747	9.77186933525178
H	15.24929470040301	6.77861522807980	10.27703981785164
H	14.23885489227208	7.16122220822018	8.06435709075522
H	11.32570902350900	6.35565899456916	12.00793819239711
H	13.80721595316350	6.38565168052263	12.27456281216996
C	12.57369234787108	6.64441967386590	3.74432010807082
C	13.87568278171247	7.18217594427159	3.71937593118194
C	14.64757344381889	7.13298670796186	2.55991568732108
C	14.13383611088592	6.56165049107565	1.39175206166343

C	12.84295435446615	6.02471309137175	1.39988970435131
C	12.07732287849844	6.06230816019320	2.56275644969922
H	11.07435970403946	5.63963878424120	2.55446183672984
H	12.42849236679175	5.57717877378919	0.49561775238614
H	14.73004035807693	6.54720213793981	0.47890898094223
H	14.25805843137834	7.69020867028141	4.60542067079459
H	15.64515631258348	7.57420673285293	2.55772666237007

For compound **3-BC₆F₅** (R = *t*Bu)

P	9.62237236569719	7.42244086021472	4.73024752770374
F	5.91461914685222	9.13832561877661	3.65702208716379
F	8.89877737573138	6.11500334042422	1.46371425316814
F	3.86384677227161	7.80320855387072	2.66148849509252
F	11.38884058212279	9.77550892929849	3.80691898413765
F	8.78176229881610	8.37122982693788	0.06719615421188
F	10.87094109711787	8.78394432480743	-1.52147945429625
F	13.44913938706128	10.24832152208281	2.17153796089766
F	13.24660365647330	9.70059615582886	-0.50967074180571
F	6.80194698575595	4.75544716796084	0.53403351708343
F	4.24236099494909	5.57827388058711	1.10354595689884
N	8.49178427288614	9.80878773507062	3.93831515628219
C	7.54606269598508	7.73977601652810	2.56728792885603
C	11.25662244620441	8.00407046688907	7.29388048719256
C	6.21810705078435	8.10019913849841	2.84073897139664
C	10.02114820410823	8.89296665069491	2.06002308552641
C	10.12178573170869	8.78199520693061	7.08172963838611
H	9.83116857059698	9.48977865506969	7.86272606303383
C	8.36615021119645	11.07420069783298	5.97279161419443
H	8.52622221451757	11.13393992663976	7.04774789782504
C	11.38102751154548	7.08520866110577	4.93122187210874
C	8.01271544939496	10.87620494399828	3.25439912613149
H	7.90246696137133	10.72876954445032	2.18068617270963
C	5.10923688371173	7.40151500675417	2.35354997131509
C	11.88031662949850	7.32088274896778	6.19785536641300
H	12.92414398561010	7.03476519854622	6.36116710359249
C	9.39128207822558	8.76298889329244	5.87461161133422
C	8.72308991936534	9.87568743661417	5.30004133369238
C	9.93806447927534	8.74004154396661	0.66932707312692
C	12.31550348861287	9.72699235920126	1.67357377750118
C	7.84790725312063	12.14165795847392	5.27537744512158
H	7.57882621752357	13.05729314882997	5.80337541875184
C	11.22932997717474	9.45586649632957	2.50200052028690
C	8.66245223201799	5.91127058218728	5.35872108908918
C	7.67931929482700	12.05693870725192	3.87487535412296
H	7.29203206998792	12.88858174972949	3.29115062812767
C	12.21248123014952	9.46116366846930	0.30911587893031
C	5.29425821029793	6.26558216853080	1.56922669198211
C	7.66792682923056	6.58826552120970	1.77865085352087
C	11.00581822173159	8.98364019315892	-0.19777975994655
C	6.59551722387001	5.85198348112518	1.28244293960742
B	8.87052699650724	8.49034486327951	3.14192669848703
C	11.93346053581110	7.98251855683549	8.60743457411742
C	12.60638244469719	6.82194003584299	9.03524254709826
C	13.25021907205789	6.77282886290623	10.27212344106306
C	13.23562660712378	7.88378566414488	11.11827706789875
C	12.57324755111082	9.04563747940828	10.70875755046218
C	11.93477153171971	9.09487840233810	9.47117789529711
H	11.45511970415733	10.02245233237932	9.15465208687710
H	13.75789686855272	5.85731670298323	10.58008042102886
H	12.60147375080202	5.93857440757286	8.39426779272819
H	12.56709805373723	9.92590039406657	11.35372238523981
H	13.73753114971441	7.84747575067071	12.08580109963039
C	12.24776383782294	6.77829878919243	3.78598358594644
C	13.58522276097912	7.22607549460145	3.75870264571789
C	14.39277748705382	7.00607710312279	2.64507231294396
C	13.88292491293004	6.35411598398609	1.51784470361321

C	12.55820385828354	5.90848554274654	1.52626905272401
C	11.75831573991324	6.11137686050917	2.64835376715121
H	10.72982368854291	5.75928698178570	2.63771977937625
H	12.14258360967610	5.40300814196780	0.65362389224467
H	14.50820268460879	6.20803846297750	0.63653692386968
H	13.97290294247162	7.80301461678069	4.59849210221434
H	15.41735142252721	7.38039197716642	2.64211203322251
C	8.93857749749476	4.70684353741132	4.45015325895399
H	8.58107935631545	4.85687706113485	3.42575128687393
H	8.41775025041603	3.82728868957366	4.85897750228732
H	10.01142941128591	4.47037213668987	4.41587980999641
C	7.16347187847052	6.23327024644525	5.42783224958352
H	6.97855530685060	7.20851705770486	5.90196383896552
H	6.66563884539983	5.46754122717599	6.04169897823422
H	6.69277600119383	6.22778078653758	4.44063271562394
C	9.15447398989230	5.57454906525513	6.77742235484737
H	10.23035465027090	5.36546923352553	6.80119975608497
H	8.62331422520598	4.66960203186520	7.11184407233915
H	8.93980316902370	6.38052083227904	7.48861376678899

For compound **4'** (R = Me)

P	10.60459260603573	5.85962305959786	6.84182255605741
F	6.98066723910351	9.79631623235911	4.46899776713270
F	8.73236789516924	5.97502951080845	2.16984083669194
F	4.55856788426832	8.76855571896838	4.27509615281352
F	12.08240580410941	9.94916930743091	3.66834958603340
F	8.51333847181856	8.66194035827248	0.76331101389795
F	9.87410388822316	9.63931695358618	-1.30796793336576
F	13.41919194697049	10.92399068204088	1.56245492627742
F	12.34981154522145	10.75701488986942	-0.95987265948763
F	6.28432959131828	4.98533854731106	2.00536612716070
F	4.13737284319991	6.34580266481720	3.04975015853118
N	9.64782641366537	9.35464771219577	4.91886954706572
C	8.04321056244662	7.91364498724242	3.40907694520835
C	12.00486556528371	6.96814303826012	3.85000789301153
C	6.89995993988473	8.57158652950018	3.88164235296269
C	10.23539384556238	9.23110861658885	2.33300427377121
C	10.52787514522065	7.16386603959074	4.16065643260509
C	9.85028414207278	9.23856548471969	7.29577342462107
H	10.05088305276903	8.64711533346111	8.18659910158213
C	11.95081094561755	7.03137666330917	6.22775957612758
C	9.39177283234501	10.67363937157728	4.98767696826140
H	9.20188532107277	11.16930510528151	4.03756780167949
C	5.59877378401195	8.07078211684355	3.78221977395793
C	12.72528386002645	6.81013059115321	4.98764667824634
C	10.50428858843741	7.32898435212865	5.69204801659765
C	9.94361661789643	8.63613196234090	6.03691617284172
C	9.71946756507291	9.21489843714853	1.03207572663230
C	12.20846740044944	10.36764015109230	1.37774023273819
C	9.55784071289362	10.59466549210253	7.37582171164583
H	9.50832906874066	11.08356635222594	8.34899148192445
C	11.48514103245993	9.85262115082498	2.44988077210926
C	10.62779821378257	4.45597673626227	5.64250576672554
C	9.35962846539182	11.33453155689325	6.20365846821349
H	9.15996878339843	12.40384368574992	6.23207249569472
C	11.66780040991017	10.28605288612700	0.09496822630151
C	5.37744572314972	6.84618014843140	3.15942103178803
C	7.74889125958774	6.70139887571978	2.76682105358034
C	10.40809736747436	9.71602050401679	-0.07525868197650
C	6.47136543238877	6.15803163760543	2.63800634344950
B	9.60557430127731	8.43256631541043	3.59785030429803
H	10.02279439585939	6.23315991310338	3.87370984023799
H	13.79144417066329	6.58917411686427	5.02820090370010
H	10.86580152082386	3.54139402515491	6.20272131566980
H	11.36971687583328	4.59655751495913	4.84449426749492
H	9.62970980065245	4.33589912706909	5.19778060796393
C	12.58105325582875	7.91764200131337	7.26036363240857

C	13.08851166296332	9.16395392523149	6.85333684001358
C	12.66634109822368	7.56669602341594	8.61348039786948
C	13.64890770273513	10.04126277071520	7.78031882302500
C	13.22713430301541	8.44524176301869	9.54420459948577
C	13.71559151448794	9.68700896624818	9.13165227390181
H	14.15340047058443	10.37310186519246	9.85797917111453
H	13.28654859693321	8.15519297017978	10.59427889602217
H	12.28242239992629	6.59672451355801	8.93393744474746
H	14.03232793830901	11.00696824120044	7.44753922712536
H	13.02813404329081	9.44077622921640	5.80043175135381
C	12.56891270544854	6.94161592362474	2.49531328460963
C	11.79327668434839	6.59483696393820	1.37487368561099
C	13.90084504680550	7.35016606120180	2.27861054234950
C	12.32674538097381	6.65620619889950	0.08790213838697
C	13.64694257475692	7.06672873036782	-0.11116186994232
C	14.43308464244976	7.41029830214108	0.99345862121251
H	14.50334701035281	7.67248936846348	3.12840227212960
H	15.45930931099503	7.75098226316578	0.84960001544116
H	14.05686075469148	7.13210329175697	-1.11959491351895
H	11.70121109609785	6.39199342212932	-0.76593407574816
H	10.76050897522134	6.28650574900503	1.51319188392733

For compound **4** (R = *t*Bu)

P	10.80750341284589	5.61386428975255	6.53685171422062
F	7.04689330856112	9.60523376940701	4.64290103067459
F	8.77064766177383	6.13935058289900	1.82069772679307
F	4.64711544611993	8.52199398999666	4.46126580767056
F	12.11217858998903	9.98108752708908	3.60698819432924
F	8.44934623677663	8.90507476119964	0.73420888435051
F	9.72586012640856	10.06585675783056	-1.29421845081654
F	13.36232841384408	11.14689353798449	1.54591154705833
F	12.20346906561322	11.17857418482124	-0.94274738874353
F	6.34712436531718	5.08495226910692	1.67847969182698
F	4.22588581053904	6.24068528611376	2.98959726085562
N	9.73126832357984	9.20877806334676	4.89433246266436
C	8.09847941671142	7.89514162359472	3.31382128664104
C	12.08289832613064	6.98352538671922	3.53837699249679
C	6.96675370471193	8.45485600699194	3.92087617374349
C	10.22774549180799	9.34929186130839	2.28229542345963
C	10.61164777623686	7.12368293382792	3.89349434687999
C	9.95815253201495	8.83527418677468	7.24153652245855
H	10.16742321559622	8.14918508049624	8.05964643545119
C	12.08832631353794	6.82475622964462	5.91875018767024
C	9.47490626021956	10.51200022423170	5.10779987636694
H	9.26874441062223	11.10530913284629	4.21872960962888
C	5.67684003665028	7.92268066695800	3.83467419117681
C	12.82861172380199	6.71501042889274	4.63656453126229
C	10.61190393847668	7.11340795090305	5.43451277649266
C	10.03894844359712	8.37249014420576	5.92402334164172
C	9.66293610922080	9.44046826257420	1.00465679030898
C	12.15241474911734	10.59016492759807	1.35685926655297
C	9.66837834412363	10.17474027384496	7.47108191219006
H	9.63062074667617	10.55539506806036	8.49195822953434
C	11.47388365424438	9.97639848109295	2.40600523862032
C	10.93396619017488	3.96650467447899	5.58768695214420
C	9.45841640319716	11.03764714875885	6.38837363675619
H	9.25998401569728	12.09746558835298	6.53504109584235
C	11.56609001031915	10.61022507432592	0.09188386880305
C	5.45524202766148	6.76956174014410	3.08784670950722
C	7.80207338783959	6.75593071580892	2.55071415729944
C	10.30596736490857	10.04159092103534	-0.08021447526570
C	6.53623102497912	6.18470187969838	2.43060472700281
B	9.65857694282391	8.42881143296001	3.49123034931477
H	10.10998515995588	6.23445877593532	3.50833657019518
H	13.89967017640232	6.51432178360656	4.63030708122459
C	12.74108035947452	7.68504104260963	6.96457542713744

C	13.20798175138504	8.95835855291944	6.59586663982887
C	12.88931354950754	7.27551745572665	8.29543069966007
C	13.78448838612468	9.80646300392241	7.54012127127667
C	13.46962469861504	8.12259457759196	9.24303372179325
C	13.91346218459594	9.39331997961337	8.87007030039388
H	14.36463638314761	10.05611917472443	9.60976625082968
H	13.57775098535925	7.78621583491496	10.27532070800337
H	12.53369032314361	6.28555683917751	8.58606223800195
H	14.13261575713757	10.79512940372837	7.23721961232605
H	13.10394150073565	9.28029635221652	5.55999994653550
C	12.61378983865239	7.09014936806794	2.17512159675473
C	11.81477124941675	6.83231911732762	1.04698017172132
C	13.93378197874312	7.53864365700700	1.96413526686856
C	12.31402408420942	7.01848427222042	-0.24184783744509
C	13.62246895884942	7.46757930564235	-0.43477719420317
C	14.43179270367194	7.72311645977332	0.67717198143925
H	14.55263539421995	7.79350760942961	2.82511031865789
H	15.44885548694970	8.09275283041905	0.53968531217873
H	14.00534338879635	7.63097718769951	-1.44272730176666
H	11.67065776387337	6.82185291714620	-1.10067650927450
H	10.79049803961290	6.49588136184925	1.18218829833235
C	12.36819146233026	3.46991708666590	5.83358397738953
H	12.45699350203924	2.42145305423597	5.50612176084698
H	12.63832622641611	3.51093427696226	6.89977322803982
H	13.09517275486041	4.07052262646202	5.27122374893619
C	9.93627118377594	3.06423720197041	6.34251644022703
H	8.89980438569335	3.40258684797004	6.19758805046699
H	10.13816702764929	3.04463540076486	7.42355903158287
H	10.01317264454001	2.03325886124984	5.96227859042240
C	10.61092672497242	3.92167398614027	4.09381314550559
H	11.33021839427256	4.49425776824962	3.49761401130289
H	9.59559391497088	4.28076938481519	3.87888250378258
H	10.66157835343193	2.87287357556722	3.75750230616219

Chapter 5

Facile C=O Bond Splitting of Carbon Dioxide Induced by Metal-Ligand Cooperativity in a Phosphinine Iron(0) Complex

Abstract: New iron complexes [Cp*FeL]⁻ (**1-σ** and **1-π**, Cp* = C₅Me₅) containing the chelating phosphinine ligand 2-(2'-pyridyl)-4,6-diphenylphosphinine (**L**) have been prepared, and found to undergo facile reaction with CO₂ under ambient conditions. The outcome of this reaction depends on the coordination mode of the versatile ligand **L**. Interaction of CO₂ with the isomer **1-π**, in which **L** binds to Fe through the phosphinine moiety in an η⁵ fashion, leads to the formation of **3-π**, in which CO₂ has undergone electrophilic addition to the phosphinine group. In contrast, interaction with **1-σ** – in which **L** acts as a σ-chelating [P,N] ligand – leads to product **3-σ** in which one C=O bond has been completely broken. Such CO₂ cleavage reactions are extremely rare for late 3d metals, and this represents the first such example mediated by a single Fe centre.



Reproduced with permission from J. Leitl, M. Marquardt, P. Coburger, D. J. Scott, V. Streitferdt, R. M. Gschwind, C. Müller and R. Wolf, *Angew. Chem. Int. Ed.* **2019**, 58, 15407–15411.

J. Leitl performed all reactions and fully characterized compounds **1-σ**, **1-π**, **2**, **3-σ** and **3-π** by single crystal X-ray analysis, NMR and UV-Vis spectroscopy and elemental analysis. J. Leitl prepared the manuscript and supporting information with assistance by D. J. Scott. M. Marquardt supplied ligand **L** and proof-read the manuscript. P. Coburger performed all DFT calculations. I. Shenderovich performed the ³¹P CP-MAS NMR spectroscopic measurement. C. Müller and R. Wolf supervised and directed the project

5.1 Introduction

The transformation of carbon dioxide into novel and useful chemicals remains one of the most important research challenges of modern chemistry. Consumption of CO₂ as a C₁ building block is highly attractive due to its relative abundance and, in particular, as a method to mitigate long-established concerns about its role as an atmospheric greenhouse gas.^[1–4] One potential method is the transformation of CO₂ into carbon monoxide, CO, which is a common feedstock for large-scale industrial processes (e.g Fischer-Tropsch alkane synthesis).^[5] This has led to great interest in the identification and study of well-defined molecular systems capable of directly cleaving the C=O bond in CO₂. Such transformations are highly challenging due to the high strength of the C=O bond (bond enthalpy 532 kJ mol⁻¹).^[6] Nevertheless, these reactions have become relatively established for highly-reducing, low-valent early 3d metals^[7–10] and a number of examples based on precious^[11–15] and f-block metals^[16–18] have also been reported. In comparison, the use of earth-abundant late 3d metals remains surprisingly underexplored, particularly given the role that such metals play in biological CO₂ reduction to CO, mediated by Ni,Fe CO dehydrogenase.^[19,20]

Currently, only a handful of examples of CO₂ cleavage based on 3d metals are known (Figure 1).^[21–23] In 2005, Sadighi *et al.* reported abstraction of an oxygen atom from CO₂ by NHC copper boryl complexes, resulting in formal O atom insertion into the Cu—B bond to give compound **A**.^[24] Subsequently, in 2007, Peters and co-workers reported the formation of a dinuclear Fe(II) complex **B** containing bridging CO and O²⁻ ligands, which was prepared by reaction of CO₂ with an Fe(I) precursor (similar results were also published by Holland *et al* shortly thereafter).^[25,26,10] Recently, the group of Milstein has described a more complex CO₂ activation sequence mediated by a nickel pincer complex, involving the cleavage of a ligand C—P bond as well as one CO₂ C=O bond to give the products **C** and **D**.^[27]

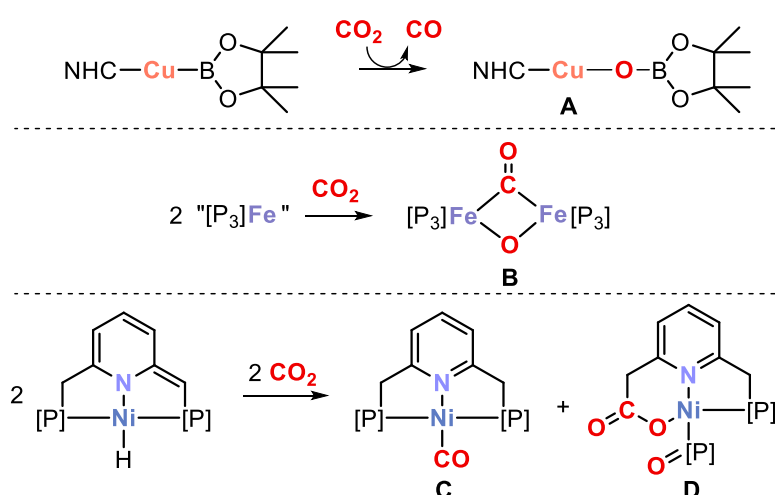


Figure 1. C=O cleavage in CO₂ mediated by well-defined late 3d metal complexes. NHC = *N*-heterocyclic carbene. [P₃] = PhB(CH₂P(CH₂Cy)₂)₃. [P] = P^{*i*}Pr₂.

The complexes **A-D** all form through some manner of cooperative CO₂ activation. In each case, the small molecule substrate is cleaved as a result of combined interaction with either more than one metal centre (**B, C/D**), or with both a metal centre and a ‘non-innocent’ ligand (**A, C/D**). On this basis, we reasoned that the use of other ligands capable of metal-ligand cooperation (MLC)^[28–33] should allow us to expand the range of structural motifs available for mediating challenging CO₂ cleavage reactions at late 3d metals.

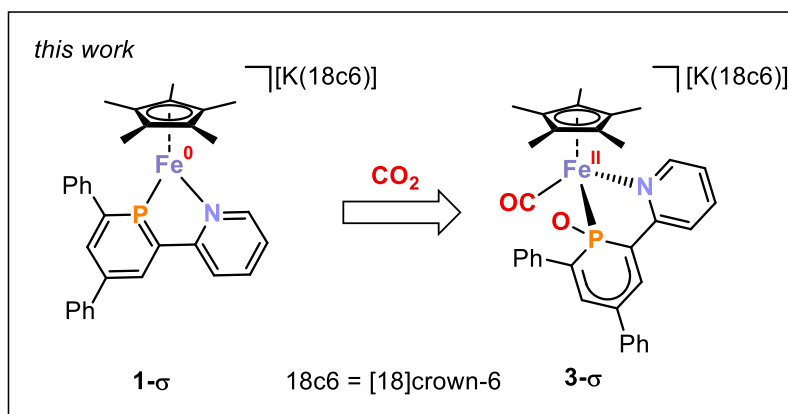


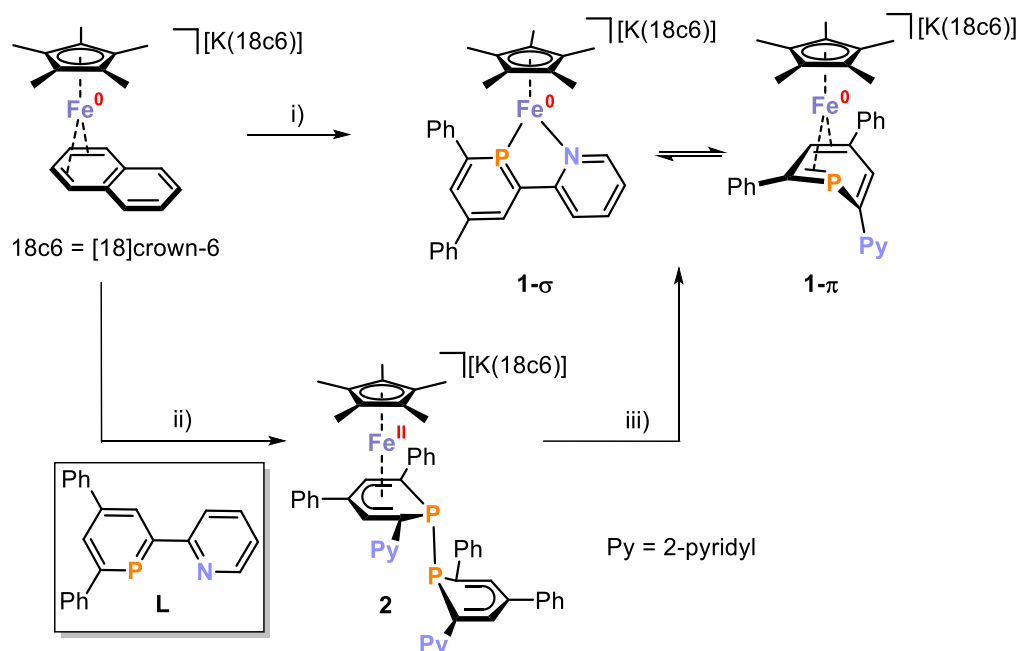
Figure 2. C=O cleavage in CO₂ mediated by **1-σ**.

In this context, we have recently become interested in the use of phosphinines as ligands in late 3d metal transition metal chemistry.^[34] Previous work has shown that these compounds exhibit a rich coordination chemistry, and are capable of displaying diverse coordination modes.^[34–36] Furthermore, we have shown that Cp*Fe complexes of the simple phosphinine TPP (TPP = 2,4,6-triphenylphosphinine) show considerable non-innocent behaviour, with the TPP ligand capable of displaying either nucleophilic or electrophilic character towards external reagents.^[37,38] We anticipated that the coordination chemistry (and, hence, onward reactivity) of these complexes might be further diversified through incorporation of the phosphinine moiety into a chelating ligand scaffold. We therefore decided to target the synthesis of an analogue of our previously-reported complex [K([18]crown-6)][Cp*Fe(η⁴-TPP)],^[39] in which TPP is replaced by the known ligand 2-(2'-pyridyl)-4,6-diphenylphosphinine (**L**).^[40]

5.2 Results and Discussion

Pursuing an analogous method to that used previously used to prepare [K([18]crown-6)][Cp*Fe(η⁴-TPP)], treatment of [K([18]crown-6)][Cp*Fe(η⁴-C₁₀H₈)] with **L** at –35 °C in dimethoxyethane (DME) gave a deep purple reaction mixture after warming to room temperature (RT) and stirring overnight. Dark purple crystals of a new product **1** were obtained in good yield (68%) by layering this reaction mixture with *n*-hexane and subsequent filtration (Scheme 1, top). X-ray analysis confirmed the expected formulation of **1** as [K([18]crown-6)][Cp*Fe**L**] (**1-σ**), in which the ligand **L** has displaced naphthalene from the anionic Cp*Fe moiety (Figure 2). The crystal structure reveals that, in contrast to the

η^4 -TPP binding mode in [K([18]crown-6)][Cp*Fe(η^4 -TPP)], the phosphinine ligand acts as a sigma-coordinated [P,N] chelate in [K([18]crown-6)][Cp*FeL], with the Cp* and L ligands coordinating the iron centre in a trigonal planar fashion.



Scheme 16. Reaction of [K([18]crown-6)][Cp*Fe(C₁₀H₈)] with 2-(2'-pyridyl)-4,6-diphenylphosphinine (L) forming **1-σ** and **1-π**; i) L, DME, -35 °C to RT, -naphthalene; ii) 1 equiv. [K([18]crown-6)][Cp*Fe(C₁₀H₈)], 2 equiv. L, toluene/THF -35 °C to RT; iii) 1 equiv. [K([18]crown-6)][Cp*Fe(C₁₀H₈)], THF.

Further structural assignment of **1-σ** in the solid state is supported by ³¹P CP MAS NMR spectroscopy, which indicates the presence of a single species with $\delta_{\text{iso}} = 121.1$ ppm, in the range expected for this coordination mode of L.^[41] In contrast, solution phase ³¹P{¹H} NMR analysis of crystalline **1** dissolved in suitable solvents^[42] shows two distinct resonances. For example, in THF-*d*₈ a sharp singlet at 130.7 ppm (or a triplet with ³J_{P-H} = 13 Hz in the coupled ³¹P NMR spectrum) is assigned to **1-σ**, but is accompanied by a second, very broad resonance ($\tau_{1/2} = 1000$ Hz) at -46.2 ppm. Attempts to selectively crystallise the species corresponding to this resonance have been unsuccessful, with XRD and ³¹P CP MAS measurements consistently showing the presence of only **1-σ** in the solid state. Nevertheless, the broadness and chemical shift of this signal are very similar to those observed previously for the complex [K([18]crown-6)][Cp*Fe(η^4 -TPP)]. In this compound the TPP ligand is rapidly equilibrating between different η^4 π -coordination modes.^[39] We therefore assign this signal to an isomeric structure of **1** (**1-π**) where the ligand L coordinates in an η^4 fashion as shown in Scheme 1, and which exists in equilibrium with **1-σ** in solution. This conclusion is supported by DFT calculations. A minimum energy structure corresponding to **1-π** is only 0.9 kcal mol⁻¹ higher in energy than the optimized structure for **1-σ** (which reproduces well the structure observed by crystallography; see the SI). Furthermore, conversion of **1-π** to **1-**

σ is calculated to proceed with a barrier of 27.0 kcal mol⁻¹, consistent with an equilibrium at RT. ³¹P{¹H} NMR integration indicates an approximately 2:1 ratio of **1- σ** to **1- π** at RT, which does not change significantly at lower temperature (-30 °C; at elevated temperatures other reactivity is observed, see SI).

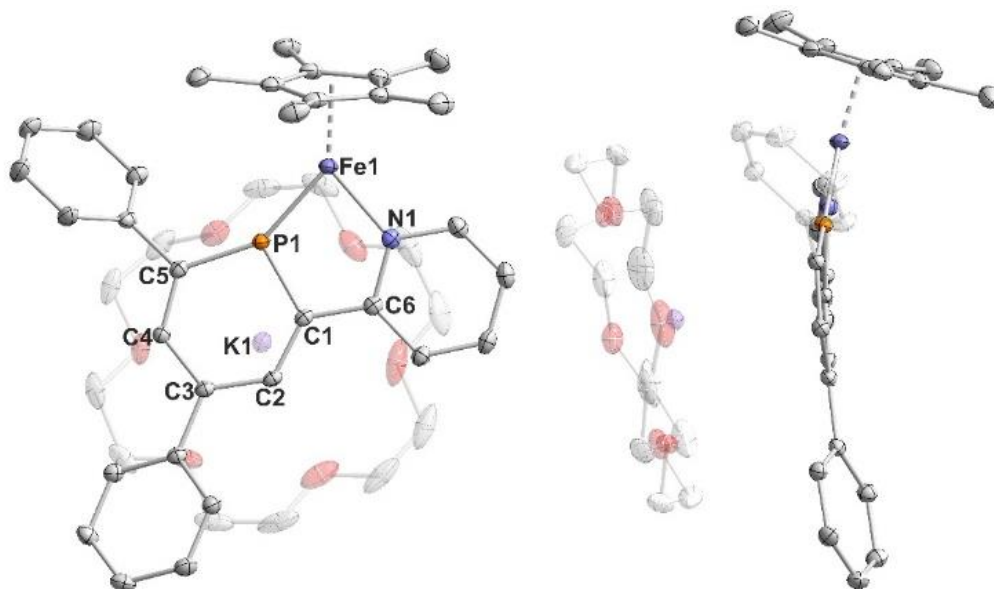


Figure 3. Solid state molecular structure of **1- σ** (left); ellipsoids are drawn at the 40% probability level; H atoms are omitted and the K[18]crown-6 cation is transparent for clarity; selected bond lengths [Å] and bond angles [°]: Fe1–P1: 2.0811(4), Fe1–N1: 1.9428(12), P1–C1: 1.7733(13), C1–C2: 1.3953(19), C2–C3: 1.3947(18), C3–C4: 1.4343(18), C4–C5: 1.3756(18), C5–P1: 1.7757(13), P1–Fe1–N1: 82.32(4), Fe1–P1–C1: 107.62(4), Fe1–N1–C6: 124.18(9), Cp*–Fe1–N1: 135.513(8), P1–Fe1–Cp*: 140.545(9). Side view of solid state molecular structure of **1- σ** (right); for clarity, one additional phenyl group is also transparent.

In the hope of gaining more insight into the formation of both isomers of **1**, the reaction of [K([18]crown-6)][Cp*Fe(C₁₀H₈)] with **L** was monitored by ³¹P{¹H} NMR spectroscopy at 273 K. The initial spectrum showed immediate, full consumption of ligand **L**, and formation of two major new groups of resonances at *ca.* -25 and -42 ppm.^[43] Only after approximately 30 minutes did signals attributable to **1- σ** and **1- π** become readily discernible, growing in steadily over the course of several hours with concomitant loss of the intermediate resonances.

Close inspection of the observed multiplets suggested that they could be assigned to a pair of AB spin systems with very similar chemical shifts and coupling constants. Notably, the chemical shifts at approximately -42 ppm are almost identical to those of the P–P bonded dimeric species [Cp*Fe(η^5 -TPP)]₂.^[39] Indeed, when the reaction between **L** and [K([18]crown-6)][Cp*Fe(C₁₀H₈)] was repeated with a 2:1 molar ratio, these resonances were seen to form selectively. Only upon addition of a further equivalent of [K([18]crown-6)][Cp*Fe(C₁₀H₈)] were the isomers of **1** observed (Scheme 1, bottom). Conversely, addition of 1 eq. **L** to an isolated sample of **1** regenerated the intermediate resonances. It was therefore proposed that these resonances might correspond to two isomers of the P–P dimer

[K([18]crown-6)][Cp*Fe(η^5 -L-L)], **2**, which differ only in the relative orientations of the L pyridyl groups. This assignment was confirmed by X-ray analysis of single crystals grown by slow diffusion of *n*-hexane into a DME solution of **2**, which resolved to show the expected L₂ dimer. One half of the molecule is coordinated in an η^5 fashion to a Cp*Fe moiety (Figure 3).^[44] The P1–P2 bond is longer than typical P–P single bonds (2.3149(14) vs. 2.04 Å)^[45] suggesting a relatively weak interaction, consistent with facile cleavage upon addition of a second equivalent of [K([18]crown-6)][Cp*Fe(η^4 -C₁₀H₈)].

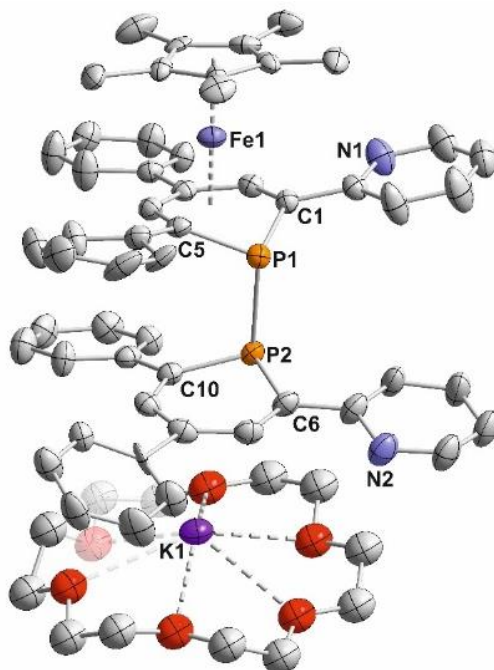
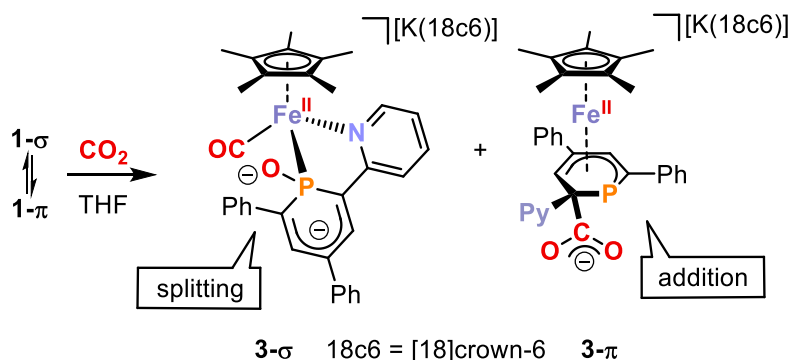


Figure 4. Solid state molecular structure of **2**; ellipsoids are drawn at the 40% probability level; H atoms are omitted for clarity; selected bond lengths [Å] and bond angles [°]: P1–P2: 2.3149(14), C1–P1–C5: 92.99(17), C6–P2–C10: 99.58(19), fold angle C1–P1–C5: 32.64, fold angle C6–P2–C10: 14.79.

Complex **2** likely arises through rapid addition of initially-formed **1** to a second equivalent of L. When L is consumed, further coordination of “Cp*Fe[−]” leads to formation of free **1**. Transiently-formed **1** is believed to act as a nucleophile in this reaction, with the second equivalent of L behaving as a formal electrophile. This is consistent with previous observations of nucleophilic character for the P atom in [K([18]crown-6)][Cp*Fe(η^4 -TPP)],^[37] as well as with DFT calculations, which suggest that the phosphinane moiety not directly bound to Fe is best described as an anionic phosphahexacyclodienyl fragment (see SI). These calculations also indicate that formation of **2** from **1- π** and L is favourable by 23.5 kcal mol^{−1}, and proceeds over a low energy barrier of 7.5 kcal mol^{−1}.

Encouraged by the evidence of both coordinative flexibility and non-innocent reactivity already displayed by the phosphinane ligand L during the synthesis of compound **1**, we were encouraged to investigate the reactivity of this complex towards CO₂. Thus, a THF solution of **1- σ** and **1- π** was charged with CO₂ (1 atm) at RT (Scheme 2). Gratifyingly, an immediate

colour change from deep purple to deep green was observed, and ³¹P{¹H} NMR spectroscopy confirmed the complete consumption of **1** within 10 minutes with concomitant formation of two major new species, identified by signals at 97.0 and 116.0 ppm, with the former splitting into a triplet in the proton-coupled ³¹P NMR spectrum (³J_{P-H} = 13 Hz). The species corresponding to these two resonances could be separated by fractional crystallisation, and the identity of both was established by single crystal X-ray diffraction studies (Figure 4).



Scheme 2. Reaction of **1-σ** and **1-π** with CO₂ (1 atm) in THF at RT.

Thus, the ³¹P{¹H} resonance at 116.0 ppm can be assigned to the new compound **3-π**, in which an intact CO₂ moiety has attached to the phosphinine carbon ‘ipso’ to the pyridyl group.^[46] The resulting carboxylate-substituted phosphacyclohexadienyl ligand coordinates to Fe in an η⁵ fashion, and the carboxylate itself interacts in a κ² manner with the potassium counteranion. It is noteworthy that no reaction is observed between CO₂ and the free ligand **L** under analogous conditions.

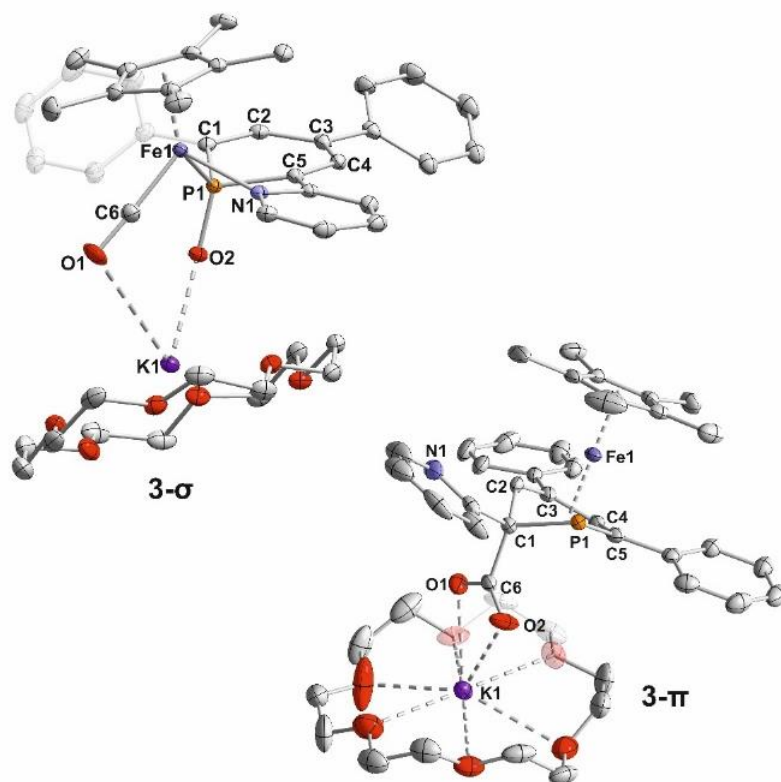


Figure 5. Solid state molecular structures of **3-σ** and **3-π**; ellipsoids are drawn at the 40% probability level; H atoms are omitted for clarity; selected bond lengths [Å] and bond angles [°] of **3-σ**: Fe1–P1: 2.2434(4), Fe1–N1: 2.0060(14), Fe1–C6: 1.7272(18), C6–O1: 1.170(2), P1–O2: 1.5272(12), K1–O1: 3.3043(16), K2–O2: 2.558(17), O1–C6–Fe1= 177.49(17), C6–Fe1–P1= 88.41(6), Fe1–P1–O2= 114.45(5), C6–Fe1–N1: 98.78(7); for **3-π**: C6–O1: 1.236(5), C6–O2: 1.229(5), C1–C6: 1.575(5), K1–O1: 2.723(3), K1–O2: 3.050(4), O1–C6–O2= 127.3(4), P1–C1–C2= 97.5(3), C1–P1–C5= 98.36(19).

A more dramatic outcome is revealed by the second major reaction product, **3-σ**. In this case, the molecular structure in the crystal clearly shows full cleavage of one C=O bond in the CO₂ substrate, with coordination of the resulting CO molecule to the Fe centre, and of the remaining O atom to the ligand P atom. Nonetheless, the coordination mode of the ligand **L** remains unchanged from **1-σ**, which may be attributed to the electronic flexibility of the phosphinine moiety. In contrast to Milstein's product **D** (as well as an Ir-based system described recently by Langer, Hamza and Pápai), O atom transfer to P does not require cleavage of any bonds in the ligand backbone.^[15,27] Again, this can be attributed to the use of an unsaturated phosphinine moiety in place of a more conventional phosphine donor. This reaction represents the first example of full CO₂ C=O cleavage mediated by a single well-defined Fe centre. That the activation is achieved under very ambient conditions using only earth-abundant elements renders this system a highly attractive starting point for further investigations into productive CO₂ utilization. Intuitively, the structures observed for **3-σ** and **3-π** suggest that they are formed through the reaction of CO₂ with isomers **1-σ** and **1-π** of **1**, respectively. This conclusion is further supported by ³¹P{¹H} spectra of the crude product mixture, which indicate the formation of **3-σ** and **3-π** in the same 2:1 ratio observed for the equilibrium between **1-σ** and **1-π**. To provide more conclusive evidence, DFT studies

were performed to establish the mechanisms of formation of both **3- σ** and **3- π** (see the SI). As expected, interaction of CO₂ with **1- σ** was calculated to lead to formation of **3- σ** , with only a very small energy barrier of 3.5 kcal mol⁻¹. Interaction with **1- π** was calculated to lead to **3- π** over a similarly small barrier (5.5 kcal mol⁻¹). Notably, both barriers are significantly lower than the barrier to isomerisation between **1- σ** and **1- π** (*vide supra*).

5.3 Conclusion

In summary, we have prepared a new anionic Fe complex **1** incorporating a chelating phosphinine ligand. **1** exists in solution as a pair of isomers in which the phosphinine adopts distinct coordination modes at the metal. Both isomers react with CO₂: for the π -coordinated isomer **1- π** addition of CO₂ to a carbon atom of the phosphinine moiety is observed, while full cleavage of one C=O bond occurs in the σ -coordinated isomer **1- σ** to give an Fe-coordinated CO moiety and P-bound O atom. This is the first reported example of C=O cleavage of a CO₂ molecule mediated by a single Fe centre, and clearly demonstrates the potential of coordinatively- and electronically-flexible phosphinine ligands to help mediate challenging bond activation reactions. Research into the further applications of such complexes, the derivatisation of CO₂ cleavage product **3- σ** , and the use of these systems to address to crucial topical challenge of efficient CO₂ transformation are currently underway in our laboratories.

5.4 Experimental Details

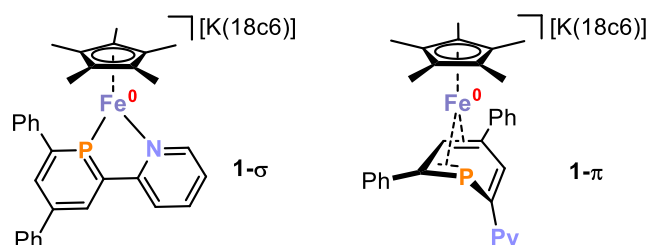
5.4.1 General Considerations

All experiments were performed under an atmosphere of dry argon using standard glovebox and Schlenk line techniques. Tetrahydrofuran, toluene and *n*-hexane were purified, dried, and degassed using an MBraun SPS800 solvent purification system. 1,4-Dioxane and 1,2-dimethoxyethane were dried over potassium and distilled under inert gas atmosphere. Deuterated tetrahydrofuran was purchased from Sigma Aldrich and used as received. [K([18]crown-6)][Cp*Fe(C₁₀H₈)] and **L** were synthesized according to literature procedures.^[40,47] CO₂ (purity 4.8) was purchased from Linde Gas and used as received.

NMR spectra were recorded on Bruker Avance 300 and Avance 400 spectrometers at 300 K and a Bruker Avance III HD 600 MHz spectrometer with a fluorine selective TBIF probe at 273 K. ¹H and ¹³C{¹H} spectra were referenced internally to residual solvent resonances, while ³¹P{¹H} and ³¹P spectra were referenced externally to 85% H₃PO₄(aq). The assignment of ¹H and ¹³C NMR signals was confirmed by two-dimensional (COSY, HSQC, and HMBC) experiments. Solid state ³¹P MAS-NMR spectra were recorded with a Bruker 400 MHz spectrometer. UV/vis spectra were recorded using a Varian Cary 50 spectrometer. Elemental analyses were determined by the analytical department of the University of Regensburg. IR spectra were recorded using a Bruker ALPHA spectrometer equipped with a diamond ATR unit.

Single-crystal X-ray diffraction data were recorded on an Agilent Technologies SuperNova diffractometer with Cu-*K*_α radiation (λ = 1.54184 Å). Either semi-empirical multi-scan absorption corrections^[48] or analytical ones^[49] were applied to the data. The structures were solved with SHELXT^[50] and least-square refinements on *F*² were carried out with SHELXL.^[51] The hydrogen atoms were located in idealized positions and refined isotropically with a riding model. CCDC 1942537 (for **1-σ**), 1942538 (for **2**), 1942550 (for **3-σ**), and 1942542 (for **3-π**) contain the supplementary crystallographic data for this paper. These data can be obtained free of charge from the Cambridge Crystallographic Data Centre.

5.4.2 Synthesis of **1**

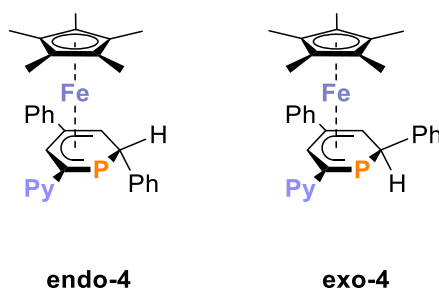


A solution of **L** (200 mg, 0.62 mmol, 1 eq.) in 1,2-dimethoxyethane (4 mL) was added dropwise to a solution of [K([18]crown-6)][Cp*Fe(C₁₀H₈)] (383 mg, 0.62 mmol, 1 eq.) in 1,2-dimethoxyethane (8 mL) at

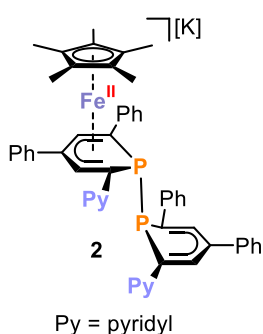
−35 °C. The orange/brown reaction mixture turned into a deep green suspension. After stirring overnight and warming up to room temperature a deep purple suspension was formed. The suspension was layered with *n*-hexane (16 mL) and stored at −35 °C over two days. Product **1** could be isolated as dark purple solid after decanting off the supernatant

solution and drying under vacuum. Crystals suitable for single-crystal XRD were grown by slow diffusion of *n*-hexane into a 1,2-dimethoxyethane solution of **1**. Yield 350 mg, 68%. Elemental analysis calcd. for C₄₄H₅₅FeKNO₆P (Mw = 819.84 g·mol⁻¹) C 64.46, H 6.76, N 1.71; found C 63.27, H 6.69, N 1.54. UV-Vis: (THF, λ_{max} / nm, ε_{max} / L·mol⁻¹·cm⁻¹): 310 (sh, 16553), 500 (3708). ¹H NMR (400.13 MHz, 300 K, [D₈]THF): δ = 1.23 (s, 15H, C₅(CH₃)₅), 3.25 (s, 24H, [18]crown-6), 6.20–10.45 (m, 16H signals for **L** of **1-σ** and **1-π**). ¹³C{¹H} NMR (100.61 MHz, 300 K, [D₈]THF): δ = 11.0 (s, C₅(CH₃)₅), 12.6 (s), 12.8 (s), 70.9 (bs, [18]crown-6), 72.6 (s), 78.7 (s), 80.9 (s, C₅(CH₃)₅), 105.3 (s), 109.6 (s), 111.7 (s), 116.1 (s), 117.0 (s), 122.1 (s), 123.5 (s), 125.00 (s), 125.3 (s), 125.7 (bs), 126.4 (s), 127.4 (s), 127.5 (s), 128.5 (s), 128.8 (s), 130.3 (d, *J* = 6 Hz), 132.0 (m), 133.8 (s), 144.1 (s), 147.5 (s), 148.7 (s), 158.5 (s). ³¹P{¹H} NMR (161.98 MHz, 300 K, [D₈]THF): δ = 131.7 (s, **1-σ**), -44.8 (bs, **1-π**). ³¹P NMR (161.98 MHz, 300 K, [D₈]THF): δ = 130.7 (t, ³*J*_{PH} = 12 Hz, **1-σ**), -46.2 (bs, **1-π**).

NMR spectroscopy and elemental analysis consistently indicate the presence of persistent, minor impurities in samples of **1** prepared in the above manner. Specifically, ³¹P{¹H} NMR analysis indicates the presence of side-products **endo-4** and **exo-4** (typically *ca.* 8%), which are presumed to arise from protonation of **1** by adventitious moisture.^[7]



5.4.3 Synthesis of **2**



A solution of **L** (100 mg, 0.31 mmol, 2 eq.) in toluene (2 mL) was added dropwise to a solution of [K([18]crown-6)][Cp*Fe(C₁₀H₈)] (96 mg, 0.15 mmol, 1 eq.) in tetrahydrofuran (0.5 mL) at -35 °C. A colour change from orange brown to wine red was observed. After stirring for 5 hours and warming to room temperature the brown reaction mixture was layered with *n*-hexane (6 mL) and stored at -35 °C overnight. Product **2** was isolated as a dark brown solid after decanting off the supernatant solution and drying under vacuum.

Crystals suitable for single-crystal XRD were grown from slow diffusion of *n*-hexane into a 1,2-dimethoxyethane solution of **2**. Yield 126 mg, 72%. Elemental analysis calcd. for C₆₆H₇₁FeKN₂O₆P₂ (Mw = 1145.19g·mol⁻¹) C 69.22, H 6.25, N 2.45; found C 69.60, H 6.26, N 2.28. UV-Vis: (THF, λ_{max} / nm, ε_{max} / L·mol⁻¹·cm⁻¹): 250 (40598), 280 (39399), 510 (8023). ¹H NMR (400.13 MHz, 300 K, [D₈]THF): δ = 0.90 (s, 15H, C₅(CH₃)₅), 3.25 (s, 44H, [18]crown-6), 5.87 (m, 1H), 6.17 (m, 2H) 6.51 7.44 (m, 40H), 7.74 8.00 (m, 10H), 8.34 (m, 1H). ¹³C{¹H} NMR (100.61 MHz, 300 K, [D₈]THF): δ = 8.9 (s, C₅(CH₃)₅), 71.6 (bs,

[18]crown-6), 84.3 (d, 1.66 Hz), 85.2 (m), 85.6 (m), 94.74 (s), 94.7 (s), 112.6 (s) 113.5 (s), 113.9 (s), 117.8 (s), 119.4 (m), 120.6 (s), 120.8 (s), 122.5 (s), 122.6 (s), 123.7 (m), 125.0 (m), 125.2 (m), 125.4 (m), 125.5 (s), 125.9 (s), 126.4 (s), 126.7 (m), 127.5 (s), 127.7 (s), 128.5 (s), 128.5 (s), 128.6 (s), 128.8 (s), 129.3 (s), 129.5 (s), 131.8 (m), 133.3 (s), 133.6 (s), 133.8 (s), 134.5 (s), 134.8 (s), 135.0 (s), 138.3 (s), 143.0 (s), 143.2 (s), 146.1 (s), 148.4 (s), 148.5 (s), 162.5 (s), 162.8 (s), 164.9 (s), 165.2 (s). ³¹P{¹H} NMR (161.98 MHz, 300 K, [D₈]THF): δ = -24.31 (AB, ¹J_{PP} = 262 Hz), -42.09 (AB, ¹J_{PP} = 262 Hz), -25.27 (AB, ¹J_{PP} = 257 Hz), -41.69 (AB, ¹J_{PP} = 257 Hz). ³¹P NMR (161.98 MHz, 300 K, [D₈]THF): δ = -24.31 (AB, ¹J_{PP} = 262 Hz), -42.09 (AB, ¹J_{PP} = 262 Hz), -25.27 (AB, ¹J_{PP} = 257 Hz), -41.69 (AB, ¹J_{PP} = 257 Hz).

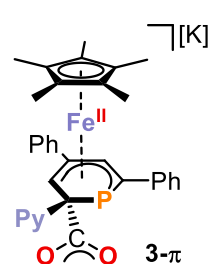
As for compound **1**, samples of **2** prepared in the above manner were found to contain trace impurities, and specifically side-products **endo-4** and **exo-4** (typically *ca.* 1%).^[7]

5.4.4 Synthesis of **3-σ** and **3-π**

Stoichiometric conversion of 1 and CO₂ leads also to 3-σ and 3-π, but leads also to more hydrolysis side products endo-4 and exo-4, due to opening of the reaction vessel and adding CO₂ via syringe. It is advisable to keep the reaction mixture in a closed system.

A sealed vessel containing a solution of **1** (100 mg, 0.122 mmol) in tetrahydrofuran (3 mL) was charged with CO₂ (1 atm). An immediate colour change from purple to deep green was observed, and the reaction mixture was stirred for 30 minutes at room temperature. The solvent was removed under vacuum, and the resulting green oil was washed with *n*-hexane (3 x 2 mL). The remaining residue was extracted with toluene (3 mL), layered with *n*-hexane (6 mL), and stored at room temperature for 7 days. The mother liquor was then decanted from the resulting orange powder.

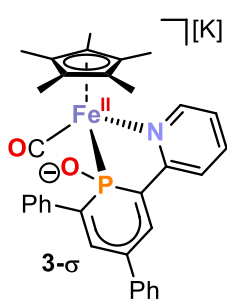
Isolation of 3-π: A small amount of orange powder was isolated and dried under vacuum to give **3-π**. This sample was used for spectroscopic characterization. The ¹H NMR spectrum of **3-π** isolated in this manner shows minor impurities with signals at 1.13 ppm and 3.86 ppm, which is believed to account for deviations in the elemental analysis. Crystals suitable for single-crystal XRD were grown by slow diffusion of *n*-hexane into a 1,4-dioxane solution of **3-π**.



Elemental analysis calcd. for C₄₅H₅₅FeKNO₈P (M_w = 863.85 g·mol⁻¹) C 62.57, H 6.42, N 1.62; found C 59.77, H 6.12, N 1.31. UV-Vis: (THF, λ_{max} / nm, ε_{max} / L·mol⁻¹·cm⁻¹): 334sh (9494). ¹H NMR (400.13 MHz, 300 K, [D₈]THF): δ = 1.28 (s, 15H, C₅(CH₃)₅), 3.29 (s, 24H, [18]crown-6), 6.62 (s, 1H, PC₅H₂Ph₂Py), 6.96–7.74 (m, 8H, PC₅H₂Ph₂Py), 7.91 (m, 2H, PC₅H₂Ph₂Py), 8.09 (m, 3H, PC₅H₂Ph₂Py), 8.52 (m, 1H, PC₅H₂Ph₂Py). ¹³C{¹H} NMR (100.61 MHz, 300 K, [D₈]THF): δ = 9.5 (s, C₅(CH₃)₅), 70.7 (s, [18]crown-6), 90.9 (s, C₅(CH₃)₅), 111.8 (s), 115.7 (s), 121.3 (s), 123.0 (s), 123.7 (s), 125.6 (s), 127.8

(s), 127.8 (s), 128.0 (s), 131.2 (s), 133.6 (s), 157.2 (s). ³¹P{¹H} NMR (161.98 MHz, 300 K, [D₈]THF): δ = -116.6 (s). ³¹P NMR (161.98 MHz, 300 K, [D₈]THF): δ = -116.6 (s).

Isolation of 3-σ: The decanted mother liquor was evaporated to dryness, and the remaining residue was extracted into tetrahydrofuran (3 mL) and layered with *n*-hexane (6 mL). Dark green crystals of **3-σ** were isolated after standing at room temperature for 6 days, filtering, and drying under vacuum. Crystals suitable for single-crystal XRD were grown from slow diffusion of *n*-hexane into a 1,4-dioxane solution of **3-σ**. Yield: 16 mg, 15%.



Elemental analysis calcd. for C₄₅H₅₅FeKNO₈P (Mw = 863.85 g·mol⁻¹) C 62.57, H 6.42, N 1.62; found C 62.57, H 6.31, N 1.60. UV-Vis: (THF, λ_{max} / nm, ε_{max} / L·mol⁻¹·cm⁻¹): 270 (sh, 16070), 340 (13458), 417 (15900), 620 (9617). ATR-IR: $\tilde{\nu}$ (CO) = 1876 cm⁻¹. ¹H NMR (400.13 MHz, 300 K, [D₈]THF): δ = 1.24 (s, 15H, C₅(CH₃)₅), 3.38 (s, 24H, [18]crown-6), 6.02 (m, 1H, pyridyl-*H*), 6.75 (m, 1H, pyridyl-*H*), 6.88 (m, 1H, pyridyl-*H*), 6.99 (m, 2H, phenyl-*H*), 7.12 (m, 4H, phenyl-*H*), 7.28 (m, 2H, phenyl-*H*), 7.40 (m, 2H, phenyl-*H*), 8.00 (bd, 1H, pyridyl-*H*, ⁴J_{PH} = 5 Hz), 8.23 (bd, 2H, ^{3,5}H of PC₅H₂, ³J_{PH} = 7 Hz). ¹³C{¹H} NMR (100.61 MHz, 300 K, [D₈]THF): δ = 9.5 (s, C₅(CH₃)₅), 70.7 (s, [18]crown-6), 90.9 (s, C₅(CH₃)₅), 111.8 (s, pyridyl-CH), 115.7 (s, ^{2,6}C of PC₅H₂), 121.8 (s, pyridyl-CH), 123.0 (s, pyridyl-CH), 123.7 (s, phenyl-CH), 125.6 (s, phenyl-CH), 127.8 (s, ^{3,5}CH of PC₅H₂), 127.8 (s, ^{3,5}CH of PC₅H₂), 128.0 (s, phenyl-CH), 128.4 (s, phenyl-CH), 131.2 (s, phenyl-CH), 133.6 (s, phenyl-CH), 146.8 (s, phenyl-C), 147.8 (phenyl-C), 157.2 (s, pyridyl-CH), 170.7 (s, CO). ³¹P{¹H} NMR (161.98 MHz, 300 K, [D₈]THF): δ = 97.9 (s). ³¹P NMR (161.98 MHz, 300 K, [D₈]THF): δ = 96.9 (t, ³J_{PH} = 17 Hz).

5.5 References

- [1] E. V. Kondratenko, G. Mul, J. Baltrusaitis, G. O. Larrazábal, J. Pérez-Ramírez, *Energy Environ. Sci.* **2013**, *6*, 3112–3135.
- [2] Q. Liu, L. Wu, R. Jackstell, M. Beller, *Nat. Commun.* **2015**, *6*, 5933.
- [3] C. Maeda, Y. Miyazaki, T. Ema, *Catal. Sci. Technol.* **2014**, *4*, 1482–1497.
- [4] D. M. D'Alessandro, B. Smit, J. R. Long, *Angew. Chem. Int. Ed.* **2010**, *49*, 6058–6082.
- [5] H. H. Storch, in *Adv. Catal.* (Eds.: W.G. Frankenburg, V.I. Komarewsky, E.K. Rideal), Academic Press, **1948**, pp. 115–156.
- [6] Data Taken from CRC Handbook of Chemistry and Physics, 73rd Ed.; Lide, D. R., Ed.; CRC Press Inc.: Boca Raton, 1992–1993.
- [7] G. Fachinetti, C. Floriani, A. Chiesi-Villa, C. Guastini, *J. Am. Chem. Soc.* **1979**, *101*, 1767–1775.
- [8] J. C. Bryan, S. J. Geib, A. L. Rheingold, J. M. Mayer, *J. Am. Chem. Soc.* **1987**, *109*, 2826–2828.
- [9] L. J. Procopio, P. J. Carroll, D. H. Berry, *Organometallics* **1993**, *12*, 3087–3093.
- [10] C. T. Saouma, C. C. Lu, M. W. Day, J. C. Peters, *Chem. Sci.* **2013**, *4*, 4042–4051.
- [11] S. I. Källäne, T. Braun, M. Teltewskoi, B. Braun, R. Herrmann, R. Laubenstein, *Chem. Commun.* **2015**, *51*, 14613–14616.
- [12] M. Feller, U. Gellrich, A. Anaby, Y. Diskin-Posner, D. Milstein, *J. Am. Chem. Soc.* **2016**, *138*, 6445–6454.
- [13] M. A. McLoughlin, N. L. Keder, W. T. A. Harrison, R. J. Flesher, H. A. Mayer, W. C. Kaska, *Inorg. Chem.* **1999**, *38*, 3223–3227.
- [14] W. C. Kaska, S. Nemeh, Ata. Shirazi, Suzan. Potuznik, *Organometallics* **1988**, *7*, 13–15.
- [15] J. Langer, A. Hamza, I. Pápai, *Angew. Chem. Int. Ed.* **2018**, *57*, 2455–2458.
- [16] N. Tsoureas, L. Castro, A. F. R. Kilpatrick, F. G. N. Cloke, L. Maron, *Chem. Sci.* **2014**, *5*, 3777–3788.
- [17] O. P. Lam, K. Meyer, *Polyhedron* **2012**, *32*, 1–9.
- [18] I. Castro-Rodriguez, K. Meyer, *J. Am. Chem. Soc.* **2005**, *127*, 11242–11243.
- [19] S. W. Ragsdale, M. Kumar, *Chem. Rev.* **1996**, *96*, 2515–2540.
- [20] D. J. Evans, *Coord. Chem. Rev.* **2005**, *249*, 1582–1595.
- [21] C. Bianchini, A. Meli, *J. Am. Chem. Soc.* **1984**, *106*, 2698–2699.
- [22] D. Sahoo, C. Yoo, Y. Lee, *J. Am. Chem. Soc.* **2018**, *140*, 2179–2185.
- [23] C. Yoo, Y.-E. Kim, Y. Lee, *Acc. Chem. Res.* **2018**, *51*, 1144–1152.
- [24] D. S. Laitar, P. Müller, J. P. Sadighi, *J. Am. Chem. Soc.* **2005**, *127*, 17196–17197.
- [25] C. C. Lu, C. T. Saouma, M. W. Day, J. C. Peters, *J. Am. Chem. Soc.* **2007**, *129*, 4–5.
- [26] A. R. Sadique, W. W. Brennessel, P. L. Holland, *Inorg. Chem.* **2008**, *47*, 784–786.
- [27] D. Oren, Y. Diskin-Posner, L. Avram, M. Feller, D. Milstein, *Organometallics* **2018**, *37*, 2217–2221.
- [28] J. R. Khusnutdinova, D. Milstein, *Angew. Chem. Int. Ed.* **2015**, *54*, 12236–12273.
- [29] B. Bichler, C. Holzhaecker, B. Stöger, M. Puchberger, L. F. Veiros, K. Kirchner, *Organometallics* **2013**, *32*, 4114–4121.
- [30] T. Zell, D. Milstein, *Acc. Chem. Res.* **2015**, *48*, 1979–1994.
- [31] Milstein David, *Philos. Trans. R. Soc. Math. Phys. Eng. Sci.* **2015**, *373*, 20140189.
- [32] C. Gunanathan, D. Milstein, *Acc. Chem. Res.* **2011**, *44*, 588–602.
- [33] C. Schulten, G. von Frantzius, G. Schnakenburg, A. Espinosa, R. Streubel, *Chem. Sci.* **2012**, *3*, 3526–3533.
- [34] N. Mèzailles and P. Le Floch, *Curr. Org. Chem.* **2006**, *10*, 3–25.
- [35] P. L. Floch, *Coord. Chem. Rev.* **2006**, *250*, 627–681.

- [36] C. Müller, L. E. E. Broeckx, I. de Krom, J. J. M. Weemers, *Eur. J. Inorg. Chem.* **2013**, *2013*, 187–202.
- [37] C. M. Hoidn, R. Wolf, *Dalton Trans.* **2016**, *45*, 8875–8884.
- [38] C. M. Hoidn, J. Leidl, C. G. P. Ziegler, I. G. Shenderovich, R. Wolf, *Eur. J. Inorg. Chem.* **2019**, 1567–1574.
- [39] B. Rezaei Rad, U. Chakraborty, B. Mühldorf, J. A. W. Sklorz, M. Bodensteiner, C. Müller, R. Wolf, *Organometallics* **2015**, *34*, 622–635.
- [40] C. Müller, D. Wasserberg, J. J. M. Weemers, E. A. Pidko, S. Hoffmann, M. Lutz, A. L. Spek, S. C. J. Meskers, R. A. J. Janssen, R. A. van Santen, et al., *Chem. – Eur. J.* **2007**, *13*, 4548–4559.
- [41] C. Müller, J. A. W. Sklorz, I. de Krom, A. Loibl, M. Habicht, M. Bruce, G. Pfeifer, J. Wiecko, *Chem. Lett.* **2014**, *43*, 1390–1404.
- [42] **1** shows poor solubility in *n*-hexane, Et₂O and PhMe, but dissolves well in more polar solvents such as THF and DME.
- [43] Additional significant resonances are also observed at *ca.* 38 ppm to 46 ppm. The corresponding species could not be identified.
- [44] The pyridyl nitrogens are hard to assign with confidence (and may plausibly be disordered over several positions), but have been located at the positions that give the lowest final R1 value.
- [45] P. Pykkö, M. Atsumi, *Chem. Eur. J.* **2009**, *15*, 186–197.
- [46] Addition of a range of electrophiles to the analogous positions in TPP has been reported previously for [K[(18)crown-6]][Cp*Fe(η⁴-TPP)]. See: C. M. Hoidn, R. Wolf, *Dalton Trans.* **2016**, *45*, 8875–8884.
- [47] R. Wolf, E.-M. Schnöckelborg, *Chem. Commun.* **2010**, *46*, 2832–2834.
- [48] a) SCALE3ABS, CrysAlisPro, Agilent Technologies Inc., Oxford, GB, **2012**. b) G. M. Sheldrick, SADABS, Bruker AXS, Madison, USA, **2007**.
- [49] R. C. Clark, J. S. Reid, *Acta Crystallogr. A* **1995**, *51*, 887–897.
- [50] G. M. Sheldrick, *Acta Crystallogr. Sect. Found. Adv.* **2015**, *71*, 3–8.
- [51] G. M. Sheldrick, *Acta Crystallogr. A* **2008**, *64*, 112–122.

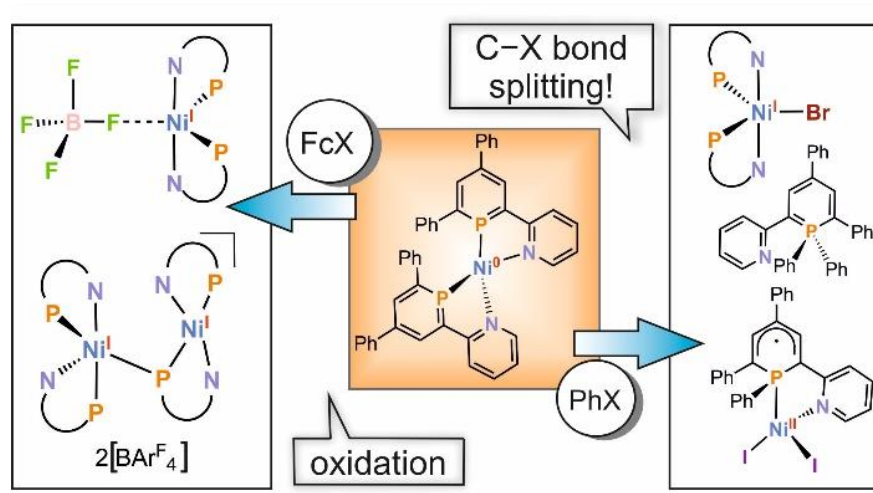
5.6 Supporting Information

The supporting information of *Chapter 5* can be found on the supplied CD-ROM and on <https://doi.org/10.1002/anie.201909240>. The supporting information contains: NMR, UV-vis and IR spectra, X-ray crystallography details and results of quantum chemical calculations including Cartesian coordinates of all optimized structures.

Chapter 6

Phosphorus-Analogues of $[\text{Ni}(\text{bpy})_2]$: Synthesis and Application in Carbon-Halogen Bond Activation

Abstract: The neutral, homoleptic, pyridyl-phosphinine Ni(0) complex $[\text{Ni}(2\text{-Py-4,6-Ph}_2\text{-PC}_5\text{H}_2)_2]$ (**1**) has been obtained by reaction of the formal Ni(0) source $[(\text{IPr})\text{Ni}(\text{H}_2\text{C}=\text{CHSiMe}_3)_2]$ with two equivalents of 2-(2'-pyridyl)-4,6-diphenyl-phosphinine (**L**). Compound **1** can be oxidized both electrochemically and through use of ferrocenium salts, to afford the corresponding Ni(I) complexes $[\mathbf{1}]\text{BF}_4$, $[\mathbf{1}(\text{THF})]\text{PF}_6$ and $[\mathbf{1}_2](\text{BAR}^{\text{F}_4})_2$. The structure of these salts shows an interesting dependence on the nature of the anion. While $[\mathbf{1}]\text{BF}_4$ and $[\mathbf{1}(\text{THF})]\text{PF}_6$ show trigonal bipyramidal coordination of Ni in the solid state, $[\mathbf{1}_2](\text{BAR}^{\text{F}_4})_2$ exists as a dinuclear Ni(I) complex and possesses a bridging phosphinine moiety in a rare μ_2 -mode. Reactions of **1** with halobenzenes highlight the non-innocent behavior of the aromatic phosphinine ligand, leading to the formation of oxidized Ni complexes but not to classical oxidative addition products. Reaction of **1** with bromobenzene affords the λ^5 phosphinine **2** and the bipyramidal Ni(I) complex $[\mathbf{1}]\text{Br}$, whereas a more unconventional oxidation product **3** is formed from reaction of **1** and iodobenzene.



Reproduced with permission from J. Leitl, P. Coburger, D. J. Scott, N. P. van Leest, C. G. P. Ziegler, G. Hierlmeier, B. de Bruin, G. Hörner, C. Müller and Robert Wolf, *Inorg. Chem.* **2020**, <https://doi.org/10.1021/acs.inorgchem.0c01115>.

[b] J. Leitl performed all reactions and fully characterized compounds **1**, $[\mathbf{1}]\text{BF}_4$, $[\mathbf{1}(\text{THF})]\text{PF}_6$ and $[\mathbf{1}_2](\text{BAR}^{\text{F}_4})_2$, **2**, $[\mathbf{1}]\text{Br}$ and **3** by single crystal X-ray analysis, NMR and UV-Vis spectroscopy and elemental analysis. C. G. P. Ziegler and G. Hierlmeier supplied $[(\text{IPr})\text{Ni}(\text{H}_2\text{C}=\text{CHSiMe}_3)_2]$. P. Coburger performed all DFT calculations and was involved in the preparation of the manuscript and supporting information. N. P. van Leest and B. de Bruin performed all EPR measurements and were involved in preparing the manuscript and supporting information. G. Hörner performed the SQUID measurement and was involved in preparing the manuscript and supporting information. J. Leitl wrote the manuscript with assistance by D. J. Scott and contributions by all authors. C. Müller and R. Wolf supervised and directed the project.

6.1 Introduction

Nickel(0) complexes have become ubiquitous in homogeneous catalysis and are used for a wide range of processes,^[1] including alkene and alkyne oligomerization reactions,^[2–7] as well as Kumada-type cross couplings.^[8] The complex bis(2,2'-bipyridine) nickel(0) (**A**, Figure 1) is an archetypal example of a Ni(0) species with versatile catalytic properties, and has found diverse applications in various (electro)chemical reactions and catalysis.^[9–13]

Replacing the pyridyl moieties in **A** with valence isoelectronic phosphinine (also referred to as phosphabenzene) units can have a significant impact on both the electronic structure and reactivity of the corresponding coordination compound.^[14–18] Considering the versatile applications of **A** and bipyridine complexes, as well as the fact that monophosphinine nickel(0) complexes are well-investigated,^[19–24] it is quite surprising that phosphorus-containing analogues of **A** are extremely rare. In fact, the known examples appear to be limited to just a single species described by Le Floch and co-workers, who reported that reactions of 2,2'-(4,5-dimethyl)biphosphinine^[25] with nickel(0) sources, such as Ni(cod)₂ (cod = 1,5-cyclooctadiene), afford the homoleptic bis(biphosphinine) complex **B** (Figure 1).^[26] However, the reactivity of this complex – and almost all related chelating phosphinine Ni complexes – remains unexplored.

We have recently become interested in the coordination chemistry of the donor-functionalized phosphinine 2-(2'-pyridyl)-4,6-diphenylphosphinine (**L**), a ‘hybrid’ P,N ligand which can be considered as a cross between previously explored biphosphinines and the ubiquitous bipyridines.^[27–29] **L** possesses two electronically distinct binding sites – a “soft” P and a “hard” N donor site – which can have a significant impact on its coordination properties and reactivity. Although a large variety of 4d and 5d transition metal complexes of **L** have been prepared, syntheses of 3d metal complexes remain scarce.^[30–38] Nevertheless, we have recently demonstrated that the combination of a late 3d metal with ligand **L** can lead to versatile coordination chemistry, and even more importantly to useful reactivity, as exemplified by the facile cleavage of one C=O bond in CO₂ by the Fe complex **C** (Figure 1).^[39]

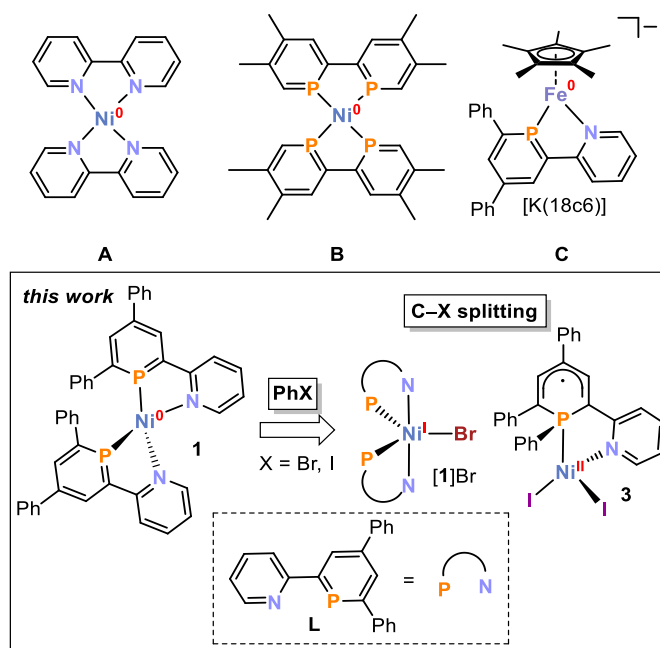
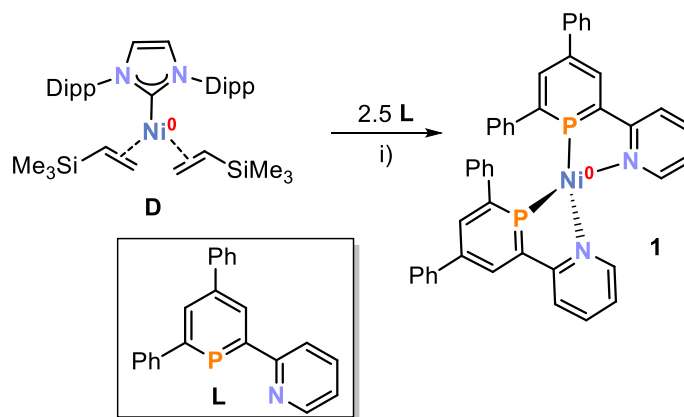


Figure 1. Previously-reported bidentate, chelated phosphinone-containing transition metal complexes (A–C), and the new nickel pyridyl-phosphinone complexes (**1**, [1]Br and **3**) described herein; 18c6 = [18]crown-6.

6.2 Results and Discussion

Encouraged by our previous results with iron, we were motivated to investigate the coordination compounds of the pyridyl-phosphinone ligand **L** with other late 3d metals. Given the paucity of prior Ni complexes containing chelating phosphinone ligands – and, in particular, the lack of corresponding reactivity studies – we were specifically motivated to study the reactivity of **L** towards suitable low-valent Ni sources, and decided to start with the formal Ni(0) source $[(\text{IPr})\text{Ni}(\text{H}_2\text{C}=\text{CHSiMe}_3)_2]$ (**D**, IPr = 1,3-bis(2,6-diisopropylphenyl)imidazolin-2-ylidene).^[40] While the 1:1 reaction of **D** and **L** resulted in a mixture of several inseparable products (see SI, Figure S11), the reaction of **D** with 2.5 equivalents of **L** led to the selective formation of a single phosphorus-containing species (**1**), characterized by a singlet in the $^{31}\text{P}\{^1\text{H}\}$ NMR spectrum at δ (ppm) = 179.4 (Scheme 1, for spectrum see Figure S5). The isolation of **1** was achieved by removal of volatiles (including $\text{H}_2\text{C}=\text{CHSiMe}_3$) under vacuum, removal of IPr by washing with *n*-hexane, and layering of a purple solution of **1** in benzene with *n*-hexane at room temperature for two days, to afford a pure, crystalline material in 35% yield.

Compound **1** was fully characterized by NMR and UV-Vis spectroscopy, elemental analysis and cyclic voltammetry (see SI). The collected data are all consistent with formulation of **1** as the 1:2 homoleptic chelate complex $[\text{Ni}(\text{L})_2]$ (Scheme 1), which is also in line with the reaction stoichiometry employed.



Scheme 1. Synthesis of $[\text{Ni}(\text{L})_2]$ (**1**), using $[(\text{IPr})\text{Ni}(\text{H}_2\text{C}=\text{CHSiMe}_3)_2]$ (**D**) as a Ni(0) precursor; i) C_6H_6 , 25 °C, 16 h; Dipp = 2,6-diisopropylphenyl.

Single crystals suitable for X-ray diffraction could be obtained by slow diffusion of *n*-hexane into a solution of **1** in benzene. As anticipated, the solid-state molecular structure shows the expected homoleptic chelate complex where the Ni center is coordinated by two 2-(2'-pyridyl)-phosphinine ligands **L** (Figure 2). This leads to a distorted tetrahedral coordination sphere around the Ni center (calculated geometry index for **1** is $\tau_4 = 0.80$, see Table 1; *c.f.* $\tau_4 = 0, 1$ for ideal square planar and tetrahedral geometries, respectively). The P–Ni–N bite-angles are $84.05(17)^\circ$ for P1–Ni1–N1 and $84.28(17)^\circ$ for P2–Ni1–N2. The C1–P1–C5 angle of **1** is approximately 102° , close to the one in free phosphinines (*ca.* 100°). This is in line with earlier observations that electron rich metal fragments cause only a marginal opening of the C1–P1–C5 angle in the coordinated phosphinine. In contrast, this effect is much more pronounced in coordination compounds, in which the phosphinine ligand is bound to more electron poor metal centers with reduced π -back donation ability. Those complexes are usually characterized by a high reactivity of the P=C double bond towards nucleophilic attack.^[28,41–43]

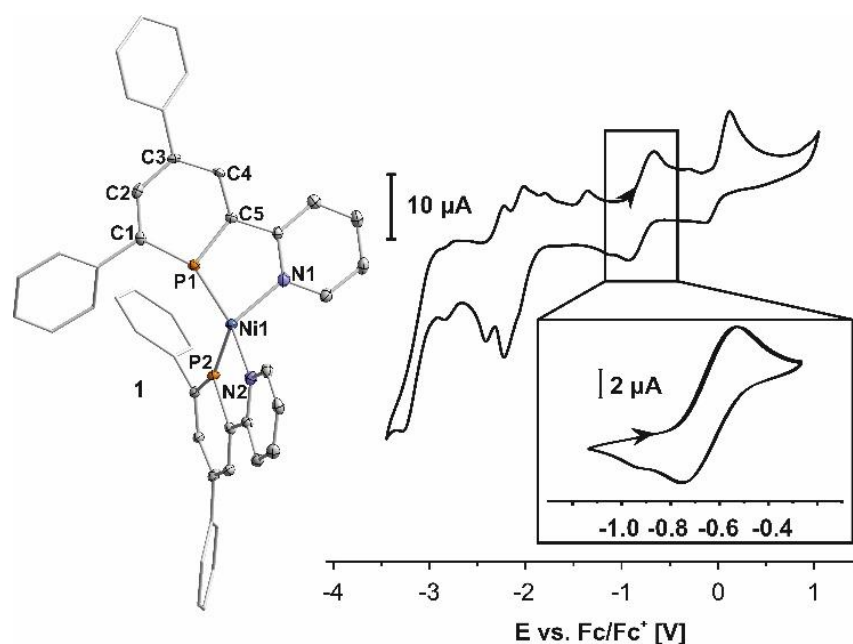


Figure 2. Molecular structure of **1** in the solid state (left); ellipsoids are drawn at the 40% probability level; H atoms are omitted for clarity; four phenyl groups are displayed in wireframe for clarity; selected bond lengths [Å] and bond angles [°]: Ni1–N1 2.005(6), Ni1–N2 1.998(6), Ni1–P1 2.091(2), Ni1–P2 2.092(2), P1–Ni1–P2 128.15(8), N1–Ni1–N2 110.4(2), P1–Ni1–N2 124.67(18), N1–Ni1–P2 129.03(17), P1–Ni1–N1 84.05(17), P2–Ni1–N2 84.28(17), C1–P1–C5 102.2(3), C1'–P2–C5' 102.0(3); cyclic voltammograms of **1** (right; from E (V) = –3.4 to +1.1 and E (V) = –1.1 to –0.2, scan rate 100 mV).

Complex **1** is the first example of a Ni complex containing a pyridyl-phosphinine ligand. The molecular structure of **1** is reminiscent of ubiquitous 2,2'-bipyridine^[44] Ni(0) complexes, which are known for their versatile redox properties and corresponding utilization in the electrochemical reduction of aryl halides, for example.^[9–11,45] Thus, in order to determine the redox properties of **1**, cyclic voltammograms were recorded in THF using $[nBu_4N]PF_6$ as a supporting electrolyte. Several irreversible and quasi-reversible oxidation and reduction processes are apparent (Figure 2). However, perhaps the most interesting process is the quasi-reversible oxidation observed at $E_{1/2} = -0.6$ V vs. Fc/Fc^+ . Because this feature is well-behaved on the CV timescale it was anticipated that **1** might also be oxidized in a preparative manner using a suitable chemical oxidant. Thus, **1** was treated with several different ferrocenium salts FcX (Fc = ferrocenium; $X = BF_4, PF_6, BAr^F_4$; $Ar^F = 3,5-(CF_3)_2C_6H_3$) in order to obtain the corresponding cationic Ni complexes $[1]BF_4$, $[1(THF)]PF_6$ and $[1_2](BAr^F_4)_2$ (Scheme 2), which could all be characterized crystallographically.

Table 1. Geometry indices (τ_4 , τ_5)^{[46][47]} and magnetic moments (μ_{eff} , THF-d₈, 300 K) of reported Ni complexes.

Compound	τ_4	τ_5	μ_{eff}
1	0.80	-	-
[1] BF_4	-	0.53	2.0(1)
[1 (THF)] PF_6	-	0.71	1.7(1)
[1] Br	-	0.79	2.1(1)
3	0.95	-	3.2(1)

The solid-state molecular structures of [**1**] BF_4 and [**1**(THF)] PF_6 reveal a common structural motif: trigonal bipyramidal Ni(I) complexes coordinated by two ligands **L**, and direct, equatorial coordination of an additional ligand (Figure 3). In [**1**] BF_4 , the tetrafluoroborate anion shows an interaction of one fluorine atom with the metal center (Ni1---F1 distance: 2.273 Å). The value of the geometry index for [**1**] BF_4 ($\tau_5 = 0.53$) is in between those expected for square pyramidal ($\tau_5 = 0$) and trigonal bipyramidal complexes ($\tau_5 = 1$; see Table 1). For [**1**(THF)] PF_6 the fifth coordination site at Ni is occupied by a THF solvent molecule (Ni1---O1 2.136 Å), rather than by the counteranion, which can be attributed to the reduced donor strength of the PF_6^- anion relative to BF_4^- (Figure 3). A similar coordination motif was observed following the electrophilic addition of Ph_3SnCl to anionic homoleptic biphosphinine cobalt and rhodium complexes, as described by Le Floch and co-workers.^[48] The magnetic moments of [**1**] BF_4 and [**1**(THF)] PF_6 [2.0(1) and 1.7(1) μ_{B} respectively in THF-d₈ at 300 K] were determined by the Evans NMR method and are consistent with $S = \frac{1}{2}$ Ni(I) centers (see Table 1). EPR measurements of [**1**] BF_4 and [**1**(THF)] PF_6 were recorded in toluene glasses at 20 and 40 K, respectively, and also confirm the presence of a single unpaired electron at each Ni center (for full details see the SI). The EPR signal of [**1**] BF_4 appears almost isotropic due to the broad and overlapping signals of the g -tensor. However, it is better described as a rhombic system which is indicated by the asymmetric shape of the signal. The observed g -tensor with the simulated principal components $g_{11} = 2.195$, $g_{22} = 2.127$, $g_{33} = 2.060$ is consistent with a nickel-centered radical in a system with small g -anisotropy (for spectrum see Figure S20). The EPR spectrum of [**1**(THF)] PF_6 displays similarly overlapping signals of the g -tensor and can again be described as a rhombic system with small g -anisotropy. Poorly resolved hyperfine interactions were observed on (at least) one g -tensor, and satisfactory simulation was achieved after inclusion of hyperfine coupling (135 and 150 MHz) to ^{31}P ($I = \frac{1}{2}$) on two g -tensors. The observed g -tensor (simulated g -tensor: $g_{11} = 2.200$, $g_{22} = 2.129$, $g_{33} = 2.035$) is again consistent with a nickel-centered radical (for spectrum see Figure S21). These results are consistent with DFT calculations carried out on [**1**] BF_4 which show a high spin density on Ni (0.85) and reproduce the experimental g -tensor quite well (TPSSh/IGLO-III+CP(PPP), see the Supporting Information).

The reaction of **1** with FcBAR^F₄ leads to a product with a notably different structure, at least in the solid state. In this case the product [1₂](BAR^F₄)₂ is formed, which crystallizes as a dicationic dinuclear nickel complex fragment with two Ni(I) centers bridged by one P atom of one phosphinine ligand **L**. The charge of the dication is balanced by two BAR^F₄[−] anions, which show no close contacts with either Ni centers (Figure 3). Compound [1₂](BAR^F₄)₂ is a rare example of a complex in which the phosphinine ligand shows a μ₂-P bridging coordination mode.^[49–57] The corresponding bipyridine μ₂-N bridging mode is even scarcer (despite the fact that these complexes were studied far more extensively), due to the reduced electronic versatility of the lighter heterocycle.^[58–60] The Ni–N and Ni–P distances in [1₂](BAR^F₄)₂ are similar to those in [1]BF₄ and [1(THF)]PF₆, except for the bridging Ni1–P3 distance, which is slightly elongated (2.4071(11) Å vs. mean distance 2.246 Å) as expected for a bridging interaction. The bridging P3 atom is tetrahedrally coordinated between the two Ni(I) centers with a geometry index of τ₄ = 0.86.

Also in contrast to [1]BF₄ and [1(THF)]PF₆, the EPR signal observed during measurement of [1₂](BAR^F₄)₂ in a toluene glass at 30 K is well resolved, and shows a rhombic system with small *g*-anisotropy and hyperfine coupling interactions with two ³¹P nuclei along all three *g*-tensors ($A^{P1}_{11} = A^{P2}_{11} = 205$ MHz, $A^{P1}_{22} = A^{P2}_{22} = 170$ MHz, $A^{P1}_{33} = A^{P2}_{33} = 175$ MHz). The spectrum again indicates that a nickel-centered radical is present (simulated *g*-tensors: $g_{11} = 2.2170$, $g_{22} = 2.1450$, $g_{33} = 2.0195$, see Figure S22). The found *g*-values (close to 2) and well-defined hyperfine coupling interactions are indicative for an isolated *S* = 1/2 species. Thus the EPR data might indicate that [1₂](BAR^F₄)₂ dissociates in solution into two monocations [Ni(I)L₂]⁺. This is also consistent with DFT calculations on the monocation, which yield a rhombic *g*-tensor ($g_z = 2.123$, $g_y = 2.116$, $g_x = 2.015$) that is in good agreement with the experimental results.

When the EPR measurement of [1₂](BAR^F₄)₂ is performed in a 2-methyl-tetrahydrofuran glass at 20 K instead of a toluene glass, a well resolved rhombic system with small *g*-anisotropy is again observed (Figure 4). However, in this case additionally resolved hyperfine coupling to two equivalent ³¹P (*I* = 1/2), two equivalent ¹⁴N (*I* = 1), and two equivalent ¹H (*I* = 1/2) nuclei are also observed. Calculations indicate that the proton hyperfine couplings are caused by the *ortho*-hydrogen atoms of the pyridyl groups (see the SI for details). The simulated *g*-tensor ($g_{11} = 2.2135$, $g_{22} = 2.146$, $g_{33} = 2.0212$) is similar to that obtained in toluene and so is again consistent with a nickel centered radical. The presence of monocationic Ni(I) centers is additionally confirmed by the magnetic moment of 1.7(1) μ_B [in THF-d₈ at 300 K] per Ni atom measured by the Evans NMR method.

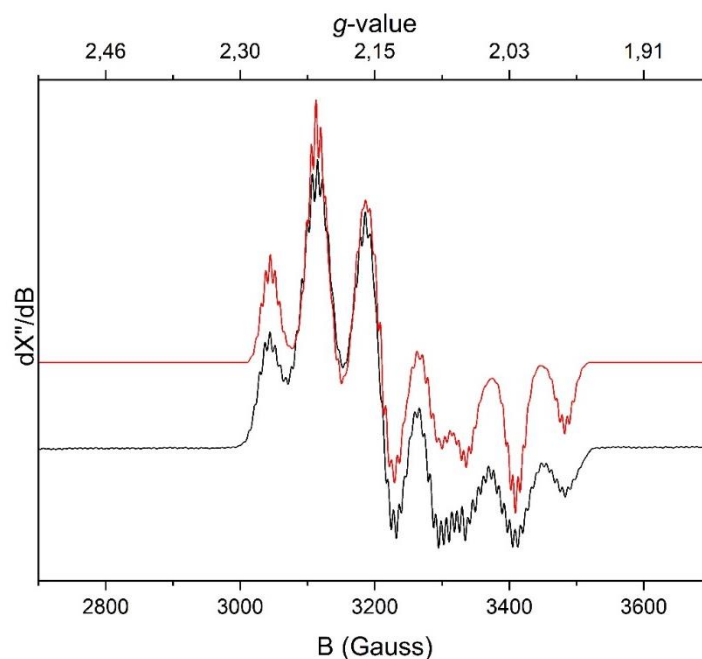
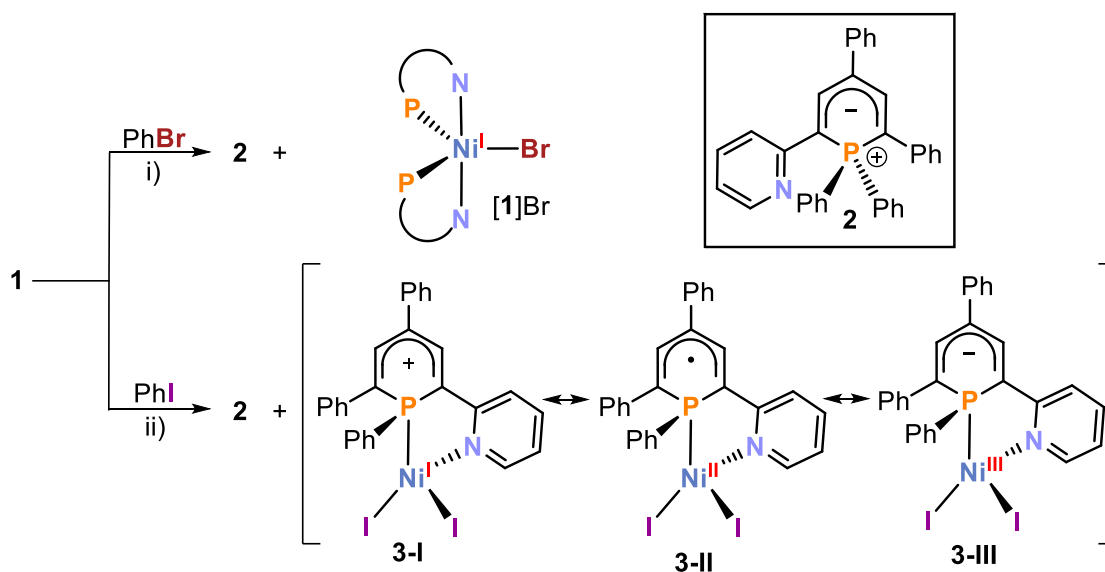


Figure 4. Experimental (black) and simulated (red) EPR spectra of $[12](BAr^F_4)_2$ recorded at 20 K in a 2-methyl-tetrahydrofuran glass; simulation parameters: $g_{11} = 2.2135$, $g_{22} = 2.1460$, $g_{33} = 2.0212$. $W_{11} = 3.0$, $W_{22} = 2.5$, $W_{33} = 3.2$. $A^{P1}_{11} = A^{P2}_{11} = 210$ MHz, $A^{P1}_{22} = A^{P2}_{22} = 212$ MHz, $A^{P1}_{33} = A^{P2}_{33} = 207$ MHz. $A^{N1}_{11} = A^{N1}_{11} = 23$ MHz, $A^{N1}_{22} = A^{N2}_{22} = 28$ MHz, $A^{N1}_{33} = A^{N2}_{33} = 21$ MHz, $A^{H1}_{11} = A^{H2}_{11} = 20$ MHz, $A^{H1}_{22} = A^{H2}_{22} = 20$ MHz, $A^{H1}_{33} = A^{H2}_{33} = 19$ MHz; experimental conditions: microwave frequencies 9.64567 GHz; power 1.589 mW; modulation amplitude 4.000 G.

In addition to simple outer-sphere oxidation, we were also interested in investigating more complex reactions of **1**, particularly given the complete lack of analogous studies for other Ni phosphinine complexes. Ni(0) complexes in general are very versatile and find various applications in electrochemistry and catalysis.^[61,62] For example, Ni(0) species play important roles in cross coupling reactions (e.g. Kumada reaction) due to their redox properties and ability to undergo oxidative additions with substrates such as aryl halides.^[63,64] Thus, we were motivated to investigate the reactivity of **1** with the simple model cross-coupling substrates bromobenzene and iodobenzene (Scheme 3). When one equivalent of bromobenzene was added to **1** in benzene no change was observed at room temperature, either by eye or by $^{31}P\{^1H\}$ NMR spectroscopy. However, when the temperature was increased to 60 °C a color change from deep purple to fluorescent red could be observed. According to GC-FID analysis, a maximum of *ca.* 70% of bromobenzene was consumed (despite complete consumption of **1** as indicated by $^{31}P\{^1H\}$ NMR spectroscopy) alongside formation of a single new $^{31}P\{^1H\}$ resonance arising as a sharp singlet at δ (ppm) = 4.7. This signal splits into a complex multiplet in the ^{31}P NMR spectrum. In order to characterize the corresponding species **2**, the solvent of the fluorescent red reaction mixture was completely evaporated, and the remaining residue was extracted into *n*-hexane.



Scheme 3. Reaction of **1** with haloarenes PhX ($X = Br, I$) at $60\text{ }^\circ\text{C}$; i) reaction in benzene, **2** (15% isolated yield) and $[1]Br$ (45%); ii) reaction in toluene, **2** (30%) and **3** (64%); possible contributions to the electronic structure of **3**, including $Ni\ d^9$ (**3-I**), $Ni\ d^8$ (**3-II**) and $Ni\ d^7$ (**3-III**) centers.

Crystals of **2** were obtained by slow evaporation of the resulting fluorescent orange *n*-hexane solution. Single crystal X-ray diffraction revealed its identity as a 1,1-diphenyl- λ^5 -phosphinine (Figure 5), which accounts for the observed fluorescent properties.^[65,27,66–68] This structure formally arises from addition of two phenyl groups to the phosphorus center of the phosphinine ligand **L**. As reported for other λ^5 -phosphinines, the P1–C1/C5 bonds are slightly shortened compared to P–C single bonds (mean distance: 1.763 \AA , vs. sum of covalent radii: 1.86 \AA), while the carbon-carbon bonds are in the range of C=C double bonds (mean distance: 1.395 \AA vs. sum of covalent radii: 1.34 \AA).^[69] The almost planar phosphorus heterocycle is characterized by the small fold angle of $1.50(8)^\circ$, and the phenyl substituents at the phosphorus atom show bond lengths consistent with P–C single bonds (mean distance: 1.817 \AA).^[69] Similar to the only other λ^5 -pyridyl-phosphinine reported in literature, the pyridyl-group is essentially coplanar with the phosphinine-ring ($N1-C6-C5-C4 = 174.9(1)^\circ$), while the phenyl-groups in 4- and 6-position of the heterocycle are not in plane with the central hexagon. This is in accordance with our expectations for the steric demand of the nitrogen lone pair, which is smaller than a CH-group of a phenyl moiety.^[68,70]

The *n*-hexane-insoluble material remaining after separation of **2** could be dissolved in THF to give a red, NMR-silent solution. Single crystals suitable for XRD were obtained after layering with *n*-hexane. The molecular structure revealed the formation of a trigonal bipyramidal Ni(I) complex $[1]Br$, containing two **L** and one additional bromide ligand (Figure 5), in a structure very similar to those observed for $[1]BF_4$ and $[1(THF)]PF_6$. The σ -bonds between the Ni center and the donor atoms of **L** (mean distance $Ni1-N$: 2.105 \AA and $Ni1-P$: 2.208 \AA) are elongated compared to **1**, most likely caused by the higher coordination number of the Ni atom. In comparison with the cationic complexes $[1]BF_4$ and $[1(THF)]PF_6$, $[1]Br$ displays similar Ni–P distances but shortened Ni–N distances. The $Ni1-Br1$ bond

length of 2.489 Å is in the range of covalent Ni–Br bonds (sum of covalent radii: 2.430 Å),^[69] while the geometry index of $\tau_5 = 0.79$ is consistent with a distorted trigonal bipyramidal structure (see Table 1). The magnetic moment of $[1]Br$ [2.1(1) μ_B in THF- d_8 at 300 K] was determined by the Evans NMR method and is consistent with an $S = 1/2$ Ni(I) center (see Table 1). Additionally, EPR measurements in a toluene glass at 20 K indicate the presence of a Ni(I) species with a metal-centered radical (see SI, Figure S24, simulated g -tensor: $g_{11} = 2.19$, $g_{22} = 2.125$, $g_{33} = 2.060$), similar to $[1]BF_4$ and $[1(THF)]PF_6$. The calculated spin-density on Ni (0.82) as well as the calculated g -tensor are in good agreement with the experimental data (see Table S5).

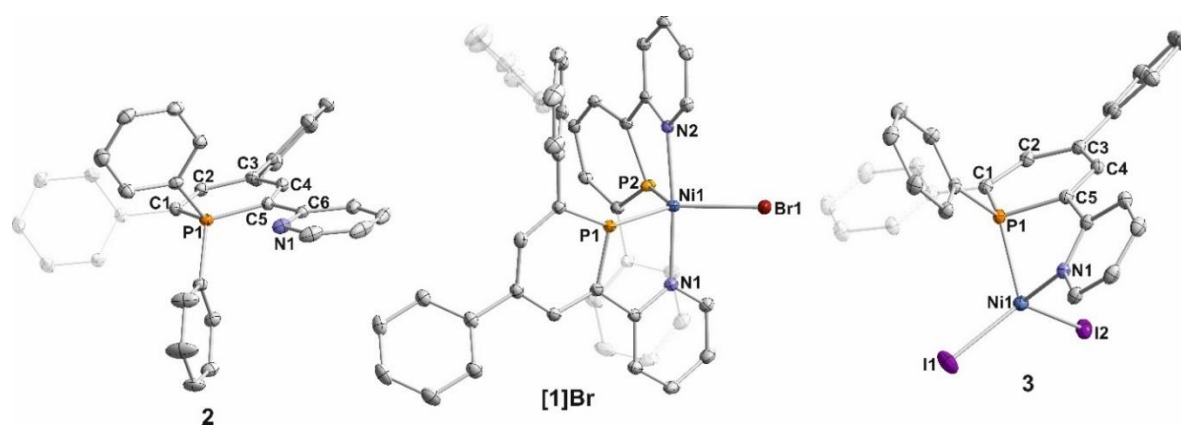


Figure 5. Solid state molecular structures of **2**, $[1]Br$ and **3**; ellipsoids are drawn at the 40% probability level; H atoms are omitted for clarity; some phenyl groups are transparent for clarity; for **2**: selected bond lengths [Å] and bond angles [°]: P1–C1 1.7719(13), C1–C2 1.3724(17), C2–C3 1.4194(17), C3–C4 1.3858(18), C4–C5 1.4038(18), P1–C5 1.7553(13), C1–P1–C5 107.49(6), fold angle C1–P1–C5 1.50(8); for $[1]Br$: selected bond lengths [Å] and bond angles [°]: Ni1–P1 2.2094(6), Ni1–P2 2.2055(6), Ni1–N1 2.1046(18), Ni1–N2 2.1045(18), Ni1–Br1 2.4889(4), P1–Ni1–P2 112.45(3), P1–Ni1–Br1 121.48(2), Br1–Ni1–P2 126.04(2), P1–Ni1–N1 80.61(4), P2–Ni1–N2 80.58(4); for **3**: toluene solvent molecule is omitted for clarity; selected bond lengths [Å] and bond angles [°]: Ni1–P1 2.2509(6), Ni1–I1 2.4893(4), Ni1–I2 2.5375(4), Ni1–N1 1.9941(19), P1–C1 1.774(2), C1–C2 1.387(3), C2–C3 1.414(3), C3–C4 1.417(3), C4–C5 1.370(3), P1–C5 1.779(2), C1–P1–C5 104.61(10), P1–Ni1–N1 82.59(6), I1–Ni1–I2 124.218(16), P1–Ni1–I1 116.93(2), N1–Ni1–I2 108.96(5).

Although Ni-mediated cross coupling reactions usually involve Ni(0) and Ni(II) species,^[71] Ni(I) complexes analogous to $[1]Br$ have also been suggested as viable intermediates and may also show pronounced catalytic activity.^[72–76] Some other Ni(I) halide complexes have also been isolated from the reaction of Ni(0) complexes with PhX.^[77,78] Nelson and Sproules reported on the formation of $[(dppf)NiX]$ complexes (dppf = 1,1'-bis(diphenylphosphino)ferrocene; X = Cl, Br, I) *via* oxidative addition of ArX to a Ni(0) precursor, and subsequent comproportionation upon addition of a second equivalent of the Ni(0) starting material. In those reactions the formation of biphenyl could be observed, due to homocoupling of concomitantly-generated phenyl radicals.^[79] It is plausible that similar formation of phenyl radicals occurs during the formation of $[1]Br$, and that these are intercepted by the phosphinine ligand **L**, ultimately resulting in formation of the co-product **2**.

The reaction of **1** was also investigated towards one equivalent of iodobenzene under analogous conditions (toluene, 60°C) but was found to lead to a significantly different outcome. In this case, full consumption (>99%) of iodobenzene took place according to GC-FID analysis. Compound **2** could again be isolated after extraction with *n*-hexane. However, the remaining residue showed a deep green color, rather than deep red as had been observed using PhBr. Crystals were obtained from a toluene solution of this residue, after layering with *n*-hexane. Single crystal X-ray diffraction revealed a new product **3**, which shows a significantly different structure in the solid state than [1]Br (Figure 5). Most notably, **3** has clearly lost one of its phosphinine ligands **L**. Moreover, the Ni center – which is tetrahedrally coordinated ($\tau_4 = 0.95$, Table 1) – is bound to *two* iodide ligands, as well as by a formally anionic 1-Ph- λ^4 -phosphinine ligand, which is derived by addition of an extra phenyl substituent to ligand **L**. The Ni1–P1 distance (2.250 Å) is in the range of Ni–P single bonds (sum of covalent radii: 2.21 Å), while the Ni1–N1 (1.994 Å) bond length is elongated in a similar manner as in **1**. The Ni1–I distances (mean value: 2.514 Å) are in the range of typical Ni–I bonds (sum of covalent radii: 2.43 Å). We anticipate that **3** is formed by oxidative addition of the carbon-halogen bond to the Ni-center and subsequent transfer of the aryl fragment to the ligand. A similar reaction of a (TPP)Ni(C₂H₅)(acac)-complex (TPP = 2,4,6-triphenylphosphinine, acac = acetylacetonate) has been proposed by Lehmkuhl et al.^[23] Unlike [1]Br, the electronic structure of **3** cannot be assigned easily. The measured value of the magnetic moment [3.2(1) in THF-d₈ at 300 K] lies between those expected for two and three unpaired electrons (Table 1).

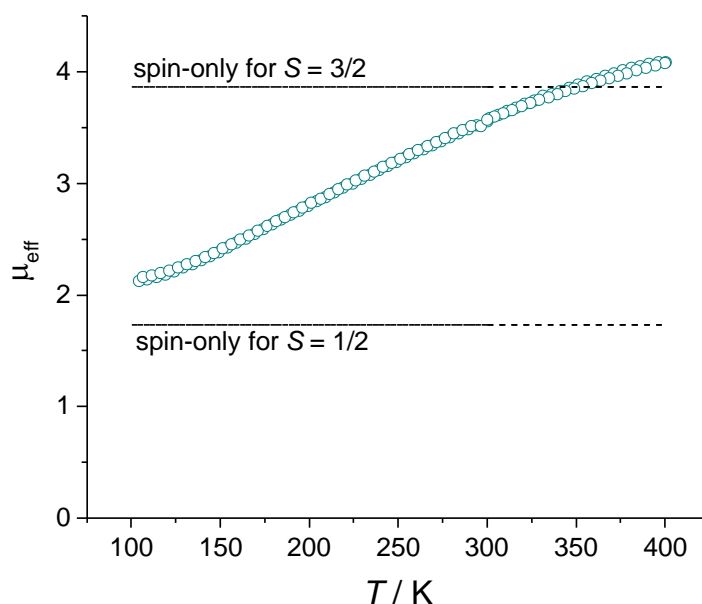


Figure 6. Magnetic susceptibility data recorded for a solid sample **3** in the temperature range 100 – 400 K in the heating and cooling mode and an applied field of 2000 Oe.

The magnetic susceptibility of a solid sample of **3** was measured with a SQUID magnetometer in the temperature range 100 K < T < 400 K. The results are shown in Figure 6. These data reveal that the magnetic moment continuously increases from $\mu_{\text{eff}} = 2$

at 105 K to $\mu_{\text{eff}} = 4$ at 400 K. These data suggest that a thermally activated spin transition occurs from an $S = 1/2$ ground state into an $S = 3/2$ excited state. The latter dominates at the upper limit of the accessible temperature window. In addition, it is noteworthy that the measured effective moment significantly exceeds the expected spin-only value for an $S = 3/2$ system at high temperature ($T > 350$ K). This observation might be explained by unquenched orbital contributions to the magnetic moment of the $S = 3/2$ species, which is a common phenomenon for complexes with a tetrahedral d^8 configuration at the metal atom. The EPR spectrum of **3** recorded at 20 K in a toluene glass shows overlapping and broad signals for the g -tensors. The simulated g -tensor ($g_{11} = 2.390$, $g_{22} = 2.242$, $g_{33} = 2.120$) is consistent with a nickel centered radical in a rhombic system (Figure 7).

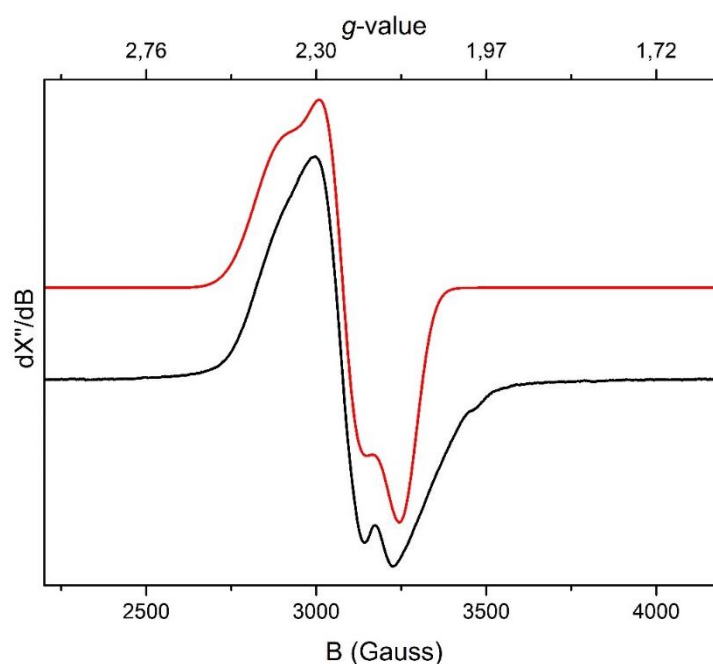


Figure 7. Experimental (black) and simulated (red) EPR spectra of **3** recorded at 20 K in a toluene glass; simulation parameters: $g_{11} = 2.390$, $g_{22} = 2.242$, $g_{33} = 2.120$; $W_{11} = 90$, $W_{22} = 55$, $W_{33} = 55$; experimental conditions: microwave frequencies 9.644902 GHz; power 0.6325 mW; modulation amplitude 2.000 G.

In the case of **3**, the experimental data could not be reproduced in good agreement using standard DFT (for details see supporting information). Furthermore, a rather large spin density was calculated at the Ni atom (1.23) hinting at a broken-symmetry solution. Indeed, a broken-symmetry treatment at the TPSS0/def2-TZVP level shows an interesting electronic structure. Here, an intermediate spin Ni center ($S = 1$, d^8) is antiferromagnetically coupled to a phosphacyclohexadienyl radical resulting in an overall $S = 1/2$ species (**3-II**, for details see Supporting Information). A small energy separation between the broken-symmetry doublet and the quartet states was calculated by DFT ($\Delta E_{\text{doublet-quartet}} = 1.1 \text{ kcal mol}^{-1}$ at the TPSS0-D3BJ/def2-TZVP level of theory). However, dedicated multireference calculations, namely CASSCF-NEVPT2 with an active space of 13 electrons in 12 orbitals, reveal a much more complicated electronic structure of the $S = 1/2$ ground state of **3**. These calculations

show that all three mesomeric structures (**3-I**, **3-II** and **3-III**) shown in Scheme 3 (*vide supra*), contribute significantly to the overall electronic structure of **3**. Thus, **3** exhibits significant multi-reference character which makes an assignment of the oxidation state of the nickel atom somewhat ambiguous. However, both broken-symmetry DFT and CASSCF clearly show the redox-active behavior of the anionic 1-phenyl-phosphacyclohexadienyl ligand in **3**. Furthermore, the CASSCF-NEVPT2 estimation of the *g*-tensor is in qualitative agreement with the experiment and reproduces the observed significant anisotropy of the *g*-tensor ($g_z = 2.562$, $g_y = 2.227$, $g_x = 2.173$).

6.3 Conclusion

In summary, we have presented the synthesis and crystallographic characterization of the homoleptic 2-(2'-pyridyl)-phosphinine Ni(0) complex [Ni(2-Py-4,6-Ph₂-PC₅H₂)₂] (**1**). First reactivity studies on the phosphinine-based Ni complex **1** show that it can be conveniently oxidized using ferrocenium salts FcX. Oxidation with FcBF₄ and FcPF₆ leads to the formation of Ni(I) complexes [1]BF₄ and [1(THF)]PF₆ which possess similar trigonal bipyramidal structural motifs. Oxidation of **1** with FcBAr^F₄, on the other hand, affords a dicationic dinuclear Ni(I) complex [1₂](BAr^F₄)₂ containing a bridging phosphinine ligand in the rare μ₂-coordination mode. The reaction of **1** with bromobenzene leads to the formation of the λ⁵-phosphinine **2** and the trigonal bipyramidal Ni(I) complex [1]Br. In contrast, reaction of **1** with iodobenzene results in the formation of **2** and the tetrahedral Ni complex **3**, which is based on a formally anionic 1-Ph-λ⁴-phosphinine. Quantum chemical calculations on **3** highlight the redox-active behavior of the phosphinine moiety which prohibits a clear assignment of an oxidation state to the nickel center. The carbon-halogen bond splitting by a transition metal complex and transfer of the aryl fragment to the ligand highlights the chemical non-innocence of phosphinine ligands in transition metal complexes. Investigations on the mechanism of the formation of [1]Br and **3** and further reactivity studies on **1** are currently underway in our laboratories.

6.4 Experimental Details

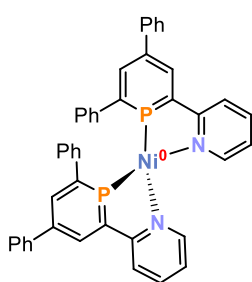
6.4.1 General Considerations

All experiments were performed under an atmosphere of dry argon using standard glovebox and Schlenk line techniques. Tetrahydrofuran (THF), toluene, diethyl ether and *n*-hexane were purified, dried, and degassed using an MBraun SPS800 solvent purification system. Benzene was distilled and degassed with Schlenk techniques. Deuterated tetrahydrofuran and benzene were purchased from Sigma Aldrich and used as received. Bromobenzene and iodobenzene were purchased from Sigma Aldrich and used as received. [(IPr)Ni(H₂C=CHSiMe₃)₂] **D** (IPr = 1,3-bis(2,6-diisopropylphenyl)imidazolin-2-ylidene)^[40], 2-(2'-pyridyl)-4,6-diphenylphosphinine **L**^[27], FcBF₄^[80], FcPF₆^[81] and FcBAR^{F₄}^[80] (Fc = ferrocenyl, BAR^{F₄} = [B{3,5-(CF₃)₂C₆H₃}₄]⁻) were synthesized according to literature procedures. NMR spectra were recorded on Bruker Avance 400 spectrometers at 300 K. ¹H and ¹³C{¹H} spectra were referenced internally to residual solvent resonances, while ³¹P{¹H} and ³¹P spectra were referenced externally to 85% H₃PO₄ (aq.). The assignment of ¹H and ¹³C NMR signals was confirmed by two-dimensional (COSY, HSQC, and HMBC) experiments. Magnetic susceptibilities in solution were determined by the Evans NMR method in THF-d₈ at room temperature. UV/vis spectra were recorded using a Varian Cary 50 spectrometer. Elemental analyses were determined by the analytical department of the University of Regensburg. Cyclic voltammograms were recorded with a CH Instruments Electrochemical Analyzer. Gas chromatography with FID (GC-FID): Shimadzu GC2010plus. Carrier gas: H₂. Column: Restek Rxi[®], (30 m x 0.25 mm x 0.25 μm) Carrier gas: H₂. Standard heating procedure: 50 °C (2 min), 25 °C/min → 280 °C (5 min). HP6890 GC-System with injector 7683B and Agilent 7820A System. Column: HP-5, 19091J-413 (30 m × 0.32 mm × 0.25 μm), carrier gas: N₂. Calibration of substrates and products with internal standard *n*-pentadecane and analytically pure samples. The experimental X-band EPR spectra were recorded on a Bruker EMX spectrometer (Bruker BioSpin Rheinstetten) equipped with a He temperature-control cryostat system (Oxford Instruments). The *g* values were calculated with the ORCA software package at the B3LYP/def2-TZVP level of theory. The spectrum was analysed and simulated using the W95EPR program of Prof. Frank Neese. Magnetic measurements on compound **3** were carried out using a SQUID MPMS-XL5 from Quantum Design with an applied field of 5000 G. Magnetic response was recorded in the temperature range 100 K < T < 400 K with scan rates of 2 K / min and 5 K / min; scan rate had no effect on the results. The sample was prepared in a sealed quartz tube held in a plastic straw. The raw data were corrected for the diamagnetic part of the sample holder and the diamagnetism of the organic ligand using tabulated Pascal's constants. Single-crystal X-ray diffraction data were recorded on an Agilent Technologies SuperNova diffractometer with Cu-K_α radiation (λ = 1.54184 Å). Either semi-empirical multi-scan absorption corrections^[82] or analytical ones^[83] were applied to the data. The structures were solved with SHELXT^[84] and least-square refinements on *F*² were carried out with SHELXL^[85]. The hydrogen atoms

were located in idealized positions and refined isotropically with a riding model. CCDC 2007973 (for **1**), CCDC 1988434 (for [1]BF₄), CCDC 1988435 (for [1(THF)]PF₆), CCDC 1988436 (for [1₂](BAr^F₄)₂), CCDC 1988437 (for **2**), CCDC 1988438 (for [1]Br) and CCDC 1988439 (for **3**) contain the supplementary crystallographic data for this paper. These data can be obtained free of charge from the Cambridge Crystallographic Data Centre. Comment for compound **1**: twin law was applied; two components rotated (UB1, UB2) = –179.9435° around –0.71 0.71 –0.00 (rec) –0.77 0.64 0.04 (dir). Comment for compound [1]Br: A solvent mask was calculated, and 40 electrons were found in a volume of 160 Å³ in 1 void per unit cell. This is consistent with the presence of 0.5[C₄H₈O] per asymmetric unit which account for 40 electrons per unit cell.

6.4.2 Synthesis of **1**

Compound 1 was prepared in an MBraun argon glove box. 1 is sensitive toward moisture and air. 1 is soluble and stable in benzene, tetrahydrofuran and toluene.

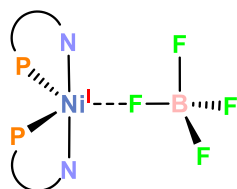


A solution of 2-(2'-pyridyl)-4,6-diphenylphosphinine **L** (2.5 equiv., 125 mg, 0.385 mmol) in benzene (2 mL) was added dropwise to a solution of [(IPr)Ni(H₂C=CHSiMe₃)₂] **D** (1 equiv., 100 mg, 0.154 mmol) in benzene at room temperature. An immediate color change from yellow to deep purple was observed. The reaction mixture was stirred for 16 hours at room temperature. Volatiles were completely removed, and the deep purple residue was washed with *n*-hexane (3 x 2 mL) in order to remove IPr. The remaining residue was extracted with benzene (4 x 2 mL) and layered with *n*-hexane (12 mL). **1** was isolated as deep purple crystals after decanting the mother liquor, washing with *n*-hexane (3 x 2 mL) and drying *in vacuo*. Crystals suitable for single-crystal XRD were grown from slow diffusion of *n*-hexane into a benzene solution of **1**. Yield: 40 mg, 37 %. Elemental analysis calcd. for C₄₄H₃₂N₂P₂Ni (M_w = 709.39 g·mol⁻¹) C 74.50, H 4.55, N 3.95; found C 74.98, H 4.70, N 3.77. UV-Vis: (THF, λ_{max} / nm, ε_{max} / L·mol⁻¹·cm⁻¹): 290 (98632), 520 (27940), 816 (20814). ¹H NMR (400.13 MHz, 300 K, [D₈]THF): δ = 7.05–7.11 (m, 6H, H of C^{2,4}-Ph), 7.18–7.21 (m, 2H, H of NC₅H₄), 7.33–7.37 (m, 2H, H of C^{2,4}-Ph), 7.41–7.45 (m, 4H, H of C^{2,4}-Ph), 7.79–7.81 (m, 4H, H of C^{2,4}-Ph), 7.85–7.86 (m, 2H, H of NC₅H₄), 7.90 (d, 4H, H of C^{2,4}-Ph, J_{HH} = 7 Hz), 8.30 (pt, 2H, H^{3,5} of PC₅H₂Ph₂Py, ⁴J_{HH} = 5 Hz), 8.43 (d, 2H, H of NC₅H₄, J_{HH} = 8 Hz), 8.55 (pt, 2H, H^{3,5} of PC₅H₂Ph₂Py, ⁴J_{HH} = 5 Hz), 8.86 (d, 2H, H of NC₅H₄, J_{HH} = 5 Hz). ¹³C{¹H} NMR (100.61 MHz, 300 K, [D₈]THF): δ = 119.3 (s, C of NC₅H₄), 122.5 (s, C of NC₅H₄), 126.7 (s, C of C^{2,4}-Ph), 126.8 (s, C of C^{2,4}-Ph), 127.0 (s, C of C^{2,4}-Ph), 127.4 (t, 7 Hz), 129.0 (s, C of C^{2,4}-Ph), 129.6 (s, C of C^{2,4}-Ph), 131.4 (s, C of C^{2,4}-Ph), 133.7 (m, C of NC₅H₄), 137.4 (t, C of C^{2,4}-Ph, J = 7 Hz), 143.2 (m, C of PC₅H₂Ph₂Py), 143.9 (m, C of PC₅H₂Ph₂Py), 145.1 (m, C of PC₅H₂Ph₂Py), 146.6 (m, C of

PC₅H₂Ph₂Py), 153.1 (m, C of NC₅H₄). ³¹P{¹H} NMR (161.98 MHz, 300 K, [D₈]THF): δ = 179.4. ³¹P NMR (161.98 MHz, 300 K, [D₈]THF): δ = 179.4.

6.4.3 Synthesis of [1]BF₄

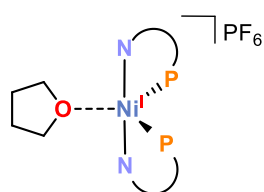
Compound [1]BF₄ was prepared in an MBraun argon glove box. [1]BF₄ is sensitive toward moisture and air. [1]BF₄ is soluble and stable in benzene, tetrahydrofuran and toluene.



1 (50 mg, 0.07 mmol) was dissolved in THF (1 mL) and FcBF₄ (12 mg, 0.07 mmol) was added at room temperature. An immediate color change from deep purple to brown was observed. The color changed further to green-brown upon stirring overnight. The solvent of the green reaction mixture was completely removed, and ferrocene was removed by sublimation under high vacuum (50 °C, ca. 10⁻⁵ mbar). The remaining brown residue was extracted with THF (2 mL) and layered with *n*-hexane (4 mL). After crystallization for two days at -35 °C, [1]BF₄ could be isolated as a brown powder. Crystals suitable for single-crystal XRD were grown from slow diffusion of *n*-hexane into a toluene solution of [1]BF₄. Yield: 43 mg, 77%. Elemental analysis calcd. for C₄₄H₃₂N₂P₂NiBF₄ (M_w = 796.20 g·mol⁻¹) C 66.38, H 4.05, N 3.52; found C 65.17, H 4.26, N 3.35. UV-Vis: (THF, λ_{max} / nm, ε_{max} / L·mol⁻¹·cm⁻¹): 284 (38665), 338 (sh, 15363), 466 (8545). μ_{eff} (THF-d₈): 2.0(1) μ_B.

6.4.4 Synthesis of [1(THF)]PF₆

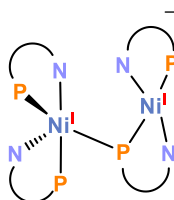
Compound [1(THF)]PF₆ was prepared in an MBraun argon glove box. [1(THF)]PF₆ is sensitive toward moisture and air. [1(THF)]PF₆ is soluble and stable in benzene, tetrahydrofuran and toluene.



1 (50 mg, 0.07 mmol) was dissolved in THF (1 mL) and FcPF₆ (23 mg, 0.07 mmol) was added at room temperature. A slow color change from deep purple to brown green was observed. The color changed further to deep brown upon stirring overnight. The solvent of the brown reaction mixture was completely removed, and ferrocene was removed by sublimation under high vacuum (50 °C, ca. 10⁻⁵ mbar). The remaining brown residue was extracted with THF (2 mL) and layered with *n*-hexane (6 mL). After crystallization for one day at -35 °C, [1(THF)]PF₆ could be isolated as a deep brown powder. Crystals suitable for single-crystal XRD were grown from slow diffusion of *n*-hexane into a tetrahydrofuran solution of [1(THF)]PF₆. Yield: 53 mg, 88%. Elemental analysis calcd. for C₄₄H₃₂N₂P₃NiF₆(C₄H₈O) (M_w = 926.47 g·mol⁻¹) C 62.23, H 4.35, N 3.02; found C 62.12, H 4.41, N 2.93. UV-Vis: (toluene, λ_{max} / nm, ε_{max} / L·mol⁻¹·cm⁻¹): 334 (sh, 6649), 450 (2617), 659 (1805). μ_{eff} (THF-d₈): 1.7(1) μ_B.

6.4.5 Synthesis of [1₂](BAR^F₄)₂

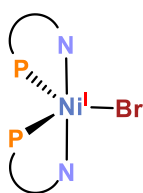
Compound [1₂](BAR^F₄)₂ was prepared in an MBraun argon glove box. [1₂](BAR^F₄)₂ is sensitive toward moisture and air. [1₂](BAR^F₄)₂ is soluble and stable in diethyl ether, benzene, tetrahydrofuran and toluene.



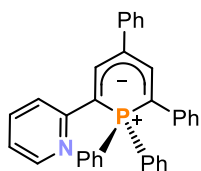
1 (50 mg, 0.07 mmol) and FcBAR^F₄ (74 mg, 0.07 mmol) were dissolved in THF (2 mL) at room temperature. An immediate color change from deep purple to brown was observed. After stirring overnight the solution turned green and the solvent of the reaction mixture was completely removed. Ferrocene was removed by washing with *n*-hexane (3 x 2 mL). The remaining oily green residue was extracted in diethyl ether (2 mL) and layered with *n*-hexane (6 mL). [1₂](BAR^F₄)₂ was isolated as a dark brown powder after crystallization at –35 °C for two days. Crystals suitable for X-ray crystallography were obtained by slow diffusion of *n*-hexane into a diethyl ether solution of [1₂](BAR^F₄)₂. Ether solutions of [1₂](BAR^F₄)₂ show a green color while ether-free [1₂](BAR^F₄)₂ appears brown. Crystals suitable for single-crystal XRD were grown from slow diffusion of *n*-hexane into a diethyl ether solution of [1₂](BAR^F₄)₂. Yield: 86 mg, 78%. Elemental analysis calcd. for C₁₅₁H₈₈B₂F₄₈N₄Ni₂P₄ (Mw = 3130.41 g·mol⁻¹) C 57.88, H 2.83, N 1.79; found C 58.48, H 3.21, N 1.58. UV-Vis: (diethyl ether, λ_{max} / nm, ε_{max} / L·mol⁻¹·cm⁻¹): 279 (55432), 330 (sh, 22957), 454 (8288), 635 (4397). UV-Vis: (toluene, λ_{max} / nm, ε_{max} / L·mol⁻¹·cm⁻¹): 330 (sh, 19450), 416 (6438), 505 (5831). μ_{eff} (THF-d₈): 1.7(1) μ_B.

6.4.6 Synthesis of **2** and [1]Br

Compounds **2** and [1]Br were prepared in an MBraun argon glove box. [1]Br is sensitive toward moisture and air. [1]Br is soluble and stable in benzene, tetrahydrofuran and toluene. **2** is soluble and stable in *n*-hexane.



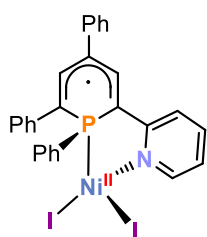
Bromobenzene (7.5 μL, 0.07 mmol) was added to a solution of **1** (50 mg, 0.07 mmol) in benzene (1 mL) and this reaction mixture was heated to 60 °C overnight. The deep purple solution turned deep red upon heating. The mixture was cooled down to room temperature and layered with *n*-hexane (5 mL). After crystallizing at room temperature over 2 days, a deep red solid was isolated by decanting the fluorescent pink solution. After washing with *n*-hexane (2 x 2 mL) and drying under vacuum, [1]Br was isolated as a deep red powder. Crystals suitable for single-crystal XRD were grown from slow diffusion of *n*-hexane into a tetrahydrofuran solution of [1]Br. Yield: 25 mg, 45%. Elemental analysis calcd. for C₄₄H₃₂BrN₂P₂Ni (Mw = 789.30 g·mol⁻¹) C 66.96, H 4.09, N 3.55; found C 64.83, H 4.27, N 3.33. UV-Vis: (THF, λ_{max} / nm, ε_{max} / L·mol⁻¹·cm⁻¹): 280 (35690), 480 (6780). μ_{eff} (THF-d₈): 2.1(1) μ_B.



The decanted fluorescent pink solution was evaporated to dryness, and the remaining pink residue was extracted with *n*-hexane (3 x 2 mL). Slow evaporation at room temperature gave pure **2** as a pink powder. Crystals suitable for single-crystal XRD were grown from slow evaporation of a *n*-hexane solution of **2**. Yield: 5 mg, 15%. Elemental analysis calcd. for C₃₄H₂₆NP (Mw = 479.56 g·mol⁻¹) C 85.16, H 5.46, N 2.92; found C 84.34, H 5.37, N 2.70. UV-Vis: (*n*-hexane, λ_{max} / nm, ε_{max} / L·mol⁻¹·cm⁻¹): 265 (6456), 300 (8900), 333 (8933), 516 (8023). ¹H NMR (400.13 MHz, 300 K, C₆D₆): δ = 6.21–6.25 (m, 1H, H of C^{3,5} of PC₅H₂Ph₂Py), 6.86–7.00 (m, 10H, H_{aromatic}), 7.08–7.12 (m, 2H, H_{aromatic}), 7.21–7.23 (m, 1H, H_{aromatic}), 7.32–7.36 (m, 2H, H_{aromatic}), 7.81–7.82 (m, 1H, H of C^{3,5} of PC₅H₂Ph₂Py), 7.91–7.97 (m, 4H, H_{aromatic}), 8.11–8.20 (m, 1H, H_{aromatic}), 8.11–8.20 (dd, 1H, H of pyridyl group, J_{HH} = 32 Hz, J_{PH} = 2 Hz). ¹³C{¹H} NMR (100.61 MHz, 300 K, C₆D₆): δ = 80.1 (s), 81.1 (s), 94.7 (s), 95.6 (s), 112.8 (s), 112.9 (s), 115.9 (d, J = 9 Hz), 116.3 (s), 123.9 (s), 124.7 (s), 125.7 (s), 128.3 (s), 128.6 (s), 129.2 (s), 129.5 (d, J = 5 Hz), 130.1 (s), 130.2 (d, J = 3 Hz), 132.6 (s), 132.7 (s), 133.4 (d, J = 10 Hz), 135.3 (s), 141.4 (s), 141.47 (s), 141.52 (s), 143.7 (s), 146.6 (s), 158.6 (s). ³¹P{¹H} NMR (161.98 MHz, 300 K, C₆D₆): δ = 4.7 (s). ³¹P NMR (161.98 MHz, 300 K, C₆D₆): δ = 4.7 (m). Reaction with two equivalents of bromobenzene (0.14 mmol, 15 μL) with one equivalent of **1** (50 mg, 0.07 mmol) afforded [**1**]Br (42 mg, 75%) and **2** (10 mg, 30%) in higher yields.

6.4.7 Synthesis of **2** and **3**

Compounds **2** and **3** were prepared in an MBraun argon glove box. **3** is sensitive toward moisture and air. **3** is soluble and stable in benzene, tetrahydrofuran and toluene. **2** is soluble and stable in *n*-hexane.



Iodobenzene (8 μL, 0.07 mmol) was added to a solution of **1** (50 mg, 0.07 mmol) in toluene (1 mL) and this reaction mixture was heated to 60 °C overnight. The deep purple solution turned deep red upon heating. The mixture was cooled down to room temperature and layered with *n*-hexane (8 mL). After crystallizing at room temperature overnight, a deep green solid was isolated by decanting the fluorescent pink solution. After washing with *n*-hexane (2 x 2 mL) and drying under vacuum, **3** was isolated as a deep green powder. Crystals suitable for single-crystal XRD were grown from slow diffusion of *n*-hexane into a toluene solution of **3**. Yield: 38 mg (64%). Elemental analysis calcd. for C₂₈H₂₁I₂NPNi·(C₇H₈)_{1.4} (Mw = 843.96 g·mol⁻¹) C 53.80, H 3.85, N 1.66; found C 53.99, H 3.58, N 1.98. UV-Vis: (THF, λ_{max} / nm, ε_{max} / L·mol⁻¹·cm⁻¹): 285 (24370), 450 (4788), 614 (2600). μ_{eff} (THF-d₈): 3,2(1) μ_B.

The decanted fluorescent pink solution was evaporated to dryness, and the remaining pink residue was extracted with *n*-hexane (3 x 2 mL). Slow evaporation at room temperature gave pure **2** as a pink powder. Yield: 10 mg, 30%.

6.5 References

- [1] S. Z. Tasker, E. A. Standley, T. F. Jamison, *Nature* **2014**, *509*, 299–309.
- [2] P. A. Wender, T. E. Smith, G. Zuo, H. A. Duong, J. Louie, *Encyclopedia of Reagents for Organic Synthesis*, American Cancer Society, **2006**.
- [3] P. Binger, J. McMeeking, *Angew. Chem. Int. Ed.* **1974**, *13*, 466–467.
- [4] P. Binger, A. Brinkmann, *Chemische Berichte* **1978**, *111*, 2689–2695.
- [5] P. Heimbach, K.-J. Ploner, F. Thömel, *Angew. Chem. Int. Ed.* **1971**, *10*, 276–277.
- [6] P. Binger, G. Schroth, J. McMeeking, *Angew. Chem. Int. Ed.* **1974**, *13*, 465–466.
- [7] D. R. Fahey, *J. Org. Chem.* **1972**, *37*, 4471–4473.
- [8] K. Tamao, Y. Kiso, K. Sumitani, M. Kumada, *J. Am. Chem. Soc.* **1972**, *94*, 9268–9269.
- [9] Yu. G. Budnikova, Yu. M. Kargin, V. V. Yanilkin, *Russ. Chem. Bull.* **1992**, *41*, 1299–1300.
- [10] Yu. G. Budnikova, Yu. M. Kargin, *Russ. J. Gen. Chem.* **2001**, *71*, 128–131.
- [11] Y. Rollin, M. Troupel, D. G. Tuck, J. Perichon, *J. Organomet. Chem.* **1986**, *303*, 131–137.
- [12] D. G. Yakhvarov, E. Hey-Hawkins, R. M. Kagirov, Yu. H. Budnikova, Yu. S. Ganushevich, O. G. Sinyashin, *Russ. Chem. Bull.* **2007**, *56*, 935–942.
- [13] D. Gelman, S. Dechert, H. Schumann, J. Blum, *Inorg. Chim. Acta* **2002**, *334*, 149–158.
- [14] P. Le Floch, D. Carmichael, L. Ricard, F. Mathey, *J. Am. Chem. Soc.* **1991**, *113*, 667–669.
- [15] P. Le Floch, D. Carmichael, L. Ricard, F. Mathey, A. Jutand, C. Amatore, *Organometallics* **1992**, *11*, 2475–2479.
- [16] P. Rosa, L. Ricard, F. Mathey, P. Le Floch, *Organometallics* **1999**, *18*, 3348–3352.
- [17] N. Mézailles, P. Rosa, L. Ricard, F. Mathey, P. Le Floch, *Organometallics* **2000**, *19*, 2941–2943.
- [18] S. Choua, H. Sidorenkova, T. Berclaz, M. Geoffroy, P. Rosa, N. Mézailles, L. Ricard, F. Mathey, P. Le Floch, *J. Am. Chem. Soc.* **2000**, *122*, 12227–12234.
- [19] C. Elschenbroich, M. Nowotny, A. Behrendt, W. Massa, S. Wocadlo, *Angew. Chem. Int. Ed.* **1992**, *31*, 1343–1345.
- [20] H. Lehmkuhl, R. Paul, R. Mynott, *Liebigs Ann.* **1981**, *1981*, 1139–1146.
- [21] N. Mézailles, P. Le Floch, K. Waschbüsch, L. Ricard, F. Mathey, C. P. Kubiak, *J. Organomet. Chem.* **1997**, *541*, 277–283.
- [22] D. G. Holah, A. N. Hughes, K. L. Knudsen, R. Perrier, *J. Heterocyc. Chem.* **1988**, *25*, 155–160.
- [23] H. Lehmkuhl, R. Paul, C. Krüger, Y.-H. Tsay, R. Benn, R. Mynott, *Liebigs Ann.* **1981**, *1981*, 1147–1161.
- [24] H. Lehmkuhl, J. Elsässer, R. Benn, B. Gabor, A. Ruffńska, R. Goddard, C. Krüger, *Z. Naturforsch. B* **1985**, *40*, 171–181.
- [25] J.-M. Alcaraz, Anne Breque, F. Mathey, *Tetrahedron Lett.* **1982**, *23*, 1565–1568.
- [26] P. LeFloch, L. Ricard, F. Mathey, A. Jutand, C. Amatore, *Inorg. Chem.* **1995**, *34*, 11–12.
- [27] C. Müller, D. Wasserberg, J. J. M. Weemers, E. A. Pidko, S. Hoffmann, M. Lutz, A. L. Spek, S. C. J. Meskers, R. A. J. Janssen, R. A. van Santen, et al., *Chem. Eur. J.* **2007**, *13*, 4548–4559.
- [28] C. Müller, D. Vogt, *C. R. Chim.* **2010**, *13*, 1127–1143.
- [29] C. Müller, J. A. W. Sklorz, I. de Krom, A. Loibl, M. Habicht, M. Bruce, G. Pfeifer, J. Wiecko, *Chem. Lett.* **2014**, *43*, 1390–1404.

- [30] A. C. Carrasco, E. A. Pidko, A. M. Masdeu-Bultó, M. Lutz, A. L. Spek, D. Vogt, C. Müller, *New J. Chem.* **2010**, *34*, 1547–1550.
- [31] A. Campos-Carrasco, L. E. E. Broeckx, J. J. M. Weemers, E. A. Pidko, M. Lutz, A. M. Masdeu-Bultó, D. Vogt, C. Müller, *Chem. Eur. J.* **2011**, *17*, 2510–2517.
- [32] I. de Krom, E. A. Pidko, M. Lutz, C. Müller, *Chem. Eur. J.* **2013**, *19*, 7523–7531.
- [33] G. Pfeifer, P. Ribagnac, X.-F. Le Goff, J. Wiecko, N. Mézailles, C. Müller, *Eur. J. Inorg. Chem.* **2015**, *2015*, 240–249.
- [34] A. Loibl, M. Weber, M. Lutz, C. Müller, *Eur. J. Inorg.* **2019**, 1575–1585.
- [35] I. de Krom, L. E. E. Broeckx, M. Lutz, C. Müller, *Chem. Eur. J.* **2013**, *19*, 3676–3684.
- [36] A. Loibl, I. de Krom, E. A. Pidko, M. Weber, J. Wiecko, C. Müller, *Chem. Commun.* **2014**, *50*, 8842–8844.
- [37] A. Loibl, W. Oschmann, M. Vogler, E. A. Pidko, M. Weber, J. Wiecko, C. Müller, *Dalton Trans.* **2018**, *47*, 9355–9366.
- [38] I. de Krom, M. Lutz, C. Müller, *Dalton Trans.* **2015**, *44*, 10304–10314.
- [39] J. Leitl, M. Marquardt, P. Coburger, D. J. Scott, V. Streitferdt, R. M. Gschwind, C. Müller, R. Wolf, *Angew. Chem. Int. Ed.* **2019**, *58*, 15407–15411.
- [40] M. R. Elsbey, S. A. Johnson, *J. Am. Chem. Soc.* **2017**, *139*, 9401–9407.
- [41] D. Carmichael, P. Le Floch, L. Ricard, F. Mathey, *Inorganica Chimica Acta* **1992**, *198–200*, 437–441.
- [42] A. Breque, C. C. Santini, F. Mathey, J. Fischer, A. Mitschler, *Inorg. Chem.* **1984**, *23*, 3463–3467.
- [43] P. Le Floch, S. Mansuy, L. Ricard, F. Mathey, A. Jutand, C. Amatore, *Organometallics* **1996**, *15*, 3267–3274.
- [44] C. Kaes, A. Katz, M. W. Hosseini, *Chem. Rev.* **2000**, *100*, 3553–3590.
- [45] D. M., D. M., P. J., *New J. Chem.* **1996**, *20*, 659–667.
- [46] A. Okuniewski, D. Rosiak, J. Chojnacki, B. Becker, *Polyhedron* **2015**, *90*, 47–57.
- [47] A. W. Addison, T. N. Rao, J. Reedijk, J. van Rijn, G. C. Verschoor, *J. Chem. Soc., Dalton Trans.* **1984**, 1349–1356.
- [48] N. Mézailles, P. Rosa, L. Ricard, F. Mathey, P. Le Floch, *Organometallics* **2000**, *19*, 2941–2943.
- [49] B. Schmid, L. M. Venanzi, T. Gerfin, V. Gramlich, F. Mathey, *Inorg. Chem.* **1992**, *31*, 5117–5122.
- [50] M. T. Reetz, E. Bohres, R. Goddard, M. C. Holthausen, W. Thiel, *Chem. Eur. J.* **1999**, *5*, 2101–2108.
- [51] M. J. Bakker, F. W. Vergeer, F. Hartl, P. Rosa, L. Ricard, P. L. Floch, M. J. Calhorda, *Chem. Eur. J.* **2002**, *8*, 1741–1752.
- [52] C. Elschenbroich, J. Six, K. Harms, *Chem. Commun.* **2006**, 3429–3431.
- [53] X. Chen, Z. Li, F. Yanan, H. Grützmacher, *Eur. J. Inorg.* **2016**, *2016*, 633–638.
- [54] P. Rosa, L. Ricard, F. Mathey, P. Le Floch, *Organometallics* **2000**, *19*, 5247–5250.
- [55] M. H. Habicht, F. Wossidlo, T. Bens, E. A. Pidko, C. Müller, *Chem. Eur. J.* **2018**, *24*, 944–952.
- [56] Y. Hou, Z. Li, Y. Li, P. Liu, C.-Y. Su, F. Puschmann, H. Grützmacher, *Chem. Sci.* **2019**, *10*, 3168–3180.
- [57] Y. Mao, K. M. H. Lim, Y. Li, R. Ganguly, F. Mathey, *Organometallics* **2013**, *32*, 3562–3565.
- [58] X. Zhao, X. Sun, Z. Han, C. Zhao, H. Yu, X. Zhai, *J. Solid State Chem.* **2013**, *207*, 178–183.
- [59] I. L. Fedushkin, T. V. Petrovskaya, F. Girgsdies, R. D. Köhn, M. N. Bochkarev, H. Schumann, *Angew. Chem. Int. Ed.* **1999**, *38*, 2262–2264.

- [60] E. Gore-Randall, M. Irwin, M. S. Denning, J. M. Goicoechea, *Inorg. Chem.* **2009**, *48*, 8304–8316.
- [61] S. Z. Tasker, E. A. Standley, T. F. Jamison, *Nature* **2014**, *509*, 299–309.
- [62] V. P. Ananikov, *ACS Catal.* **2015**, *5*, 1964–1971.
- [63] K. Tamao, K. Sumitani, M. Kumada, *J. Am. Chem. Soc.* **1972**, *94*, 4374–4376.
- [64] L. Guo, W. Srimontree, C. Zhu, B. Maity, X. Liu, L. Cavallo, M. Rueping, *Nat. Commun.* **2019**, *10*, 1–6.
- [65] N. Hashimoto, R. Umano, Y. Ochi, K. Shimahara, J. Nakamura, S. Mori, H. Ohta, Y. Watanabe, M. Hayashi, *J. Am. Chem. Soc.* **2018**, *140*, 2046–2049.
- [66] J. Huang, J. Tarábek, R. Kulkarni, C. Wang, M. Dračinský, G. J. Smales, Y. Tian, S. Ren, B. R. Pauw, U. Resch-Genger, et al., *Chem. Eur. J.* **2019**, *25*, 12342–12348.
- [67] A. Yoshimura, H. Kimura, A. Handa, N. Hashimoto, M. Yano, S. Mori, T. Shirahata, M. Hayashi, Y. Misaki, *Tetrahedron Lett.* **2020**, 151724.
- [68] G. Pfeifer, F. Chahdoura, M. Papke, M. Weber, R. Szücs, B. Geffroy, D. Tondelier, L. Nyulászi, M. Hissler, C. Müller, *Chem. A Eur. J.* **2020**, 10.1002/chem.202000932.
- [69] P. Pyykkö, M. Atsumi, *Chem. Eur. J.* **2009**, *15*, 12770–12779.
- [70] J. A. W. Sklorz, S. Hoof, N. Rades, N. De Rycke, L. Könczöl, D. Szieberth, M. Weber, J. Wiecko, L. Nyulászi, M. Hissler, et al., *Chem. Eur. J.* **2015**, *21*, 11096–11109.
- [71] M. Foà, L. Cassar, *J. Chem. Soc., Dalton Trans.* **1975**, 2572–2576.
- [72] N. D. Schley, G. C. Fu, *J. Am. Chem. Soc.* **2014**, *136*, 16588–16593.
- [73] J. Cornella, E. Gómez-Bengoa, R. Martin, *J. Am. Chem. Soc.* **2013**, *135*, 1997–2009.
- [74] L. M. Guard, M. Mohadjer Beromi, G. W. Brudvig, N. Hazari, D. J. Vinyard, *Angew. Chem. Int. Ed.* **2015**, *54*, 13352–13356.
- [75] M. Mohadjer Beromi, A. Nova, D. Balcells, A. M. Brasacchio, G. W. Brudvig, L. M. Guard, N. Hazari, D. J. Vinyard, *J. Am. Chem. Soc.* **2017**, *139*, 922–936.
- [76] I. Kalvet, Q. Guo, G. J. Tizzard, F. Schoenebeck, *ACS Catal.* **2017**, *7*, 2126–2132.
- [77] I. Funes-Ardoiz, D. J. Nelson, F. Maseras, *Chemistry* **2017**, *23*, 16728–16733.
- [78] D. J. Nelson, F. Maseras, *Chem. Commun.* **2018**, *54*, 10646–10649.
- [79] S. Bajo, G. Laidlaw, A. R. Kennedy, S. Sproules, D. J. Nelson, *Organometallics* **2017**, *36*, 1662–1672.
- [80] C. Hua, J. A. DeGayner, T. D. Harris, *Inorg. Chem.* **2019**, *58*, 7044–7053.
- [81] M. Deb, S. Hazra, P. Dolui, A. J. Elias, *ACS Sustainable Chem. Eng.* **2019**, *7*, 479–486.
- [82] a) SCALE3ABS, CrysAlisPro, Aglient Technologies Inc., Oxford, GB, **2012**; b) G. M. Sheldrick, SADABS, Bruker AXS, Madison, USA, **2007**.
- [83] R. C. Clark, J. S. Reid, *Acta Cryst. A* **1995**, *51*, 887–897.
- [84] G. M. Sheldrick, *Acta Cryst. A* **2008**, *64*, 112–122.
- [85] G. M. Sheldrick, *Acta Cryst. C* **2015**, *71*, 3–8.

6.6 Supporting Informartion

The supporting information of **Chapter 6** can be found on the supplied CD-ROM and on <https://pubs.acs.org/doi/10.1021/acs.inorgchem.0c01115>. The supporting information contains: Experimental details, NMR, UV-vis and EPR spectra, X-ray crystallography details, cyclic voltammograms and results of quantum chemical calculations including Cartesian coordinates of all optimized structures.

Chapter 7

Summary and Conclusion

Chapter 1: Phosphinines – Versatile Ligands in Coordination Chemistry and Catalysis

Chapter 1 reviews the chemistry of phosphinines, their properties and utilization in coordination chemistry and catalysis. The pioneering work of Gottfried Märkl introduced a novel ligand class in organometallic chemistry with 2,4,6-triphenylphosphinine. A range of different synthetic routes to substituted phosphinine ligands have been developed. Among these, the pyrylium salt route is the most popular one. Phosphinines have been utilized as ligands for transition metal complexes due to their special electronic properties. Phosphinine complexes can possess variable coordination modes. The most common mode is the σ -coordination to the metal center *via* the phosphorus lone pair electrons. π -Coordination occurs mostly through η^6 -mode, but also η^4 - and η^5 -phosphinine coordination compounds are accessible. The introduction of a donor-substituent leads to chelating phosphinines. Biphosphinines and pyridyl-phosphinines proved as effective chelating ligands for transition metals. Finally, phosphinine complexes were successfully utilized as potent catalysts in a range of reactions, including hydroformylation, hydroboration and transfer hydrogenation.

Chapter 2: Halide-Substituted Phosphacyclohexadienyl Iron Complexes:

Covalent Structures vs. Ion Pairs

The aim of *Chapter 2* was the synthesis of rare examples of halide-substituted phosphacyclohexadienyl complexes **2-2-X** (X = F, Cl, Br, and I). **2-2-X** can be synthesized by reacting the anionic iron phosphinine complex $[\text{K}([\text{18}]\text{crown-6})(\text{thf})_2][\text{Cp}^*\text{FeTPP}]$ (**2-1**) with different electrophilic halogenating agents ($[\text{1-F-NC}_5\text{H}_5]\text{BF}_4$, $\text{C}_6\text{H}_4\text{Cl}_6$, Br_2 , I_2). The related complex $[\text{Cp}^*\text{Fe}(\text{PC}_5\text{Ph}_3\text{H}_2)][\text{BAr}^{\text{F}}_4]$ (**2-2-[BAr^F]₄**, $\text{Ar}^{\text{F}} = 3,5\text{-(CF}_3)_2\text{C}_6\text{H}_3$), which contains a more weakly coordinating anion, is likewise accessible in high yield by salt metathesis from **2-2-I**. The properties of **2-2-X** were extensively studied by means of single-crystal X-ray diffraction, NMR and UV-vis spectroscopy, cyclic voltammetry, mass spectrometry, conductivity measurements and DFT calculations. Single crystal X-ray analysis revealed that the solid-state molecular structures of **2-2-F** and **2-2-Cl** show covalent P–X bonds. To the best of our knowledge, these compounds represent the first structurally authenticated transition metal complexes with π -coordinated λ^3 -halophosphacyclohexadienyl ligands. On the contrary, ionic structures with dissociated halide anions were observed for **2-2-Br**, **2-2-I** and **2-2-[BAr^F]₄**.

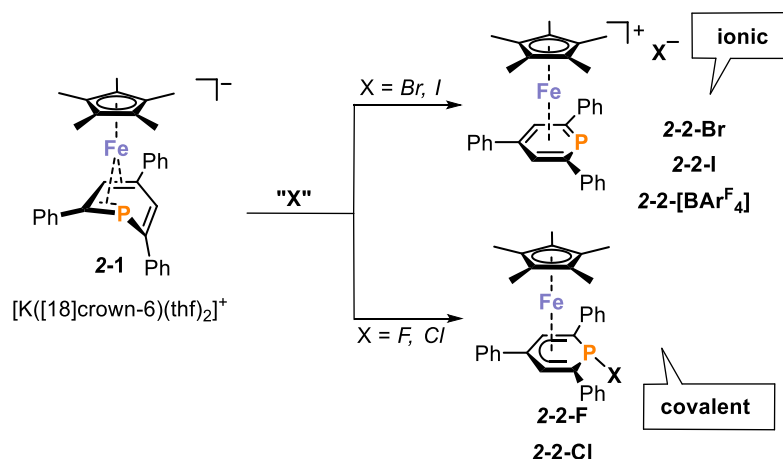


Figure 1. Synthesis of ionic and covalent phosphacyclohexadienyl iron complexes; “X” = [1-F-NC₅H₅]⁺BF₄⁻, C₆H₄Cl₆, Br₂, I₂.

DFT calculations at the OPBE/TZ2P level of theory indicate that the covalent isomers are favoured in the gas phase independent of the halogen substituent. The P–X bonds are cleaved for X = Br and I probably due to the weaker P–X bonds and packing effects in the solid-state. **2-2-Cl**, **2-2-Br**, and **2-2-I** possess ionic structures in solution according to ³¹P NMR, UV-vis, CV and computational data. ³¹P NMR studies in the solid state and in solution show very similar shifts for **2-2-Cl**, **2-2-Br**, **2-2-I** and **2-2-[BAr^F₄]**, especially in deuterated acetonitrile. Calculated NMR shieldings for covalent and ionic isomers at the ZORA-OPBE/def2-TZVP level are in agreement with the observed ³¹P NMR data. Molar conductivity measurements additionally confirm the high ionic character for **2-2-Cl**, **2-2-Br**, **2-2-I** and **2-2-[BAr^F₄]** in solution. By contrast, all analytical data for **2-2-F** differ significantly from **2-2-Cl**, **2-2-Br** and **2-2-I** indicating that the covalent P–F bond is retained in solution.

Chapter 3: A Phosphinine-Derived 1-Phospha-7-Bora-Norbornadiene: Frustrated Lewis Pair Type Activation of Triple Bonds

The goal of *Chapter 3* was the synthesis of an unusual phosphinine-based frustrated Lewis pair (FLP). This was achieved by reacting the λ⁴-phosphinine anion Li[1-Me-PC₅H₂Ph₃] (**3-1**) with Lewis acidic chloroborane (C₆F₅)₂BCl which results in the formation of 1-phospha-7-bora-norbornadiene derivative **3-2**. Compound **3-2** is the first bicyclic system of phosphorus and boron which possesses a direct, polar and strained P–B bond. Compound **3-2** was thoroughly characterized by means of single crystal X-ray diffraction, NMR and UV-Vis spectroscopy as well as elemental analysis, all of which provided data that are consistent with the molecular structure depicted in Figure 2. ³¹P{¹H} NMR monitoring as well as DFT calculations of the reaction of **3-1** with (C₆F₅)₂BCl confirmed the presence of the intermediate **3-Iso-2a**. Additionally, characterization of **3-2** and its isomer **3-Iso-2a** via variable temperature NMR studies were conducted. Although **3-2** represents a classical

Lewis acid-base adduct, its reactivity is reminiscent of FLPs. Reaction of **3-2** with nitriles affords insertion products **3-3a–3-3e**, where the nitrile fragment is bound to the Lewis base P and Lewis acid B. The insertion is accompanied with B–C bond splitting. DFT calculations at the ω B97X-D/6-311+G** level of theory revealed that the activation of nitriles involves splitting of the polar P–B bond, addition of the nitrile, cyclization and degradation to **3-3a–3-3e**. Encouraged by the high reactivity of **3-2** toward the strong, polar triple bond of nitriles, the reactivity of **3-2** was tested toward similarly strong, but apolar triple bonds of phenylacetylenes. In contrast to the reaction with nitriles, treatment of **3-2** with phenylacetylene derivatives affords phosphabarrelenes **3-5a–3-5c**. DFT calculations were used to elucidate the mechanism of formation, which involves migration of “(C₆F₅)₂B”, through formal insertion into a C–C bond. This work highlights the ability of seemingly classical Lewis pairs to form reactive intermediates by reversible heterolytic element-element bond dissociation, while also illustrating the ability of phosphinine-derived Lewis bases to engage in interesting FLP reactivity that is not easily accessible using more conventional λ^3, σ^3 -phosphines.

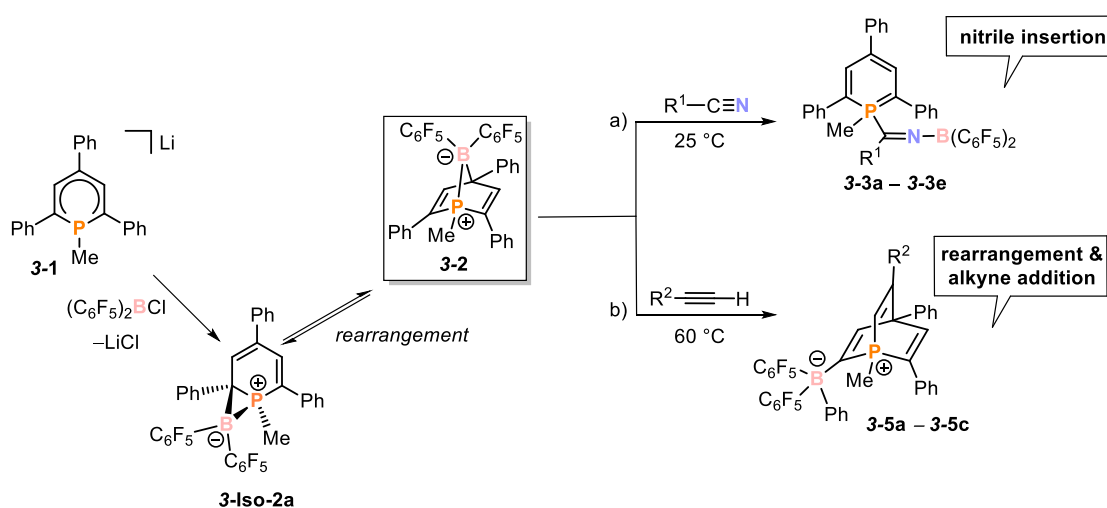


Figure 2. Synthesis of 1-phospha-7-bora-norbornadiene **3-2** and its reactivity toward a) nitriles (**3-3a–3-3e**) and b) phenylacetylenes (**3-5a–3-5c**); R¹ = Me, Ph, 3,5-Br₂-C₆H₃, CH₂Cl, Et; R² = Ph, 4-CF₃-C₆H₄, 4-Br-C₆H₄.

Chapter 4: 2-(2'-Pyridyl)-4,6-diphenylphosphinine as platform for the synthesis of phosphorus/boron-based Lewis pairs

Chapter 4 reports on the synthesis of a range of pyridyl-phosphinine-based P-B Lewis pairs obtained from salt elimination reactions. The reaction of λ^4 -phosphacyclohexadienyl anion **4-1-Me** with different chloroboranes [(C₆F₅)₂BCl, {C₆H₃(CF₃)₂}₂BCl, (catechol)BCl and Ph₂BCl] affords zwitterionic phosphinineborates **4-2-BCF₅**, **4-2-BCF₃**, **4-2-Bcat** and **4-2-BPh** in moderate to good yields. All of these compounds display the same Lewis pair structure motif in the solid state. The pyridyl-phosphinine anion **4-1-Me** chelates *via* the lone pair electrons of the P and N atom to the boron moiety resulting in a five-membered heterocycle. By contrast, the combination of 2,4,6-triphenylphosphinine and chloroborane

affords a phospho-bora-norbornadiene derivative as shown in *Chapter 3*. The flanking pyridyl group in 2-(2'-pyridyl)-4,6-diphenyl-phosphinine [**P,N**] provides bidentate chelating abilities, which inhibits the norbornadiene formation. Altering the substituents on the borane has little effect on the reaction outcome. However, changing the steric bulk on the P atom, has a more dramatic effect on the reactivity. The reaction of *tert*-butyl-substituted **4-1-*t*Bu** with (C₆F₅)₂BCl results in a mixture of products in a 1:2 ratio. Again, P/B/N-heterocycle **4-3-BC₆F₅** is formed, but the major species in this reaction is the unprecedented phosphirane **4-4**. The latter compound presumably is the kinetic product, because DFT calculations show that **4-4** is +20.2 kcal·mol⁻¹ higher in energy than **4-3-BC₆F₅**. Although **4-1-*t*Bu** forms a phosphirane when treated with (C₆F₅)₂BCl, the reaction of **4-1-*t*Bu** with other chloroboranes possessing electron-withdrawing or electron-pushing substituents mainly affords P/B/N-heterocycles **4-3-BCF₃**, **4-3-Bcat** and **4-3-BPh**. This work reveals the decisive impact of an auxiliary donor on the reactivity of phosphacyclohexadienyl anions.

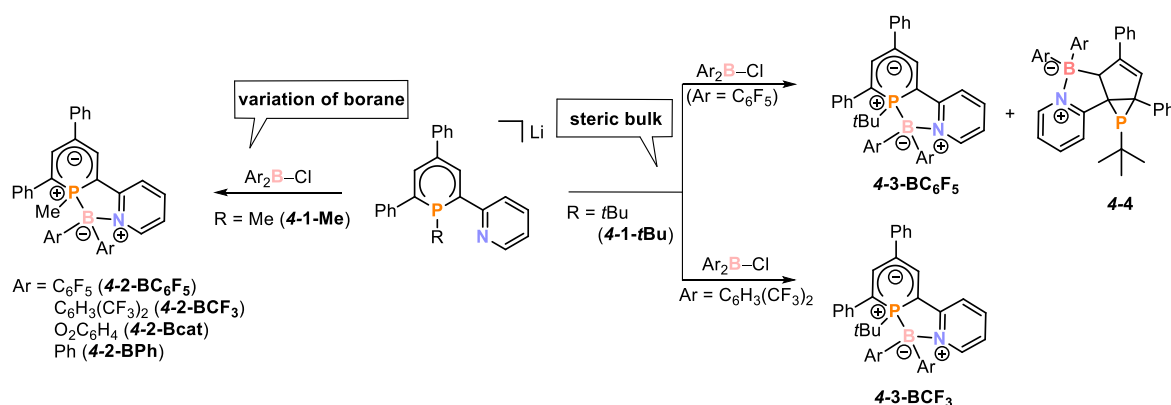


Figure 3. Synthesis of phosphinoborates **4-2-BC₆F₅**, **4-2-BCF₃**, **4-2-Bcat**, **4-2-BPh**, **4-3-BC₆F₅** and **4-3-BCF₃** via alkyated pyridyl-phosphinine lithium salt; synthesis of phosphirane **4-4** from reaction of **4-1-*t*Bu** with (C₆F₅)₂BCl.

Chapter 5: Facile C=O Bond Splitting of Carbon Dioxide Induced by Metal-Ligand Cooperativity in a Phosphinine Iron(0) Complex

Chapter 5 presents the synthesis of the first anionic Fe complexes **5-1** incorporating a chelating 2-(2'-pyridyl)-4,6-diphenyl-phosphinine ligand [**P,N**]. **5-1** exists in solution as a pair of isomers in which the phosphinine adopts σ - and π -coordination modes. The isomer **5-1- σ** shows chelating σ -donation of the pyridyl-phosphinine ligand to the metal center, while isomer **5-1- π** possesses ligand [**P,N**] in η^4 -coordination mode. **5-1- σ** is observed in the solid state, while **5-1- σ** and **5-1- π** are in equilibrium in solution which is supported by DFT calculations. ³¹P{¹H} NMR monitoring of the formation of **5-1- σ** and **5-1- π** reveals the presence of an anionic asymmetric phosphinine-dimer Fe(II) complex **5-2** as an intermediate. Complex **5-2** is readily accessible via reaction of anionic “Cp*Fe(0)” precursor with two equivalents of [**P,N**]. Its molecular structure shows a dimeric phosphinine ligand.

Both isomers **5-1- σ** and **5-1- π** react with CO₂. For the isomer **5-1- π** containing the π -coordinated phosphinine ligand, addition of CO₂ to a carbon atom of the phosphinine moiety is observed. By contrast, cleavage of one C=O bond occurs in **5-1- σ** containing a σ -coordinated phosphinine ligand to give an Fe-coordinated CO moiety and P-bound O atom. This is the first reported example of C=O cleavage of a CO₂ molecule mediated by a single Fe centre, and clearly demonstrates the potential of coordinatively- and electronically-flexible phosphinine ligands to help mediate challenging bond activation reactions.

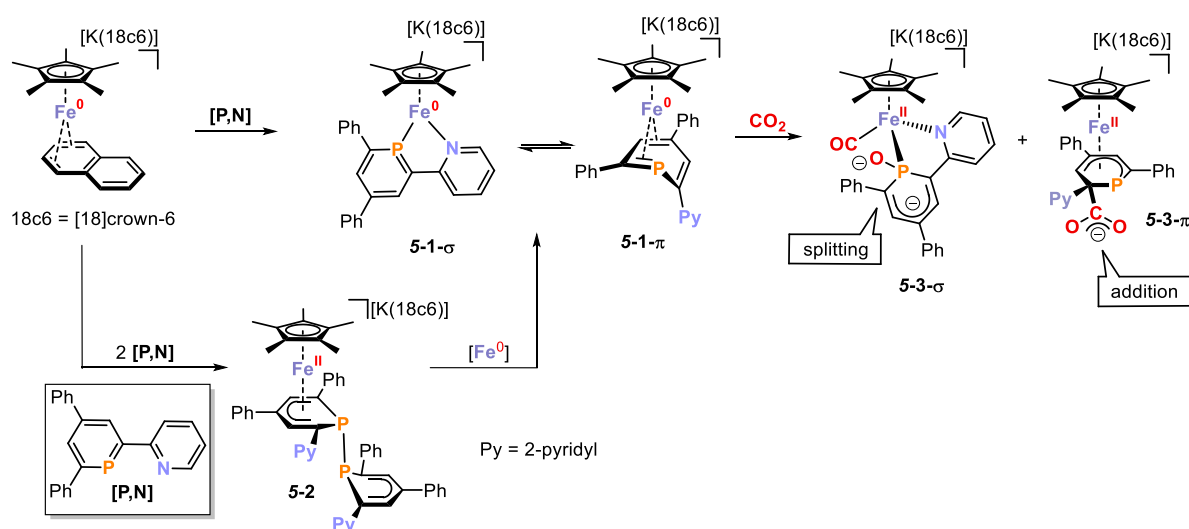


Figure 4. Synthesis of anionic pyridyl-phosphinine iron(0) complexes **5-1- σ** and **5-1- π** via anionic phosphinine dimer **5-2** and their reaction with CO₂ affording **5-3- σ** and **5-3- π** .

Chapter 6: Phosphorus-Analogues of [Ni(bpy)₂]: Synthesis and Application in Carbon-Halogen Bond Activation

Chapter 6 presents the synthesis and characterization of the homoleptic 2-(2'-pyridyl)-phosphinine Ni(0) complex [Ni(2-Py-4,6-Ph₂-PC₅H₂)₂] (**6-1**) and its reactivity toward phenyl halides. Complex **6-1** is readily accessible by replacing [IPr] and H₂C=CHSiMe₃ in the formal Ni(0) source [(IPr)Ni(H₂C=CHSiMe₃)₂] with two equivalents of 2-(2'-pyridyl)-4,6-diphenyl-phosphinine ([P,N]). Complex **6-1** is the first example of a Ni complex containing a pyridyl-phosphinine ligand. The molecular structure of **6-1** is reminiscent of ubiquitous 2,2'-bipyridine Ni(0) complexes, which are known for their versatile redox properties and utilization in the electrochemical reduction of aryl halides. Thus, the redox properties of **6-1** were investigated. It turned out that **6-1** can be oxidized both electrochemically and also chemically through use of ferrocenium salts FcX (Fc = ferrocenium; X = BF₄, PF₆, BAr^F₄; Ar^F = 3,5-(CF₃)₂C₆H₃), to afford the corresponding Ni(I) complexes **6-[1]BF₄**, **6-[1](THF)]PF₆** and **6-[1₂](BAr^F₄)₂**. The solid-state structures of these salts show an interesting dependence on the nature of the anion. While **6-[1]BF₄** and **6-[1](THF)]PF₆** show trigonal bipyramidal coordination of Ni in the solid state,

6-[**1**₂](BAR^F₄)₂ exists as a dinuclear Ni(I) complex with a bridging phosphinine moiety in a rare μ₂-mode. Magnetic measurements (EPR and Evans NMR measurements) suggest the presence of Ni(I) complexes and Ni-centered radicals. Due to the reminiscence of **6**-**1** to 2,2'-bipyridine Ni(0) complexes, which play an important role in cross-coupling reactions and which are able to undergo oxidative additions with aryl halides, the reactivity toward model substrates such as bromobenzene and iodobenzene was investigated. The reaction of **6**-**1** with bromobenzene leads to the formation of the λ⁵-phosphinine **6**-**2** and the trigonal bipyramidal Ni(I) complex **6**-[**1**]Br. In contrast, reaction of **6**-**1** with iodobenzene results in the formation of **6**-**2** and the tetrahedral Ni complex **6**-**3**, which is based on a formally anionic 1-Ph-λ⁴-phosphinine. Magnetic measurements on **6**-**3** indicate that this species undergoes a spin transition from an S = 1/2 to an S = 3/2 spin state. Quantum chemical calculations for **6**-**3** are in agreement with this observation. The calculations revealed the significant multireference character of the wavefunction and suggest that the electronic structure may be described as a 3d⁸ Ni center antiferromagnetically coupled with a ligand-centered radical. The observed carbon-halogen bond splitting and aryl group transfer highlights again the chemical non-innocence of phosphinine ligands in transition metal complexes.

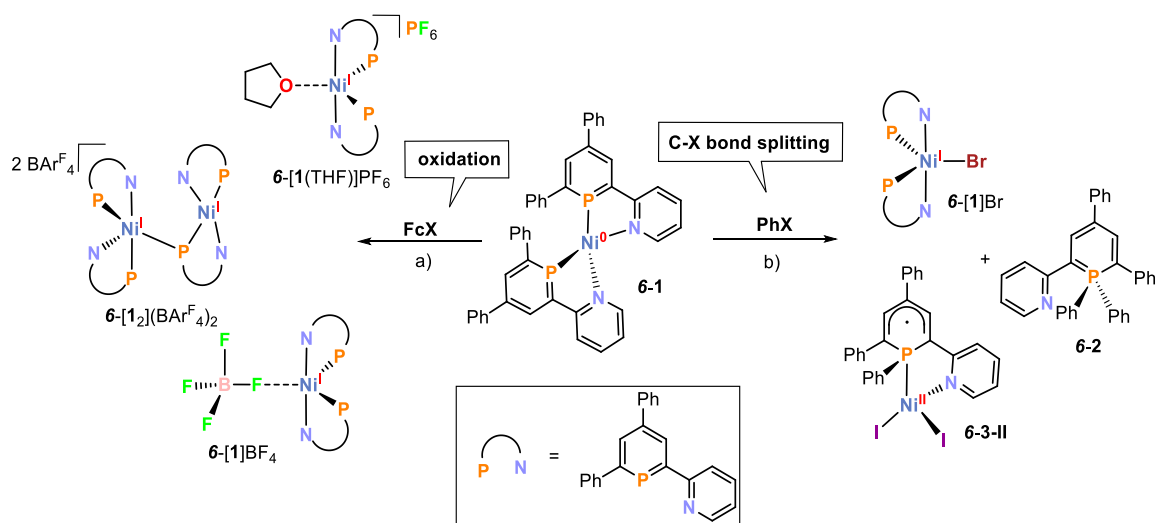


Figure 5. Homoleptic pyridylphosphinine Ni(0) chelate complex **6**-**1** and reactivity toward a) ferrocenium salts FcX (X = BF₄, PF₆, BAR^F₄; Ar^F = 3,5-(CF₃)₂C₆H₃) and b) phenyl halides PhX (X = Br, I).

Conclusion

In summary, this doctoral thesis clearly highlights the chemical non-innocence of phosphinine ligands and their versatility in a wide array of reactions. Although these six-membered heterocycles have been intensively investigated over the past five decades, many novel facets of this ligand class were discovered during this work. The selective halogenation of π -phosphinine complexes, their utilization as FLPs, activation of carbon dioxide and splitting of aryl halides were, prior to this thesis, unknown for phosphinines. This work clearly broadens the spectrum of phosphinine chemistry, nevertheless, there is still much to discover, for example with regard to the ability of phosphinines to stabilize highly-reduced metal complexes and the use of chiral phosphinines for enantioselective catalysis. This work has shown that phosphinines are a wellspring of divergent applications while still possessing a considerable amount of untapped potential which will likely be uncovered in the coming years.

List of Publications

- 1) M. J. Margeson, J. Leidl, F. Seeberger, R. Szlosek, P. Coburger, J. A. Kelly, C. Müller, R. Wolf, “Phosphacyclohexadienyl Anion Catalyzed Hydrofunctionalization of Carbonyls and Imines”, *submitted*.
- 2) J. Leidl, P. Coburger, D. J. Scott, N. P. van Leest, C. G. P. Ziegler, G. Hierlmeier, B. de Bruin, G. Hörner, C. Müller, R. Wolf, “Phosphorus-Analogues of [Ni(bpy)₂]: Synthesis and Application in Carbon-Halogen Bond Activation”, *Inorg. Chem.* **2020**, <https://doi.org/10.1021/acs.inorgchem.0c01115>.
- 3) J. Leidl, A. R. Jupp, E. R. M. Habraken, V. Streitferdt, P. Coburger, D. J. Scott, R. M. Gschwind, C. Müller, J. C. Slootweg, R. Wolf, “A phosphinine-derived 1-phospha-7-bora-norbornadiene: frustrated Lewis pair type activation of triple bonds”, *Chem. Eur. J.* **2020**, *26*, 7788–7800. Front cover: *Chem. Eur. J.* **2020**, *26*, 7731. Cover profile: *Chem. Eur. J.* **2020**, *26*, 7735–7736.
- 4) J. Leidl, M. Marquardt, P. Coburger, D. J. Scott, V. Streitferdt, R. M. Gschwind, C. Müller, R. Wolf, “Facile C=O Bond Splitting of Carbon Dioxide Induced by Metal-Ligand Cooperativity in a Phosphinine Iron(0) Complex”, *Angew. Chem. Int. Ed.* **2019**, *58*, 15407–15411.
- 5) C. M. Hoidn, J. Leidl, C. G. P. Ziegler, I. G. Shenderovich, R. Wolf, “Halide-Substituted Phosphacyclohexadienyl Iron Complexes: Covalent Structures vs. Ion Pairs”, *Eur. J. Inorg. Chem.* **2019**, 1567–1574. Front cover: *Eur. J. Inorg. Chem.* **2019**, 1433. Cover profile: *Eur. J. Inorg. Chem.* **2019**, 1434.
- 6) U. Chakraborty, J. Leidl, B. Mühldorf, M. Bodensteiner, S. Pelties, R. Wolf, “Mono- and Dinuclear Tetraphosphabutadiene Ferrate Anions”, *Dalton Trans.* **2018**, *47*, 3693–3697.

Curriculum Vitae

Education

Since Nov. 2016	Ph.D. in the group of Prof. Dr. Robert Wolf at the University of Regensburg, Institute of Inorganic Chemistry
Sept. 2018	Research Visit during Ph.D. at the Freie Universität Berlin with Prof. Dr. Christian Müller
Oct. 2014 – Sept. 2016	Master of Science in Chemistry at the University of Regensburg Master Thesis in the group of Prof. Dr. Robert Wolf (Institute of Inorganic Chemistry): “ <i>Synthesis and Reactivity of Phosphinine Iron Complexes</i> ”
Oct 2011 – Sept 2014	Bachelor of Science in Chemistry at the University of Regensburg Bachelor Thesis in the group of Prof. Dr. R. Wolf (Institute of Inorganic Chemistry): “ <i>Synthese von NCH-stabilisierten Übergangsmetallkomplexen</i> ”
Sept 2003 – July 2011	Allgemeine Hochschulreife (A-levels) at the Gymnasium Waldkraiburg

Conferences and Presentations

Feb. 2020	Talk – 17 th European Workshop on Phosphorus Chemistry, Rennes, France
Aug. 2019	Talk – Wissenschaftliches Kolloquium von Arbeitsgruppen für Anorganische Chemie 2019, Hirschegg, Austria
April 2019	Poster – 16 th European Workshop on Phosphorus Chemistry, Bristol, UK
March 2019	Poster – 16. Koordinations-Chemie Treffen, München, Germany
Sept. 2018	Poster – 19. Vortragstagung für Anorganische Chemie der Fachgruppen Wöhler-Vereinigung und Festkörperchemie und Materialforschung, Regensburg, Germany
March 2018	Poster – 15 th European Workshop on Phosphorus Chemistry, Uppsala, Sweden
Aug. 2017	Talk – Wissenschaftliches Kolloquium von Arbeitsgruppen für Anorganische Chemie 2017, Hirschegg, Austria
July 2017	Poster – 22 nd Conference on Organometallic Chemistry (EuCOMC XXII), Amsterdam, the Netherlands
March 2017	Poster – 14 th European Workshop on Phosphorus Chemistry, Cluj-Napoca, Romania

Acknowledgement

Zuallererst möchte ich mich bei meinem Doktorvater *Prof. Dr. Robert Wolf* für die hervorragende Betreuung bedanken. Danke Robert, dass du mir die Möglichkeit gegeben hast, meine Doktorarbeit an deinem Arbeitskreis unter den bestmöglichen Arbeitsbedingungen anzufertigen. Danke, dass du mir so viele Freiheiten in der Forschung gegeben hast und mich immer unterstützt hast. Danke für deine Geduld und deinen Glauben in meine (chemischen) Fähigkeiten.

Zudem möchte ich mich noch herzlichst bei meinem zweiten Mentor *Prof. Dr. Christian Müller* für das Anfertigen des Zweitgutachtens seine Betreuung bedanken. Danke Christian, dass du den tollen Pyridylphosphinin-Liganden in mein Promotionsleben gebracht hast. Er hat mir nicht nur Publikationen verschafft, sondern auch Freude an der Forschung. Danke nochmal für die schöne Zeit während meines Forschungsaufenthaltes in Berlin. Ich bin für unsere Kooperation sehr dankbar!

Ich danke Prof. Dr. Frank-Michael Matysik (Drittprüfer) und Prof. Dr. Manfred Scheer (Vorsitz) für die Bereitschaft, die restlichen Plätze der Prüfungskommission zu besetzen.

Ich möchte mich auch bei den Mitarbeitern der zentralen Analytik für ihre jahrelange Unterstützung bedanken, insbesondere Sabine Stempfhuber und Birgit Hischa (Röntgenstrukturanalyse), Annette Schramm, Georgine Stühler, Veronica Scheidler, Fritz Kastner und Ilya Shenderovich (NMR-Abteilung), Barbara Baumann und Helmut Schüller (Elementaranalyse), Josef Kiermaier und Wolfgang Söllner (Massenspektrometrie).

Many thanks to my collaboration partners from Amsterdam: Prof. Dr. J. Chris Slootweg, Dr. Evi R. M. Habraken, Dr. Andrew R. Jupp, Prof. Dr. Bas de Bruin and Nicolaas P. van Leest. Thank you so much for the chemical, theoretical and analytical support!

Thank you so much Evi for being not only an excellent collaboration partner but also for becoming a very good and lovely friend!

Ein großer Dank gilt auch meinem Kooperationspartner aus Berlin: Michael Marquardt. Danke Michael für die Liganden-Lieferungen und für die schöne Zeit in Berlin!

Danke an alle aktuellen und ehemaligen Arbeitskreismitglieder: Dirk, Stefan, Bernd, Christian Rödl, Uttam, Anup, Christian Hoidn, Uli, Thomas, Sigggi, Gabi, Julia, Marion, Felix, Jose, Daniel, John, Percia, Rafael, Sebastian, Peter, Karo, Robin, Maxi, Martin und Matti. Danke für die gute und harmonische Arbeitsatmosphäre, für coole Küchenparties und unterhaltsame Kaffee-/Mittagspausen!

Besonderer Dank gilt all meinen Laborkollegen: Anup, Christian, Uttam, Uli, Felix, Matti, Rafael und Gabi. Danke für tolle Stimmung im Labor und für eure Unterstützung! Thanks Matti for your daily portion of positive energy!

Danke Gabi, dass du mir nicht nur eine exzellente Laborkollegin warst, sondern auch eine sehr gute Freundin! Jede Kaffeepause ohne dich ist eine verlorene Kaffeepause!

A massive hug for John and Daniel, who rescued my thesis and PhD life by proofreading all of the stuff I gave to them (sorry guys)! Special thanks to John, who is not only a good colleague, but also a caring friend and roommate! Thanks for your support!

Ein riesiges Dankeschön geht an meine liebsten Studienkolleginnen: Verena, Marlene und Nele! Danke für die coole Studienzeit, die (exzessiven) Parties, NMR-Messungen, die schönen Ausflüge und an all die schönen Momente, die wir miteinander geteilt haben.

Tausend Dank an meine Familie (Mama, Papa, Melanie, Klaus, Oliver, Alex, Evi), Familie Coburger (Antje, Karli, Liese) und Freunde (Bibi, Lisa, Nina), die mich aus der Ferne immer und bedingungslos unterstützt haben! Eure lieben Worte und positive Energie haben mich in weniger schönen Zeiten der Promotion immer wieder motiviert!

Ich möchte noch von ganzem Herzen meiner Schwester *Gela* danken! Ohne dich wäre ich jetzt nicht da, wo ich bin.

Zuletzt möchte ich meinem Verlobten Peter danken, der seit Tag eins meiner Promotion immer an meiner Seite war. Danke für deine enorme Unterstützung egal, ob im privaten Leben oder im Labor! Ohne dich hätte ich die Promotion wahrscheinlich nicht durchgestanden und ohne dich wäre das Leben auch nur halb so schön!

Appendix

The Appendix of this thesis contains the supporting informations of all published publications. These supporting informations contain analytical data in terms of NMR spectra, UV-Vis spectra, IR spectra, EPR spectra, X-ray crystallography and cyclic voltammograms, as well as DFT calculations. These supporting informations are stored on an external CD-ROM, which is supplied with this thesis.

Eidesstattliche Erklärung

Ich erkläre hiermit an Eides statt, dass ich die vorliegende Arbeit ohne unzulässige Hilfe Dritter und ohne Benutzung anderer als der angegebenen Hilfsmittel angefertigt habe; die aus anderen Quellen direkt oder indirekt übernommenen Daten und Konzepte sind unter Angabe des Literaturzitats gekennzeichnet. Die Arbeit wurde bisher weder im In- noch im Ausland in gleicher oder ähnlicher Form einer anderen Prüfungsbehörde vorgelegt.

Julia Leitl

